A HYPOMORPHIC MUTATION IN *POLD1* DISRUPTS THE COORDINATION OF EMBRYO SIZE EXPANSION AND MORPHOGENESIS DURING GASTRULATION

by

Tingxu Chen

A Dissertation

Presented to the Faculty of the Louis V. Gerstner, Jr.

Graduate School of Biomedical Sciences,

Memorial Sloan Kettering Cancer Center

in Fulfillment of the Requirements for the Degree of

Doctor of Philosophy

New York, NY

September 2022

Dedication

I would like to dedicate this thesis to my mother, Ping Peng, my husband, Zhenhao Guo, my daughter, Kathy Guo. Of all the great people whom I have met over my lifetime, these three individuals have always stood by me. If it wasn't for their love, sacrifice and perseverance, none of this work would have been possible.

A HYPOMORPHIC MUTATION IN *POLD1* DISRUPTS THE COORDINATION OF EMBRYO SIZE EXPANSION AND MORPHOGENESIS DURING GASTRULATION

Tingxu Chen, Ph.D.

Louis V. Gerstner Sloan Kettering Graduate School of Biomedical Sciences,

2022

Formation of a properly sized and patterned embryo during gastrulation requires a well-coordinated interplay between cell proliferation, lineage specification and tissue morphogenesis. Following transient physical or pharmacological manipulations of embryo size, pre-gastrulation mouse embryos show remarkable plasticity to recover and resume normal development. However, it remains unclear how mechanisms driving lineage specification and morphogenesis respond to defects in cell proliferation during and after gastrulation. Null mutations in DNA replication or cell cycle-related genes frequently lead to cell cycle arrest and reduced cell proliferation, resulting in developmental arrest before the onset of gastrulation; such early lethality precludes studies aiming to determine the impact of cell proliferation on lineage specification and morphogenesis during gastrulation. From an unbiased ENU mutagenesis screen, we discovered a mouse mutant, *tiny siren* (*tyrn*), that carries a hypomorphic mutation producing an aspartate to tyrosine (D939Y) substitution in Pold1, the catalytic subunit of DNA polymerase δ. Impaired cell proliferation in the *tyrn* mutant leaves anterior-posterior patterning unperturbed during gastrulation but results in reduced embryo size and severe morphogenetic defects. Our analyses show that the successful execution of morphogenetic events during gastrulation requires that lineage specification and the

ordered production of differentiated cell types occur in concordance with embryonic growth.

Biosketch

Tingxu was born on January 8th, 1993, in Nanjing, Jiangsu, China. At the age of six, she attended her first year of elementary school. Tingxu graduated from Jinling High School in 2011 and began college at Shanghai Jiao Tong University (SJTU) in Shanghai, China that same year. Tingxu graduated with a bachelor of science (BS) in Biological Sciences, honor program in 2015. During her time at SJTU, Tingxu worked in Dr. Shigang He's lab as a research undergraduate for 2 years. Tingxu completed her undergraduate senior thesis project in the Howard Hughes Medical Institute, Department of Physiology, University of California, San Francisco (UCSF) under the mentorship of Dr. Lily. Yeh. Jan. On August 17th, 2015, Tingxu moved to New York, New York, where she began the first year of her PhD at the inaugural Louis V. Gerstner Jr. Graduate School of Biomedical Sciences at Memorial Sloan Kettering Cancer Center.

Acknowledgments

I would like to thank my Ph.D. mentor, Kathryn. V. Anderson (1952-2020), for her enthusiastic and continuous support and encouragement over the past 5 years. I also sincerely appreciate the scientific advice from Kathryn and academic independence from the lab. More importantly, I learned from Kathryn the invaluable scientific attitudes: be curious about life, be honest about observations, be open-minded about unexpected results, be careful about the data interpretation and conclusion. I will carry on her legacy forward in the next period of my life.

I would like to thank my Ph.D. mentor, Danwei Huangfu, for her continuous support and encouragement during the last year of my graduate student life. I am very grateful for everything she has done to help me go through the most difficult time, prepare and submit the manuscript, and eventually get me ready for the defense. I would like to thank Dr. Elizabeth Lacy for her advice and input on my thesis project and manuscript preparation. I would not be able to complete my research without her help and support.

I would like to thank our lab manager Edward Espinoza, who has been an irreplaceable person not only for his essential support in lab work, but also for those incredible daily non-scientific conversations which make my graduate career much more joyful. I am also very grateful to Heather Alcorn for performing the ENU mutagenesis screen with Kathryn, and for continuous support on mouse colony management. I would also like to thank all other Anderson Lab and Huangfu Lab members for their support and kindness.

I would like to thank my thesis committee members, Drs Jennifer Zallen and Dirk Remus. In particular, I would like to thank Dr. Remus and Dr. Sujan Devbhandari for

performing the primer extension assay, and Dr. Zallen for helpful advice throughout the years. I am grateful for the support from the whole SKI community: Dr. Devanshi Jain from Dr. Scott Keeney's lab for sharing the methods of data analysis; MSKCC Integrated Genome Operation for performing whole-exome sequencing and exome-wide SNP dataset, MSKCC Molecular Cytogenetics Core Facility for the karyotype test, MSKCC Center of Comparative Medicine and Pathology for the pathogen exam, MSKCC Mouse Genetics Core Facility for ESC clone injection, MSKCC Molecular Cytology Core Facility (Dr. Boyko, Dr. Tipping, Mr. Feng) for assistance with confocal imaging and image processing. I would like to thank Dr. Anna-Katerina Hadjantonakis for providing the Hhex-GFP mouse strain, and Mr. Jonathan Pai from Hadjantonakis' lab for methods of clearing embryos. Without their enormous generosity, professional skills and knowledge this thesis is impossible.

Lastly, I would like to thank our graduate school, particularly our dean, Dr. Michael Overholtzer, for his help and support during my most difficult time in graduate school, Drs. Kenneth Marians, Harold Varmus, and our benefactor Louis V. Gerstner. If it wasn't for their vision, initiative, and generosity, our graduate program would not exist today. Additionally, I would like to thank David McDonagh for helping format this dissertation.

Table of Contents

List of Figures

Chapter 1 Introduction

Section 1 Lineage specification, tissue morphogenesis, and embryo size expansion in early embryogenesis

1.1 Lineage segregation in blastocyst

1.1.1 Overview

3.5 days after fertilization, a single-cell zygote undergoes multiple rounds of cell cleavage, reaching the blastocyst stage (**Figure 1.1**). The embryo at this stage consists of an outer cell layer termed trophectoderm (TE), and a group of inner cell mass (ICM) surrounded by the TE. The ICM is composed of two cell lineages: epiblast (EPI) and primitive endoderm (PrE). TE, EPI, and PrE are the three fundamental lineages specified in the blastocyst stage. The TE gives rise to the ectoplacental cone and the extraembryonic ectoderm (ExE), which become the placenta. The PrE differentiates into the parietal endoderm and the visceral endoderm (VE). The parietal endoderm becomes part of the parietal yolk sac. The VE covers the ExE and the epiblast, contributing to the formation of the visceral yolk sac. The TE and PrE envelop the epiblast layer, which gives rise to all fetal tissues and some of the extraembryonic tissues during embryonic development (Arnold and Robertson, 2009; Rivera-Perez and Hadjantonakis, 2014).

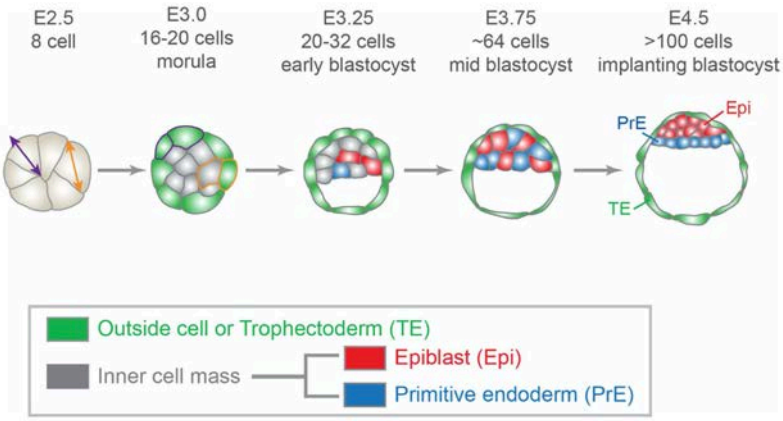

Figure 1.1 Schematic representation of early mouse embryonic development before implantation. The outer cell/trophectoderm is labeled in green. The epiblast is labeled in red and the primitive endoderm is labeled in blue. (Artus and Chazaud, 2014)

1.1.2 Lineage segregation of trophectoderm and inner cell mass

The mechanisms driving cell fate decision and cell layer segregation inside the blastocyst are the two deeply studied topics in blastocyst lineage specification. The first round of binary lineage segregation occurs between the TE and ICM (**Figure 1.2**). Segregation of progenitors of TE and ICM is realized through asymmetrical cell divisions along a basolateral cleavage plane at the 8-cell morula stage, as observed by the time-lapse cinemicrography (Sutherland et al., 1990). The outer cells become the TE and the inner cells comprise the ICM. The molecular mechanism driving the binary cell fate specification of TE and ICM is extensively explored by a series of genetic and cell biology studies in blastocysts and pluripotent stem cells (PSCs). Expression of *Cdx2*, the mouse orthologue of the *Drosophila* homeobox gene *caudal* (*cad*) (Mlodzik et al., 1985; Mlodzik and Gehring, 1987), is detected exclusively in the TE (Beck et al., 1995). Genetic ablation of *Cdx2* in mouse blastocysts shows that *Cdx2*$^{-/-}$ embryos fail to maintain TE differentiation and fail to implant (Strumpf et al., 2005). Loss of *Cdx2* is also associated with ectopic expression of ICM-specific genes in outer cells (Strumpf et al., 2005). On the contrary, expression of the gene encoding murine POU transcription factor OCT4 (also known as POU5F1) is required for promoting ICM lineage formation. *Oct4* is exclusively expressed in the ICM and is required for maintaining the pluripotency of ESCs or ICM cells in mammalian embryos (Niwa et al., 2000). Repressing *Oct4* expression in mouse ESCs leads to loss of pluripotency and differentiation to trophoblast stem cells (TSCs) (Niwa et al., 2000). The mutual-exclusive expression pattern of *Cdx2* and *Oct4* raises the new question that how such expression pattern is generated. Studies in pre-implantation embryos indicate that *Cdx2* and *Oct4* are initially co-expressed in all cells at the morula stage (Niwa et al., 2005). *Cdx2* expression is enhanced after the asymmetrical division of the morula and further increased through a positive regulatory-feedback mechanism in outer cells (Dietrich and Hiiragi, 2007; Niwa

et al., 2005; Ralston and Rossant, 2008). *Oct4* expression is also positively regulated by a similar mechanism, although restricted to the ICM cells (Okumura-Nakanishi et al., 2005). CDX2 and OCT4 adopt a reciprocal-inhibition mechanism that interferes with the transcriptional activation of each other (Niwa et al., 2005) (Figure 1.2). Taken together, these studies demonstrate that CDX2 and OCT4 are the major transcription factors required for TE and ICM lineage segregation. The binary cell fate decision is achieved by the reciprocal inhibition of transcriptional activities between CDX2 and OCT4.

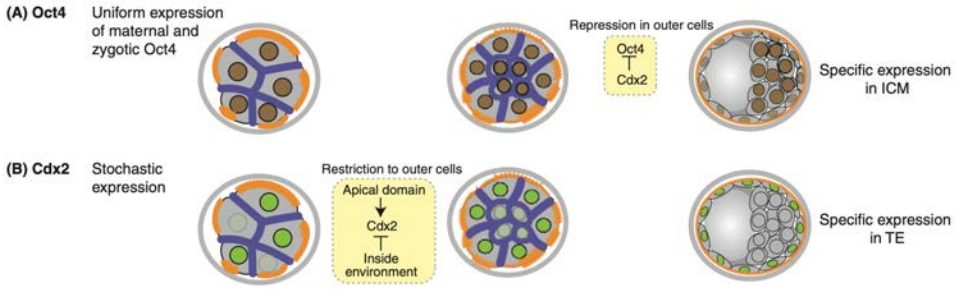

Figure 1.2 Critical transcription factors in the segregation of the trophectoderm and ICM lineages. (Rossant and Tam, 2009a)

The apical domain is tightly correlated with the enhanced CDX2 expression in outer cells (Ralston and Rossant, 2008), raising the question whether the cell polarity acquired in outer layer cells at the morula stage is the primary cue that drives TE and ICM lineage specification. Genetic analysis in *Tead4*$^{-/-}$ embryos shows that TEAD4 is required for TE specification, suggesting that the Hippo/YAP signaling pathway serves as the link between cell polarization and TE differentiation (Nishioka et al., 2008; Yagi et al., 2007) (**Figure 1.3**). The Hippo/YAP signal pathway was originally discovered in *Drosophila* that controls tissue growth and it is now proven to be a well-conserved signaling cascade in mammals (Pan, 2010; Yu et al., 2015). A subsequent study shows that in TE, where Hippo signaling is OFF, free YAP proteins translocate to the nucleus and bind to TEAD4, activating TE-specific genes such as *Cdx2* and *Gata3* (Nishioka et al., 2009; Ralston et

al., 2010). Whereas in ICM, where Hippo signaling is ON, YAP is phosphorylated by LATS kinases and sequestered in the cytoplasm (Lorthongpanich et al., 2013). The differential activity of Hippo/YAP signaling is only required for a short period of time for establishing the binary gene expression pattern in the TE and ICM (Lorthongpanich et al., 2013). Hippo/YAP signaling is sufficient to modulate CDX2 expression, the Hippo/YAP signaling cascade itself, however, does not change the cell position and cell polarity.

It has been shown that loss of function of apical components such as aPKC, PAR6, and CDC42 prevents TE formation, with YAP/TAZ sequestered in the cytoplasm (Alarcon, 2010; Cao et al., 2015; Hirate et al., 2015; Hirate et al., 2013; Korotkevich et al., 2017). Outer cells in these mutant embryos adopt ICM cell fate expressing ICM-specific markers like *Nanog*. These results validate the idea that the apical-basal polarity is essential to interpret polarity information to promote YAP/TAZ localization. Studies on junction-associated scaffold protein Angiomotin (AMOT) show that the differential sub-localizations of AMOT are observed in outer/TE cells and inner/ICM cells (Hirate et al., 2013; Leung and Zernicka-Goetz, 2013). In inner/ICM cells, AMOT is phosphorylated and is located on the whole plasma membrane, whereas in outer/TE cells, AMOT is localized strictly on the apical domain and excluded from the basal lateral domain (Hirate et al., 2013). The phosphorylation of AMOT prevents its binding to F-actin in both *in vitro* biochemical assays and in cultured cells (Chan et al., 2013; Mana-Capelli et al., 2014). The phosphorylated AMOT enhances its interaction with LATS kinase to promote YAP phosphorylation (Hirate et al., 2013). These data suggest that AMOT is the mediator that transmits cell polarity to Hippo/YAP signaling cascade controlling TE specification. A recent comprehensive comparative embryology study using published single-cell RNA-sequencing (scRNA-seq) data in human preimplantation embryos combined with

immunofluorescence analysis on the human, mouse, and cow embryos shows that at the morula stage, the outer layer cell expresses aPKC and sequesters AMOT to the apical domain, inhibiting Hippo signaling pathway activation. YAP translocates to the nucleus and activates the expression of TE-specific genes, suggesting that the cell polarity- Hippo/YAP signaling is a conserved mechanism driving TE/ICM specification in mammals (Gerri et al., 2020). Other mechanisms that link apicobasal polarity to YAP/TAZ nuclear localization are demonstrated in cell line studies. For example, apical component PAR3 mediates dephosphorylation of LATS kinase by protein phosphatase 1A (PP1A). Knockdown of apical component PAR3 prevents YAP/TAZ nuclear localization (Lv et al., 2015). DLG5, another apical regulator, directly regulates MST1/2 to block YAP/TAZ nuclear localization (Kwan et al., 2016). However, it remains unknown whether these components act in the same way in preimplantation embryos.

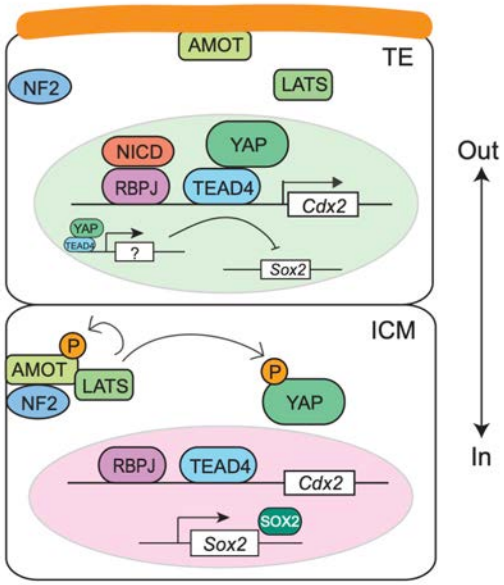

Figure 1.3 The Hippo/YAP signaling cascade controlling TE/ICM lineage segregation. (Chazaud and Yamanaka, 2016)

Interestingly, although Hippo signaling is proved to be the central player in TE/ICM specification, the requirement of TEAD4 during TE formation can be bypassed under the

condition of hypoxia that TE is formed in *Tead4*$^{-/-}$ embryos cultured in low oxygen conditions (Kaneko and DePamphilis, 2013). This suggests that YAP may have other co-effectors to activate target genes. Analyses of TE-specific enhancers of *Cdx2* reveal that Notch signaling cooperates with Hippo/YAP signaling for *Cdx2* activation (Rayon et al., 2014). It remains to be seen whether the components of Notch signaling are the compensatory factors of TEAD4 under the hypoxia condition.

1.1.3 Segregating epiblast and primitive endoderm

The ICM cells differentiate into EPI and PrE lineages. This process contains three steps: 1) Binary EPI/PrE specification, 2) EPI/PrE lineage maturation, and 3) cell sorting to form EPI cluster and PrE epithelium. In this section, we will focus on the binary EPI/PrE specification and cell sorting for PrE layer formation.

The initial ICM is a group of cell mixtures expressing either *Nanog* or *Gata6* (Chazaud et al., 2006; Kurimoto et al., 2006). Lineage tracing and live-cell imaging experiments reveal that this mosaic “salt and pepper” expression pattern can be observed at the early blastocyst stage (E3.75) in an asynchronous, position-independent manner: *Nanog* is expressed exclusively in epiblast cells and required for maintaining pluripotency, whereas *Gata6* is expressed only in PrE cells (Chazaud et al., 2006; Kurimoto et al., 2006; Meilhac et al., 2009; Plusa et al., 2008; Xenopoulos et al., 2015). Lineage-specific marker staining with live imaging of embryos expressing *Pdgfra*-HistoneH2B-GFP fusion protein, together with single-cell transcriptomic analysis suggest that these lineage-specific markers are initially co-expressed in 8-cell embryos (Guo et al., 2010; Plusa et al., 2008). The overlapping expression of these markers is gradually lost during the developmental progression and the mutual-exclusive pattern of NANOG and GATA6 is finally established in the early blastocysts (Guo et al., 2010; Plusa et al., 2008).

Although these two studies show the process of pattern establishment, it does not explain how such pattern is generated. It seems that the NANOG and GATA6 mutually repress the transcription activities of each other, similar to CDX2 and OCT4 seen in the TE/ICM lineage specification (Niwa et al., 2005). All ICM cells express *Nanog* in *Gata6* mutants (Bessonnard et al., 2014; Schrode et al., 2014) whereas all ICM cells express *Gata6* in *Nanog* mutants (Frankenberg et al., 2011). NANOG and GATA6 might directly repress each other's transcription given their binding site identified in co-immunoprecipitation studies of ESCs (Singh et al., 2007) and induced extra-embryonic endoderm cells (Wamaitha et al., 2015). But what are the upstream components of GATA6 and NANOG? A series of studies reveal that the FGF (fibroblast growth factor) signaling plays a pivotal role in defining PrE lineage (**Figure 1.4**). *Fgf4* is specifically expressed in the EPI cells (Frankenberg et al., 2011; Guo et al., 2010; Kurimoto et al., 2006; Ohnishi et al., 2014) and its expression is missing in *Nanog* mutants (Frankenberg et al., 2011). *Fgfr2* is expressed in all ICM cells before being restricted in PrE at E3.5, suggesting that all early ICM cells are able to respond to FGF ligands (Boroviak et al., 2015; Ohnishi et al., 2014). Blocking FGF signaling leads to the adoption of EPI fate in the ICM (Chazaud et al., 2006; Kang et al., 2013; Krawchuk et al., 2013; Nichols et al., 2009; Yamanaka et al., 2010), whereas exogenous addition of FGF promotes PrE cell differentiation (Nichols et al., 2009; Yamanaka et al., 2010). However, FGF itself is not required for the initiation of *Gata6* expression, as demonstrated by the presence of *Gata6* expression before the blastocyst stage in *Fgf4* mutant embryos (Kang et al., 2013; Krawchuk et al., 2013). These data suggest that FGF is required for the mosaic pattern of ICM but the initiation of *Gata6* expression is regulated by other unknown factors. Notably, even though the mutual-exclusive pattern of NANOG and GATA6 is generated, EPI and PrE cells are not fully committed to their final fate yet. Modulating

FGF signals or changing neighbor cells by transplantation at E3.75 pushes cells to adopt an alternative cell fate (Nichols et al., 2009; Yamanaka et al., 2010). This plasticity gradually disappears at E4.0 (Yamanaka et al., 2010) (Grabarek and Plusa, 2012) and is first lost in the EPI cells (Grabarek and Plusa, 2012), indicating that the EPI cell lineage is specified earlier than the PrE cell lineage.

Due to the complexity of the FGF-NANOG-GATA6 regulatory network in driving EPI/PrE lineage specification, the method of computational modeling is applied to address how the mutually exclusive salt-and-pepper is established in the ICM. The initial settings of this modeling include the mutual expression of *Gata6* and *Nanog*, and the positive and negative regulatory effects of FGF signaling on GATA6 and NANOG, respectively (Bessonnard et al., 2014). This model successfully recapitulates the *in vivo* developmental process. A few cells in the early ICM promote *Nanog* expression, leading to an increase in local FGF4 secretion. A high concentration of FGF4 induces neighboring cells into PrE cells, suggesting that the individual ICM cells adopt an EPI or PrE fate asynchronously and is dependent on FGF4 concentration. In addition, *Fgfr2* is homogenously expressed in all ICM cells at E3.25 (Ohnishi et al., 2014), indicating that differential ERK signaling activities occur upon local FGF4 concentration. Later, *Fgfr2* is downregulated by NANOG in EPI cells whereas, in PrE cells, *Fgfr2* expression is maintained by the ERK-mediated NANOG inhibition (Bessonnard et al., 2014). Another computational model is based on ectopic *Gata6* expression in ESCs (Schroter et al., 2015). In this ESC system, the *Gata6* transcriptional reporter is insensitive to ERK inhibition upon GATA4 induction (Schroter et al., 2015). This model only takes mutual repression of NANOG and GATA6 and the inhibition of FGF signaling on NANOG into consideration but still successfully recapitulates the binary fate choice. Therefore, it remains to be seen whether the FGF4 acts on NANOG only or also on GATA6

expression at both the RNA and protein levels *in vivo.* In general, it remains elusive regarding how FGF4 and/or NANOG expression increases in just a few ICM cells at very early stages. A few theories have been proposed like 1) congenital cell-to-cell difference in FGF4 secretion (Dietrich and Hiiragi, 2007; Ohnishi et al., 2014), 2) the presence or absence of certain other modulators (Bessonnard et al., 2014), 3) asymmetrical divisions leading to uneven amounts of FGF4 or FGFR2 (Mihajlovic et al., 2015; Morris et al., 2013; Morris et al., 2010), etc. None of them are favored or discarded. It is possible that a random beginning, including partial or all of these above, determines the cells that stand out among the others.

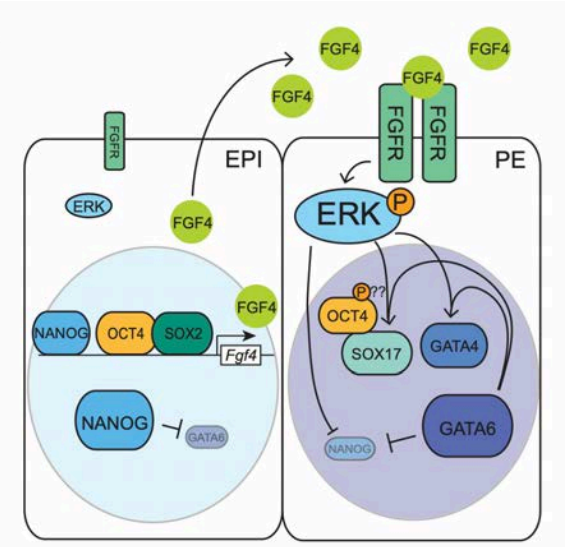

Figure 1 4 The NANOG-OCT4-FGF regulatory loop controlling EPI/PrE formation. (Chazaud and Yamanaka, 2016)

Compared to the deep insights of binary lineage specification of EPI and PrE, the cell sorting process that segregates PrE to the surface of epiblast remains poorly understood (**Figure 1.5**). Live imaging of embryos expressing PrE-specific *Pdgfr1*-H2B-GFP fluorescent reporter shows that these cellular rearrangements are achieved through multiple process (Plusa et al., 2008). First, PrE cells originally located on the surface of ICM express *Sox7* and become epithelial cells, as marked by apical expression of polar

proteins LRP2 and DAB2 (Artus et al., 2011; Gerbe et al., 2008; Yang et al., 2002). Loss of DAB2 leads to the failure of PrE cell sorting or the contact with the blastocoel (Gerbe et al., 2008; Yang et al., 2002). Once all PrE cells reach the surface, they start to redistribute the aPKC to the apical surface of the cells (Saiz et al., 2013). aPKC anchors PrE cells to prevent remixing of PrE and EPI cells (Moore et al., 2009; Saiz et al., 2013). These observations raise the possibility that cell polarity may influence cell position and sorting. Nevertheless, this theory is not sufficient to explain PrE cells moved from deep layers of the ICM. It is possible that the directional movement may also be involved in facilitating cell sorting (Meilhac et al., 2009). Lineage-specific transcription factors have been shown to modulate adhesive molecule expression such as laminin 1 and collagen IV (Gerbe et al., 2008; Niakan et al., 2010), indicating differential adhesive properties might be the driving force for directional cell movement. However, modulating other adhesion molecules such as integrin β1 only leads to failure of epithelium formation, with cell sorting occurring normally (Liu et al., 2009). Similar results are also obtained in an *in vitro* cellular assay where cell sorting process remains intact in the mixture of null E-cadherin ES cells and extraembryonic endoderm cells (Moore et al., 2009). Mathematical modeling also suggests that differential adhesion alone is not sufficient to drive cell sorting (Krupinski et al., 2011). The directional cell movement of PrE cells may also be influenced by the cortical tension created through the differential pressure between the blastocoel and the polar TE (Krupinski et al., 2011). It has been shown in zebrafish that the actomyosin network is the major contributor to the cortical tension (Krieg et al., 2008). Breaking F-actin polymerization by cytochalasin D perturbs cell movement (Meilhac et al., 2009). These observations suggest that the combined effects of differential adhesion, cortical tension, and cell polarization may be the comprehensive model driving cell sorting process for the PrE layer formation. In addition, the sorting process is also accompanied by cell apoptosis in both Epi and PrE cells (Plusa et al.,

2008). Such apoptosis may be involved in the segregation of PrE/EPI, but the detailed mechanism is still unclear.

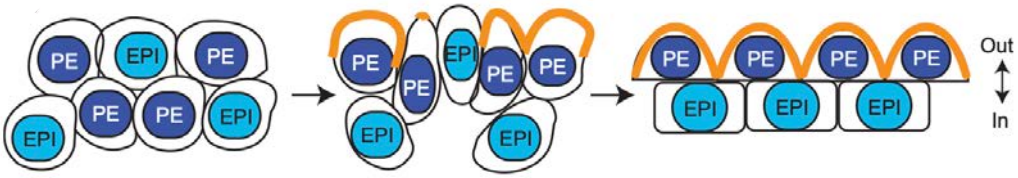

Figure 1.5 The cell sorting and PrE epithelization after PrE/EPI lineage specification. (Chazaud and Yamanaka, 2016)

A very recent study brings a new concept of “cell surface fluctuation” into the regulation of cell sorting (Yanagida et al., 2022). By combining physical modeling and experimental analysis, they discover the high surface fluctuation in PrE and consider it as the key mechanical factor in segregating these early embryonic lineages. ESCs expressing low levels of Ezrin show enhanced surface fluctuations compared to wildtype cells and are preferentially located on the outside of the aggregates. Transplanting ES cells with high surface fluctuation into cultured mouse blastocysts leads to the integration of ES cells onto the corresponding PrE cells. This study provides a new angle of addressing cell sorting process. It will be meaningful to link the intrinsically high surface fluctuation with the underlying structure of the actomyosin network and the surface distribution of signaling molecules.

1.1.4 Differences in early lineage specification among mammalian embryos

The current understanding of lineage segregation in blastocyst is primarily based on mouse embryo or mouse ESC studies. Although common features are shared, variations do exist among different species. For the past 10 years, the improved conditions to maintain *in vitro* blastocyst culture for an extended period as well as the development of stem cell-based models of blastocyst or peri-implantation embryos have provided new

information regarding early human embryogenesis. So far, our knowledge and understanding of human blastocyst are still very rudimentary, but the differences between the human and mouse blastocyst lineage specification have been identified. In general, the major genes involved in mouse lineage specification such as *Pou5f1*(*Oct4*), *Nanog*, *Cdx2,* and *Gata6*, are conserved in human embryos (Blakeley et al., 2015; Niakan and Eggan, 2013). the timing of their expression in lineage specification, however, is not always the same as in mice. Gene expression analysis by immunofluorescence in cultured human embryos reveals that OCT4, one of the key transcription factors for ICM formation in mice (Nichols et al., 1998), is broadly expressed in ICM and TE up till late blastocyst stage (Niakan and Eggan, 2013), while *CDX2*, the gene required for TE specification in mouse (Strumpf et al., 2005), is not expressed until blastocyst formation (Niakan and Eggan, 2013). Knocking out *OCT4* using CRISPR/Cas9 in human zygotes leads to the failure of blastocyst formation, but the requirement of *OCT4* in human embryo seems earlier than ICM specification (Fogarty et al., 2017). CDX2 and OCT4 show a mutually exclusive pattern in the mouse blastocyst (Niwa et al., 2005; Strumpf et al., 2005), but in the human embryo *CDX2* expression is dependent on *OCT4* (Fogarty et al., 2017). GATA3 plays a minor role in mouse TE formation, whereas in humans *GATA3* is expressed in TE precursors and is downregulated when inhibiting aPKC at the morula stage (Gerri et al., 2020; Petropoulos et al., 2016; Zhu et al., 2021), suggesting its major role in initial TE specification. These findings are supported by the results from scRNA-seq analyses of gene expression patterns and trajectories in human embryos (Petropoulos et al., 2016; Stirparo et al., 2018; Yan et al., 2013). A recent single-cell RNA-seq analysis of a pile of scRNA-seq data produces a pseudo-time trajectory indicating that the TE/ICM lineage separation may occur only after the blastocyst has formed (Meistermann et al., 2021), in contrast to the mouse where distinct gene signatures of TE and ICM are already expressed at the

late morula stage (Posfai et al., 2017). Therefore, the lineage commitment in the human embryo is delayed compared to the mouse embryo, and cells at this stage may have higher plasticity in human embryos (Rossant and Tam, 2017). Consistent with this idea, Outer layer cells isolated from human E5 blastocyst can generate a blastocyst with ICM cells (De Paepe et al., 2013). ICMs dissected from E6 human embryos can generate trophoblast outgrowth in *ex vivo* culture (Guo et al., 2021). These results suggest that the morphological events driving blastocyst formation precede the TE/ICM lineage specification. In the mouse embryo, EPI/PrE separation is dependent on local FGF/ERK signaling intensity in ICM (Saiz et al., 2016; Yamanaka et al., 2010). The binary cell fate decision in the human blastocyst, however, is not dependent on FGF/ERK signal cascade (Kuijk et al., 2012; Roode et al., 2012). What replaces the FGF/ERK signaling is still unknown. Taken together, the knowledge and information of human blastocyst remain largely unknown. More experimental data are needed to help understand the process. In recent years, the generation of the stem cell-based blastoid has shed light on the blastocyst study (Rivron et al., 2018). The quality of blastoids has been improved in recent 2-3 years to more closely mimic the real mouse blastocyst (Li et al., 2019; Sozen et al., 2019; Yang et al., 2017a; Yang et al., 2017b). However, questions remain regarding the equivalence of blastocyst and blastoid (Posfai et al., 2021). Problems also occur in human blastoid regarding how similar it is to the real blastocyst and how to match the blastoid model to the real blastocyst stage (Fan et al., 2021; Kagawa et al., 2022; Liu et al., 2021; Sozen et al., 2021; Yu et al., 2021). Data coming from both sides need to be carefully compared in a detailed and comprehensive way.

Studies in other species such as cattle also reveal spatiotemporal differences in lineage-specific gene expression. In fact, the process of bovine lineage specification is even closer to humans due to higher similarity. For example, CDX2 is present only at the

blastocyst stage (Goissis and Cibelli, 2014; Madeja et al., 2013), not at the morula stage as seen in the mouse (Beck et al., 1995; Ralston and Rossant, 2005; Strumpf et al., 2005). OCT4 is detected in TE and ICM cells (Kirchhof et al., 2000; Kuijk et al., 2008). Knocking out OCT4 in bovine embryos fails to form blastocysts, suggesting that the requirement of OCT4 is much earlier in the cattle than in the mouse (Daigneault et al., 2018; Nichols et al., 1998; Niwa et al., 2000). These findings are similar to what we observed in the human blastocyst (Fogarty et al., 2017; Gerri et al., 2020; Niakan and Eggan, 2013). During EPI/PrE specification, *Nanog* (Chambers et al., 2003; Mitsui et al., 2003) and *Gata6* (Fujikura et al., 2002) are co-expressed at the 8-cell morula stage and become mutually exclusive at the blastocyst stage in mouse (Chazaud et al., 2006; Plusa et al., 2008). In cattle, *Nanog* expression begins primarily at the early blastocyst stage while *Gata6* expression is detected in all cells from the morula stage and restricted to ICM cells at the blastocyst stage (Kuijk et al., 2012). In mice, FGF4 is required for maintaining *Gata6* expression in ICM (Kang et al., 2013). In cattle, addition of exogenous FGF2 is also able to induce PrE formation *in vitro*, indicating other FGF signal sources can be applied to activate cell differentiation (Yang et al., 2011). Blocking FGF signaling through FGFR or MEK inhibitors in the mouse embryo leads to loss of PrE cells (Yamanaka et al., 2010). In cattle, inhibition of FGF signaling leads to a significant decrease in TE and ICM cell number and predominant *Nanog* expression in ICM cells (Canizo et al., 2019), suggesting that FGF signaling in cattle may influence blastocyst formation more than just EPI/PrE specification.

In conclusion, the knowledge obtained from mouse studies provides the basis for understanding lineage specification and segregation in the blastocyst and is very instructive for human embryo research. However, the genetic distance between mice and humans determines that not all mechanisms are shared among humans and mice.

The logic of embryo morphogenesis and lineage specification can be quite different and more comparative studies among different mammalian embryos are required to help us understand the process, especially in humans.

1.2 Breaking the symmetry: specification of the anterior-posterior axis

1.2.1 Conceptus shaping

At the peri-implantation stage, the mouse embryo undergoes rapid growth, with the epiblast quickly expanding into the yolk sac cavity (Snell and Stevens, 1966; Snow, 1977). A proamniotic cavity is formed in the center of the embryo, surrounded by the epiblast layer. In mice, the polar TE proliferates and develops into extraembryonic ectoderm and ectoplacental cone in response to FGF signaling (Corson et al., 2003; Gardner et al., 1973). The mouse conceptus is elongated, forming an egg-cylinder structure. The connection site to the uterus is defined as the proximal pole along the proximodistal axis of the embryo. The differential rates of proliferation and mechanical constraints from the uterus are proposed to be the cause of proximodistal conceptus elongation as well as the formation of the columnar shape of the extraembryonic ectoderm (Copp, 1979).

In humans, the morphological events are very different from those in mice. The human embryo does not form the ectoplacental cone at the peri-implantation stage (Kunath et al., 2014). The nascent proamniotic cavity is formed when the EPI is separated from the amniotic epithelium, which does not exist in the mouse embryo at this stage. While in the mouse embryo, the proamniotic cavity is connected to the prospective chorionic cavity surrounded by the ExE. The extra-embryonic mesenchyme, which fills the space between the trophoblast and the EPI, is also unique in the human pre-gastrula embryo. Lineage tracing from rhesus monkeys and human shows that some of these cells may

originate from the hypoblast (Deglincerti et al., 2016; Enders and King, 1988). Finally, the human embryo develops into a discoid shape, instead of an egg-cylinder structure seen in mice. Whether and how these differences in spatial arrangements may affect tissue-tissue interaction and pattern formation needs further comparative investigation.

1.2.2 Specification of distal visceral endoderm

Multicellular organisms adopt different strategies to determine the body axes. For example, in *Drosophila*, the anterior-posterior (A-P) polarity is determined by the asymmetric distribution of maternal determinants in the oocyte, and this asymmetric localization is well maintained during embryogenesis (Cox et al., 2001; Cox and Spradling, 2003; Huynh et al., 2001). In mammalian embryos, however, specification of body polarity does not rely on maternal determinants and the timing of the specification occurs after the implantation. In mouse embryos, specification of the distal visceral endoderm is the first step in generating the A-P axis that breaks the radial-symmetrical structure of the egg cylinder embryo (**Figure 1.6**). After conceptus elongation, the embryo naturally establishes the proximal-distal (P-D) axis. The DVE is induced in a small population of embryonic visceral endoderm (emVE) cells located at the distal pole underlying the epiblast (Lu and Robertson, 2004; Takaoka et al., 2017). At E5.5, the proximal epiblast secrets pro-NODAL, which is converted to the active NODAL through proteolytic cleavage by FURIN and PACE4 convertases located at the ExE. After that, NODAL spreads out through the whole epiblast, creating a NODAL gradient along the P-D axis (Ben-Haim et al., 2006). BMP4 secreted from the ExE inhibits the formation of DVE, restricting the DVE to the distal pole (Yamamoto et al., 2009). The DVE expresses the Nodal antagonists *Cer1* and *Lefty1*, which in turn inhibits the NODAL/SMAD2 signaling that initially induces the *Cer1* and *Lefty1* expression (Yamamoto et al., 2009). Loss of SMAD2 functionally fails to induce the expression of Nodal antagonists, leading

to ectopic activation of posterior/proximal genes such as *Brachyury* (also known as *T*), *Fgf8,* and *Wnt3* (Perea-Gomez et al., 2002; Waldrip et al., 1998). This inhibitory feedback loop further enhances the NODAL signaling gradient along the P-D axis (Yamamoto et al., 2009). The DVE cells subsequently migrate unidirectionally to determine the future anterior side of the embryo.

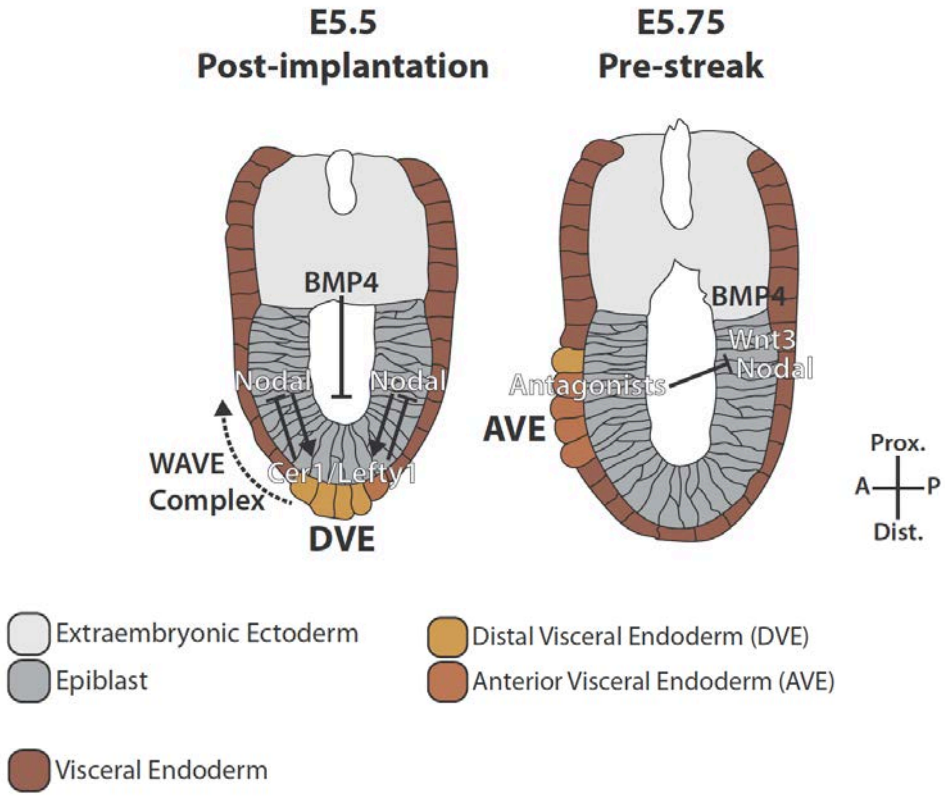

Figure 1.6 Anterior-posterior polarity establishment. DVE and AVE are specified sequentially after conceptus elongation. The DVE/AVE migration breaks the symmetry of the mouse embryo. (Bardot and Hadjantonakis, 2020)

1.2.3 Specification of anterior visceral endoderm

The similarity of gene expression, location, and morphology between DVE and AVE cells makes people think that the DVE migrates to the anterior part of the embryo, directly becoming the AVE. This theory is later demonstrated to be wrong through a detailed lineage tracing analysis of mouse embryos between E5.5 to E6.5. AVE cells arise from a subpopulation of VE cells located more proximally which initially do not express *Lefty1*

(Takaoka et al., 2011). *De novo* expression of *Lefty1* in AVE cells is observed when the *Lefty1*+ DVE cells already migrate anteriorly (Takaoka et al., 2011) (**Figure 1.7**). Depleting EOMES also leads to the failure of AVE formation, but DVE remains intact (Nowotschin et al., 2013). These data demonstrate that AVE and DVE cells originate from different subpopulations in VE. Similar to DVE, AVE expresses NODAL inhibitors CER1 and LEFTY1 (Hoshino et al., 2015; Thomas et al., 1998). It also expresses HHEX and Wnt inhibitor DKK1 (Hoshino et al., 2015; Kimura-Yoshida et al., 2005). Once migrating to the anterior side, the AVE serves as the signal center to restrict the NODAL and WNT to the proximal/posterior and posterior side of the embryo, respectively (Belo et al., 1997; Kemp et al., 2005; Perea-Gomez et al., 2002). Although the embryo is morphologically symmetric, the A-P polarity is established and sets up the basis for initiating gastrulation.

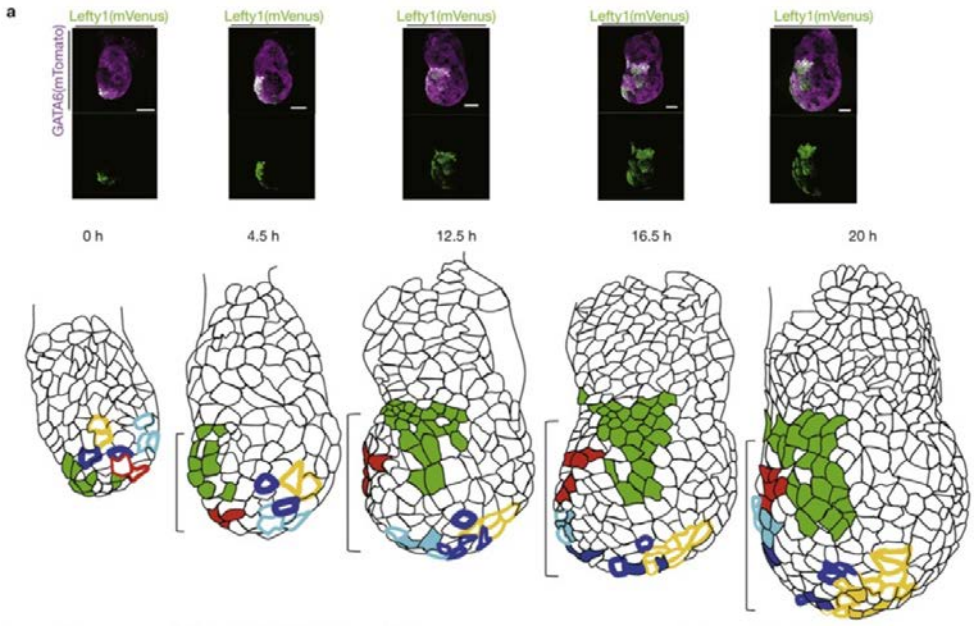

Figure 1.7 Time-lapse imaging of E5.5 transgenic embryos expressing *Lefty1* and *Gata6* BACs. DVE cells are marked in green. AVE-fated cells are outlined in red, light blue, dark blue, or yellow. AVE cells are labeled with solid red, light blue, dark blue, or yellow. (Takaoka et al., 2011)

1.2.4 AVE and DVE migration: where and how

The migratory behaviors of AVE and DVE cells have been extensively investigated in the past decade. There have been a lot of debates on the determinants guiding the direction of cell collective migration as well as the mechanisms driving cell movements. It has been shown that an imbalanced expression of *Lefty1* is observed in the PrE at the implantation stage. The biased expression of *Lefty1* can also be recapitulated in *in vitro* culture (Takaoka et al., 2011; Takaoka et al., 2006). Besides, the localization of β-catenin, the downstream effector of the canonical WNT signal cascade, is asymmetrical in implanting embryos (Chazaud and Rossant, 2006). Cells expressing *Cer1* are also asymmetrically located after implantation (Torres-Padilla et al., 2007). These results suggest that the orientation of the A-P polarity is already established prior to DVE/AVE migration. However, whether the biased expression of these markers is only predictive or is the real determinant of DVE/AVE migration direction remains elusive. The details of guiding DVE/AVE migration are still under active investigation.

The migration of DVE/AVE is facilitated by multiple signaling pathways. It has been shown that NODAL signaling is required to maintain DVE/AVE migration (Kumar et al., 2015; Takaoka et al., 2006; Yamamoto et al., 2009). Inhibition of *Nodal* transcription prevents DVE migration (Norris and Robertson, 1999; Perea-Gomez et al., 2002). Embryos lacking CRIPTO, the NODAL co-receptor, also show defective DVE migration (Ding et al., 1998). Based on the biased expression of NODAL signaling, one model proposes that DVE/AVE cells are passively pushed forward towards the anterior side, as a result of enhanced cell proliferation in response to asymmetric Nodal signaling on the prospective posterior side (Yamamoto et al., 2004). However, given the rapid transition from DVE to AVE (5~7 hours)(Rivera-Perez et al., 2003; Srinivas et al., 2004), the cell proliferation rate (~10 hours) (Stuckey et al., 2011) is not sufficient to drive DVE/AVE

migration. In contrast to the passive migration model, time-lapse imaging of mouse embryos expressing the *Hhex*-GFP reporter reveals localized filopodia projections on migrating DVE cells (Srinivas et al., 2004), indicating that DVE cell movement is mediated by the filopodia protrusion. The filopodia projection extends basally while cells are moving forward (Srinivas et al., 2004). The directional extension of filopodia may also indicate the existence of chemoattractant or chemorepellent (Kimura-Yoshida et al., 2005; Srinivas et al., 2004). Alternatively, DVE/AVE cells might move through the planar polarity-dependent mechanism based on the expression of various planar cell polarity proteins in DVE/AVE (Crompton et al., 2007). The strong evidence supporting the active cell migration comes from the genetic study that functional loss of NAP1, a regulator of the WAVE-WASP1 complex required for the reorganization of F-actin and the formation of filopodia, results in defective DVE migration (Rakeman and Anderson, 2006). Further studies on RAC-1, a GTPase downstream of WAVE-WASP1 and functions in actin polymerization in lamellipodia, matrix adhesion and cell survival, show that *Rac-1* mutant embryos fail to specify the A-P axis. AVE-specific markers are retained at the distal tip (Migeotte et al., 2011; Migeotte et al., 2010). Genetic ablation of *Rac-1* regulator in VE disrupts spatial localization of RAC-1, the activity of which is essential for driving directional AVE migration (Omelchenko et al., 2014). However, caveats still exist in these genetic studies as Rac-1-dependent signaling is also involved in shaping cell morphology, maintaining epithelial integrity, and controlling the cell cycle. Moreover, these components are expressed in multiple cell types inside the VE. Inevitably, the behaviors of other cells may also be affected at the same time.

Although the current genetic evidence favors the active cell migration as the predominant mechanism driving DVE/AVE cell movements, evidence for subsequent events after protrusion is still lacking, such as establishing new adhesion sites at the

leading edge, cell body contraction, and detachment of adhesions at the trailing edge of the cell (Rivera-Perez and Hadjantonakis, 2014). These observations are very difficult to obtain *in vivo* given the size and complexity of the embryos. It might be an alternative way if we can develop an embryoid body mimicking embryos at this stage to observe these active migratory events in higher magnification. In conclusion, the DVE/AVE migration is still a complex developmental process waiting to be deconvoluted.

1.3. Gastrulation: the beginning of a real life

1.3.1 Overview of gastrulation

Gastrulation is a tissue reorganization process transforming blastomeres into a multi-layered embryo. In triploblastic organisms, the gastrula consists of three germ layers: 1) ectoderm, which gives rise to the nervous system and epidermis; 2) mesoderm, which differentiates into muscle, bone, connective tissue, urogenital and circulatory systems; 3) endoderm, which becomes internal organs including the liver, pancreas, gastrointestinal tract, etc. The detailed process of gastrulation can be very different among different species. In invertebrates, for example, *Drosophila*, gastrulation starts with a single blastoderm epithelium generated from cellularization (FOE, 1993; Foe and Alberts, 1983; Zalokar, 1976). Multiple transient furrows are formed from the blastoderm and some of these furrows will be the sites where future germ layers are generated. In amniotic vertebrates like reptiles, birds, and mammals, gastrulation involves 1) the epithelial-mesenchymal transition (EMT), which transforms the epithelial cells from the epiblast to the mesenchymal cells; 2) the formation of the primitive streak, a transient structure that passes mesenchymal cells into the interior side of the embryo, giving rise to mesoderm and endoderm. In non-amniotic vertebrates such as zebrafish, gastrulation is initiated after epiboly movements. Mesoderm and endoderm progenitors are internalized at the germ ring margin below the remaining neuroectoderm. Although the

detailed patterning and morphogenetic events during gastrulation vary among species, some key signaling pathways are shared in these processes. In this section we will discuss some critical morphogenetic events occurring during gastrulation and compare these events among different model organisms.

1.3.2 Epithelial-mesenchymal transition

The epithelial-mesenchymal transition (EMT) is first described in the chick embryo when epithelial cells lose their original characteristics and switch to mesenchymal cells. EMT is driven by the expression of genes that are required to dissociate cell adhesion, and apical-basal polarity and promotes cell migration. In adult tissues, EMT is involved in wound healing and is also activated in cancer cells undergoing metastasis. In development, EMT is seen in a broad range of developmental events. Studies of these events lead to some major findings in the EMT process. We will discuss some major findings in EMT in two typical developmental processes: gastrulation and neural crest cell development.

Gastrulation EMT

In the *Drosophila* embryo, EMT occurs after the mesoderm internalization, where a tube is formed by mesodermal cells with epithelial characters like apicobasal polarity and apical adherens junction (AJs) (Clark et al., 2011; Leptin and Grunewald, 1990; Sweeton et al., 1991; Tepass and Hartenstein, 1994). The tube is later collapsed, and a multilayered cell aggregate is formed beneath the neuroectoderm. Disassembly of AJs is the first step of EMT (**Figure 1.8**). Live imaging of fluorescent *Drosophila* embryos provides many critical insights into the dynamics of AJs during development. The transcription factor Snail is critical for promoting AJ disassembly during EMT (Hemavathy et al., 1997). Embryos harboring a hypomorphic *sna* allele (sna^{v2}) can

invaginate, but some of the cells show features of both mesoderm and neuroectoderm with reduced mesoderm derivatives. During EMT, an E-cadherin to N-cadherin switch occurs under the control of Twi and Sna (Oda et al., 1998). Although the cadherin switch is observed in EMT, overexpression of E-cad does not impair EMT, while N-cad mutants can still undergo EMT (Schafer et al., 2014). The maternal-provided E-cad proteins still exist on mesoderm cells even after EMT is complete (Clark et al., 2011). This indicates that Sna (and Twi) may promote AJ disassembly through a posttranscriptional mechanism. Notably, the AJ dynamics are not directly correlated with the *snail* expression level before gastrulation (Dawes-Hoang et al., 2005; Kolsch et al., 2007). Live confocal imaging of embryos with fluorescent-tagged AJs or AJ-associated proteins reveals that the actomyosin activity mediates AJ reorganization and controls the timing of AJ disassembly. Visualizing mCherry-tagged Myosin II shows accumulated Myosin II at AJs (Martin et al., 2010). Activation of Myosin II in dorsal cells promotes AJs remodeling while reducing Myosin II level delays AJ remodeling in ventral cells (Martin et al., 2010). Therefore, these findings indicate that increasing actomyosin-based contractility promotes AJs remodeling and prevents Snail-mediated AJ disassembly. In addition, increased expression of *snail* downregulates the apical polar protein Baz (Par3) before mesoderm internalization (Coopman and Djiane, 2016; Weng and Wieschaus, 2017). Once the mesodermal tube is internalized, the myosin contractions cease, the AJs start to dissociate, and reduced Baz further promotes the AJ disassembly.

The FGF signaling is considered to be the critical upstream signaling in regulating EMT. In the mouse embryo, FGF regulates SNAIL expression to repress E-cadherin expression level (Ciruna and Rossant, 2001; Thisse and Thisse, 2005). In the fly embryo, however, EMT can still occur in the absence of FGF signaling, although in a delayed manner. It seems that, in the *Drosophila* embryo, FGF signaling regulates AJ

dynamics in a Snail-independent way, as modulating FGF signaling does not alter the expression level of *snail*. In general, the detailed mechanism of FGF controlling EMT in fly embryos is largely unclear.

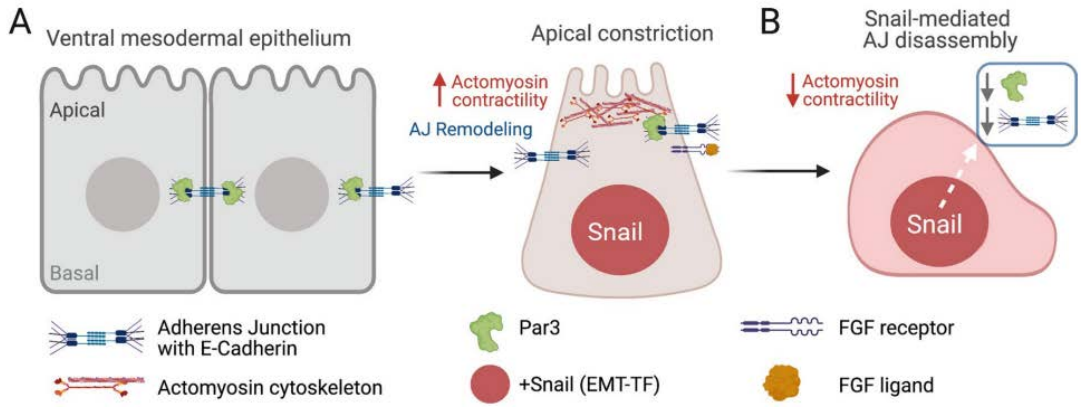

Figure 1.8 Actomyosin contractility and adherens junction (AJs) dynamics during *Drosophila* gastrulation. (Amack, 2021)

In the mouse embryo, EMT is the hallmark of primitive streak initiation. Cells at the posterior-proximal epiblast undergo EMT and delaminate from the epiblast. Epiblast cells lose cell polarity and adherens junctions after the laminin break. This process starts from the posterior-proximal epiblast and continues as the primitive streak elongates until reaching the distal pole of the embryo. The conserved signaling pathways, such as FGF, BMP, and WNT are involved in regulating EMT (Ciruna and Rossant, 2001; Ciruna et al., 1997; Huelsken et al., 2000; Mohamed et al., 2004; Sun et al., 1999; Winnier et al., 1995). Exposure to the correct combination of these signaling is pivotal for triggering a series of critical events in EMT such as E-cadherin to N-cadherin switch, mesenchymal cell fate adoption, and cell movement away from the primitive streak (Ciruna and Rossant, 2001). Mutants of *Fgf4*, *Fgf8* or *Fgfr1* fail to complete EMT and cells do not migrate away from the streak (Ciruna and Rossant, 2001; Ciruna et al., 1997; Sun et al., 1999). Embryos losing BMP4 or the receptors like BMPRII, ALK2, or ALK3, are arrested in gastrulation due to multiple defects in AVE specification and primitive streak formation

(Lawson et al., 1999; Mishina et al., 1999; Mishina et al., 1995). Similar to the *Drosophila* embryo, induction of EMT relies on transcription factor SNAIL1, the mouse orthologue of Snail in fly (Cano et al., 2000; Hemavathy et al., 1997). *Snail1* is expressed in nascent mesoderm, which is regulated by FGF signaling and is required for suppressing E-cadherin expression (Ciruna and Rossant, 2001; Thisse and Thisse, 2005). Loss of *Snail1* results in the accumulation of cells in the streak region where these cells are supposed to leave (Carver et al., 2001). Instead of being mesenchymal, these cells retain the epithelial characteristics (Carver et al., 2001). Downregulation of *Sox2* prior to *Snail1* expression is necessary, though not sufficient for successful mesoderm migration. *Eomes* is also crucial for EMT (Arnold et al., 2008; Costello et al., 2011). Genetic ablation of *Eomes* shows that epiblast cells accumulate at the posterior side, with no delamination occurring (Arnold et al., 2008).

Recent advances in mouse embryo culture protocols and microscopy allow the imaging of living mouse embryos in an easier way, which enables us to explore new mechanisms controlling EMT in other species. For example, genetic perturbations on *Crumbs2* (*Crb2*) cause defects in gastrulation (**Figure 1.9**)(Ramkumar et al., 2016; Xiao et al., 2011). In *Drosophila*, the Crumbs protein participates in organizing apical-basal polarity in epithelial cells (Tepass et al., 1990). In mouse embryos harboring *Crumbs2* mutations, however, the apical-basal polarity is normal during the gastrulation (Ramkumar et al., 2016). This finding indicates that CRUMBS2 proteins have unknown functions during mouse embryonic development. To dissect the function of CRUMBS2 during gastrulation, transgenic mouse embryos that were mosaically labeled with membrane Tomato or GFP (mTmG) (Muzumdar et al., 2007) are generated through *EIIA*-Cre-mediated activation (Lakso et al., 1996). Imaging E7.5 living mosaic embryos reveals that during cell ingression, wildtype epiblast cells undergo apical constriction and basal

positioning of the cell body, detaching from the epithelium (Ramkumar et al., 2016). While epiblast cells in *Crb2*$^{-/-}$ mutants remain attached to the epithelium with normal apical constriction and basal cell body positioning (Ramkumar et al., 2016). The E-cadherin is located at the protrusions where cells are attached to the epithelium (Ramkumar et al., 2016). These results indicate that *Crb2*$^{-/-}$ epiblast cells fail to disassemble AJs. Additional work shows that CRB2 participates in apical accumulation of Myosin II in mouse epiblast cells that are destined for cell ingression, indicating a role of CRB2 in regulating actomyosin activity (Ramkumar et al., 2016). More data and experiments are needed to incorporate the CRB2 into the actomyosin cytoskeleton dynamic network that controls EMT in mouse gastrulation.

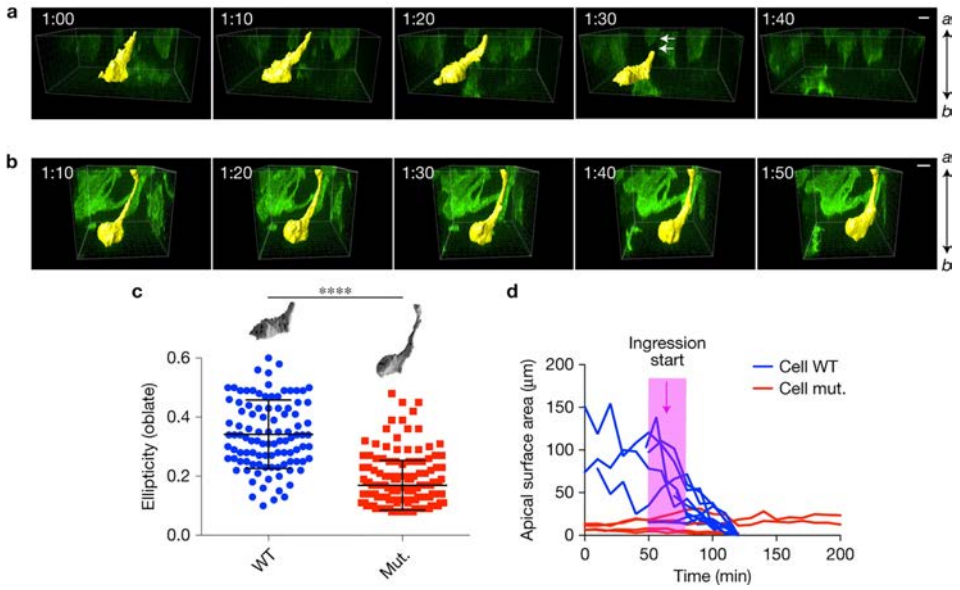

Figure 1.9 Live imaging defines defects in cell ingression in *Crumbs2* mutants. (a)(b). Snapshots of cell delaminating at the streak. (c) Quantification of cell shape at the streak. (d) Ingression dynamics of streak cells (Ramkumar et al., 2016).

EMT in other developmental contexts.

In addition to gastrulation, other developmental progress, such as the detachment of neural crest cell (NCC) from the neural tube in vertebrates, is another paradigm for studying EMT in embryonic development (Piacentino et al., 2020). NCCs, migrate to

different parts of the embryo, giving rise to multiple cell types such as smooth muscle cells, peripheral neurons, glial cells, melanocytes, etc. Zebrafish is one of the classic model organisms that has been extensively exploited to study NCC development. During EMT, zebrafish NCCs detach from the apical midline of the neuroepithelium, with basal neuroepithelium membrane rounded up, then delaminate and migrate away from the neural tube (Berndt et al., 2008). The planar cell polarity (PCP) signaling is required for the detachment and migration of NCCs. The core components of PCP signaling are first identified through genetic screens in *Drosophila* (Yang and Mlodzik, 2015). These molecules localize to AJs at specific domains, establishing proximal-distal asymmetry in epithelial cells, with Frizzled (Fz), Disheveled (Dsh) and Diego (Dgo) localized distally to the AJs and VanGogh (Vang) and Prickle (Pk) localized proximally (Butler and Wallingford, 2017). These components are functionally conserved in establishing planar cell polarity in vertebrate embryos. PCP signaling also regulates cell movements in embryos in other developmental contexts such as convergence and extension of mesoderm in chick embryos (Roszko et al., 2009). Vertebrate PCP signaling is controlled by the non-canonical WNT pathway (independent of β-catenin) through the binding of specific ligands Wnt5 and Wnt11 (Gray et al., 2011). PCP signaling activates downstream Rho GTPases to modulate actin arrangements critical for cell polarity or cell migration (Devenport, 2016). In zebrafish (also in *Xenopus* and chick), PCP signaling is required for NCC migration. Genetic and live imaging analyses of zebrafish embryos reveal that loss of core PCP gene *prickle 1* (*pk1*) results in the failure of the NCC migration (Ahsan et al., 2019). NCCs in *pk1* mutants remain rounded and accumulated at the neural tube (Ahsan et al., 2019). Live imaging of NCCs labeled with *sox10*-driven EGFP shows that in contrast to wildtype embryos, where NCCs migrate laterally out of the neural tube, mutant NCCs maintain cell-cell contacts and move anteriorly (Carney et al., 2006). Labeling actin-rich filopodia and lamellipodia in NCCs using Lifeact-GFP

shows that wildtype NCCs quickly transition to a mesenchymal morphology, becoming protrusive and migratory. *pk1* mutant cells, though detached from the epithelium, fail to become mesenchymal cells (Banerjee et al., 2011). Immunofluorescence staining of mutant NCCs shows a high level of E-cadherin and a low level of N-cadherin expression in *pk1* deficient NCCs compared to wildtype NCCs (Banerjee et al., 2011). Taken together, these data support the idea that in zebrafish the Pk1 regulates NCC EMT by modulating cell adhesion molecules, potentially via the PCP-mediated feedback loop.

Interestingly, work with *Xenopus* embryos has provided a new view of how PCP signaling regulates NCC EMT. The PCP signaling may transmit biophysical cues, like mechanical forces to trigger EMT (Barriga et al., 2018). The convergence and extension movements may increase the stiffness of the mesoderm underneath the neural crest, which is the substrate for neural crest migration (Barriga et al., 2018). Measuring the mesoderm stiffness using atomic force microscopy (AFM) at the non- and pre- NCC migratory stage demonstrates that the mesoderm stiffness is increased from the non- to the pre- migratory stage. Reducing mesoderm stiffness by laser ablation stops NCC migration (Barriga et al., 2018). In Dsh-DEP mutants, where the PCP signaling is inhibited (Axelrod et al., 1998), the mesoderm stiffness is decreased and the initiation of NCC migration is blocked (Barriga et al., 2018). Adding compression force through AFM rescues NCC migration in the Dsh-DEP (Barriga et al., 2018). These results provide a link between the PCP-mediated mechanical force transmission to migration of NCCs. However, all these experiments focus on post-EMT migration, not the process of EMT itself. Future work focusing on the direct impact of mechanical force on the EMT is required to address the concept of mechanical cues on EMT.

1.3.3 Primitive streak formation

Primitive streak is a transient structure that only appears in amniote vertebrates (birds, mammals, reptiles). For the past decades, the chick and mouse are the most classical organisms to study primitive streak formation. The initial findings are primarily from the grafting study of chick embryos due to the suitable size and easiness of manipulation. Later, the power of mouse genetics allows us to gain deeper insights into the molecular basis of streak formation. Studies from mouse and chick embryos are complementary to each other and may enlighten future studies for both sides.

Chick

In chick embryos, the developmental stages before gastrulation are labeled by the Eyal-Giladi and Kochav (EGK) system using the Roman numerals I-XIV (Eyal-Giladi and Kochav, 1976). The labeling system is switched to Hamburger and Hamilton (HH) when the primitive streak first becomes visible (Hamburger and Hamilton, 1951). The chick embryo has a flat disc shape (Pasteels, 1940). The whole embryo elongates posteriorly, acquiring a pear shape as the primitive streak extends (Pasteels, 1940). The marginal zone (Tabrizian et al.) (Tabrizian et al.), a ring of epiblast tissue, is important for separating the area pellucida (central region of the epiblast) and the area opaca (peripheral region of the embryo, giving rise to extraembryonic tissues)(Azar and Eyal-Giladi, 1979; Bachvarova et al., 1998; Eyal-Giladi and Khaner, 1989; Eyal-Giladi and Kochav, 1976; Khaner et al., 1985; Pasteels, 1940; Spratt Jr, 1942; Stern, 1990; Vakaet, 1970) (**Figure 1.10**). The MZ, especially the posterior MZ (PMZ), is indispensable for the initiation of the primitive streak (Figure 1.11) (Azar and Eyal-Giladi, 1979; Eyal-Giladi and Khaner, 1989; Khaner and Eyal-Giladi, 1986; Khaner and Eyal-Giladi, 1989; Mitrani et al., 1983). The MZ becomes visible when Koller's sickle appears at stage X (Eyal-Giladi and Khaner, 1989). The sickle is attached to the posterior, ventral side of the

epiblast, separating the inner area pellucida from the PMZ (Bachvarova et al., 1998; Callebaut and Van Nueten, 1994; Kochav et al., 1980). Experiments transplanting various sizes of PMZ suggest that the PMZ from stage X to stage XII are capable of inducing primitive streak, with stage XII being the highest (Eyal-Giladi and Khaner, 1989; Khaner and Eyal-Giladi, 1989). However, further fate-mapping experiments argue that it is the sickle and the adjacent inner epiblast, not the PMZ that contribute to the primitive streak (Bachvarova et al., 1998; Izpisua-Belmonte et al., 1993; Streit et al., 2000). Another study transplanting X-XII quail PMZ (without Koller's sickle) to the anterior halves of the MZ shows an ectopic primitive streak formation (Bachvarova et al., 1998). These experiments suggest that the avian PMZ functionally corresponds to the amphibian Nieuwkoop center (Bachvarova et al., 1998; Skromne and Stern, 2001), which is capable of inducing cell fate change in adjacent cells without really contributing to the structure. Investigation of the molecular basis in PMZ for streak induction shows that expression of the *chick Vg1* (*cVg1*) (Seleiro et al., 1996), a ligand similar to Activin (Thomsen and Melton, 1993), is seen in the primitive streak when the streak starts forming. Vg1 is initially identified from the *Xenopus* that can initiate axis development (Thomsen and Melton, 1993). Its expression, however, is downregulated as the streak progresses (Seleiro et al., 1996; Shah et al., 1997). Grafting mammalian COS cells expressing *cVg1* 180° from the putative posterior site at stages X-XII shows ectopic primitive streak formation in more than half of the cases (Shah et al., 1997). Such induction is stage-dependent as grafting the same cells at stages HH2-4 does not induce any streak formation (Shah et al., 1997). The ectopic streak expresses canonical marker genes like *Brachyury* and *Goosecoid* and a new axis is formed in the embryo (Shah et al., 1997). The *Wnt8C* is expressed throughout the MZ in a posterior-to-anterior gradient (Hume and Dodd, 1993). Inhibiting Wnt signaling by truncated Frizzled-8 receptor in the PMZ leads to impaired streak formation (Skromne and Stern, 2001). The ectopic

primitive streak formation is disrupted when the Wnt inhibitors Dkk1 and Crescent are co-grafted with cVg1-secreting cells in the anterior MZ (Skromne and Stern, 2001). Combined grafting of Wnt1-secreting (A Wnt family member with the same function as Wnt8C) fibroblast and cVg1-secreting COS cells at the anterior area pellucida induces expression of *cVg1*, *Nodal,* and primitive streak genes like *Brachyury* and *Chordin* (Shah et al., 1997). None of these genes can be induced with cVg1 or Wnt1 alone (Shah et al., 1997). *Lef1* is also expressed in the anterior area pellucida in the presence of both Wnt1 and cVg1, which is only expressed in the PMZ (Shah et al., 1997). These results suggest that the Wnt signaling cooperates with the cVg1 for streak initiation.

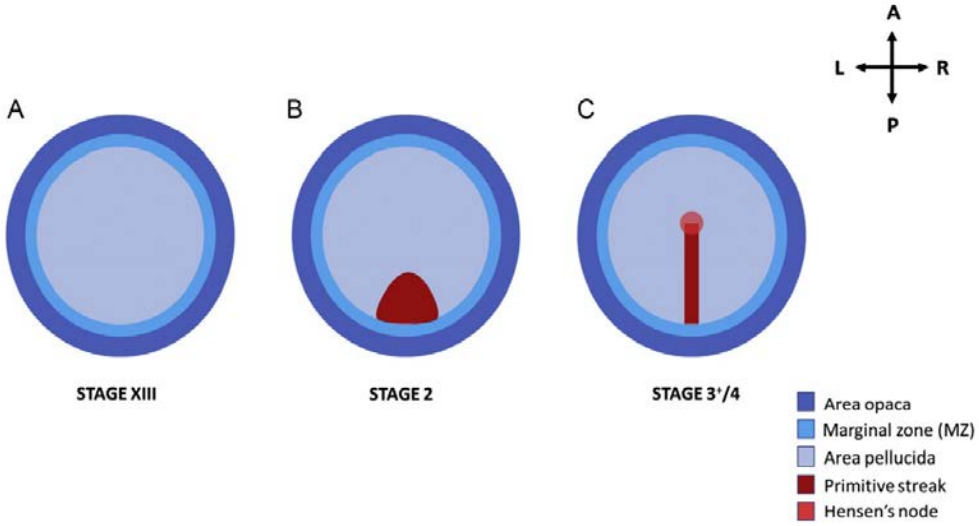

Figure1.10 The chick discoid embryo and primitive streak development. (Raffaelli and Stern, 2020)

In addition to MZ, the hypoblast is also important for primitive streak development (**Figure 1.11**). The hypoblast is an extraembryonic layer located underneath the epiblast (Azar and Eyal-Giladi, 1979). The orientation of primitive streak can be realigned after hypoblast rotation and therefore, hypoblast was initially identified as a second primitive streak inducer (Azar and Eyal-Giladi, 1981; Vakaet, 1967; Waddington, 1933;

Waddington, 1932). However, later experiments labeling the organizer-fated cells with DiI/DiO show that rotation of hypoblast changes cell movement, not cell fate (Foley et al., 2000; Voiculescu et al., 2007). Furthermore, in contrast to MZ, which induces primitive streak formation, the hypoblast is thought to be the inhibitor of primitive streak initiation. Placing the hypoblast far away from the center of the pellucida is sufficient to form a second axis (Azar and Eyal-Giladi, 1981). Ablating hypoblast completely in stage XII-XIII embryos leads to one or more ectopic primitive streaks expressing *Brachyury* (Bertocchini and Stern, 2002). Ectopic expression of *Nodal* and *Chordin*, the downstream target genes of Vg1 and Wnt signaling, is also found after hypoblast ablation (Bertocchini and Stern, 2002). The hypoblast prevents ectopic primitive streak formation when grafting Nodal-secreted COS cells, while such inhibition is lost when the hypoblast is removed (Bertocchini and Stern, 2002). These data suggest that the hypoblast acts as a signal center to antagonize Vg1 and Wnt signaling activities. Indeed, the hypoblast expresses Nodal and Wnt antagonists like *Cerberus*, *Dkk,* and *Crescent*, preventing the expansion of Nodal and Wnt signaling and are important for single axis formation in the embryo (Bertocchini and Stern, 2002). The function of hypoblast is very similar to the AVE, the mouse anterior signaling center critical for the AP axis establishment (Perea-Gomez et al., 2002).

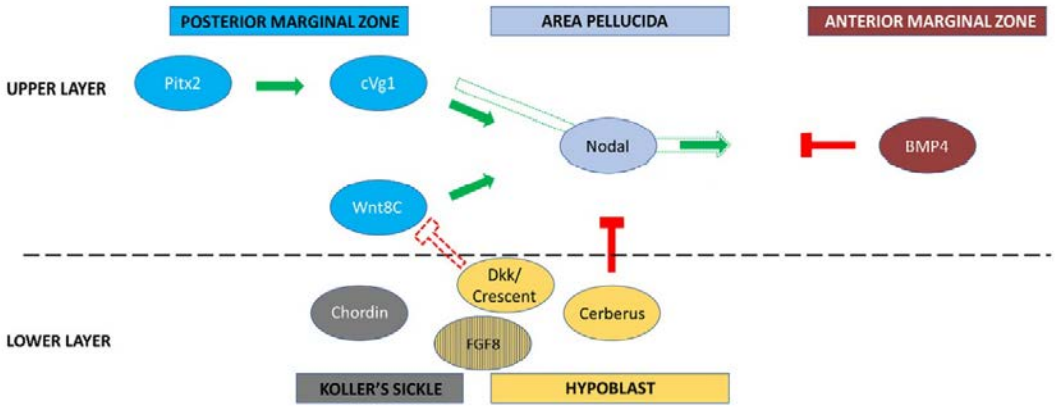

Figure1.11 Signaling inputs from various sites regulating the primitive streak in the chick embryo. (Raffaelli and Stern, 2020)

The intercalation of posterior area pellucida epiblast cells is a prerequisite of cell ingression during streak formation and occurs right before streak initiation (stage XII-XIII) (Voiculescu et al., 2007). These epiblast cells preferentially incorporate at right angles to the radius of the blastoderm, leading to convergence and extension (Voiculescu et al., 2007). Components of the non-canonical Wnt planar cell polarity (PCP) pathway such as *Prickle1*, *Celsr1,* and *Vangl2* are expressed in the same region of the posterior epiblast where these cells intercalate (Voiculescu et al., 2007). The FGF8 from the hypoblast is found to induce *Celsr1* and *Prickle1* expression, suggesting the role of hypoblast in driving cell intercalation and extension of the prospective primitive streak domain along the midline of the embryo (Voiculescu et al., 2007). Embryos harboring a dominant-negative allele of *Disheveled* (*Dsh-ΔDEP*) inhibit the PCP pathway only and impair primitive streak extension. A similar phenotype is also observed by introducing morpholinos against PRIKCLE1, CELSR1, and VANGL2 into embryos by electroporation (Voiculescu et al., 2007).

After the intercalation, the primitive streak moves anteriorly along the midline, driven by convergence and extension. Meanwhile, the anterior and lateral epiblast cells move to the medial posterior region to compensate for the cells that have left (Rozbicki et al., 2015; Voiculescu et al., 2007; Voiculescu et al., 2014). A subpopulation of cell express HNK-1 in a salt and pepper pattern inside the epiblast (Canning and Stern, 1988). Loss of HNK-1 positive cells at pre-primitive streak stages results in loss of the primitive streak and mesodermal cells (Stern and Canning, 1990). These cells ingress before the gastrulation and eventually give rise to the mesoderm and endoderm during the gastrulation (Stern and Canning, 1990). Upon ingression, the mesendodermal cells initiate EMT in the nearby cells, creating mesenchymal cell flows. More lateral cells are pulled into the primitive streak and exposed to the Wnt-PCP signaling, enhancing intercalation and extension to the midline and therefore, maintaining the structure of the primitive streak (Stern and Canning, 1990; Voiculescu et al., 2014).

Mouse

Starting from E6.0, epiblast cells start to converge toward the posterior-proximal pole of the embryo (Lawson et al., 1991). These posterior epiblast cells undergo EMT and delaminate from the epiblast. Chimera experiments reveal that the NODAL signaling is required for primitive streak initiation, as *Nodal*-deficient cells mainly contribute to the embryonic tissues residing in the anterior side (Lu and Robertson, 2004). Cells lacking NODAL receptors show impaired ability to form the posterior tissues (Gu et al., 1998). Embryos lacking NODAL or its downstream effector SMAD2 and SMAD3 are arrested before gastrulation (Dunn et al., 2004). Other signal pathways such as BMP and WNT signaling, are also necessary for streak formation and mesoderm induction (Conlon et al., 1994; Liu et al., 1999; Mishina et al., 1995). Loss of BMP receptor BMPR1A fails to form mesoderm (Mishina et al., 1995). In WNT3 and β-catenin mutants, embryos are

also blocked with no mesoderm induction (Huelsken et al., 2000; Liu et al., 1999). On the other hand, depleting NODAL antagonists CER1 and LEFTY1 result in the formation of multiple streaks or enlarged primitive streak regions due to the failure of the AVE specification (Perea-Gomez et al., 2002). A similar phenotype is also observed in embryos lacking AXIN2, a negative regulator of the WNT pathway (Zeng et al., 1997). These results suggest that the proper dosage of the signaling is important for normal primitive streak induction.

After the initial induction at the proximal pole, the primitive streak elongates towards the distal pole. The BMP, NODAL signaling generates two-dimensional signal gradients that are important for streak patterning and the subsequent specification of the mesoderm subpopulations and the definitive endoderm (DE). BMP is highly expressed at the posterior side of the embryo (Mishina et al., 1995), whereas the NODAL signaling is confined to the anterior domain and eventually expressed distally from the node (Conlon et al., 1994; Norris and Robertson, 1999). During the mid-gastrulation stage, the primitive streak is molecularly segmented based on the balance of BMP and NODAL signaling along the A-P axis (Rodes et al., 2005; Vincent et al., 2003). Cells ingressing through different positions in the streak eventually adopt differential cell fates. The establishment of the delicate BMP/NODAL signaling requires the concomitant primitive streak elongation and size expansion, indicating that the coordination of embryo size expansion and signaling activity is required for normal streak patterning and embryonic morphogenesis.

The formation of the primitive streak can be generally divided into three steps: dissolution of basal membrane between epiblast and VE, cell ingression, and streak elongation (Williams et al., 2012). For the first step, cells need to repress the expression

of genes encoding extracellular matrix (ECM) components and/or degrade basal membrane proteins (Williams et al., 2012). It has been tested in chick embryos that this process is mediated by the relocation of RhoA small GTPase (Nakaya et al., 2008). However, this observation has not been validated in mouse embryos yet. After the breakdown of the basal membrane, epiblast cells ingress into the primitive streak. This process is made through the apical constriction of these cells followed by the translocation of the cell body (Williams et al., 2012). As mentioned in the previous section, the BMP, FGF, and WNT signaling are required for cell ingression and EMT (Ciruna and Rossant, 2001; Huelsken et al., 2000; Mohamed et al., 2004; Sun et al., 1999; Winnier et al., 1995). Transcriptional factors such as SNAIL1, and EOMES, which are pivotal for the downregulation of genes encoding adhesion molecules and successful EMT, are also essential for driving cell ingression (Arnold et al., 2008; Cano et al., 2000; Costello et al., 2011). In general, mutations on any genes that substantially disrupt EMT will block the primitive streak formation. Elongation is the last step of streak formation (Williams et al., 2012). Similar to cell ingression, this process is accompanied by continuous EMT from proximal-posterior epiblast to the distal-anterior side (Williams et al., 2012). Expansion of the primitive streak requires the recruitment of epiblast cells outside the EMT region. Little is known regarding how this process is accomplished without disrupting the epithelium integrity of the epiblast. One theory proposed that these epiblast cells are pulled passively to the neighboring streak region. The epiblast cells are compensated by rapid cell proliferation in the posterior epiblast region, yet evidence supporting this theory is still lacking (Williams et al., 2012; Wilson and Beddington, 1996).

1.3.4 Germ layer formation: lineage specification and tissue morphogenesis

The germ layer formation includes two aspects: 1) the lineage specification that cells at the pre-gastrulation stage have been destined to give rise to one of the three lineages based on their position in the blastula; 2) the tissue morphogenesis that cells undergo a series of rearrangements, forming new layers. In this section, we will show the germ layer formation in the *Drosophila*, Zebrafish, and Mouse as an example of invertebrate, non-amniote vertebrate and amniote vertebrate, respectively. As we will see in the following paragraphs, each model organism has its featured morphogenetic events during germ layer formation. Most of them are related to cell movements. We will discuss the major findings from these most well-studied events.

Drosophila

The germ layer formation in *Drosophila* is based on a sequential formation of transient furrows within the blastoderm where the mesoderm and endoderm (mesendoderm) progenitors have been pre-mapped onto (**Figure 1.12**). The cephalic furrow (CF) arises in the anterior domain of the embryo. The function of CF during development is still unknown. Two transient folds are formed on the dorsal side of the embryo and are therefore called dorsal transversal folds (DTFs) (Utikal et al.). From the imaging of scanning electron microscopy, these folds will disappear after when the germband elongation reaches the dorsal side of the embryo (Turner and Mahowald, 1977). The DTFs seem to be the structures marking the dorsal positions of the embryo since the positioning of DTFs is controlled by the maternal patterning systems only. The DTF expands around the entire embryo in embryos from *dl* mutant mothers (Nüsslein-Volhard, 1979). In mutant alleles of *toll*, DTFs were formed in partially ventralized embryos but not in completely ventralized embryos (Anderson et al., 1985; Roth et al., 1991).

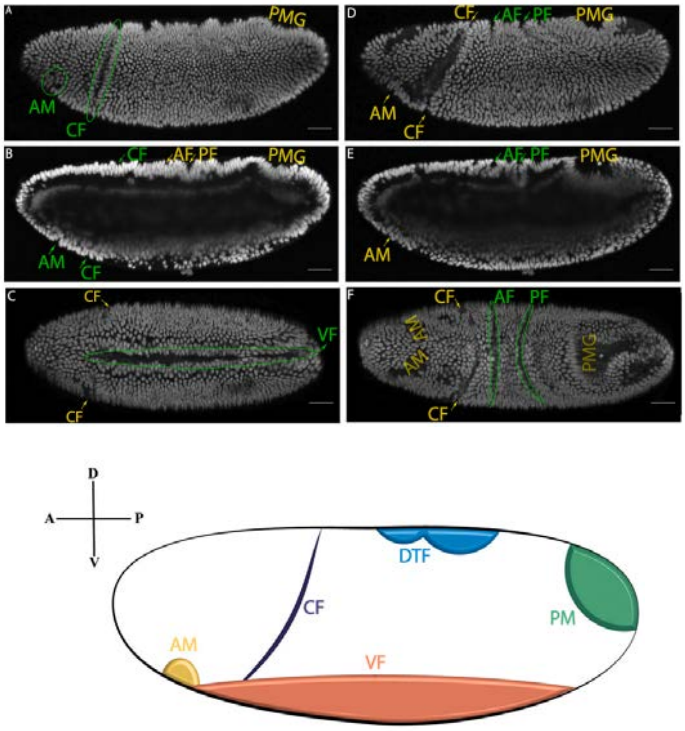

Figure 1. 12 Gastrulation movement and the mapping of furrows onto the blastoderm in *Drosophila*. AF: anterior furrow; AM or AMG: anterior midgut; CF: cephalic furrow; DTF: dorsal transverse fold; GBE: germband extension; PF: posterior furrow; PM or PMG: posterior midgut; VF: ventral furrow. Adapted from (Gheisari et al., 2020).

At the beginning of gastrulation, A large anterior-to-posterior furrow, named the ventral furrow (VF), is generated in the ventral domain. During VF formation, cells at the midventral domain of the blastoderm epithelium invaginate to form an interior tube, giving rise to the future mesoderm layer (Hartenstein and Campos-Ortega, 1985; Leptin and Grunewald, 1990; Poulson, 1950; Sweeton et al., 1991; Turner and Mahowald, 1977). The invagination process involves the apical constriction and the apical flattening of ventral cells (Kam et al., 1991; Sweeton et al., 1991). While it is still unclear how the cells are flattened, the control of apical membrane turnover may be the potential mechanism (Miao et al., 2019). During apical constriction, cells are elongated along the apical-basal axis and the nuclei are shifted basally (COSTA, 1993). Cell lengthening is

balanced by the yolk cell, resulting in cell shortening and the formation of a narrow furrow (**Figure 1.13**). The furrow is further deepened through the propagation of apical constriction on presumptive mesoderm cells inside the cleft, while cells adjacent to the furrow undergo apical expansion and flattening. By the end of VF formation, a transient tube is formed interior to the embryo.

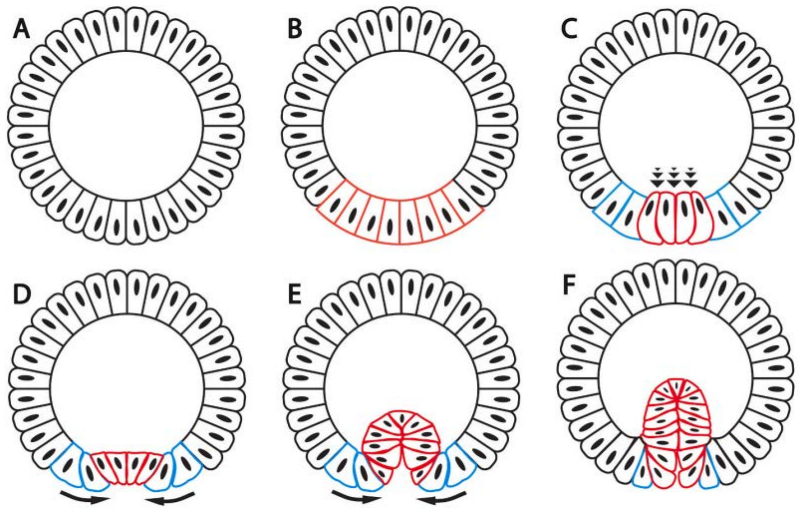

Figure1.13 The process of ventral furrow formation. The red labels invaginating cells that flatten their apices first and then constrict at later time points. Blue cells represent adjacent cells that undergo apical expansion and flattening. (Gheisari et al., 2020)

VF formation is dependent on the activity of transcription factors Twist (Twi) and Snail (Sna) by the fact that VF formation does not occur in *twi*,*sna* double mutants (Grau et al., 1984; Leptin and Grunewald, 1990; Simpson, 1983; Thisse et al., 1988). *twi* and *sna* are expressed in the mesoderm-fated cells before VF formation and are the zygotic genes controlling mesoderm formation (Sandmann et al., 2007) (Simpson, 1983). However, more recent studies show that Sna serves as a transcriptional modulator instead of directly activating or repressing gene expression in the mesoderm (Rembold et al., 2014). It is also suggested that the VE formation can be initiated by Sna independently from Twi as VF does not form by expression of *twi* in *sna* mutants, while the expression of *sna* in *twi* mutants leads to ventral invagination of the blastoderm (Hemavathy et al.,

1997; Ip et al., 1994; Leptin and Grunewald, 1990). Mutations that lead to the similar phenotype of *twi* and *sna* have also been identified and are later demonstrated to locate on genes that are direct targets of Twi and Sna. For example, mutations on the transcriptional Twi-target gene *folded gastrulation* (*fog*) (Dawes-Hoang et al., 2005; Peters and Rogers, 2013; Zusman and Wieschaus, 1985), resulting in uncoordinated cell shape change and abnormal VF morphology (Costa et al., 1994; Dawes-Hoang et al., 2005). Overexpression of *fog* causes apical flattening of cells outside the VF (Morize et al., 1998), suggesting that Fog is important for cell shape changes. Studies show that Fog binds to G-protein coupled receptors and promotes the activation of small GTPase Rho1, which activates Rho Kinase (Kerridge et al., 2016; Manning et al., 2013). The Rho signaling controls myosin II activity and thereby regulates the actomyosin-based apical constriction (Barrett et al., 1997; Dawes-Hoang et al., 2005; Hacker and Perrimon, 1998). These data suggest that the Twi promotes apical constriction during mesoderm invagination via Fog-mediated control of Rho signaling.

After internalization, the mesoderm cells undergo EMT followed by embryo elongation along the A-P axis, a process termed germband extension. At the same time, the mesenchymal cell spread along the distal-ventral (D-V) axis under the neuroectoderm layer, forming a single layer between the yolk cell and the neuroectoderm (Winklbauer and Muller, 2011). Mesoderm cell adopts different cell fate based on their relative positions along the D-V axis. The ectoderm secrets position-specific signals to induce muscle-specific genes in the mesoderm cells (Baker and Schubiger, 1995). Cells attached to the dorsal ectoderm develop into cardiac cells, whereas cells attached to the ventral ectoderm become somatic muscle cells (Azpiazu and Frasch, 1993; Baker and Schubiger, 1995). A group of conserved signaling pathways, including FGF, Dpp, Wingless, and EGF signaling, are involved in mesoderm specification.

The emergence of endoderm in *Drosophila* comes from the posterior midgut (PMG) and anterior midgut (AMG) invagination shortly after mesoderm invagination. The PMG arises slightly earlier than AMG. Cells in the PMG primordium move anteriorly and interiorly, giving rise to the posterior part of the gut epithelium. Cells in the AMG migrate posteriorly and interiorly, giving rise to the anterior part of the gut epithelium (Hartenstein and Campos-Ortega, 1985; Turner and Mahowald, 1977). The PMG invagination is dependent on maternal A-P pattern genes such as *torso and trunk*, as no cell shape change or invagination occur in *torso* or *trunk* mutants (Degelmann et al., 1986; Nusslein-Volhard et al., 1987; Schupbach and Wieschaus, 1986). Like ventral furrow formation, it also requires the Fog-mediated Rho signaling that triggers the actomyosin-based apical constriction (Casanova, 1990; Dawes-Hoang et al., 2005; Weigel et al., 1990). The anterior movement of PMG, however, is not well understood compared to PMG invagination. Recent studies provide evidence supporting the idea that the anterior movement relies on the propagation of the MyoII-dependent contraction (Bailles et al., 2019). Similar to PMG, AMG invagination is controlled by maternal pattern genes such as bicoid (*bcd*), *torso* and *trunk* (Frohnhofer et al., 1986; Schupbach and Wieschaus, 1986), as well as zygotic genes such as *forkhead* (*fkh*) (Jurgens and Weigel, 1988; Weigel et al., 1990). The detailed mechanisms controlling AMG invagination are yet to be discovered.

Mouse

The formation of the mesoderm and definitive endoderm (DE) starts from the primitive streak. Epiblast cells undergo EMT, ingressing at the primitive streak and migrating away. Subsequently, A new layer emerges between the epiblast and the overlying VE. The FGF, BMP, NODAL-SMAD2/3, and canonical WNT signaling are required for the

mesoderm specification (Brennan et al., 2001; Ciruna and Rossant, 2001; Conlon et al., 1994; Huelsken et al., 2000; Mishina et al., 1999; Mishina et al., 1995; Sun et al., 1999; Winnier et al., 1995), which has been discussed in the previous section. Cells that stay inside the epiblast expand anteriorly and proximally, and eventually give rise to the ectoderm layer comprising neurectoderm (NE) and surface ectoderm. NE is considered the default stage of epiblast differentiation. Lack of BMP or NODAL signals results in precocious neural cell fate adoption and early loss of pluripotency (Camus et al., 2006; Di-Gregorio et al., 2007).

Despite lineage specification, the germ layer patterning is another critical question that has been deeply investigated for the past decades, especially the patterning of mesoderm and DE progenitors along the primitive streak. The mesoderm can be divided into distinct mesodermal subtypes, giving rise to different organs and tissues (Lawson, 1999). These subpopulations are defined based on the timing and position of ingression through the streak (**Figure 1.14**) (Lawson, 1999). During early gastrulation (E6.5), the cranial and cardiac mesoderm cells ingress from the early streak and migrate anteriorly, forming the leading edge of the mesodermal wings (Kinder et al., 1999). The extraembryonic mesoderm, which is located at the posterior-most region and is also formed at the earliest time point, constitutes the mesodermal layer of the amnion, visceral yolk sac mesoderm, and blood islands (Arnold and Robertson, 2009; Lawson et al., 1991). During the mid-late gastrulation stage, cells exiting from the posterior streak become the lateral plate, intermediate, and posterior paraxial mesoderm in a posterior-anterior order; cells located at the anterior-most region of the primitive streak (anterior primitive streak, or APS) give rise to the anterior paraxial, axial mesoderm and DE (Lawson et al., 1991; Lawson and Pedersen, 1987; Tam and Beddington, 1987). The DE

cells intercalate and disperse into the VE layer on the surface of the embryo (Kwon and Hadjantonakis, 2009; Kwon et al., 2008b).

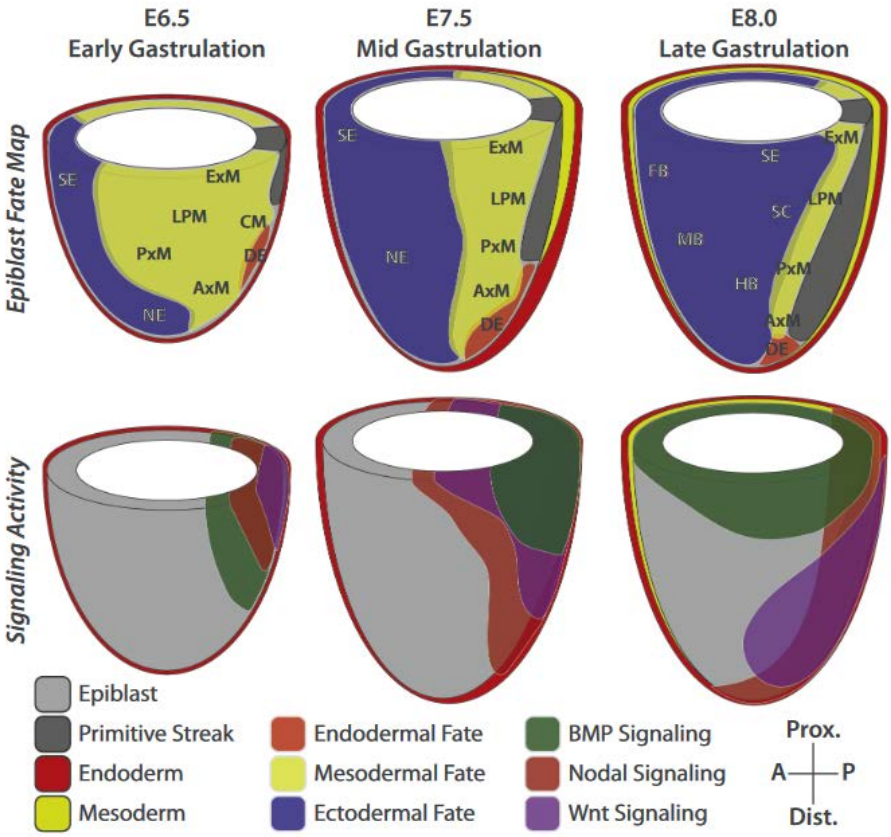

Figure1.14 Epiblast fate mapping and the corresponding morphogen gradients among different streak stages. DE, definitive endoderm; CM, cardiac mesoderm; ExM, extraembryonic mesoderm; LPM, lateral plate mesoderm; PxM, paraxial mesoderm, AxM, axial mesoderm; SE, surface ectoderm; SC, spinal cord; NE, neurectoderm; FB, forebrain; MB, midbrain; HB, hindbrain. (Bardot and Hadjantonakis, 2020)

Again, the patterning of mesoderm and DE is accomplished by the interplay of those conserved signaling pathways including BMP, FGF, WNT, and NODAL (Brennan et al., 2001; Ciruna and Rossant, 2001; Conlon et al., 1994; Huelsken et al., 2000; Mishina et al., 1999; Mishina et al., 1995; Sun et al., 1999; Winnier et al., 1995). The cardiac and cranial mesoderm induction at the early gastrulation stage requires signal inputs from all

of them (Conlon et al., 1994; Klaus et al., 2007; Yamaguchi et al., 1994). Extraembryonic mesoderm is induced posteriorly by exposure of the high BMP signaling and exclusion of the NODAL signaling (Lawson et al., 1999). During mid-late gastrulation, The BMP and the NODAL signaling mutually inhibit each other along the A-P axis and the cell fate of mesoderm derivatives is determined by the dosage of these signals that cells are exposed to. The posterior streak derivatives require a high BMP signal level, whereas derivatives of the anterior streak depend on high levels of the NODAL signaling (Winnier et al., 1995).

A number of transcription factors are expressed in the primitive streak and these genes are mostly target genes activated by the combination of various morphogen inputs. These genes are also critical for mesoderm patterning along the streak. *Brachyury* (*T*). a gene encoding T-box transcription factor, is expressed throughout the primitive streak (Chapman et al., 1996; Rashbass et al., 1991; Wilson et al., 1995). Loss of *T* expression results in failure of posterior mesoderm cells exiting the primitive streak and consequently loss of posterior somites, as well as cell accumulation at the tail bud (Rashbass et al., 1994; Wilson and Beddington, 1996). The expression domain of *Brachyury* is restricted by *Mixl1*, which is also expressed in the streak (Hart et al., 2002). Loss of *Mixl1* in gastrulating embryos leads to a thickened primitive streak and a morphologically disrupted node at the anterior streak as well as the accumulation of mesoderm-like cells in the anterior streak (Hart et al., 2002). The *Brachyury* expression is required for maintaining *Tbx6* expression, which labels paraxial mesoderm progenitors in the streak (Chapman et al., 1996). Disruption of *Tbx6* causes impaired caudal somite formation and triple neural tube formation (Chapman et al., 1996). *Mesp1* labels cardiac mesoderm at the early streak stage and is essential for the development of cardiac mesoderm (Kitajima et al., 2000; Saga et al., 1999). *Eomes* is expressed in the anterior-

mid streak (also ExE) at the mid-late streak stage and is required for DE induction (Costello et al., 2011). *Eomes* also acts upstream of *Mesp1* at the early streak to specify the cardiac mesoderm lineage (Costello et al., 2011). Mutants with ectopic or loss of *Eomes* expression show defects in the DE and cardiac mesoderm specification (Arnold et al., 2008; Costello et al., 2011; Simon et al., 2017). *Foxa2* marks the anterior region of the streak and has a partially overlapping expression domain with *T*. *Foxa2* mutant exhibits disorganized node structure and defective neural tube patterning without affecting DE lineage specification (Ang and Rossant, 1994). Cells co-expressing *T* and *Foxa2* give rise to a subset of cardiac mesoderm in early gastrulation and axial mesoderm during the late gastrulation (Bardot et al., 2017; Burtscher and Lickert, 2009). Specification of DE lineage requires another set of transcription networks. *Eomes* is activated in response to high NODAL signaling and is the first transcription factor required for DE specification. Other transcription factors such as SOX17. GATA6, Mix/Bix-type homeobox gene families are also crucial in DE formation (Grapin-Botton and Constam, 2007). In mice, *Sox17* is not required for early DE specification but is crucial for DE cell survival (Kanai-Azuma et al., 2002).

As nascent mesoderm cells migrate away from the streak, cells move anteriorly and laterally, forming a mesodermal wing (Ferretti and Hadjantonakis, 2019). Compared to the upstream signaling that induces lineage specification and patterning, the migratory behavior of mesendoderm cells during gastrulation remains relatively elusive. Classical electron microscopy studies reveal that the nascent mesoderm cells have cellular protrusions, suggesting that these cells use protrusions to migrate (Spiegelman and Bennett, 1974). Recent advances in live imaging of post-implantation embryos have provided new insights into cell migration, for example, during DVE/AVE migration (McDole et al., 2018). The knowledge of mesoderm migration, including how cells

ingress between the epiblast and the VE, and how they travel long distances to expand and cover the epiblast, is still lacking. So far, the most detailed description of mesoderm cell migration comes from the study in zebrafish (Tada and Heisenberg, 2012; Williams and Solnica-Krezel, 2017). However, mechanisms that zebrafish embryos adopt for mesendoderm migration may not be applied in the mouse embryo. For example, the mesoderm migration in zebrafish embryos is dependent on non-canonical Wnt/PCP signaling while in mouse embryos, non-canonical Wnt/PCP signaling is not required prior to the somite stage (Sepich et al., 2005; Williams and Solnica-Krezel, 2017; Yin et al., 2009a).

Mouse genetics and recent advances in imaging of living mouse embryos have identified several molecules regulating cell biological processes that are downstream of morphogen signaling or transcription factors (Bazzi et al., 2017; Migeotte et al., 2011; Rakeman and Anderson, 2006; Ramkumar et al., 2016; Saykali et al., 2019). The most classical *tw9* (also known as *tw18*) mutant, is the earliest mutant defective of mesoderm migration that is analyzed at the cellular level in detail (Lange et al., 2017; Spiegelman and Bennett, 1974). Transmission electron microscopy shows that the mutant embryo lacks the thin filopodia necessary for linking neighboring cells (Spiegelman and Bennett, 1974). A recent study revisiting the *tw9* mutant reveals that this mutant disrupts a scaffolding subunit of the protein phosphatase PP2A (Lange et al., 2017). This phenotype is consistent with the function of PP2A in cell migration (Bousquet et al., 2016). Another mutant that impairs mesoderm migration potentially via interference of PP2A function is the *Strip1* (*straiting-interacting protein 1*) mutant (Bazzi et al., 2017). The *Strip1* mutant is initially identified from mouse mutagenesis screens showing defective body plan (Bazzi et al., 2017). Further *in vivo* and *ex vivo* phenotypic analyses show that mutation in *Strip1* disrupts the mesoderm migration (Bazzi et al., 2017).

STRIP1 is the core component of the mammalian striatin-interacting phosphatases and kinases (STRIPAK) complex that appears to regulate PP2A activity, indicating that STRIP1 may regulate mesoderm migration via PP2A activity (Madsen et al., 2015). Deletion of the epiblast *Rac-1*, a classical Rho GTPase essential for cell adhesion and motility, results in impaired mesodermal cell migration, leading to deficient paraxial mesoderm lineage, somite formation, and cardia bifida (Machacek et al., 2009; Saykali et al., 2019). A similar phenotype is also seen in mutants on NAP1, a regulatory component of the WAVE complex (Rakeman and Anderson, 2006). *Nap1* mutants show cardia bifida, failed neural tube closure, as well as delayed mesoderm and endoderm migration (Rakeman and Anderson, 2006). These results suggest that the RAC-1 acts upstream of the WAVE complex to promote mesoderm migration. These experiments, however, compared to the study of *tw9* mutants, did not address the migratory behaviors at the cellular level.

A very recent study performing optimized high-resolution confocal imaging of gastrulating embryos has directly visualized the movement of nascent mesoderm and provided new insights into mesoderm migration at the cellular level (**Figure 1.15**) (Omelchenko et al., 2020). This study focuses on the β-Pix, a guanine nucleotide exchange factor (GEF) of RAC1 and CDC42 GTPases and localizes to the focal adhesion (Manser et al., 1998; ten Klooster et al., 2006). Previous genetic studies show that *β-Pix* null embryos are arrested at the late gastrulation stage without specifying the A-P axis (Omelchenko et al., 2014). By combining membrane GFP-tagged cell labeling and volumetric 3-Dimensional image analysis, researchers can measure the protrusions and directionality of these nascent mesoderm cells in their native environment (Omelchenko et al., 2020). This study shows that depleting β-Pix in the epiblast causes disorganized cell movements in random directions (Omelchenko et al., 2020). This

random cell movement is associated with the disorientated protrusions in mesoderm cells and the uncoordinated cell-cell alignments (Omelchenko et al., 2020). This observation is consistent with the findings that β-pix promotes protrusion formation in fibroblast cells (Kuo et al., 2011). These results suggest that the collective migration of nascent mesoderm is directed by the β-pix-dependent protrusions. β-Pix regulates cell adhesion and movement in a RAC-1 and CDC42-dependent way. The collective migration, however, may not completely rely on the protrusions. It is possible that other factors, such as changes of cell-matrix interaction, cell division, and cell morphology, may also be part of the factors affecting cell migration.

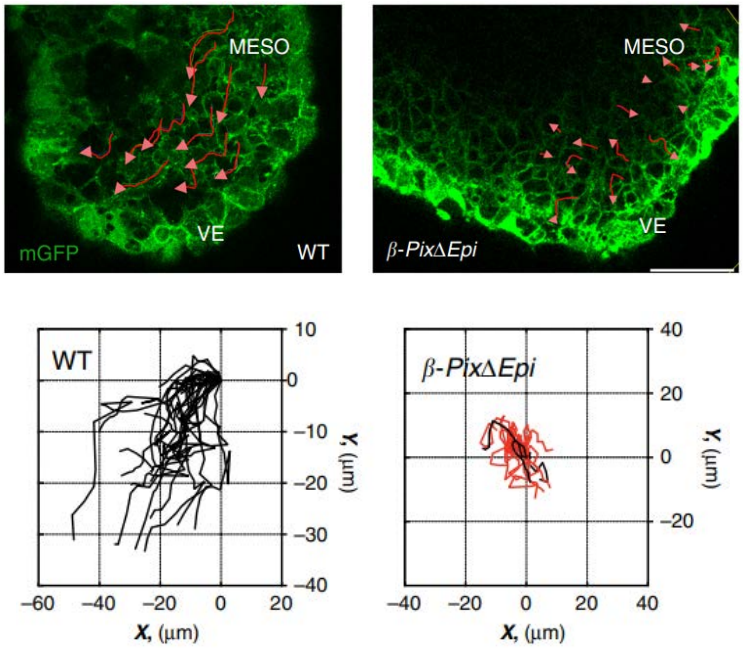

Figure1.15 The mesoderm wing migration between the wildtype and the *β-Pix* mutants. (Omelchenko et al., 2020)

Formation of the DE does not end with the cell migration step. Instead of forming a continuous layer, the DE emerges and disperses onto the surface of the embryo, intercalating into the VE layer and generating a new layer with a mixture of VE and DE cells (Kwon and Hadjantonakis, 2009; Kwon et al., 2008b). Unlike mesodermal cells, the

DE progenitors undergo a partial EMT that retains E-cadherin expression (Viotti et al., 2014). DE cells migrate from the primitive streak over the migrating mesoderm and quickly undergo MET to re-epithelialize with the VE cells (Kwon et al., 2008b; Nowotschin et al., 2019; Viotti et al., 2014). Therefore, the future gut, instead of being composed of DE cells only, is a mixture of DE and embryonic VE (emVE) cells, with the highest proportion of VE cells in the hindgut and the lowest in the foregut (Kwon et al., 2008a; Nowotschin et al., 2019; Pijuan-Sala et al., 2019).

Recently, mechanisms behind the DE-VE intercalation have drawn a lot of attention and some pioneering studies start to untangle this complicated process. It is proposed that to coordinate the behaviors of DE and VE cells, DE cells need to quickly adopt epithelial cell states like apicobasal polarity and cell-cell adhesion. The partial EMT of DE cells might be the critical mechanism that can drive MET with a fast rate (Viotti et al., 2014). This fast and partial EMT-MET is frequently seen in tumor progression, which may also be the case in VE-DE intercalation (Ye and Weinberg, 2015). Meanwhile, for VE cells, they must temporally partially disassemble, or loosen their junctions to allow DE intercalation, and quickly resume epithelial state. Phenotypic analysis of *Sox17* mutants shows that DE cells are unable to intercalate into the VE epithelium (Viotti et al., 2012; Viotti et al., 2014). It has been shown that before gastrulation, the VE is a rigid, cuboidal layer epithelium (Viotti et al., 2014). As the embryo starts gastrulation and expanding, VE cells become squamous and flattered (Viotti et al., 2014). Such morphology change is not seen in *Sox17* mutants, which may indicate that the *Sox17* in VE is essential for modulating their epithelial character that facilitates DE intercalation during the gastrulation stage (Viotti et al., 2014). Although this theory seems plausible, it lacks direct evidence regarding how Sox17 affects cell shape changes.

While the mesoderm and DE undergo rapid rearrangements along the streak, cells that stay inside the epiblast expand anteriorly and proximally and eventually give rise to the ectoderm layer comprising NE and surface ectoderm (Arkell and Tam, 2012). NE is considered the default stage of epiblast differentiation. Lack of BMP or NODAL signal results in precocious neural cell fate adoption and early loss of pluripotency (Camus et al., 2006; Di-Gregorio et al., 2007). The NE covers two-thirds of the area of the ectoderm layer and develops into the central nervous system (Arkell and Tam, 2012; Arnold and Robertson, 2009), displaying a pattern of regionalized neural progenitors. Progenitors of the forebrain, midbrain, and hindbrain are localized in the respective anterior-posterior order. The relative size of the domain of progenitors is not proportional to the final size of the brain part. Specifically, the forebrain will undergo a wide expansion during head morphogenesis (Arkell and Tam, 2012). This disproportional tissue outgrowth requires rapid cell proliferation in the forebrain region and, consequently, is very vulnerable to cell proliferation errors that lead to head truncation (Arkell and Tam, 2012).

Maintenance of the NE fate requires sustained expression of NODAL, WNT, and BMP antagonists. In pre-gastrulating embryos, AVE serves as the signal source to inhibit these signals. During gastrulation, the domain previously occupied by AVE is gradually colonized by the anterior definitive endoderm (ADE) and axial mesoderm (AME), both of which are derived from APS (Lawson, 1999; Lawson and Pedersen, 1987; Tam and Beddington, 1987; Tam et al., 2007). Embryos lacking APS progenitors exhibit anterior central nervous system truncation (Dunn et al., 2004; Vincent et al., 2003). During gastrulation, ADE and AME replace AVE as the new source expressing antagonists like CER1, DKK1, Chordin, and Noggin to maintain NE (Arkell and Tam, 2012; Arnold and Robertson, 2009). The ADE and AME are crucial in promoting anterior patterning as

demonstrated in the phenotypic analysis of head truncations when ADE and/or AME development or function is perturbed (Dunn et al., 2004; Vincent et al., 2003). The prechordal plate (PCP) and the anterior notochord, both of which are derived from AME, functionally interact with each other (Camus et al., 2000; Warr et al., 2008). PCP is not maintained in the absence of the anterior notochord and is required to inhibit the ectopic *Gsc* (*Goosecoid*) expression in the anterior notochord (Camus et al., 2000; Warr et al., 2008). It has also been shown that the presence of PCP is also required for sustaining the differentiation of the ADE (Hallonet et al., 2002). Therefore, the crosstalk between AME and ADE is important for maintaining their tissue identity as well as the neural characteristics of the neurectoderm.

The transcriptional activities that suppress the NODAL, BMP, and WNT signaling are required for the anterior specification and patterning (Lewis et al., 2008; Mukhopadhyay et al., 2001). Loss of *Dkk1* causes a major disruption of head development while reducing WNT3 activity in the *Dkk1*-null background can partially restore the head formation (Lewis et al., 2008; Mukhopadhyay et al., 2001). Similarly, mutations of other two transcription factors, *Lhx1* and *Otx2* also produce truncated head phenotypes (Ang et al., 1996; Shawlot and Behringer, 1995). *Dkk1*, *Lhx1,* and *Otx2* triple mutations are associated with head truncation phenotype, although the degree of severity varies among individuals (Ip et al., 2014). The LHX1-SSDP1-LDB1 transcription complex regulates the expression levels of several WNT antagonists. Lack of either *Ssdp1* or *Ldb1* is causative to head defects and reduced expression of antagonists including *Dkk1* in the prechordal plate (Mukhopadhyay et al., 2003; Nishioka et al., 2005). Similar phenotypes are also observed in mutant embryos lacking both *Cer1* and *Lefty1* that show expanded mesoderm at the expense of the NE. Loss of either one of them fails to disrupt NE, suggesting that CER1 and LEFTY1 have overlapping functions (Perea-

Gomez et al., 2002). Finally, mutants lacking both of BMP inhibitors *Chordin* and *Noggin*, phenocopy the head truncation phenotype (Bachiller et al., 2000). Taken together, the integration of graded morphogen signaling and transcriptional activities in anterior signal centers (AVE, AME, and ADE) are instrumental for anterior specification and morphogenesis.

Zebrafish

In zebrafish, the germ layer specification is associated with the successful establishment of the D-V axis. The localized activation of canonical Wnt signaling in the dorsal region translocates β-catenin into the nuclei of the dorsal blastomeres (Gore et al., 2005; Lu et al., 2011; Schneider et al., 1996; Tran et al., 2012; Yan et al., 2018). The β-catenin binds to Lef family proteins to induce expression of dorsal-specific genes like *Bozozok* to counteract the effects of BMP signaling from the ventral side, initiating mesendoderm specification at the dorsal side (Leung et al., 2003; Melby et al., 2000; Ryu et al., 2001; Schulte-Merker et al., 1997; Shimizu et al., 2002; Shimizu et al., 2000; Stachel et al., 1993; Yamanaka et al., 1998). Nodal signaling induced by the β-catenin at the dorsal side is required for mesendoderm specification and patterning (Feldman et al., 1998; Gritsman et al., 1999; Long et al., 2003; Shimizu et al., 2000). Nodal is also essential for the formation of the dorsal organizer, a structure that inhibits BMP signal expansion by expressing BMP antagonists (Schulte-Merker et al., 1997). The zebrafish-specific Nodal ligands Ndr1(Sqt) and Ndr2 (Cyclops, Cyc) are necessary for the germ layer specification (Feldman et al., 1998; Gritsman et al., 1999; Long et al., 2003). Recent studies have identified a new Nodal ligand, growth differentiation factor 3 (Gdf3, or Dvr1, Vg1) that is essential for mesendoderm specification (Bisgrove et al., 2017; Montague and Schier, 2017; Pelliccia et al., 2017). This ligand is maternally provided and can form heterodimers with Ndr1 or Ndr2 (Bisgrove et al., 2017; Montague and Schier, 2017;

Pelliccia et al., 2017). Thus, Gdf3 is considered to act as a cofactor to facilitate the activation of robust signaling. Similar to the observations in *Xenopus* and mouse embryos, zebrafish embryos rely on Smad2 as the main transducer of the Nodal signaling (Dubrulle et al., 2015; Howell et al., 2001; Robertson, 2014). Mutants lacking Smad2 fail to form mesoderm and endoderm, identical to the phenotype of embryos with the loss-of-function mutation in Nodal (Dubrulle et al., 2015; Feldman et al., 1998; Gritsman et al., 1999). Upon binding of Smad4, the Smad2/4 complex is phosphorylated and is associated with other transcription factors like Foxh11 to regulate target gene expression. These genes include Nodal antagonists *lefty1/2*, mesoderm-specific genes (*goosecoid*, *brachyury*), and endoderm specific genes (*sox32*) (Bennett et al., 2007; Bisgrove et al., 1999; Dickmeis et al., 2001; Meno et al., 1999; Pogoda et al., 2000).

The ectoderm arises from more animal positions within the gastrula (**Figure 1.16**). Compared to the mesendoderm specification, the ectoderm specification represents a default developmental state that the ectoderm rises in the absence or upon the reduced level of the Nodal signaling (Ho and Kimmel, 1993; Kiecker et al., 2016). Indeed, repressing mesoderm formation leads to an enlarged ectoderm domain, whereas reducing ectoderm development results in mesoderm expansion (Feldman et al., 2002; Feldman et al., 2000; Gritsman et al., 1999; Londin et al., 2007; Thisse et al., 2000). Ectoderm patterning requires inputs from BMP, FGF, Retinoid acid, and WNT signaling (Schier and Talbot, 2005). Ectodermal cells progressively lose the ability to respond to Nodal signaling, which may be the mechanism that prevents ectoderm from becoming mesendoderm (Ho and Kimmel, 1993). The exact mechanisms that lead to the incompetence of ectodermal cells in response to Nodal signaling are still unclear.

Like in *Xenopus*, a Nodal gradient is generated along the D-V axis. Therefore, a dose-dependent response is established to induce different target gene expressions along the axis, producing different tissue types. Low levels of Nodal signaling are sufficient to induce *no tail* (Palles et al.) or *floating head* (*flh*) gene expression in the notochord, whereas high levels of Nodal signaling are needed to express target genes in endoderm and anterior axial mesendoderm (prechordal plate, ppl) such as *sox32* and *goosecoid* (Gritsman et al., 2000). Consistent with this observation, the transient Nodal signaling is enough to induce notochord formation, while sustained Nodal signaling is required for the endoderm and ppl cell specification (Aoki et al., 2002; Dougan et al., 2003; Dubrulle et al., 2015; Gritsman et al., 2000; Hagos and Dougan, 2007). Modulating Nodal signaling duration using photoactivable Nodal receptors reveals that extending the exposure time of Nodal signaling lead to ppl specification at the expense of endoderm cells (Sako et al., 2016). Recent studies have shown that the FGF signaling can activate Nodal target genes independently, suggesting that FGF also participates in the mesendoderm patterning (Chen and Schier, 2001; Rodaway et al., 1999; van Boxtel et al., 2015; Van Boxtel et al., 2018). It remains to be seen how these two signal pathways cooperate spatiotemporally in defining the mesendoderm pattern.

In the mid-epiboly stage, the mesendoderm progenitors are specified at the blastoderm margin, creating a transient structure called the “germ ring” (Keller et al., 2008; Montero et al., 2005; Warga and Kimmel, 1990). Internalization of mesendoderm progenitors preferentially occurs at the dorsal side of the germ ring (Keller et al., 2008; Warga and Kimmel, 1990). Cells move across the margin and underneath the surface ectoderm progenitors, then spread along the germ ring margin, eventually form a shield structure homologous to the blastopore lip in frogs (**Figure 1.17**) (Keller et al., 2008; Solnica-Krezel and Sepich, 2012; Warga and Kimmel, 1990). The embryo ends up with two

layers: the outer epiblast consists of ectoderm and pre-internalization mesendoderm progenitors, and the inner hypoblast composes of internalized mesendoderm progenitors (Keller et al., 2008; Montero et al., 2005; Warga and Kimmel, 1990). The internalized mesendoderm progenitors migrate away from the germ ring margin and eventually form the body axis along the dorsal side (Dumortier et al., 2012; Montero et al., 2005; Montero et al., 2003; Norris et al., 2017; Pauli et al., 2014; Pezeron et al., 2008; Sepich et al., 2005). Unlike the frog embryo, mesendoderm internalization is not affected by the subsequent convergence and extension movements as the mutant defective of convergence and extension movements can still internalize mesendoderm normally (Solnica-Krezel et al., 1996).

Figure 1. 16 Initiation of gastrulation and mesendoderm patterning in zebrafish embryos. AP: animal position, VP: Vegetal position. Adapted from (Pinheiro and Heisenberg, 2020)

The molecular mechanism driving mesendoderm internalization remains poorly understood. It seems that Nodal signaling plays a dual role in mesendoderm specification and internalization. Blocking Nodal signaling leads to the failure of mesendoderm specification and internalization, whereas ectopic expression of Nodal signaling at the stage prior to the gastrulation, induces endoderm specification and internalization (Carmany-Rampey and Schier, 2001; David and Rosa, 2001; Feldman et al., 2000; Gritsman et al., 1999; Keller et al., 2008). These results indicate that the

mesendoderm specification and internalization may intrinsically link to each other. However, another transplantation assay suggests that the function of Nodal signaling may partially be separable, given the fact that ectopic induction of endoderm cells is not sufficient to trigger cell internalization (Liu et al., 2018). Another observation points out that the mesendoderm internalization is always initiated within the edge of the marginal region of the germ ring, where Nodal signaling activity is the highest (Dubrulle et al., 2015; Harvey and Smith, 2009; Keller et al., 2008; Montero et al., 2005; van Boxtel et al., 2015; Warga and Kimmel, 1990), and dorsal marginal cells are both the first cells to activate Nodal signaling and undergo internalization (Keller et al., 2008; Shimizu et al., 2000; Warga and Kimmel, 1990). However, it still cannot tell whether the high Nodal signaling activity is required for the initiation of internalization.

After internalization, mesendodermal cells move away from the margin and differentiate into the mesoderm and endoderm lineages (Dumortier et al., 2012; Keller et al., 2008; Matsuo et al., 2017; Montero et al., 2003; Myers et al., 2002; Pauli et al., 2014; Pezeron et al., 2008; Sepich et al., 2005; Warga and Nusslein-Volhard, 1999). Cells located at different positions show distinct migratory behaviors (**Figure 1.17**). In the dorsal domain, the ppl cells migrate toward the animal pole in an active and collective way, contributing to the A-P axis extension (Dumortier et al., 2012; Montero et al., 2005; Smutny et al., 2017; Ulrich et al., 2003). The Wnt/PCP signaling is suggested to play a critical role in dorsal mesendoderm migration (Heisenberg et al., 2000; Miyagi et al., 2004; Montero et al., 2003; Yamashita et al., 2002; Yamashita et al., 2004). Functional loss of Wnt11, the non-canonical Wnt ligand, and its receptor Frizzled 7 (Fz7) causes slow, not-so-well oriented ppl migration, along with other defects (Capek et al., 2019; Heisenberg et al., 2000; Ulrich et al., 2003). Overexpressing Wnt11 or activating Fz7 by light stimulation is sufficient to rescue ppl migration in *wnt11* or *fz7* mutant embryos, respectively (Capek et

al., 2019; Heisenberg et al., 2000). Inhibiting PDGF-PI3K signaling pharmacologically causes a similar phenotype as shown in the *wnt11* and *fz7* mutants, but the crosstalk between these two signaling pathways remains unclear (Montero et al., 2003). A recent study shows that downregulation of Sin1, a component of the Torc2 complex, affects the speed and the directionality of ppl migration, suggesting that Sin1 may be a key regulator of ppl cell migration (Dumortier and David, 2015). It is not known whether the Wnt/PCP or PDGF/PI3K also regulates Sin1 to affect ppl cell migration.

In the ventral and lateral side of the germ ring margin, mesendoderm cells first migrate toward the animal pole from the early- to mid-gastrulation stage (Keller et al., 2008; Myers et al., 2002; Sepich et al., 2005). Apelin signaling is recently shown to regulate ventral-lateral mesendoderm migration (Chng et al., 2013; Norris et al., 2017; Pauli et al., 2014). Apela, the ligand of Apelin signaling that binds to its APJ/Apelin G-protein-coupled-receptors (GPCR), is considered to promote motility of the ventrolateral mesendoderm cells, yet the detailed mechanism is still unclear (Chng et al., 2013; Pauli et al., 2014). Transcriptional profiles of *apela* mutants do not show major changes in gene expression during gastrulation compared to the wildtypes (Norris et al., 2017), but *apela* mutants do show delayed epiboly movements (Chng et al., 2013; Pauli et al., 2014), raising the possibility that the defective mesendoderm migration is related to the reduced epiboly movements in the outer layer. It has been shown that the frictional forces generated at the interface between the ppl (moving towards the animal pole) and the neuroectoderm epiboly movements (moving towards the vegetal pole) influence neuroectoderm cell movements and their position along the A-P axis (Smutny et al., 2017). A similar interaction may also occur between the migrating ventrolateral mesendoderm and the ectoderm. In general. the molecular basis of this observation remains largely unknown.

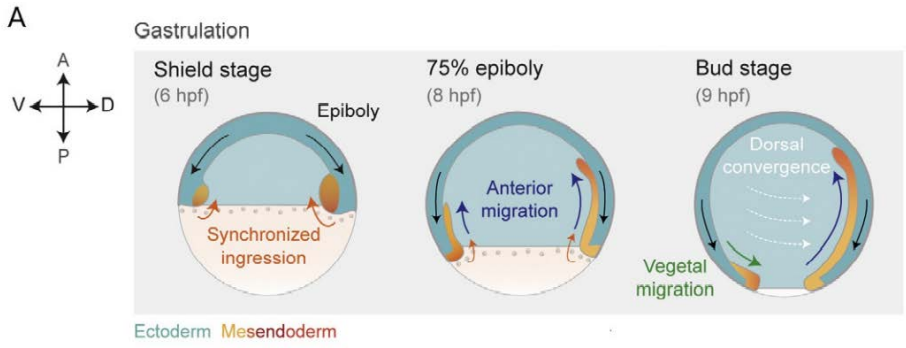

Figure1.17 The movements of mesendoderm cells at different positions inside the surface layer. (Pinheiro and Heisenberg, 2020).

Migration of endoderm progenitors is a completely different story from mesoderm progenitors that, at the early stage, instead of being a continuous monolayer, the endoderm progenitors form a non-continuous monolayer (Warga and Nusslein-Volhard, 1999). These cells seem to undergo a random walk, simply disperse on the yolk surface, with no rules to follow (Pezeron et al., 2008). Interestingly, the definitive endoderm cells in mouse embryos, also disperse and intercalate into the visceral endoderm layer, a process similar to the endoderm cells in zebrafish. It is not known whether such a random walk is an intrinsic feature for endoderm cells. Finally, from late gastrulation, the mesodermal and endodermal cells initiate convergence movements towards the dorsal side of the embryo, lining the gastrointestinal tract (Pezeron et al., 2008). The Rho GTPase Rac1 activity, which is triggered by the Nodal transcriptional target Prex1, is required for endoderm migration at both the early “random walk” stage and late convergence stage, while cell-matrix adhesion Cxcl12a chemokine signaling is required specifically for dorsal convergence (Norris et al., 2017; Woo et al., 2012). The endoderm convergence is thought to rely on the overlying mesoderm convergence as endoderm cells are tethered to mesoderm cells through integrin-ECM adhesion (Norris et al., 2017). Disrupting integrin-fibronectin adhesions of Cxcl12a/b signaling leads to

prolonged endoderm migration (Latimer and Jessen, 2010; Mizoguchi et al., 2008; Nair and Schilling, 2008; Norris et al., 2017). It is possible that the switch of migration mode in the endoderm is a mechanism that guarantees fast cell dispersion at the early stage and coordinates the convergence with the mesoderm convergence toward the dorsal side at the later stage.

Conclusion marks

By comparing the gastrulation process from different species, it is not difficult to find out that the lineage specification relies on the establishment of morphogen gradients along the body axis. In *Drosophila* and *Zebrafish* (also in *Xenopus* and *chick*), the patterning of progenitors starts from the morphogen gradient established along the D-V axis. Elongation of the embryo body along the A-P axis seems always to be the last step before gastrulation. While in mice, the concept of the D-V axis is replaced by the P-D axis and the A-P axis is established before the gastrulation occurs. Patterning of lineage progenitors relies on the two-dimensional morphogen gradients that are established along the P-D axis and the A-P axis. The morphogenesis during gastrulation of different species, though named differently, all rely on the formation of a transient structure(s). Invertebrates rely on furrows, nonamniote vertebrates form germ rings and amniote vertebrates form primitive streaks. The transient structure breaks the original topology of the embryo, serving as the gateway for cells to collectively migrate (mesenchymal cells), or invaginate (epithelial cells) to form new germ layers. The signaling pathways required for lineage specification and morphogenesis are very conserved. Among all of them, Nodal signaling plays a central role in embryo axis development and patterning. The activation of Nodal signaling, however, is context-specific. So far, the molecular basis and cellular process have been deeply investigated during gastrulation and some common features are shared among various organisms. However, most of our current

knowledge can help answer the questions of “how”, but not the questions of “why” in development. Many open questions may not even have answers. For example, the ectoderm, which is always considered a “default setting” and usually draws less attention due to the relatively simple scenario. But why does the ectoderm, not mesoderm or endoderm, adopt the default setting? Is it simply a matter of position? Why do the epidermis and the nervous system share one germ layer? These open *evo-devo* questions are also meaningful and worth extensive discussion.

1.4 Coordination between cell proliferation and lineage specification, embryo patterning, and morphology

Cell proliferation is not independent of other developmental events. Instead, it can substantially affect lineage specification, tissue patterning, and morphogenesis. Cell proliferation participates in these events in multiple ways like increasing cell number at different rates to coordinate with tissue patterning and morphogenesis, or undergoing asymmetrical cell division in lineage specification. All these events are seen in different kinds of organisms throughout the whole developmental process and are very content-specific. In this section, we will discuss some examples to get a deep insight into the importance of cell proliferation in embryogenesis.

1.4.1 Asymmetric cell division

Asymmetric cell division is a common and evolutionary conserved process that a mother cell divides to generate two daughter cells with distinct developmental potentials. Asymmetric cell division can be divided into four steps. First, the mother cell acquires and/or re-orients a polarity axis. Second, cell fate determinants, including molecules and/or organelles are unequally distributed inside the cytoplasm to influence the fate of daughter cells. Third, the mitotic spindle lines up along the cell polarity axis, and fate determinants become asymmetrically segregated at cytokinesis. Lastly, these fate

determinants regulate a binary fate choice to implement fate asymmetry (Schweisguth, 2015). The mechanism of asymmetric division is a huge topic worth another 100 pages of review, which will not be included in our discussion. In this section, we only bring about the facts of asymmetric division to highlight its importance for embryonic development across different species.

During development, asymmetric cell division plays a significant role in generating cell fate diversity and setting up the embryonic axes. In the early embryo of *C.elegans*, five asymmetric divisions produce six founder cells: AB, MS, E, C, D, and P4. The first asymmetric division cleaves the one-cell zygote into a two-cell embryo with a larger anterior cell (AB) and a smaller posterior cell (P1). P1 cell is divided asymmetrically, giving rise to two blastomeres named EMS and P2. The EMS undergoes further asymmetric divisions that produce two daughter cells MS and E, then P2 into C and P3, and finally P3 into D and P4. Three body axes are established during these early cleavages (Sulston et al., 1983). The A-P axis is generated from the first asymmetric division of the one-cell embryo, with the sperm-derived centrosome determining the future posterior side. The D-V axis is established by the four-cell stage, with EMS marking the ventral side. The left-right (L-R) axis is defined by the location of ABal and ABpl cells (Sulston et al., 1983). In *Xenopus,* the two first embryonic divisions are perpendicular to each other and generate two pairs of blastomeres with different sizes (Nieuwkoop, 1967). The two small blastomeres proliferate and give rise to embryonic dorsal structures, whereas the large pair develops into ventral structure (Moody and Kline, 1990; Nieuwkoop, 1967). In the mouse embryo at the morula stage, segregation of progenitors of TE and ICM is realized through asymmetric cell division along a basolateral cleavage plane at the 8-cell morula stage, as observed by the time-lapse cinemicrography (Sutherland et al., 1990). The outer cells become the TE and the inner

cells comprise the ICM. In *Drosophila*, the differentiation of neuroblasts is predominantly controlled by asymmetric cell division. Neuroblasts are the neural stem cells critical for the development of the central nervous system. Neuroblasts are specified during embryonic stages 9-11 through Notch/Delta and Wingless signaling (Artavanis-Tsakonas et al., 1995; Brand and Campos-Ortega, 1988; Chu-LaGraff and Doe, 1993; Ghysen et al., 1993; Skeath and Carroll, 1992). Upon specification, neuroblasts undergo EMT and delaminate from the neuroepithelium in the ventrolateral region of the *Drosophila* embryo (Hartenstein et al., 1994). Delaminated neuroblasts undergo a series of asymmetric cell divisions, producing a self-renewed neuroblast and a differentiation ganglion mother cell (GMC). GMCs divide and give rise to glia, neurons or both (Hartenstein et al., 1994).

Asymmetric cell division is also seen in the oogenesis in both insects and vertebrate species. In *Drosophila*, cyst cells are joined together, with one of them differentiating into the oocyte and the remaining cells forming the nurse cells (Bilinski, 1998; Buning, 1993; Büning, 1994; Jaglarz, 1998; Kubrakiewicz, 1997). The germline stem cells (GSCs) divide asymmetrically to produce new GSCs and cystoblasts, the progenitor germ cells (Cuevas et al., 1997; King, 1970; Pepling et al., 1999). Each cystoblast divides synchronously four times, forming the germline cysts composed of 16 interconnected cystocytes. Only the two central cystocytes are connected by four bridges (Ong and Tan, 2010; Pepling et al., 1999). The intercellular bridges connecting cystocytes contain specialized cytoplasma termed fusomes (Cuevas et al., 1997). The fusomes anchor mitotic spindles of dividing cystocytes, ensuring the orientation of the division planes, which is indispensable for asymmetric localization of transcripts into one of the two cystocytes with four bridges that eventually differentiate into the oocyte (De Cuevas and Spradling, 1998; Deng and Lin, 1997; King, 1970; Lin and Spradling, 1995). The rest 15 cyst cells become highly polyploid and transcriptionally active nurse cells. In vertebrate

species such as *Xenopus,* the cyst formation is similar to *Drosophila* in that each cystoblast undergoes four consecutive asymmetrical divisions with incomplete cytokinesis, giving rise to 16 interconnected cystocytes (Kloc et al., 2004). However, in *Xenopus* all 16 cystocytes enter the meiotic prophase and become the oocytes after the breakdown of the cytoplasmic bridges (Kloc et al., 2004). Similar to *Drosophila*, the intercellular bridges in *Xenopus* also contain fusomes, which are required for anchoring the poles of mitotic spindles critical for asymmetric division (Kloc et al., 2004). These findings suggest that oogenesis is a conserved process and many common features are shared in various multicellular organisms. The asymmetric cell division plays a fundamental role in oocyte generation.

1.4.2 Cell proliferation

In mouse development, cell number growth is correlated with some of the developmental milestones in embryogenesis. The relationship between cell number and developmental progression in pre-gastrulating embryos is addressed through embryological manipulations. In blastocyst formation, inhibiting DNA replication affects the timing of cavitation (Alexandre, 1979). Treatment of aphidicolin in embryos at the 4-8 cell stage blocks 90% of DNA synthesis, leading to precocious cavitation at the 8-16 stage instead of the 16-32 cell stage in the untreated embryos (Dean and Rossant, 1984). After lineage specification, TE, EPI, and PrE exhibit differential proliferative activities. TE cells are proliferating at a faster rate compared to EPI/PrE cells during the 5^{th} to 6^{th} division and then slow down rapidly. At the 7^{th} to 8^{th} division, the EPI/PrE cells proliferate faster than TE cells (Handyside and Hunter, 1986). At E6.5, the primitive streak becomes apparent in the post-implantation embryos (Tam et al., 1993). Embryos enter gastrulation typically contain an average of 1000 cells (Power and Tam, 1993). Other embryos at the same age but have about 660 cells have yet to undergo gastrulation,

indicating a cell-number threshold required for initiation of gastrulation (Power and Tam, 1993). Double-sized embryos, formed by aggregating two 8-cell stage morulae, undergo size regulation before gastrulation. The double-sized embryos show an increase in cell-cycle length compared to controls; in addition, they lack the proliferative burst that normally occurs before gastrulation. These two modes of regulating cell proliferation allow the aggregated embryos to reach a normal size and cell number before E7.0 (Buehr and McLaren, 1974; Lewis and Rossant, 1982) and then to gastrulate. Conversely, undersized mouse embryos generated by removing one or two blastomeres from the 4-cell stage preimplantation embryo, form blastocyst with a significantly reduced number of inner cell mass cells. Post-implantation embryos derived from these reduced embryos are approximately half-sized and show a delay in gastrulation. These embryos have to sustain a prolonged proliferative burst until reaching the 1000 cells before the initiation of the gastrulation (Power and Tam, 1993). Another study on size regulation in the mammalian embryo examined the response to reduced cell number in the early post-implantation embryo, an experimentally more refractory stage. Following treatment with mitomycin to inhibit cell proliferation, E7.0 embryos, with ~80% of their cells eliminated, could still recover and complete the gastrulation (Snow and Tam, 1979), although an extended period of time is required before gastrulation.

In organ development, size control and organ morphology are tightly correlated as demonstrated through extensive genetic studies. In *Drosophila*, the hindgut is the first asymmetric organ that forms during embryogenesis. In *pebble* and *string* mutants, which show no blastoderm mitosis and reduced cell number, the hindgut still forms asymmetrically, though some embryos display inversion of the left/right asymmetry (Hartenstein and Posakony, 1990; Nakamura et al., 2013). A detailed analysis of *string* mutants shows that ~20% of the mutant embryos display morphological defects.

Mutations on E-Cadherin and MYoIA also affect left/right asymmetry (Nakamura et al., 2013). Perturbations of Dpp or Hh signaling significantly alter hindgut morphology. Dpp positively regulates endoreplication during hindgut elongation. Mutations in Dpp pathways result in severe morphology phenotypes, while Hh mutants have a smaller gut size with twisted left/right morphology (Takashima and Murakami, 2001). In wing development, Dpp is essential for stimulating cell proliferation (Rogulja and Irvine, 2005). Ectopic expression of Dpp is sufficient to drive wing growths and this growth can be organized into partial wing duplications (Zecca et al., 1995).

Hippo signaling is always the central regulator when comes to organ growth and size expansion. Later studies also define important roles of the Hippo pathway in tissue morphogenesis (Pan, 2010). In mouse cardiac development, loss of Hippo pathway components SAV1 leads to substantial cardiomegaly (Heallen et al., 2011). The change of myocardium thickness and heart size is due to the over-proliferation of cardiomyocytes in the absence of SAV1 (Heallen et al., 2011). Conversely, loss of YAP in early development or cardiac muscle leads to severe myocardium hypoplasia with severely reduced cardiomyocyte proliferation (von Gise et al., 2012; Xin et al., 2011). In eye development, knockdown of YAP results in reduced eye size in zebrafish (Jiang et al., 2009). Deletion of YAP in the lens at E14.5 leads to severe atrophy due to lens fiber (LF) defect and the hypocellularity in the lens epithelium (LE) in mouse embryos (Cvekl and Duncan, 2007). LE cells are progenitor cells and YAP is required to maintain the self-renew of LE cells (Menko, 2002). YAP-null LE cells exit from the cell cycle and differentiate into LF cells, causing a reduced LE cell pool important for replacing new LF cells (Song et al., 2014). In kidney development, knockout of YAP in cap mesenchyme, which develops into nephrons, leads to dramatic reductions in Henle's loop, glomeruli, and proximal tubule formation (Reginensi et al., 2013). Knocking out CDC42, an

activator of YAP/TAZ during kidney development shows phenotypes similar to YAP knockout (Reginensi et al., 2013).

Taken together, cell proliferation is regulated by a series of conserved signaling pathways to coordinate the size expansion with tissue patterning and morphogenesis. It is not uncommon to see reduced embryo size from mutations on these signaling pathways. However, the caveat of these studies is that these signal pathways control too many things that it is hard to tease out other defects and focus primarily on cell proliferation. Therefore, studies targeting cell-cycle-related proteins will be potentially more informative to look at how the cell cycle could affect embryogenesis or organ development, which will be discussed in the next section.

Section 2 Cell Cycle

2.1 Overview of Cell Cycle

Cell cycle is a ubiquitous and complex process indispensable for cell proliferation and tissue growth. The cell cycle can be morphologically divided into two parts, the interphase stage, which usually occupies more than 90% of the time during the cell cycle, and the M (mitosis) stage for cell division. The interphase contains G1, S, and G2 phases while the M phase can be subdivided into prophase, metaphase, anaphase, and telophase. S phase and M phase are two periods when the major cell cycle events happen: nascent DNAs are synthesized in the S phase, while the duplicated genomes are evenly distributed when the mother cell is dividing in the M phase. The G1 and G2 phases of the cell cycle are the “gaps” occurring between the S phase and M phase. In the G1 phase, proteins required for DNA replication are synthesized and cells are prepared for the S phase. The G2 phase is the second gap to prepare cells entering the M phase. Incompletely replicated genomes or any DNA damages will trigger the damage

responses to cause a delay in G2/M transition or even cell cycle arrest in the G2 phase. Cells that are not in the active cell cycle but with the potential for division are referred to as G0 cells such as hepatocytes. However, the concept of G0 has later been loosely, and probably incorrectly applied to any terminally differentiated cells including adult neurons and epidermis.

The cell cycle is tightly regulated by a large group of proteins (**Figure 1.18**). The cyclin-dependent kinases (CDKs) and the paired cyclin proteins are the central players in this process (Morgan, 1997). These proteins regulate the cell cycle progression and are also regulated by a peripheral protein network. Dysregulated cell cycle is frequently seen in a broad spectrum of neoplasia and tumors and has always been a research hot spot in the cancer field. In embryo development, the cell cycle is also regulated by a series of developmental genes, mostly transcription factors critical for lineage specification and embryo patterning. In this section, we will first discuss the principles of cell cycle regulation in a generic view, primarily in multicellular eukaryotes. Then we will discuss how the cell cycle is regulated in the context of developmental biology. Finally, we will provide examples showing how the cell cycle is involved in cell fate determination in the context of pluripotent stem cell differentiation, cell trans-differentiation, and cell reprogramming.

2.2 Cell cycle regulation

2.2.1 CDKs and cyclins: the major players of cell cycle progression

The cell cycle is primarily catalyzed by the CDK-cyclin complexes. CDKs are a group of serine/threonine protein kinases activated at specific time points in the cell cycle (Pines, 1995). In single-cell eukaryotes such as yeast, cell cycle progression is governed by one CDK paired with cyclins. Cyclins are named due to their cyclic expression during the cell

cycle (Darzynkiewicz et al., 1996). In multicellular eukaryotes, multiple CDKs and cyclins are identified. Cyclins are important for binding and phosphorylating CDKs to activate CDKs activities (Darzynkiewicz et al., 1996; Pines, 1991). Therefore, CDKs can be activated only at specific times due to the cyclic expression of the cyclins. We will talk about the activities of CDK-cyclin complexes in a time-specific manner during the cell cycle.

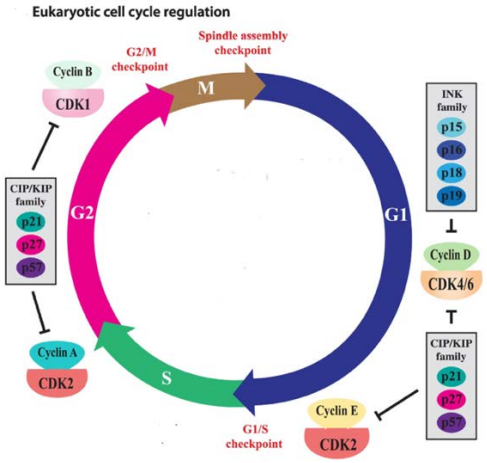

Figure1.18 Regulation of cell cycle by CDK-cyclin complexes. The CDK-cyclin complex activity is also regulated by CDK inhibitors. Adapted from (Bury et al., 2021).

G1 phase

In the mid/late G1 phase, the cyclin D/CDK4/6 phosphorylates pRB, the retinoblastoma tumor suppressor protein (Connell-Crowley et al., 1997; Lees et al., 1991; Zarkowska and Mittnacht, 1997). The hypophosphorylated pRB binds to the E2F transcription factor and represses transcription (Bandara and La Thangue, 1991; Chellappan et al., 1991; Chittenden et al., 1991). Phosphorylation of pRB by CDK4/6-cyclin D releases E2F, initiating the transcription of genes required for the G1/S transition (Arroyo and Raychaudhuri, 1992; Mudrak et al., 1994). RB remains hyperphosphorylated through the rest of the cell cycle until the end of the mitosis (Weinberg, 1995). The p16 family,

including p15, p16, p18, and p19 are the inhibitors of CDK4 and CDK6. The p16 family proteins bind to CDK4/6 and prevent the phosphorylation of and inactivation of pRB (Guan et al., 1994; Hirai et al., 1995; Kamb et al., 1994; Serrano et al., 1993; Washimi et al., 1995).

Studies in mammals have been focusing on the requirement of CDK4/6-cyclin D in the G1/S phase transition. *Cdk4*$^{-/-}$ mouse embryonic fibroblasts (MEFs) initially divided normally. However, the S phase entry is delayed when cells re-enter the cell cycle from the quiescence (Tsutsui et al., 1999). *Cdk4* null mice are viable but smaller than wildtype mice, with defects in endocrine tissues leading to diabetes and infertility (Rane et al., 1999; Tsutsui et al., 1999). *Cdk6* null mice are viable and are of normal size but develop hypoplasia in the spleen and thymus (Malumbres et al., 2004). *Cdk6*$^{-/-}$ MEFs can proliferate normally, but *Cdk6*$^{-/-}$ T lymphocytes display a delayed response to mitogens after cell arrest (Malumbres et al., 2004). These results suggest that genetic depletion of *Cdk4* or *Cdk6* shows tissue-specific effects in mice and *Cdk4* is more important than *Cdk6*. Meanwhile, these studies also point out that the functions of CDK4 and CDK6 can be substituted, although only partially, by other CDKs in the single knockout mice to promote G1/S transition. The *Cdk4/6* double knock-out mice die shortly after birth and display major defects in the hematopoietic system, suggesting that CDK4/6 is not important for embryogenesis (Malumbres et al., 2004). Although *Cdk4/6* null MEFs can exit from quiescence, the cell cycle re-entry from quiescence is delayed (Malumbres et al., 2004). pRB phosphorylation in *Cdk4/6* null MEFs seems to be partially achieved by the pairing of CDK2-cyclin D2 (Malumbres et al., 2004). Inhibiting CDK2 by shRNA completely blocks the cell proliferation of *Cdk4/6* null cells, suggesting that CDK2 becomes essential for pRB phosphorylation and cell cycle progression in the absence of CDK4/6 (Malumbres et al., 2004).

Mice without cyclin D1 are viable with reduced size (Sicinski et al., 1995). *Ccnd1* null mice display proliferation defects in the retina and mammary epithelium, which is completely different from *Cdk4* null mice (Rane et al., 1999; Sicinski et al., 1995; Tsutsui et al., 1999). In *Ccnd2* null mice, ovarian granulosa cells do not respond to follicle-stimulating hormone (FSH) (Sicinski et al., 1996). Although *Cdk4* null mice also display ovarian follicular defects, the phenotype is not similar to *Ccnd2* null mice (Rane et al., 1999; Sicinski et al., 1996; Tsutsui et al., 1999). These tissue-specific defects probably reflect the relative abundance of these cyclin D members in different tissues. Depleting all D-type cyclins in mice leads to embryonic lethality before E17.5 of gestation (Kozar et al., 2004). These embryos die with severe anemia and cardiac output failure (Kozar et al., 2004). Since most tissues and organs are formed prior to E13.5, this may indicate that cyclin D family proteins are not essential for embryogenesis. However, D-type cyclins are essential for the expansion of hematopoietic stem cells as a deficiency in hematopoiesis is observed in embryos losing all D-type cyclins (Kozar et al., 2004). While other non-hematopoietic tissues can still proliferate in the absence of all D-type cyclins (Kozar et al., 2004). Meanwhile, since CDK4/6 exclusively pairs with cyclin D, cells null for all D-type cyclins should be resistant to $p16^{INKa}$, an inhibitor of CDK4 and CDK6 (Serrano et al., 1993). Indeed, introduction of $p16^{INKa}$ by retroviral infection into cyclin D null MEFs does not affect cell proliferation, whereas $p27^{KIP1}$, an inhibitor of CDK4/6 and CDK2 (cyclin A and cyclin E-dependent kinase) blocks cell proliferation in MEFs without any D-type cyclins (Kozar et al., 2004; Polyak et al., 1994a; Polyak et al., 1994b; Toyoshima and Hunter, 1994). Like in *Cdk4/6* null cells, CDK2 is important for driving cell proliferation in *Ccnd1*$^{-/-}$*Ccnd2*$^{-/-}$*Ccnd3*$^{-/-}$ cells. Knockdown experiments using siRNAs against CDK2 block cell proliferation in cyclin D null MEFs but not wildtype MEFs (Kozar et al., 2004). The cyclin A/E-dependent phosphorylation of pRB is

sufficient for cell cycle progression in the absence of all cyclin D genes (Kozar et al., 2004). Taken together, these studies suggest that tissue-specific proliferation-associated defects occur in cyclin D, CDK4, or CDK6 null mice. All three D-type cyclins and CDK4/6 are not essential for the G1/S phase transition in most cell types in mice, as their functions can be mostly compensated by CDK2 and cyclin A/E.

S phase

The CDK2 and its paired cyclin A/E are found to be required for G1/S transition and progression through S phase (Ohtsubo et al., 1995; Pagano et al., 1993; Pagano et al., 1992; van den Heuvel and Harlow, 1993). The E2F activity, which is essential for the G1/S phase transition, is terminated by cyclin A/CDK2 phosphorylation, which probably results from its inability to bind the chromatin (Dynlacht et al., 1994; Krek et al., 1994). Loss of E2F binding guarantees the completion of the S phase as constitutive E2F binding to chromatin leads to S phase delay or arrest (Krek et al., 1995). Sequestering cyclin A or E by neutralizing antibodies, or introducing dominant-negative *CDK2* mutants in cultured human cells blocks the S phase progression (Ohtsubo et al., 1995; Pagano et al., 1993; Pagano et al., 1992; van den Heuvel and Harlow, 1993). In mouse studies, CDK2 null mice are small, viable but sterile, indicating the role of CDK2 in germ cell development and meiosis (Berthet et al., 2003; Ortega et al., 2003). *Cdk2*$^{-/-}$ MEFs can proliferate but the S phase entry is delayed (Berthet et al., 2003; Ortega et al., 2003). Depleting CDK2 in human tumor cells using RNAi does not disrupt mitotic cell cycle progression, suggesting that the role of CDK2 in somatic cells can be compensated by other CDKs (Tetsu and McCormick, 2003). In frog embryos, CDK1-cyclin B can promote S phase progression by artificially promoting nuclear entry of cyclin B, indicating that the CDK1 may assume the functions of CDK2 in the S phase (Moore et al., 2003).

In contrast to the loss of CDK2, depleting cyclin A2 results in developmental arrest shortly after implantation (Murphy et al., 1997; Winston et al., 2000). Cyclin A2 is necessary for both the G1/S and G2/M transitions, as well as centrosome and DNA replication (Girard et al., 1991; King et al., 1994; Knoblich and Lehner, 1993; Pagano et al., 1992). Expression of cyclin A1 is restricted to germ cells and cannot compensate for the loss of cyclin A2 (Howe et al., 1995; Murphy et al., 1997; Sweeney et al., 1996). Loss of cyclin A1 results in infertility in males, but not in females (Liu et al., 1998). Increased germ cell apoptosis, defective desynapsis, and reduced levels of CDK1 activity are observed in cyclin A1-deficient mice (Liu et al., 1998). Deletion of cyclin E1 or E2 can be tolerated by animals (Geng et al., 2003). Cyclin E1-deficient mice appear normal, suggesting that the function of cyclin E1 is fully compensated by other cyclins (Geng et al., 2003). Half of the *Ccne2* null males, however, are infertile due to testicular atrophy, suggesting that cyclin E2 is involved in meiosis and germ cell development (Geng et al., 2003). Deletion of both cyclin E genes, however, leads to no embryogenesis in uterus (Geng et al., 2003). Further rescue experiments in placenta indicate that the cyclin E is critical for the endoreduplication of the trophoblast giant cells inside the placenta, which is required for embryogenesis (Geng et al., 2003). The embryonic cells, however, do not require cyclin E for normal proliferation (Geng et al., 2003). It is not clear why trophoblasts specifically required cyclin E. Studies in *Drosophila* salivary glands provide some hints to this question. Multiple rounds of DNA synthesis can occur in *Drosophila* salivary glands without mitosis (Rudkin, 1972; Smith and Orr-Weaver, 1991). Chromatin competent for replication is marked by the presence of minichromosome maintenance (MCM) proteins (Su and O'Farrell, 1997). MCM binds to DNA prior to the S phase and disengages from DNA during S phase (Su and O'Farrell, 1997). Cyclin E promotes the loading of MCM proteins onto chromatin before the initiation of DNA synthesis undergoing endoreduplication (Su and O'Farrell, 1998). Therefore, MCM cannot bind to

chromatin in the absence of cyclin E (Su and O'Farrell, 1998). In support of this, the cyclin E-/- MEFs cannot load MCM proteins onto chromatin after serum stimulation (Geng et al., 2003). However, it seems that only cells undergoing endoreduplication rely on cyclin E-dependent MCM loading. This function of cyclin E is exclusive and cannot be substituted by other cyclins such as cyclin A.

G2/M phase

The G2/M transition and M phase progression in multicellular eukaryotes requires cyclin A2 and B1 paired with CDK1. CDK1 is the most essential gene as no viable *CDK1*-/- cells are produced. RNAi-mediated knockdown of CDK1 in HeLa cells displays cell cycle arrest right before spindle formation (Harborth et al., 2001). Cyclin A2 is required at the G1/S transition and during mitosis (King et al., 1994; Knoblich and Lehner, 1993; Pagano et al., 1992). The embryonic lethality of cyclin A2-deficient embryos may be due to loss of either or both functions (Murphy et al., 1997; Winston et al., 2000). Microinjection of cyclin A/CDK2 promotes mitotic entry of human G2 phase cells while injecting cyclin A-specific antibodies after S phase prevents mitosis progression (Furuno et al., 1999; Pagano et al., 1992). In *Drosophila* cells, depleting maternal cyclin A causes cell cycle arrest in G2 phase (Knoblich and Lehner, 1993). Cyclin B1/CDK1 complex is involved in the suppression of RNA polymerases, which is important for mitotic transcriptional suppression. Cyclin B1/CDK1 phosphorylates the promoter selectivity factor SL1, which is required for Pol I gene expression (Heix et al., 1998). In RNA Polymerase III, one of the subunits of the basal transcription factor TFIIIB is phosphorylated by cyclinB1/CDK1 (Gottesfeld et al., 1994). Cyclin B2 is highly expressed during spermatogenesis in germ cells (Brandeis et al., 1998). Disruption of cyclin B2, however, does not cause reproductive abnormalities in mice (Brandeis et al., 1998). Instead, cyclin B1 turns out to be the essential factor for spermatogenesis, as

shown by the phenotype of cyclin B1 null mice (Brandeis et al., 1998). These studies indicate that cyclin B1 is able to compensate for the absence of cyclin B2, not vice versa. A number of CDK1-cyclin B substrates have been identified as being critical for mitosis (Ubersax et al., 2003). One of the most important targets is the anaphase-promoting complex (APC), which is also the substrate of CDK2-cyclin A (Ohtoshi et al., 2000; Zou et al., 1999). Phosphorylation of APC leads to the degradation of certain proteins including securin, an inhibitor of the sister chromatid separation (Zou et al., 1999). Emi1, an inhibitor of APC, is accumulated in cells starting from late G1 and remains high through G2 (Reimann et al., 2001). Entry into mitosis requires the destruction of Emi1 (Reimann et al., 2001). Failure of Emi1 destruction stabilizes APC substrates, leading to mitotic catastrophe (Margottin-Goguet et al., 2003; Reimann et al., 2001). It has been shown that Emi1 destruction requires poly-ubiquitination by SCF-E3 ligase (Margottin-Goguet et al., 2003). Phosphorylation of Emi1 by Cyclin B/CDK1 stabilizes the association between Emi1 and the βTrCP, the adaptor protein inside the E3 ligase, therefore promoting the poly-ubiquitination and destruction of Emi 1 (Margottin-Goguet et al., 2003). Chromosomal localization of condensin, a multi-subunit protein complex, is also phosphorylated by CDK1-cyclin B in *Xenopus* and humans, which is crucial for promoting chromosome condensation *in vitro* (Hirano et al., 1997; Hirano and Mitchison, 1994; Kimura et al., 2001; Kimura et al., 1998).

2.2.2. Homeobox genes: a set of cell-cycle modulators in development

Homeobox genes are among the most well-studied genes during embryonic development. These genes encode a large family of transcription factors featuring a well-conserved DNA-binding motif (usually containing 60 amino acids) known as homeodomain (HD) (Scott et al., 1989). The homeobox genes were initially identified in *Drosophila*, where mutants show defects in body segmentation (Gehring et al., 1994;

Scott et al., 1989). In mammals, 39 Hox genes are identified as the closest vertebrate homologs of the genes initially identified in *Drosophila* (Tupler et al., 2001). For the past two decades, numerous amounts of work have demonstrated the central role of homeobox genes in embryonic development ranging from early embryo patterning to organogenesis and cell-type specification. In addition to these traditional work, homeobox transcription factors are also found to be involved in controlling cell proliferation by modulating cell-cycle-related proteins. As cell proliferation must be tightly controlled and coordinated with pattern signals and morphogenetic movements for normal development, it is not surprising to see the homeobox transcription factors, despite determining lineage specification and tissue patterning, are also the master regulators of cell proliferation during the development.

The patterning and morphogenesis of the anterior neural plate is the most well-characterized context for investigating the role of Homeobox transcription factors in controlling cell proliferation in vertebrates (Wilson and Houart, 2004) (**Figure 1.19**). The anterior neural plate develops into the forebrain, which gives rise to part of the central nervous system including the telencephalon, eyes, and diencephalon (Wheeler et al., 2005). Cells from the anterior neural plate need to undergo extensive cell proliferation in order to expand the tissue size large enough for differentiation and morphogenesis (Hartenstein, 1993; Korzh et al., 1993). In this region, the concomitant expression of a few transcription factors, such as Rx and Six3 are required for anterior fate specification and promoting cell proliferation (Andreazzoli et al., 2003; Bovolenta et al., 1998; Casarosa et al., 2003; Kobayashi et al., 1998; Loosli et al., 1998; Oliver et al., 1995; Seo et al., 1998; Zhou et al., 2000). *Rx* genes are broadly expressed in non-amniote and amniote vertebrates including *Xenopus*, zebrafish, chick, and mouse (Casarosa et al., 1997; Furukawa et al., 1997; Loosli et al., 2003; Loosli et al., 2001; Mathers et al., 1997;

Ohuchi et al., 1999). Gain-of-function studies in *Xenopus* demonstrate that *Rx* genes are essential for maintaining the proliferative state of anterior neural plate cells (Andreazzoli et al., 2003; Casarosa et al., 2003). Overexpressing *xrx1*, one of the *Rx* gene family members, is sufficient to induce expanded expression of cyclin D1 and increased cell proliferation (Andreazzoli et al., 2003). Meanwhile, Xrx1 also has the capacity to restrict the expression of p27, an inhibitor of cyclin-dependent kinases (CDKs)(Andreazzoli et al., 2003; Polyak et al., 1994b; Toyoshima and Hunter, 1994). This function has not been clearly tested in other model organisms yet due to the early effects on morphogenesis and eye organogenesis occurring before later defects in autonomous functions in loss-of-function experiments (Mathers et al., 1997). In mice, conditional knock-out of *Rx* in early retinal progenitors leads to reduced cell proliferation and changes in cell fate, indicating *Rx* is important for maintaining the retinal progenitor pool (Rodgers et al., 2018). However, the detailed mechanism regarding how Rx regulates cell cycle in retinal progenitor cells is unknown.

Homeobox transcription factors Six3 and Six6 play a similar role in controlling cell cycle progression in the anterior neural plate and other central nervous system regions. Both genes belong to the *Six*/*sineoculis* family and are considered to be the orthologue of the *Drosophila* gene *optix* (Kawakami et al., 2000; Kobayashi et al., 1998; Oliver et al., 1995; Seimiya and Gehring, 2000). *Six3* is expressed in the anterior neural plate and the presumptive eye field (Bovolenta et al., 1998; Kobayashi et al., 1998; Loosli et al., 1998; Oliver et al., 1995; Seo et al., 1998; Zhou et al., 2000). Overexpressing *six3* in medaka, a Japanese rice fish, leads to ectopic induction of eyes and retinal hyperplasia (Loosli et al., 1999). Gain-of-function test in zebrafish also shows enlarged rostral forebrain in response to *six3* overexpression (Kobayashi et al., 1998). *Six6* expression is detected in retinal progenitor cells, ventral hypothalamus, and pituitary precursors (Jean et al., 1999;

Lopez-Rios et al., 1999; Toy et al., 1998). Overexpression of *Six6* promotes cell proliferation in the developing eye (Zuber et al., 1999). Six3 and Six6 are considered to act as transcriptional repressors (Kobayashi et al., 2001; Lopez-Rios et al., 2003; Zhu et al., 2002). The CDKs inhibitor p27kip1 is identified as the potential target of Six3 and Six6, given the fact that p27kip1 is upregulated in *Six6* null retinal cells and the cell proliferation is reduced (Li et al., 2002).

The Chx10, a paired-like homeodomain/CVC domain-containing transcription factor, is exclusively expressed in the proliferating neuroblasts of the neuroretina and plays a pivotal role in promoting cell proliferation (Chen and Cepko, 2000; Levine et al., 1997; Liu et al., 1994). Mutations in *Chx10* cause severe hypoplastic neuroretina in mice without affecting cell fate specification and differentiation (Burmeister et al., 1996; Green et al., 2003; Liu et al., 1994). Cells with *Chx10* mutation have extended cell cycle progression due to delayed G1 phase (Green et al., 2003). Studies show that Chx10 regulates p27Kip activity in a post-transcriptional mechanism (Green et al., 2003). The *Chx10* mutant can be rescued by introducing p27Kip1, indicating a genetic regulation between a homeobox gene and a cell cycle inhibitor (Green et al., 2003). It remains unclear what is the direct target of Chx10 in regulating p27Kip1 activity.

In contrast to the genes mentioned above, which promote cell proliferation, *Prox1*, plays a negative role in cell proliferation. Prox1 is the vertebrate orthologue of the *Drosophila* Prospero, which is required for asymmetric cell division and cell cycle exit (Jan and Jan, 2001; Li and Vaessin, 2000). Prospero represses transcription of the central cell cycle genes including *cdc25*, *cyclin E,* and *cyclin A* in *Drosophila* (Jan and Jan, 2001; Li and Vaessin, 2000). In vertebrates, *Prox1* expression precedes the CDKs inhibitors such as p27Kip1 and p57Kip2 and is involved in promoting cell cycle exit (Dyer et al., 2003). The

detailed molecular basis, including whether Prox1 plays a direct role in cell cycle exit remains to be investigated.

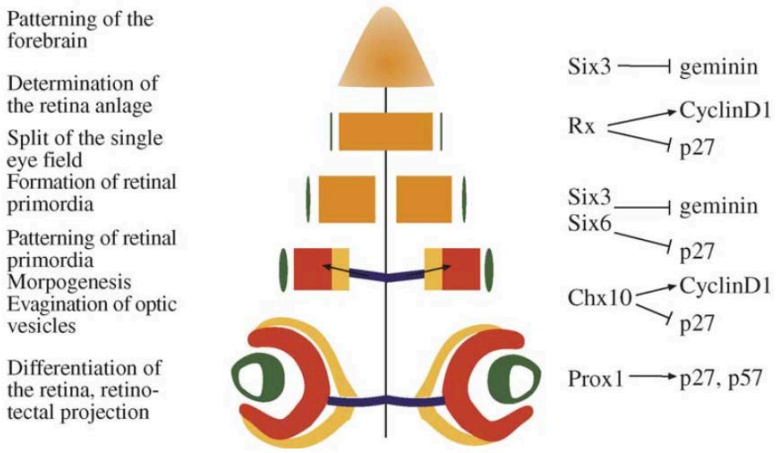

Figure 1.19 Homeobox genes controlling cell proliferation during anterior neural plate development. Adapted from (Del Bene and Wittbrodt, 2005).

Outside the central nervous system, there are a number of examples showing the role of homeobox genes in regulating cell cycle. Homeobox genes *Msx1* and *Msx2* are crucial for the embryonic mammary gland development (Chen and Sukumar, 2003; Visvader and Lindeman, 2003). Both genes are expressed in the epithelium of the developing mammary bud and have partially redundant functions (Chen and Sukumar, 2003; Phippard et al., 1996; Visvader and Lindeman, 2003). *Msx1*, *Msx2* double mutant mice display developmental arrest of the mammary gland (Satokata et al., 2000). Overexpression of *Msx1*, however, leads to failure in normal differentiation of mature lobule-alveolar tubule-alveolar structures (Hu et al., 2001). It has been proposed that the Msx1 may inhibit terminal differentiation by preventing cell cycle exit and cyclin D1 might be the primary target of Msx1 (Hu et al., 2001). Consistent with this idea, overexpressing Msx1 in the mammary gland leads to impaired differentiation of multiple mesenchymal and epithelial cell types with increased cyclin D1 and CDK4 activity (Hu et al., 2001).

Intriguingly, *Msx1* overexpression does not increase cell proliferation and the cyclin D1 is not directly activated by Msx1. These results suggest that the relationship between Msx1 and cell cycle is more complex than initially expected and worth more investigation.

In skeletal muscle regeneration, satellite cells compose the stem cell pool, re-entering the cell cycle to proliferate and repair the tissue (Seale et al., 2001). Once the repair process is done, some of these cells become quiescent again without terminal differentiation, maintaining their stem-cell property (Seale et al., 2001). It has been shown that the Pax7, a homeobox transcription factor, is required for maintaining the satellite cell pool (Seale et al., 2000). Mice lacking *Pax7* do not form satellite cells while overexpressing *Pax7* forces proliferating myoblasts to exit the cell cycle and repress myogenic markers like MyoD (Olguin and Olwin, 2004; Oustanina et al., 2004; Seale et al., 2000). These results indicate that the right dosage of *Pax7* is crucial for maintaining the stem cell population. It does not show, however, which cell cycle genes are the potential target of Pax7. Another homeobox gene *Gax* is expressed in adult vascular smooth muscle and embryonic cardiac, smooth and skeletal muscle (Gorski et al., 1993; Skopicki et al., 1997). Gax is downregulated in the G0/G1 transition in response to the mitogenic activation in *in vitro* experiments (Gorski et al., 1993). The Cdk inhibitor p21Cip1 is implicated as the direct target of Gax (Gorski and Leal, 2003; Smith et al., 1997). Under normal conditions, Gax maintains the quiescent state of the cells via direct activation of p21Cip1 (Gorski and Leal, 2003; Smith et al., 1997). In tissue regeneration, the Gax expression is decreased in response to vascular injury, and cell proliferation is activated for tissue repair (Gorski et al., 1993).

Since the homeobox genes encode transcription factors, it is very natural to think that the cell-cycle regulation by homeobox transcription factors occurs only at the

transcriptional level, either through activation or repression of cell cycle genes. These transcription factors can act more directly through protein-protein interaction. For example, the homeobox protein Tlx1 (also known as Hox11), which is required for spleen development, physically interacts with the protein phosphatases PP2A and PP1 (Kawabe et al., 1997). Yeast two-hybrid experiments show that Tlx1 directly binds to the catalytic subunit of PP2A and PP1 (Kawabe et al., 1997). This interaction is further validated in Jurkat cells (Kawabe et al., 1997). In *Xenopus* oocytes and mammalian cells, overexpression of *tlx1* releases the G2 arrest, which can also be achieved by selectively inhibiting PP2A and PP1 via okadaic acid treatment (Kawabe et al., 1997). During cell cycle, PP2A and PP1 dephosphorylate and inactivate Cdc25 family proteins, which are required for the activation of the Cdk1/Cyclin B complex that is essential for the G2/M transition (Perdiguero and Nebreda, 2004). Some homeobox transcription factors like Six3 and Six6 adopt a novel mechanism regulating the cell cycle by direct binding to and inhibiting the cell cycle modulator Geminin (Bene et al., 2004; Luo et al., 2004). Gemini is identified in two independent and parallel screens that in one screen, Geminin can arrest cell cycle by inhibiting the initiation of S-phase (McGarry and Kirschner, 1998). Whereas in the other screen, Geminin is shown to induce premature neural cell differentiation (Kroll et al., 1998). Geminin inhibits S-phase initiation by sequestering Cdt1, a key component of the pre-replicative complex (Tada et al., 2001; Wohlschlegel et al., 2000). Two independent yeast two-hybrid screen shows that Geminin physically binds with Six3 and other Hox proteins (Luo et al., 2004; Tessmar et al., 2002). In medaka, the Geminin and Six3 act in an antagonistic manner to regulate cell proliferation in the early-stage eye development (Bene et al., 2004). Overexpressing Geminin phenocopies the Six3 loss-of-function mutant, whereas inhibiting Geminin promotes the proliferation of retinal progenitor cells, similar to the Six3 overexpression (Bene et al., 2004; Loosli et al., 1999). Studies have shown that Geminin binds to Hox

proteins, preventing Hox proteins from binding to DNA (Luo et al., 2004). On the other hand, Hox proteins can displace Geminin from Cdt1, suggesting a bi-directional regulation between cell cycle and Hox proteins (Luo et al., 2004). Interestingly, in a screen for human cDNAs that can rescue budding yeast from lethality caused by ectopic expression of human cyclin E, they isolated a cDNA encoding *ESXR1* (Ozawa et al., 2004). *EXSR1* is a paired-like homeobox gene mainly expressed in the placenta and testis in human (Fohn and Behringer, 2001). ESXR1 harbors a proline-rich repeat in its C-terminal domain and mammalian cells, and the protein undergoes proteolytic cleavage (Ozawa et al., 2004). The C-terminal fragment stays in the cytoplasm and arrests cells in the M-phase by inhibiting the degradation of ubiquitinylated cyclins. While the N-terminal fragments containing the HD translocate to the nucleus and may act as a transcription factor (Ozawa et al., 2004). These results show that a single homeobox protein may have the capacity to "multitask" at the same time to coordinate developmental patterning and proliferation.

2.3 Cell cycle and cell fate determination

2.3.1 G1 phase: The major time window of differentiation signal exposure

The G1 phase is the time window for cells to get exposed to induction signals. In *Dictyostelium* development, amoeba becomes pre-spore cells if they sense starvation in the G1 phase (Gomer and Firtel, 1987). The duration of the G1 phase can vary among different cell types. In peri-implantation embryos, pluripotent stem cells (PSCs) have a shorter cell cycle length, primarily due to the shorter G1 phase. As cells differentiate into germ layer species, the G1 phase is extended and so does the total cell cycle (Lawson and Pedersen, 1992; Mac Auley et al., 1993; Snow and Bennett, 1978). This trend is also applied in cultured PSCs in that PSCs undergo rapid cell division with truncated G1 phase and G2 phase (Boward et al., 2016). Consequently, PSCs spend more than half

of the time in the S phase. When cells differentiate into other lineages, the G1 phase lengthens, increasing the cell cycle duration (Boward et al., 2016). The change of cell cycle duration is primarily due to the altered regulation of CDK activity (Faast et al., 2004; Stead et al., 2002; White et al., 2005). The prevalent model explaining the relationship between pluripotency and cell division proposes that the low G1-phase/high S-phase maintains pluripotency by limiting the G1 time window when cells get exposed to differentiation signals. This model is partially supported by studies showing that inhibiting CDK activity to selectively extend the G1 phase in human PSCs leads to spontaneously differentiation of the PSCs (Neganova et al., 2009; Ruiz et al., 2011). However, inhibiting CDK activity in mouse ESCs has no impact on the spontaneous differentiation (Li et al., 2012). Whether these differences may be organism or cell-line specific remains to be determined.

The fact that PSCs respond to specification signals in the G1 phase has been demonstrated for a long time (Mummery et al., 1987; Pierce et al., 1984; Wells, 1982). However, it is not until the development of the fluorescence ubiquitin cell cycle indicator (FUCCI) reporter system that people can start to directly visualize this process in a detailed manner (Sakaue-Sawano et al., 2008). It has been shown that the mesoderm and endoderm lineage commitments occur in the early G1 phase, whereas ectoderm is specified only in the late G1 phase (Pauklin and Vallier, 2013). Such difference is due to the elevated activity of SMAD2/3 activity in the early G1 phase and the inactivation of SMAD2/3 in the late G1 phase ((Pauklin and Vallier, 2013). The inactivation of SMAD2/3 at a late stage is dependent on the CDK4/6-cyclin D activity (Pauklin and Vallier, 2013). These experiments demonstrate how lineage specification is partitioned into different stages of the G1 phase. Another study focuses on changes of epigenetic events during cell cycle (Singh et al., 2015). In human PSCs, researchers find that the H3K4

trimethylation (H3K4me3) level in bivalent domains of developmental genes is increased in the G1 phase, while the level of repressive H3K27me3 remains constant throughout the cell cycle (Singh et al., 2015). Consistent with this observation, the developmental genes with increased H3K4me3 become transcriptionally competent in the G1 phase, suggesting that these genes are primed for activation in G1 phase and can be triggered whenever the proper upstream signaling is on (Singh et al., 2013). Chromatin conformation-capture (4C) assays show the formation of DNA loops connecting distal enhancers with proximal promoters concomitant to the G1-specific epigenetic changes and increased CDK2 activity (Singh et al., 2015). These results indicate a synergistic effect of epigenetics, chromosome architecture, and transcription factor recruitment for priming developmental genes for G1-specific differentiation. These activities may potentially be coordinated by CDKs. The Cyclin D activity is also involved in G1-specific cell fate determination in a CDK-independent manner (Pauklin et al., 2016). Cyclin D is able to independently recruit transcriptional co-activators and co-repressors to target developmental genes in the late G1 phase (Pauklin et al., 2016). In ectoderm differentiation, cyclin D1 recruits the co-activator p300 to ectoderm genes and increases H3K4me3 at these genes. Recruitment of cyclin D1 is dependent on SP1 (Pauklin et al., 2016). In endoderm differentiation, the p300 is initially recruited to the target genes at the early G1 phase when cyclin D1 is absent. When cyclin D1 accumulates in late G1, it recruits histone deacetylases (HDACs) to replace p300, leading to increased repressive H3K27me3 and decreased histone acetylation on these genes. The cyclin D1 recruitment in endoderm is dependent on E2F (Pauklin et al., 2016). These results suggest that the cyclin D1 can directly interact with transcription factors and the mechanism of recruiting cyclin D1 is context-specific. In summary, these studies point out that the cell fate decision and the cell cycle machinery are tightly linked, primarily through epigenetic modifications.

2.3.2 Mitotic advantage in nuclear reprogramming and cell identity switching

In contrast to the G1 phase, which plays important role in cell fate decision during cell differentiation. Mitosis opens a time window for efficient reprogramming of terminally differentiated cells (Campbell et al., 1996; Egli et al., 2008; Halley-Stott et al., 2014; Soufi et al., 2012; Soufi et al., 2015). In M phase, most transcription-associated factors are dissociated from the chromatin (Egli et al., 2008; Gottesfeld and Forbes, 1997; Spencer et al., 2000). Global histone acetylation also disappears during mitosis, while many repressive histone methylations are retained (Kruhlak et al., 2001; McManus and Hendzel, 2006). The whole-genome landscape seems to be reset and ready for rewriting. It has been shown that the condensed chromatin structure in M phases is favored by reprogramming factors like OCT4, SOX2, and KLF4 (Soufi et al., 2012; Soufi et al., 2015). These factors preferentially access to closed chromatin, facing less competency during M phase (Soufi et al., 2012; Soufi et al., 2015). One hypothesis is that these reprogramming factors bind to chromatin to mark the mitotic chromatin, enabling gene priming immediately following exit from mitosis and prior to gene reactivation. However, it is not known whether the priming of these factors is random or regulated by other factors. It is hard to predict which genes will be prioritized for activation after mitosis and whether they will be beneficial for acquiring pluripotency.

In studies of somatic nuclear transfer in *Xenopus*, using nuclei from actively dividing cells promotes rapid cell cycle entry and progression, which is essential for embryo development (Lemaitre et al., 2005). Permeabilizing mouse embryonic fibroblasts (MEFs) to *Xenopus* mitotic egg extract, not interphase extract leads to decreased H3K9, H3K4, and H4K20 di- and trimethylation as well as an increase in expression of pluripotency-associated genes (Ganier et al., 2011). Using mouse fibroblast nuclei

exposed to the mitotic extract for somatic cell nuclear transfer (SCNT) results in a 4-fold increase in the reprogramming efficiency (Ganier et al., 2011). To understand why the mitotic status of a donor nucleus can enhance the efficiency of cell reprogramming, permeabilized adult mouse myoblast cells of different cell cycle stages are transferred into *Xenopus* oocytes of which the nuclei have been removed (Halley-Stott et al., 2014). These experiments show that transferring cells with nuclei in the late G2 or M-phase leads to a robust increase in response to reprogramming factors in *Xenopus* oocytes (Halley-Stott et al., 2014). The expression of pluripotency genes is up to 100 times faster than observed with interphase donor nuclei (Halley-Stott et al., 2014). This phenomenon is termed “mitotic advantage” (Halley-Stott et al., 2014). The mitotic advantage, however, cannot be explained by histone acetylation, phosphorylation, or methylation (Halley-Stott et al., 2014). It seems that the loss of ubiquitination on histones H2A and H2B is necessary, but not sufficient to confer a mitotic advantage (Joo et al., 2007). Studies using the cytoplasm of interphase cells from mouse two-cell stage embryos show that somatic cells in SCNT can be reprogramed in the cytoplasm, as long as the donor nucleus and recipient cytoplasm are synchronized (Kang et al., 2014). This suggests that the mitotic advantage is a matter of cell cycle coordination, not the presence of special proteins present in the recipient cytoplasm only, or a special chromatin configuration of the donor nucleus. One explanation could be that the nuclear envelope acts as the major barrier to cell synchronization, which is diminished in the mitosis and therefore, promotes cell synchronization and cell reprogramming in SCNT (Blow and Laskey, 1988; Campbell et al., 1993).

2.3.3 Cell cycle exit and terminal differentiation

Exit from the cell cycle in G1 phase is usually the prerequisite for terminal differentiation. In most cases, terminal differentiation is linked to the upregulation of CDK inhibitors

(CDKIs). CDKIs inhibit CDK activity during G1 phase and cause hypophosphorylation of the retinoblastoma (RB) tumor suppressor protein family, repressing the E2F target genes for further cell cycle activity (Bandara and La Thangue, 1991; Chellappan et al., 1991; Chittenden et al., 1991). In general, the terminal differentiation and the cell cycle progression are mutually antagonistic. In skeletal myogenesis, the myogenic transcription factors like MYOD are inhibited by CDKs, keeping cells in an immature, proliferative state (Guo and Walsh, 1997; Rao et al., 1994; Skapek et al., 1995). In neurogenesis process, the CDKs inhibit pro-differentiation factors such as NGN2 (NEUROG2) (Hardwick and Philpott, 2014). On the other hand, MYOD, once expressed, counteracts the impact of CDKs by activating the expression of genes encoding CDKIs such as $CIP1^{p21}$ and $KIP2^{p57}$ (Busanello et al., 2012; Halevy et al., 1995; Parker et al., 1995). Inhibiting CDKs leads to cell cycle arrest concomitant with the activation of neurogenic events (Choksi et al., 2006; Li and Vaessin, 2000). In *Drosophila* neuroblasts, the homeodomain transcription factor *prospero* inhibits expression of central cell cycle genes such as *Cyclin E* and *string*, as well as activates transcription of the CDKI gene *dacapo*, suggesting an inverse relationship between the cell cycle and terminal differentiation (Choksi et al., 2006; Li and Vaessin, 2000). Therefore, the balance of the CDK activity and transcription factor activity is crucial for cell fate determination.

2.3.4 Cell cycle, not always required for cell fate changes

The cell cycle is tightly linked to cell fate decision in many cases. However, the cell cycle is not always required for changing cell identity. Ectopic expression of NGN3 (NEUROG3), PDX1, and MAFA in mice lead to cell fate switch from exocrine to endocrine pancreatic cells without cell proliferation (Zhou et al., 2008). Ectopic expression of ASCL1, BRN2(POU3F2), and MYT1L in fibroblasts leads to trans-

differentiation into neurons (Vierbuchen et al., 2010). Notably, ASCL1 drives adult hippocampal stem cells to re-enter the cell from the quiescent state during differentiation, whereas ASCL1 drives somatic cells to exit from the cell cycle in trans-differentiation (Treutlein et al., 2016; Urban et al., 2016). Again, these results suggest that the mechanisms of transcription factors regulating cell cycle and determining cell fate can be very context-specific, probably determined by the dosage of the protein and the pre-existing molecular landscape of the starting cell (Masserdotti et al., 2016). Conversion of pre-B cells to macrophage-like cells can be achieved under proliferative and non-proliferative conditions, although detailed molecular mechanisms remain unknown (Di Tullio and Graf, 2012). Although these examples do show that cell division is not always the pre-requisite for cell fate determination, in most cases, active cell division plays a central role in switching cell fate. In zebrafish, cardiac regeneration is tightly linked to cell cycle regulators including polo-like kinase 1 (plk1) in proliferating cardiomyocytes (Jopling et al., 2010; Poss et al., 2002). Reprogramming cells back to the pluripotent state is often impeded by the reduced proliferative capacity of the starting cells (Hong et al., 2009; Kawamura et al., 2009; Ruiz et al., 2011; Utikal et al., 2009). These observations raise the question that why the cell cycle re-entering is not always required in cell fate changes. One theory proposed that whether cells need to re-enter the cell cycle for cell fate change is determined by the barriers that cells confront when changing cell fate. Reprogramming fibroblasts to the pluripotent cells requires erasure and rewriting of the DNA-methylation signature, which usually occurs in the S phase (Lister et al., 2009; Lister et al., 2011). While conversing pre-B cells to macrophage-like cells does not require the change of epigenetic landscapes, and cells do not need to re-enter the cell cycle (Di Tullio and Graf, 2012). So far, evidence supporting this theory is still very limited. It is also possible that whether cells enter cell cycle for cell fate switch is solely dependent on whether the transcription factors activate CDKs activity or not.

Section 3 DNA replication

3.1 Overview of DNA replication

DNA replication is the fundamental biological process to transmit genetic information to descendants. It has been recognized nowadays that eukaryotic DNA replication requires three major polymerases for synthesizing nascent DNA, DNA polymerase α (Pol α), DNA polymerase ε (Pol ε), and DNA polymerase δ (Pol δ). However, decades have been taken to build the current canonical model of DNA replication. Pol α is the first polymerase discovered and was considered to be the sole polymerase responsible for bulk DNA synthesis during replication (Bollum and Potter, 1957). The identification of Pol δ as a new mammalian DNA polymerase with proofreading exonuclease activity breaks the prior assumption (Byrnes et al., 1976). Studies of simian virus 40 (SV40) confirm that both Pol α and Pol δ are required for efficient DNA replication (Lee et al., 1989; Prelich and Stillman, 1988; Weinberg and Kelly, 1989). A third eukaryotic DNA polymerase, which was initially categorized as Pol δ, is shown structurally distinct from Pol δ and therefore reclassified as Pol ε (Chang, 1977; Syvaoja et al., 1990; Wintersberger and Wintersberger, 1970). Pol ε is also essential in yeast proliferation and like Pol δ, Pol ε contains proofreading exonuclease activity (Morrison et al., 1990). Based on these observations, a replication model is proposed: Pol α initiates synthesis by adding primers onto both strands, after which Pol ε synthesizes the leading strand and Pol δ replicates the lagging strand (Morrison et al., 1990; Sugino, 1995).

For the following decades, this model has been strongly supported by numerous pieces of evidence. In *Saccharomyces cerevisiae* (budding yeast), a Pol ε mutant strain shows that DNA synthesis errors are specifically accumulated in a reporter gene in leading strands, not lagging strands (Pursell et al., 2007). Another experiment using a Pol δ

mutant strain shows that more than 90% of Pol δ synthesis occurs on the lagging strand (McElhinny et al., 2008). The same results are also seen in the later study using *Schizosaccharomyces pombe* (fission yeast) (Miyabe et al., 2011). Ribonucleotide-promiscuous polymerase variants are used to map polymerase usage during replication, which generates higher resolution and statistically stronger data (McElhinny et al., 2010). Ribonucleotide incorporation by a Pol ε variant is biased to the leading strand in budding yeast and fission yeast, while ribonucleotide incorporation by a Pol δ variant is mapped to the nascent lagging strand (Lujan et al., 2014; Lujan et al., 2012; McElhinny et al., 2010; Miyabe et al., 2011). In recent five years, advances in the protocols and methods of ribonucleotide incorporation have further increased the mapping resolution (Clausen et al., 2015; Koh et al., 2015; Lujan et al., 2016; Reijns et al., 2015). In both budding and fission yeast, the Pol ε variant predominantly incorporates ribonucleotides in the leading strand, while Pol δ preferentially incorporates ribonucleotides in the lagging strand (Clausen et al., 2015; Daigaku et al., 2015; Koh et al., 2015; Lujan et al., 2016; Reijns et al., 2015). These data, again, support the generally accepted model that Pol ε and Pol δ are responsible for leading strand and lagging strands synthesis, respectively.

During DNA replication, a group of proteins constitutes the replisome at the progressing eukaryotic replication fork (**Figure 1.20**). The DNA helicase, CMG (Cdc45-Mcm2-7-GINS), encircles and translocates along the leading strand and excludes the lagging strand (Fu et al., 2011; Georgescu et al., 2017). Mcm2-7 comprise the ATP-dependent motor subunits to unwind the DNA double strand. On the lagging strand, Pol α-primase synthesizes multiple short RNA-DNA primers before strand polymerization by Pol δ. On the leading stand, only one RNA-DNA primer is needed for Pol ε-mediated leading strand synthesis. Pol ε is targeted to the leading strand by direct interaction with CMG

(Langston et al., 2014; Sun et al., 2015). Pol2 is the catalytic subunit of Pol ε and contains tandem repeats of polymerase modules. The N-terminal repeat is required for DNA synthesis and the C-terminal repeat (with no catalytic activity) interacts directly with Mcm2 and Mcm5 (Goswami et al., 2018). In *in vitro* biochemical experiments, Pol ε is preferentially recruited to CMG when CMG was preloaded onto the leading strand of the replication fork (Georgescu et al., 2014; Sun et al., 2015). The association between Pol δ and the leading strand is not stable and can be displaced by Pol ε in the presence of CMG (Georgescu et al., 2014). Pol ε is more intrinsically processive than Pol δ (Chilkova et al., 2007). The processivity of Pol ε is further enhanced by the low binding affinity with proliferating cell nuclear antigen (PCNA), the eukaryotic sliding clamp (Chilkova et al., 2007). On the contrary, Pol δ binds tightly to PCNA regardless of the presence of DNA (Johansson et al., 2004). This strong interaction allows Pol δ to outcompete Pol ε to get access to a primed DNA template in the presence of PCNA (Burgers, 1991; Georgescu et al., 2014). Furthermore, the presence of the single-stranded DNA binding protein RPA further slows down synthesis by Pol ε in the primer extension assay (Georgescu et al., 2014). The tight interaction with PCNA and the presence of RPA promote the recruitment of Pol δ for the primed lagging-strand synthesis (Georgescu et al., 2014). In addition, Pol δ shows higher efficiency in strand displacement synthesis than Pol ε, an activity critical for Okazaki fragment maturation (Balakrishnan and Bambara, 2013; Garg et al., 2004). The recent structural analysis of DNA-bound human Pol δ-PCNA-FEN1(flap endonuclease 1) complex also supports the idea that Pol δ is suitable for the lagging-strand synthesis (Lancey et al., 2020).

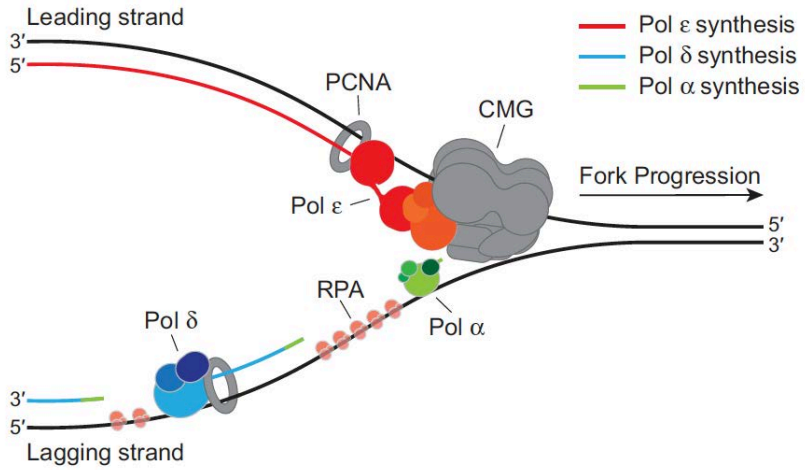

Figure 1.20 Distribution of DNA polymerases at the replication fork. Pol δ (blue), Pol ε (red), Pol α (green) (Guilliam and Yeeles, 2020a)

Recently, origin-dependent eukaryotic DNA replication is reconstituted *in vitro* using proteins purified from budding yeast (Yeeles et al., 2015). Pol δ can partially perform leading-strand synthesis when Pol ε is catalytically inactive (Yeeles et al., 2017). The synthesis rate, however, cannot reach the maximum as seen *in vivo* unless the wildtype Pol ε is present (Yeeles et al., 2017). Pol ε still preferentially synthesizes the leading strand even the interaction between Pol ε and PCNA is disrupted (Aria and Yeeles, 2019). On the contrary, Pol δ is not required for rapid synthesis of leading strand but is important for maximal lagging-strand synthesis and Okazaki fragment maturation (Devbhandari et al., 2017; Guilliam and Yeeles, 2020b; Yeeles et al., 2017). These studies further support the current canonical model of polymerase labor of division.

Although the prevailing model is generally accepted, a series of recent studies point out the involvement of Pol δ in leading-strand synthesis. For example, in genome-wide mapping of polymerase usage in fission yeast, leading-strand synthesis by Pol δ at the initiation period is observed (Daigaku et al., 2015). In *in vitro* reconstitution assays, the

total amount of leading-strand synthesis is increased in the presence of Pol δ (Yeeles et al., 2017). Since the CMG-coupled leading-strand synthesis by Pol ε cannot be displaced by Pol δ, the increase in DNA synthesis might be due to the involvement of Pol δ at the initiation stage before the CMG-coupled synthesis is established (Yeeles et al., 2017). Recent ribonucleotide mapping experiments have confirmed that Pol δ is present in the initiation of leading-strand synthesis in all *S.cerevisiae* origins (Garbacz et al., 2018; Zhou et al., 2019). These results clearly demonstrate that Pol δ is required for the initiation of leading-strand synthesis. A series of other *in vitro* reconstitution studies show that Pol δ is also involved during the elongation of the leading strand synthesis (Aria and Yeeles, 2019; Devbhandari and Remus, 2020; Yeeles et al., 2017). An estimated 18% of leading-strand synthesis in budding yeast is executed by Pol δ (Zhou et al., 2019). Apparently, more work is required to investigate the role of Pol δ synthesis and to determine whether the canonical model needs to be modified based on the incoming discoveries.

3.2 DNA polymerase delta (Pol δ)

3.2.1 Structure of Pol δ

In budding yeast, Pol δ contains three subunits: the catalytic subunit Pol3 and two structural subunits Pol31 and Pol32 (Boulet et al., 1989; Gerik et al., 1998; Sitney et al., 1989). X-ray scattering studies of yeast Pol δ reveal that Pol δ is a heterotrimer (Jain et al., 2009). Pol31 tethers to the C-terminal cysteine-rich domain of Pol3 while Pol31 binds tightly to Pol3 (Jain et al., 2009). In mammalian cells, Pol δ consists of 4 subunits: the catalytic subunit p125 (POLD1, corresponding to yeast Pol3), which is the core factor for DNA polymerization; the other 3 subunits, p50 (POLD2, corresponding to Pol31), p66 (POLD3, corresponding to Pol32) and p12 (POLD4), are thought to be the regulatory proteins to facilitate PCNA binding (Byrnes et al., 1976; Hughes et al., 1999; Lancey et

al., 2020; Lee et al., 1984; Liu et al., 2000; Swan et al., 2009; Zhou et al., 2012). Human POLD1 protein is encoded by the *POLD1* gene, which is also known as *CRCS10*, *CDC2,* and *MDPL*. *POLD1* is located on chromosome 19 at q13.3-q13.4. The *POLD1* transcript contains 27 exons, which translates into a 1107 amino acid (Chung et al., 1991; Kemper et al., 1992; Nicolas et al., 2016). A detailed structure of human Pol δ has been deciphered through Cryo-Electron Microscopy (Cryo-EM) (Lancey et al., 2020). During DNA synthesis, Pol δ associates tightly with PCNA (Bravo et al., 1987). The p125 and p50 comprise the core mammalian enzyme capable of being stimulated by PCNA (Wang et al., 2011; Zhou et al., 2012). At least one accessory subunit, either p68 or p12, is required to be associated with p125/p50 core complex for DNA synthesis, as shown in the presence of PCNA on the M13 gapped plasmid (Zhou et al., 2011). The p12 subunit can enhance the processivity of p125/p50/p68 by up to 15-fold *in vitro* (Podust et al., 2002). The p125 catalytic subunit of Pol δ consists of two major functional domains: an exonuclease domain close to the N-terminus with 3'-5' exonuclease activity for DNA proofreading, and a polymerase domain near the C-terminus that catalyzes 5'-3' DNA synthesis (Jain et al., 2009; Swan et al., 2009). The polymerase domain is divided into the palm, finger, and thumb domains (Franklin et al., 2001; Swan et al., 2009). The palm contacts the nascent duplex DNA, providing the catalytic side chains. The thumb domain holds the DNA duplex to maintain the structural integrity during DNA synthesis. The finger domain is responsible for dNTP incorporation (Franklin et al., 2001; Swan et al., 2009). The C-terminal domain contains two cysteine-rich motifs and a subdomain critical protein-protein interaction (Brocas et al., 2010; Cullmann et al., 1993).

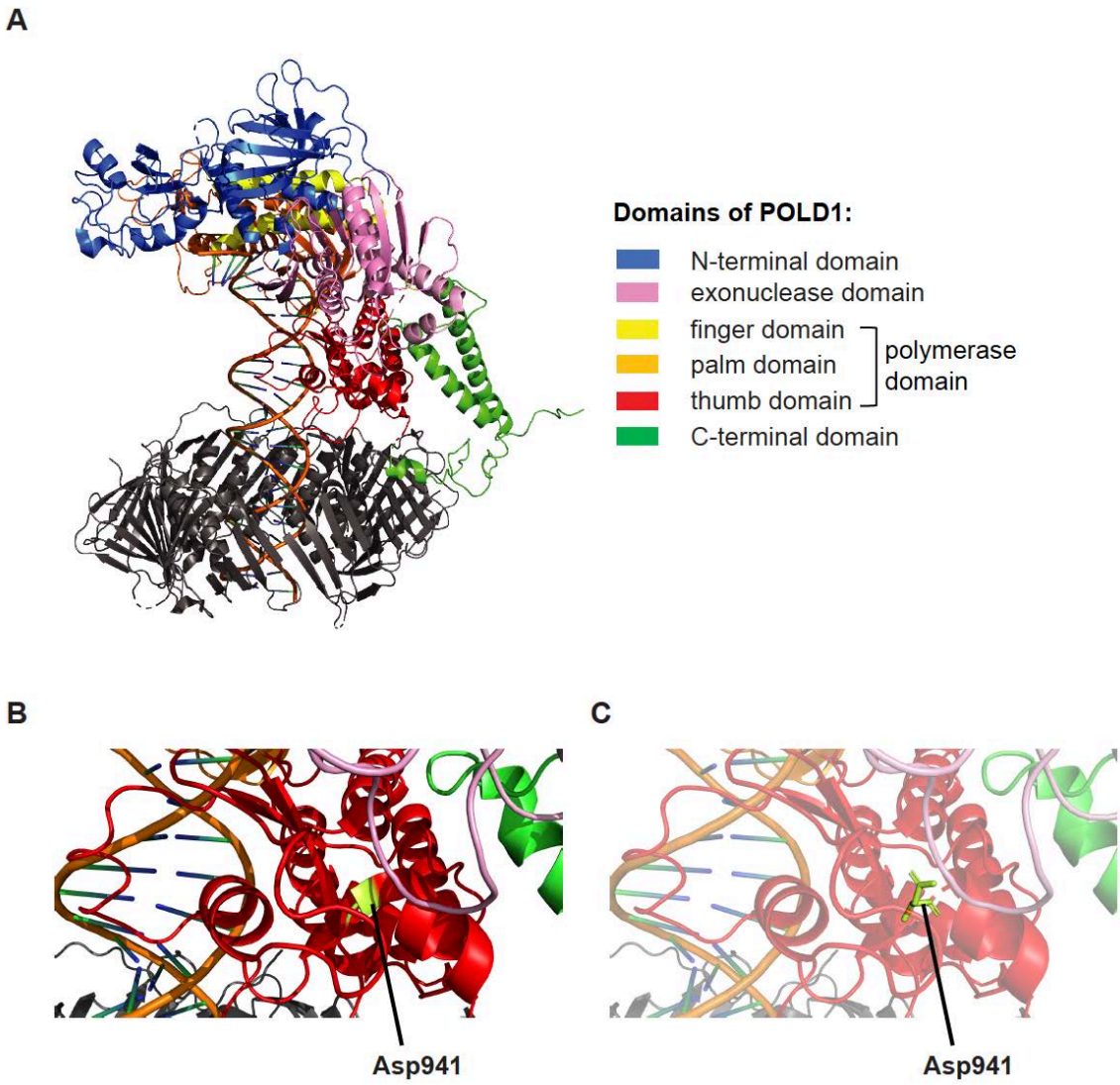

Figure1.21 Cryo-EM structure of human POLD1 associated with DNA duplex and PCNA. Cryo-EM structure of human POLD1 associated with DNA duplex and PCNA. (A) Colored-coded domain structure of the POLD1-PCNA complex bound to DNA. (B) Zoomed-in image showing the POLD1 thumb domain (red). The mutated Asp941(D941) corresponding to mouse Asp939 (D939) residue is highlighted in lime. (C) Zoomed-in image showing the POLD1 thumb domain. The mutated Asp 941(D941) residue is shown as the lime stick. The protein structure information was extracted from protein data bank (PDB). Structure ID: 6TNY. PDB DOI: 10.2210/pdb6TNY/pdb. The original protein structure was adapted using PyMOL to convey information relevant to this study.

3.2.2 Regulation of Pol δ expression in cell cycle

During cell cycle, *POLD1* transcription reaches the highest level in the late G1/S phase when genomic DNA is replicated before mitosis. *POLD1* transcription activity is tightly regulated by a series of cell-cycle-related proteins through a series of protein binding motifs inside its promoter region. The Sp1 (Special protein 1) and Sp3 (Special protein 3) bind to the 11-bp direct repeats to induce *POLD1* expression upon serum stimulation (Zhao and Chang, 1997). p53 competes with Sp1 binding to this site and represses Sp1-stimulated *POLD1* expression (Li and Lee, 2001). The *POLD1* promoter also contains a cell cycle element/cell cycle gene homology region (CDE/CHR) that is only 50 bp downstream of the transcription start site. The CDE/CHR is crucial for transcription activity in the G2/M phase (Song et al., 2009). Mutations inside this region cause defects in regulating POLD1 activity by E2F and p21 (Song et al., 2009). *POLD1* promoter activity is also positively regulated by Forkhead family proteins such as FOXO3a (Chen et al., 2016). Overexpression of microRNA miR-155 suppresses *FOXO3a* expression and inhibits *POLD1* transcripts and protein expression (Czochor et al., 2016). Besides, the *POLD1* promoter can be epigenetically repressed by PRMT7 (protein arginine methyltransferase 7) and BRG1-based hSWI/SNF chromatin remodeling complex in response to DNA damage. Knocking down PRMT7 results in a decreased methylation level of histone H2A and H4 in the *POLD1* promoter region and increased POLD1 protein level, making cells more resistant to DNA-damaging agents (Karkhanis et al., 2012).

3.2.3 Pol δ in DNA replication and repair

The molecular function of Pol δ in DNA replication is mainly addressed through biochemical studies and yeast genetics: *In vitro* DNA replication assay reveals that plasmids containing the Simian Virus 40 (SV40) DNA replication origin can be fully

synthesized by adding purified mammalian cell extracts containing Pol δ (Tsurimoto et al., 1990; Tsurimoto and Stillman, 1991). In fission yeast, the temperature-sensitive *cdc2* (the orthologue of *POLD*1) mutant causes cell-cycle arrest, with about 70% of the genomic DNA being synthesized before the cell cycle was arrested. This thermosensitive *cdc2* allele can be complemented by wildtype Pol δ+ isolated from fission yeast. Conversely, replacing wildtype Pol δ in fission yeast with the other three Pol δ thermosensitive conditional lethal alleles results in cell cycle arrest in the S phase, indicating that Pol δ is required for DNA synthesis (Francesconi et al., 1993). In addition, numerous pieces of evidence supports the central role of Pol δ in lagging strand synthesis as well as its participation in leading strand synthesis, which has been discussed before.

The high-fidelity DNA replication depends on the proofreading function of Pol δ. Wildtype Pol δ is highly accurate due to the presence of a fully functional exonuclease domain (Byrnes et al., 1976; Morrison et al., 1993; Simon et al., 1991). When encountering aberrant DNA structures, Pol δ pauses dNTP incorporation and activates the exonuclease activity (Meng et al., 2009). The exonuclease domain harbors the metal-coordinating site which is essential for removing the terminal nucleoside from the primer strand (Beese and Steitz, 1991; Lancey et al., 2020; Swan et al., 2009). Mutations in either the coordinating aspartate or the glutamate disrupt the exonucleolytic activity (Morrison et al., 1991; Morrison et al., 1993; Simon et al., 1991). *In vitro* mutation rate measurements on M13mp2-*LacZ* gapped plasmid show that purified yeast proofreading-deficient Pol δ (*Pol3-01,* D321A/E323A) displays a 10- to 100- fold higher mutation rate than the wildtype Pol δ (Fortune et al., 2005; Jin et al., 2001; Morrison et al., 1993; Venkatesan et al., 2006). In human Pol δ, deficient exonuclease activity also increases

the misincorporation rate to a similar extent compared to the wildtype exonuclease activity in the same assay (Schmitt et al., 2009). Exonuclease function can also be triggered when dNTP concentration is high (Reha-Krantz, 2010).

The high-fidelity DNA replication not only relies on the precise removal of mismatched nucleotides by Pol δbut also depends on its activity in the post-replicative DNA repair system. Pol δ heterotetramer turns to POLD1/2/3 heterotrimer when encountering DNA damage or replication stress induced by UV irradiation or other DNA damage agents (Lee et al., 2014; Meng et al., 2010). In human embryonic kidney 293 (HEK293) cells, depleting POLD1 leads to cell cycle arrest in G1 and G2/M phases, indicating DNA damage checkpoint responses (Song et al., 2015). Inhibiting *POLD1* expression through miR-155 overexpression increases the genome instability (Czochor et al., 2016). Mouse embryonic fibroblasts (MEFs) harboring D400A amino acid change in the exonuclease domain display impaired single-strand break repair (Parsons et al., 2007). Replication errors that escape the proofreading process by polymerases are subject to mismatch repair (MMR) (Kunkel and Erie, 2005; Modrich, 2006). HeLa cell nuclear extracts without mismatch repair activity can be complemented by adding repair proficient cell extracts together with Pol δ or by purified calf thymus Pol δ alone (Longley et al., 1997; Modrich, 1997). Genetic studies of MMR-deficient yeast and the biochemical assays of human MMR proteins show that Msh2/Msh6 or Msh2/Msh3 use the interactions with PCNA and/or the nicks at the 5'end of Okazaki fragments to identify the nascent strand (Iams et al., 2002; Pavlov et al., 2003; Umar et al., 1996). The Exol, the subdomain inside the exonuclease may enter through these nicks to digest the regions containing mismatches on the lagging strand (Modrich, 1997). An ExoI-independent mechanism is also proposed by the observation that Pol δ undergoes strand displacement synthesis

(Kadyrov et al., 2009). A nicked strand is dissociated away from the complementary strand, creating a flap of DNA cleaved by Flap Endonuclease 1 (Fen1). Pol δ then synthesizes new DNA fragments through the flap (Kadyrov et al., 2009). Taken together, Pol δ plays a diverse role in multiple types of DNA repair and is essential for high-fidelity DNA replication.

3.2.4 POLD1 in human diseases

A broad spectrum of somatic mutations has been identified in multiple cancer types, most of which are missense mutations accumulated in the exonuclease domain and polymerase domain. Germline *POLD1* mutations in the proofreading domain have been discovered and are considered in association with oligo-adenomatous polyposis, endometrial cancer, and colorectal cancer (CRC) (Rayner et al., 2016). Germline POLD1 S478N is detected in patients with MMR-proficient multiple colorectal adenomas and early-onset CRC (Palles et al., 2013). Other POLD1 germline variants, including P327L and L474P, are detected in a multiple adenoma patient and a hereditary nonpolyposis CRC family, respectively (Briggs and Tomlinson, 2013; Valle et al., 2014). POLD1 proofreading domain-specific mutations in hereditary CRC is dominant with high penetrance. This condition is clinically defined as “polymerase proofreading associated polyposis” (PPAP) (Briggs and Tomlinson, 2013). Nevertheless, the PPAP syndrome accounts for only 0.1-0.4% of hereditary cancer cases, suggesting a low prevalence of POLD1 germline alterations in the familial cancer predisposition (Mur et al., 2020). It has been recently brought to the attention that POLD1 variants can be served as potential biomarkers to select patients suitable for cancer immunotherapy (Bourdais et al., 2017). *In vitro* analysis of POLD1 R689W, for example, has shown synthetic lethality with mutations in ATR (ataxia telangiectasia and Rad3 related), a DNA damage response regulator involved in PD-L1 regulation at the post-translational level. This could increase

the sensitivity of CRC cells to ATR inhibitors and potentially, immunotherapeutic treatments (Hocke et al., 2016; Job et al., 2020).

POLD1-related genetic disorders are extremely rare in the population. The mandibular hypoplasia, deafness, progeroid features, and lipodystrophy (MDPL) syndrome is the representative genetic disease considered to be associated with *POLD1* mutation (Weedon et al., 2013). Patients with this multisystem disorder feature sensorineural deafness, mental retardation, insulin resistance, progressive lipodystrophy with lack of subcutaneous adipose tissue and accumulation of abdomen adipose tissue, as well as low testosterone level observed in male patients (Elouej et al., 2017; Fiorillo et al., 2018; Nicolas et al., 2016; Sasaki et al., 2018; Weedon et al., 2013). Whole-genome sequencing of 5 unrelated MDPL patients revealed a *de novo* serine 605 deletion inside a conserved motif containing the catalytic aspartate inside the polymerase activity site. S605 deletion causes the loss of catalytic function of POLD1. Mutated POLD1 binds to DNA strand but no polymerization occurs (Nicolas et al., 2016; Weedon et al., 2013). A six patient carries an R507C mutation located in the highly conserved ExoIII domain (amino acid 504 - 525), the function of which has not been characterized yet (Nicolas et al., 2016; Weedon et al., 2013). The exact molecular mechanism behind the phenotype remains a mystery, but it does indicate that the ubiquitously expressed *POLD1* gene may have tissue-specific effects.

3.2.5 POLD1 in development and gene expression control

In contrast to detailed structure and molecular function studies of Pol δ in cell extracts or yeast genetics, the function of POLD1 in development remains largely unclear, especially in the field of development. A preliminary study in *Arabidopsis* brings out the potential function of *POLD1* in gene expression control through epigenetic regulation:

gis5 (*gigantea suppressor 5*) mutant isolated from *Arabidopsis* causes early flowering phenotype (Iglesias et al., 2015). The *gis5* harbors a C to T transition in exon 18 of *POLD1*, leading to an Alanine to Valine substitution in amino acid position 707 (A707V) (Iglesias et al., 2015). Further epigenetic analysis reveals that the SEP3 and FT genes controlling flowering process are upregulated as a consequence of increased levels of H3K3me3, raising the possibility that POLD1 might involve in histone rearrangement or epigenetic modulation (Iglesias et al., 2015). In animals, zebrafish mutants harboring homozygous *pold1* mutant allele *flathead* (*fla*), display specific defects in late proliferative zones such as eyes, brain, and cartilaginous elements of the visceral head skeleton (Plaster et al., 2006). Cells in late proliferative zones show reduced DNA replication followed by apoptosis and can be rescued by p53 deficiency (Plaster et al., 2006). In rodents, *Pold1* homozygous null allele leads to peri-implantation lethality (Uchimura et al., 2009). Although $Pold1^{-/-}$ blastocysts appear normal, *ex vivo* culture of $Pold1^{-/-}$ blastocysts shows drastic defects in cell outgrowth, with high apoptosis and low DNA synthesis (Uchimura et al., 2009). A few other *Pold1* mutants have been generated in mice to study tumorigenesis: In the same study, $Pold1^{exo/exo}$ or $Pold1^{exo/-}$ mice harboring D400A exchange in the exonuclease domain suffered from tumorigenesis (Uchimura et al., 2009). Another study in heterozygous $Pold1^{+/L604K}$ mice indicates that these mice are viable and fertile but display accelerated tumor progression and reduced lifespan compared to wildtype littermates (Venkatesan et al., 2007). In primary embryonic fibroblasts culture, $Pold1^{+/L604K}$ cells show higher chromosome aberration, indicating increased chromosome instability (Venkatesan et al., 2007). $Pold1^{L604K/L604K}$ embryos died in uterus around E8.5 post-fertilization, with no phenotype being reported from this line (Venkatesan et al., 2007). In general, the very limited number of mouse models makes it challenging to explore the function of POLD1 in embryonic development.

Section 4 Introduction to the thesis

Gastrulation is a critical developmental process required for germ layer formation and the establishment of the body plan (Arnold and Robertson, 2009). Gastrulation initiates with the emergence of the primitive streak in the proximal posterior epiblast. As the streak extends to the distal tip of the embryo, epiblast cells undergo an epithelial-mesenchymal transition (EMT) to form the mesoderm layer between the epiblast and the visceral endoderm (VE)(Kinder et al., 1999; Lawson, 1999; Lawson et al., 1991). Epiblast cells ingressing through the anterior region of the elongating primitive streak intercalate into the VE to form the definitive endoderm layer, which will give rise to the gut tube, and subsequently, the epithelium of endodermal organs, such as the pancreas and intestine(Kwon et al., 2008b; Lawson et al., 1986; Lawson and Pedersen, 1987). Gastrulation requires tight spatiotemporal coordination of cell number expansion, cell migration, and cell fate determination. Despite extensive research on these topics, it has been challenging to untangle the complex interplay among these three key components. Previous studies used embryological methods in pre-implantation embryos to investigate size regulation during the pre- and early-gastrulation stages. These experiments found that double-sized embryos, formed by aggregating two 8-cell stage morula, underwent size regulation before gastrulation. The double-sized embryos showed an increase in cell-cycle length compared to controls; in addition, they lacked the proliferative burst that normally occurs before gastrulation. These two modes of regulating cell proliferation allowed the aggregated embryos to reach a normal size and cell number before E7.0 and then to gastrulate (Buehr and McLaren, 1974; Lewis and Rossant, 1982). Conversely, undersized mouse embryos generated by removing one or two blastomeres from the 4-cell stage preimplantation embryo, sustained a prolonged proliferative burst, leading to an increase in cell number before the initiation of gastrulation(Power and Tam,

1993). Another study on size regulation in the mammalian embryo examined the response to reduced cell number in the early post-implantation embryo, an experimentally more refractory stage. Following treatment with mitomycin to inhibit cell proliferation, E7.0 embryos, with ~80% of their cells eliminated, could still recover and complete gastrulation (Snow and Tam, 1979). These elegant studies suggest that intrinsic mechanisms operate within the pre- and early post-implantation embryo to monitor and control cell number both before and at the onset of gastrulation, supporting regulative development as an important feature of early mammalian embryogenesis. However, it is technically challenging to apply standard embryological and pharmacological methods to investigate how altered cell number in the gastrulating embryo impacts tissue patterning and morphogenesis. Therefore, to ask whether mechanisms of size regulation continue to act during gastrulation, it is beneficial to explore alternative approaches to perturbing cell number, such as genetic manipulation.

Although many genes encoding cell cycle-related proteins have been genetically inactivated to explore the effects of cell proliferation on embryo size and morphogenesis, the resulting phenotypes are generally not suitable for studies of gastrulation. For example, *Cyclin A2* (*Ccna2*) homozygous null mutants can be recovered only up to E5.5(Murphy et al., 1997), whereas embryos lacking all D-type cyclins survive past gastrulation, with no overt phenotypes(Kozar et al., 2004). Other targets for genetic perturbation of cell proliferation are the polymerases that replicate DNA. DNA Polymerase Delta (Pol δ), the subject of this report, plays multiple critical roles in DNA replication, with functions in DNA synthesis and repair(Jain et al., 2018). In mammalian cells, the Pol δ contains 4 subunits: the catalytic subunit, p125 (Pold1), and three regulatory subunits, p50 (Pold2), p66 (Pold3), and p12 (Pold4). Pold1 consists of two

functional domains: an N-terminal 3'-5' exonuclease with DNA proofreading activities and a C-terminal DNA polymerase that catalyzes DNA synthesis. Several mutant alleles have been generated for Pold1, but similar to targeted cell cycle-related genes mentioned above, the homozygous mutants either fail to survive beyond the onset of gastrulation or show no phenotypic defects during gastrulation. Null mutations in *Pold1* cause peri-implantation lethality (Uchimura et al., 2009). Two missense mutations have been reported for Pold1: a D400A substitution in the exonuclease domain and an L604K substitution in the DNA polymerase activity site (Fig. S1A)(Uchimura et al., 2009; Venkatesan et al., 2007). While developmentally normal, $Pold1^{D400A/D400A}$ mice frequently died with swollen thymuses 3 months after birth (Uchimura et al., 2009). $Pold1^{+/L604K}$ heterozygous mice underwent normal development but had a reduced lifespan and developed multiple tumor types, including lymphoma, adenoma, and carcinomas of the liver and lung (Venkatesan et al., 2007). Although no specific phenotypes were reported for $Pold1^{L604K/L604K}$ embryos, notably they died around E8.5, suggesting that missense mutations in the polymerase domain might perturb cell proliferation at a level compatible for the investigation of gastrulation phenotypes.

In this study, we report a *Pold1* hypomorphic mutation identified in a phenotype-based genetic screen for recessive mutations causing gastrulation defects in mouse embryos. This mutation altered a conserved residue (D939Y) in the Pold1 DNA polymerase domain, caused reduced Pold1 protein expression, and resulted in compromised DNA synthesis. Mutant embryos could be retrieved up to E8.5; at this stage, they were small with a siren-like morphology; hence we named the mutant *tiny siren* (*tyrn*). We investigated embryo growth and cell lineage differentiation in *tyrn* mutants at developmental stages between E6.5 and E8.5. The *tyrn* mutation impaired cell proliferation without affecting anterior-posterior patterning, but severely disrupted tissue

morphogenesis during gastrulation. Our findings suggest normal cell proliferation is essential for mesoderm lineage allocation and is required to coordinate embryo size with cell movement for proper morphogenesis.

Chapter 2 Results

Section 1. Identification of *tyrn* mutant from ENU mutagenesis screen.

2.1.1 *tyrn* mutant embryos show abnormal morphology but proper anterior-posterior polarity

To study the genetic regulation of gastrulation, we performed mouse ENU mutagenesis screens to uncover genetic disruptions in embryos with abnormal morphology at E8.5 (Garcia-Garcia et al., 2005; Hernandez-Martinez et al., 2019; Huangfu et al., 2003; Migeotte et al., 2011). We isolated a mutant (later named *tyrn*) that exhibited not only a smaller overall size, but also a striking body shape and orientation (**Figure 2.1**) that was distinct from other mutant phenotypes we had observed at this stage (Bazzi et al., 2017; Garcia-Garcia et al., 2005; Hernandez-Martinez et al., 2019; Huangfu et al., 2003; Migeotte et al., 2011; Zhou and Anderson, 2010). Instead of forming a U-shaped embryo with a well-extended A-P axis, the *tyrn* mutant embryos had a short A-P axis and lay relatively flat along the posterior side of the yolk sac, with the head misoriented towards the distal tip (**Figure 2.1**). *tyrn* embryos occupied approximately 25% of the total embryos harvested from pregnant mice among various dissection stages, consistent with the ratio predicted by Mendel's Law (**Table 2.1**). To determine if the irregularly shaped mutants had established and correctly positioned the A-P axis, we performed whole-mount *in situ* hybridizations (WISH) at E8.5 to a diagnostic set of markers. We found that although *tyrn* mutant embryos did not form a well-structured head, they did express *Foxg1* and *Otx2*, markers of forebrain and forebrain/midbrain, respectively, in discrete overlapping regions (**Figure 2.2A-B**). In addition, WISH detected relatively normal expression of *T* (*Brachyury*), which marks the posterior tail bud and notochord (**Figure 2.2C**), and of *Foxa2*, which labels the floor plate of the neural tube, posterior notochord, notochordal plate, and gut endoderm (**Figure 2.2D**). Therefore, despite causing a highly unusual body shape, the *tyrn* mutation does not affect A-P patterning.

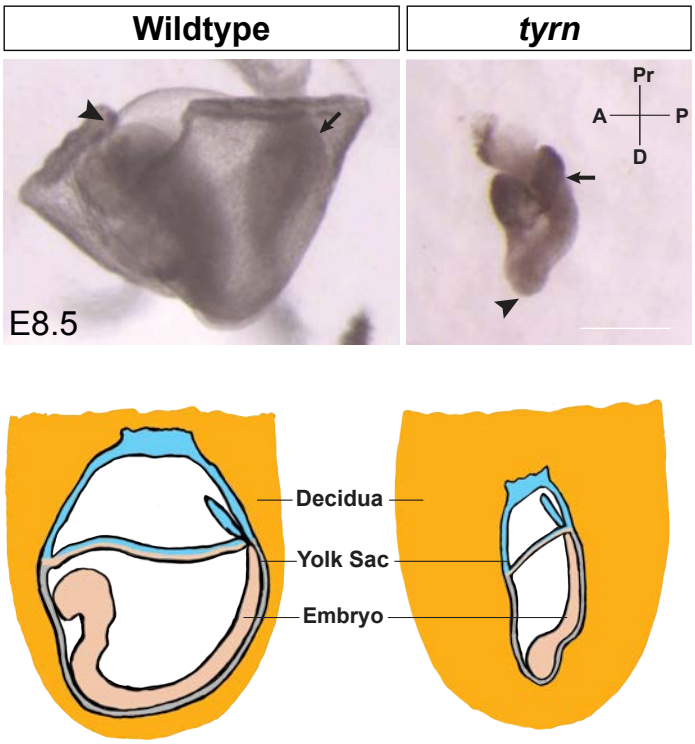

Figure 2.1 Characterization of "*tiny siren* (*tyrn*)" phenotype recovered from ENU Screen. (A) Top: Wildtype and *tyrn* embryos recovered at E8.5. Embryos were aligned as they were in the decidua. Mutant embryos showed a shifted A-P body axis, with a small head located at the distal tip (arrowhead) and the tail at the posterior-proximal side (arrow). Scale Bar = 500 μm. Bottom: A cartoon that shows the orientation of wildtype and mutant embryos inside the decidua.

Stage	Wildtype	*tyrn*	Total
E6.5	64(0.76)	20(0.24)	84
E7.5	50(0.79)	13(0.21)	63
E8.5	47(0.80)	12(0.20)	59

Table 2.1. The number and ratio of wildtype and *tyrn* embryos dissected at E6.5, E7.5 and E8.5 stages. The value in parentheses showed the ratio of wildtype and *tyrn* embryos in total embryos. Embryos were collected from at least 5 pregnant females and were calculated for the ratio.

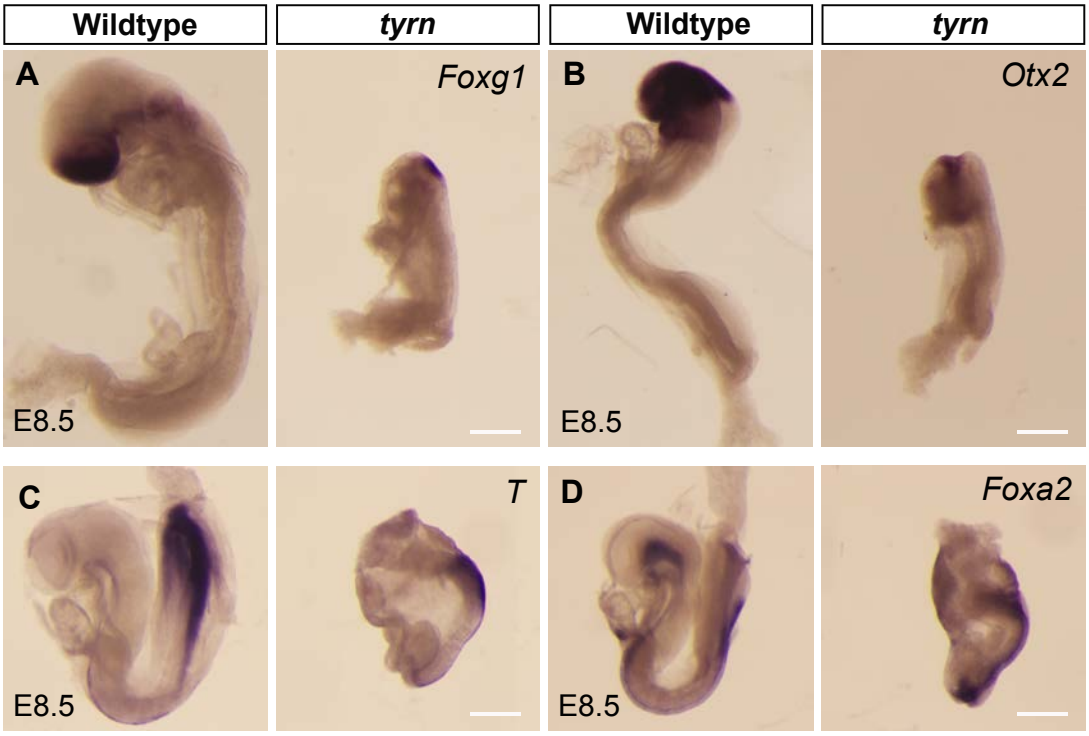

Figure 2.2 Whole-mount *in situ* hybridizations (WISH) of wildtype and *tyrn* embryos at E8.5 stage. (A) *Foxg1* labels forebrain and (B) *Otx2* labels midbrain and forebrain in wildtype embryos. Mutant embryos expressed both *Foxg1* (A) and *Otx2* (B) in the head region. (C)*T* (*Brachyury)* marks the primitive streak and notochord in E8.5 wildtype and *tyrn* embryos. (D) Both wildtype and *tyrn* embryos expressed *Foxa2* in the floor plate, posterior notochord, notochordal plate and gut endoderm. n = 3 embryos per genotype. Scale Bar = 200 μm.

2.1.2 *tyrn* is a hypomorphic allele of *Pold1*

To identify the causative mutation for the *tyrn* phenotype, we collected both wildtype and *tyrn* embryos at E8.5 and performed whole-exome sequencing (Jain et al., 2017). We found a G to T transversion at nucleotide position 2815 of the *Pold1* open reading frame that generated an aspartate to tyrosine substitution (D939Y) within the DNA polymerase domain (**Figure 2.3A**). The mutated aspartate residue is highly conserved across eukaryotic organisms from budding yeast to humans (**Figure 2.3B**). Sequencing results of cDNA from wildtype and *tyrn* embryos showed that *tyrn* produces 2 cDNA fragments around exon 23: The 400bp fragment harbours the G2815T missense mutation; the 700 bp contained unspliced intron 22-23 in addition to G2815T mutation, indicating defects in

exon splicing. The unspliced intron 22-23 contained a stop codon, predicting the presence of a truncated POLD1 protein. However, western blot analysis only showed a reduced level of POLD1 in *tyrn* mutant embryos without any additional bands (**Figure 2.3C**).

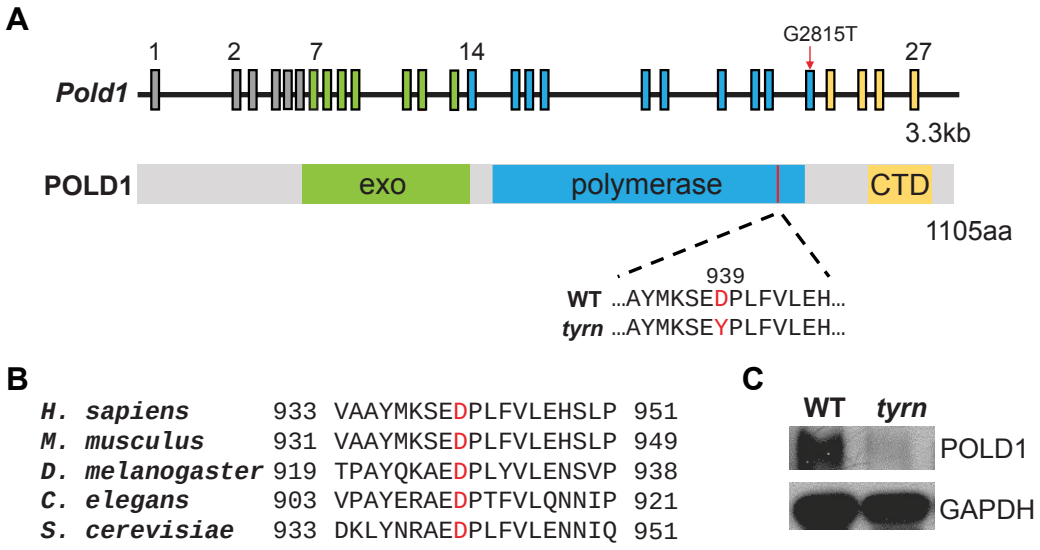

Figure 2.3 Identification of the *Pold1* missense mutation in *tyrn*. (A) Schematic diagrams of the murine *Pold1* genomic locus (upper panel) and of the POLD1 domain structure (lower panel). The G2815T nucleotide change (red arrow) was located in exon 23. The corresponding D939Y amino acid substitution was located in the DNA polymerase domain close to the C-terminal domain (CTD). exo: exonuclease domain. (B) Multiple alignments of orthologous POLD1 amino acid sequences around D939Y among different eukaryotic organisms. The mutated aspartate residue was highly conserved. (C) POLD1 expression level in wildtype (left lane) and *tyrn* (right lane) embryos at E8.5 shown by western blot.

To confirm that *Pold1* is the causative gene underlying the *tyrn* mutant phenotype, we performed a complementation test using the $Pold1^{tm1b}$ null allele, derived from embryonic stem cells carrying a "knockout-first" *tm1a* allele (Skarnes et al., 2011) (**Figure 2.4A**). No $Pold1^{tm1b/tm1b}$ embryos were recovered at post-implantation stages, consistent with the phenotype previously reported for *Pold1* null mutants (Uchimura et al., 2009). The $Pold1^{tyrn/tm1b}$ embryos produced from a $Pold1^{tm1b/+}$ and *tyrn*/+ cross failed to survive past ~E7.5 (**Figure 2.4B**), demonstrating that the *tm1b* and *tyrn* mutations failed to

complement. Moreover, the phenotype displayed by *Pold1*$^{tyrn/tm1b}$ embryos was more severe than that of the *Pold1*$^{tyrn/tyrn}$ embryos, but milder than that of *Pold1*$^{tm1b/tm1b}$ null mutants (**Figure 2.4B-C**). These findings indicate that perturbation of *Pold1* is responsible for the phenotypes observed in *tyrn* mutants and that *Pold1*^{tyrn} is a hypomorphic allele.

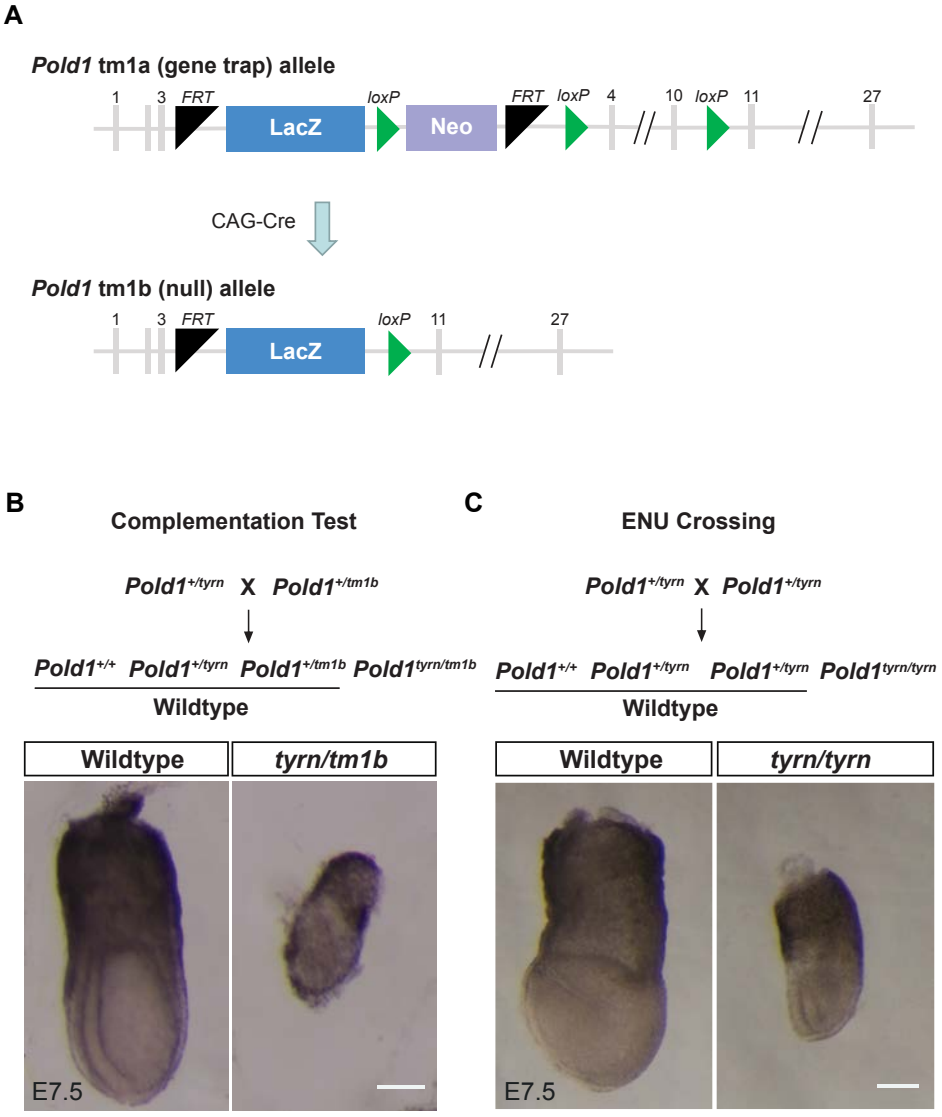

Figure 2.4 Complementation test for validating *Pold1* as the causative gene. (A) Structure of the *Pold1* tm1a (gene trap) allele and the tm1b (null) allele generated after CAG-Cre-mediated recombination. Exons are represented in grey vertical blocks. (B). Complementation test crossing strategy (upper panel). Wildtype and *tyrn/tm1b* embryos acquired at E7.5 from the complementation test (lower panel). *tyrn/tm1b* embryos were not able to survive past E7.5. (C) Crossing strategy to harvest homozygous mutants from

heterozygous mice carrying *tyrn* allele (upper panel). E7.5 wildtype and *tyrn* embryos (lower panel). n = 3 per genotype. Scale Bar = 100 μm.

2.1.3 The *tyrn* mutation impairs DNA synthesis and cell proliferation

Based on the published cryo-electron microscopy structure of the human Pol δ (Lancey et al., 2020), the aspartate residue mutated in *tyrn* embryos resides in the thumb domain of the C-terminal DNA polymerase domain of POLD1 (**Figure 2.3A, Figure 1.21**). Because of the important role of the thumb domain in stabilizing Pol δ at the primer-template junction during DNA synthesis (Jain et al., 2018), we hypothesized that the *tyrn* mutation may impair and reduce the DNA synthesis activity of Pol δ. We used a primer extension assay and mouse EdU labeling to test Pol δ polymerase activity *in vitro* and *in vivo*, respectively. For the primer extension assay, we modeled the mouse Pold1 D939Y missense mutation in budding yeast Pol δ by introducing the equivalent mutation, D941Y, in the yeast catalytic subunit, Pol3 (Devbhandari and Remus, 2020) (**Figure 2.5A**). We purified wildtype Pol δ or Pol δ^{D941Y} (with $Pol3^{D941Y}$) after overexpression in budding yeast (**Figure 2.5B**). Analysis of the DNA synthesis products by denaturing gel-analysis reveals that both overall DNA synthesis and the level of full-length DNA products were significantly reduced in the presence of $Pol3^{D941Y}$ when compared to the wildtype Pol δ (**Figure 2.5C-E**). These data demonstrate that the D941Y substitution in Pol3, and by extension the corresponding D939Y substitution in POLD1, impairs the DNA polymerase activity of Pol δ, possibly by decreasing its processivity.

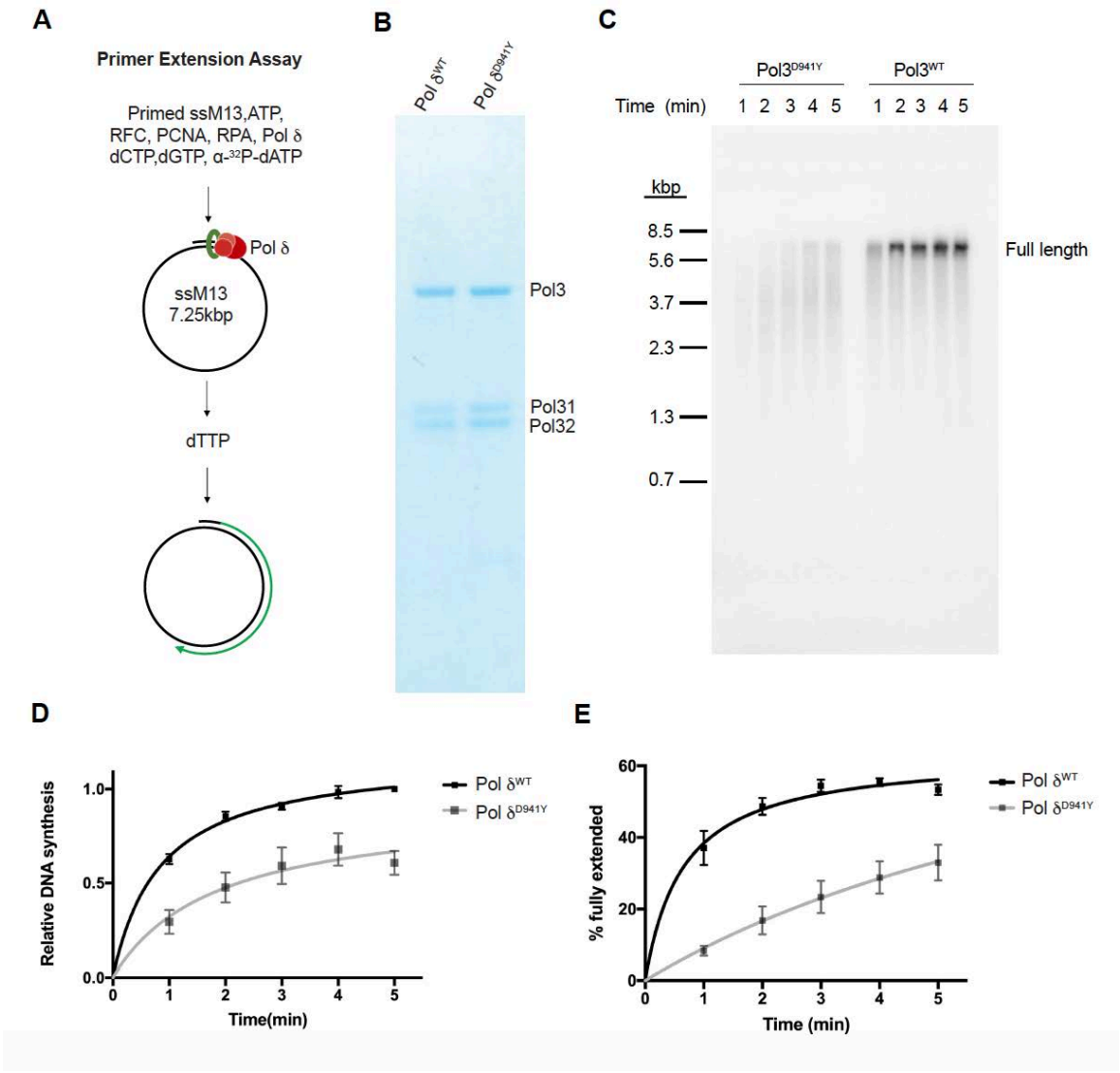

Figure 2.5 The effects of the D941Y mutation in Pol3 on DNA synthesis. (This assay was performed by Dr. Sujan Devbhandari supervised by Dr. Dirk Remus.) (A) Workflow of the *in vitro* primer extension assay. (B) Denatured protein gel showing the overexpressed yeast Pol δ^{WT} and Pol δ^{D941Y}. The Pol3^{WT} and Pol3^{D941Y} corresponds to mouse POLD1^{WT} and POLD1^{D939Y}, respectively. The Pol31 and Pol32 are the associated subunits in Pol δ corresponding to POLD2 and POLD3 in mouse. (C) *In vitro* primer extension assay showing reduction of DNA synthesis efficiency of Pol3^{D941Y}, the yeast orthologue which harbors the corresponding D939Y mutation identified in mouse. (D) Nonlinear-fitted curves of total amount of newly synthesized DNAs at different time points. The mean is represented by black squares (Pol δ^{WT}) and grey squares (Pol δ^{D941Y}). (E) Nonlinear-fitted curves of the percentage of full-length circular DNAs among total products. The mean is represented by black squares (Pol δ^{WT}) and grey squares (Pol δ^{D941Y}). Error bars represent s.e.m. For all time points in (D) and (E), n=3 per genotype. Multiple Student's *t*-test, two-tailed, $p<0.05$.

To test if DNA synthesis is affected in *tyrn* embryos, we performed *in vivo* EdU labeling at E6.0, E6.5, and E7.0, the window of time during which the size difference between wildtype and *tyrn* embryos emerges. We observed a significant reduction in EdU incorporation in *tyrn* mutants compared to wildtype embryos at all stages (**Figure 2.6A-B**). Both wildtype and *tyrn* embryos showed a substantial increase in cell number from E6.0 to E7.0, but *tyrn* embryos exhibited a slower growth rate starting from E6.5; by E7.0 *tyrn* embryos had significantly lower numbers of cells compared to wildtype embryos (**Figure 2.7**). Consistent with the observation in *tyrn* embryos, the *Pold1*$^{tyrn/tm1b}$ embryos from the complementation test also showed reduced EdU incorporation and embryo size compared to wildtype embryos at E6.5 (**Figure 2.8**). The reduction in cell number in *tyrn* embryos is not due to increased cell death; based on cleaved Caspase-3 staining, levels of cell apoptosis were similar between wildtype and *tyrn* embryos during this period (**Figure 2.9**). However, mutant embryos showed increased cell apoptosis at around E7.5, with apoptotic cells concentrated at the distal tip, the prospective location of the abnormal small head at E8.5 (**Figure 2.10**). Taken together, we conclude that the D939Y missense mutation impairs POLD1 polymerase activity, which, together with the reduced POLD1 protein expression in *tyrn* embryos, impedes cell proliferation and leads to a reduction in embryo size during gastrulation.

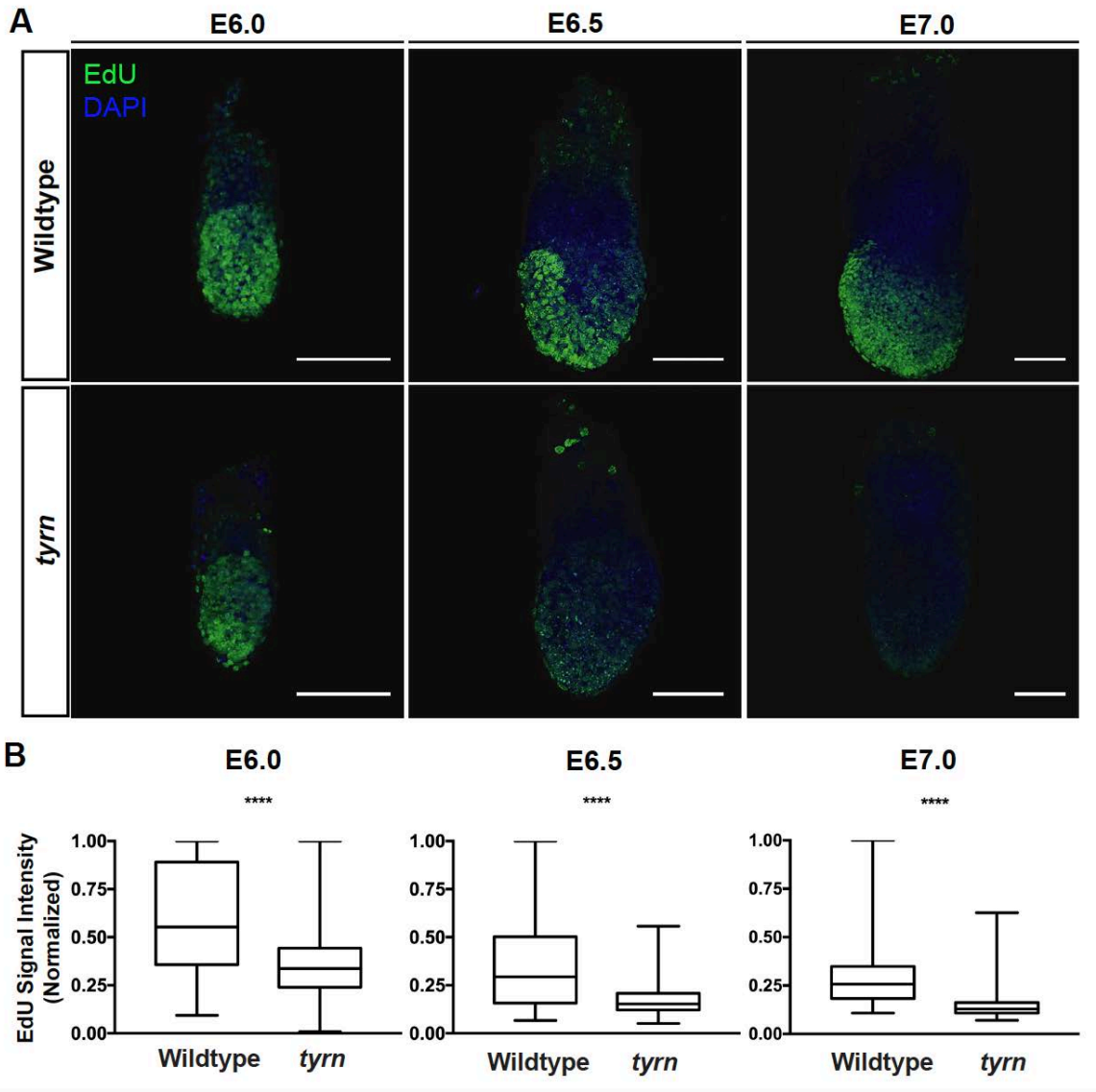

Figure 2.6 Analysis of DNA synthesis in tyrn mutants. (A) EdU incorporation levels in wildtype and *tyrn* embryos at E6.0, E6.5 and E7.0. Green: EdU, Blue: DAPI. n=3 embryos per genotype. Scale Bar = 100 μm. (B) Quantification of EdU signal intensity by box whisker plots. EdU signals of the embryos at the same stage were normalized to the maximum intensity in that stage. Total embryos quantified per genotype: n=3. Unpaired Student's *t*-test, two-tailed. The 4 asterisks indicate $p<0.0001$. In all box plots, the median is represented by the horizontal dividing line; the top and bottom of the box represent, respectively, the seventy-fifth and twenty-fifth percentile, with the whiskers indicating the maximum and minimum points.

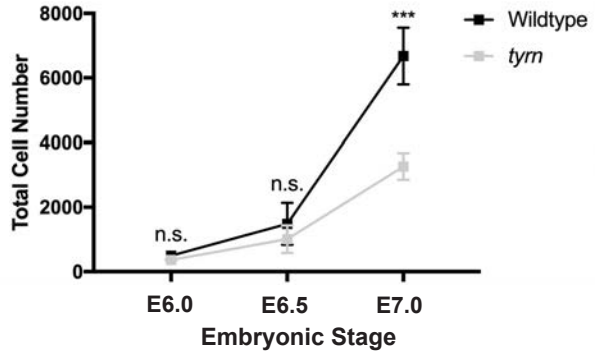

Figure 2.7 Difference of cell number growth between wildtype and *tyrn* embryos. Curves of total cell number in wildtype and *tyrn* embryos at E6.0, E6.5 and E7.0; n=3 embryos per genotype per stage. Unpaired Student's *t*-test, two-tailed, $p<0.001$. Within the curve, the mean is represented by the black (wildtype) and grey (*tyrn*) squares. Error bars represent s.d.

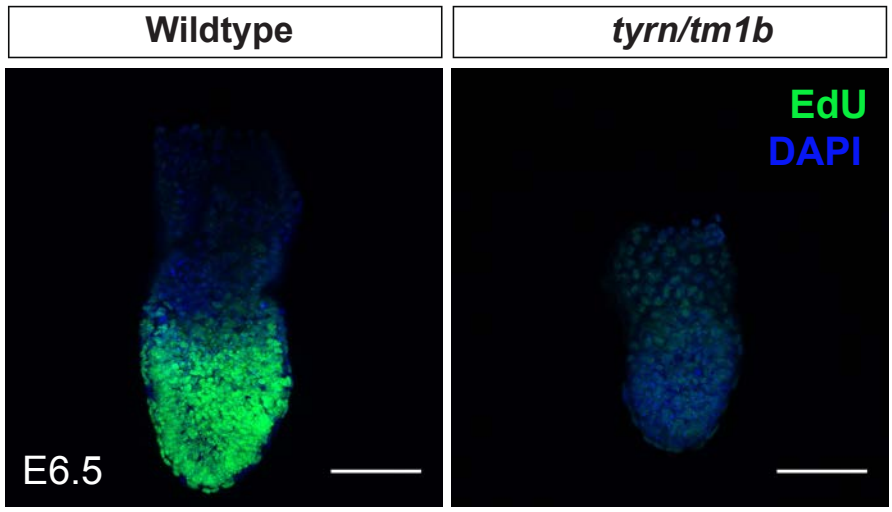

Figure 2.8 EdU incorporation in E6.5 *tyrn/tm1b* embryos. Whole mount staining of E6.5 wildtype and *tyrn/tm1b* embryos from complementation test. EdU (Green) stained for cells undergoing DNA synthesis. DAPI (blue) stained nucleus of all cells. n = 3 per genotype. Scale Bar = 100 μm.

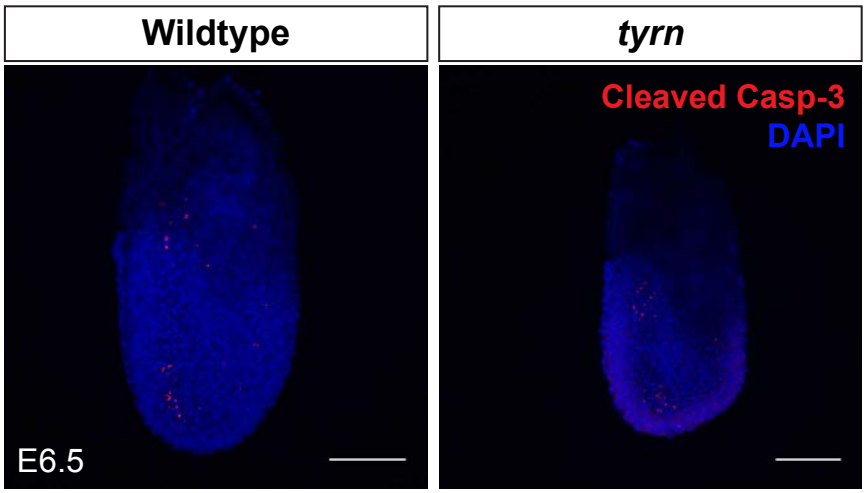

Figure 2.9 Cell apoptosis in E6.5 *tyrn* embryos. Immunofluorescence staining of Cleaved Caspase-3 in wildtype and *tyrn* embryos at E6.5; n = 3 per genotype. Scale Bar = 50 μm.

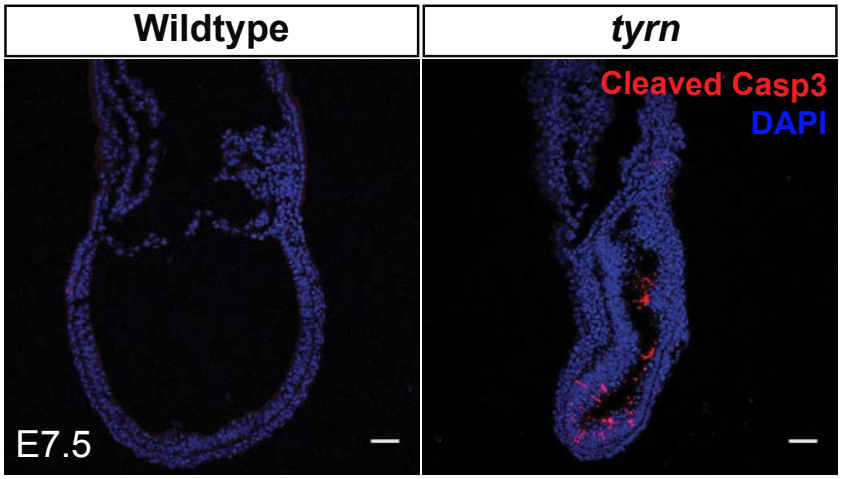

Figure 2.10 Cell apoptosis level in wildtype and *tyrn* embryos at E7.5 stage. Whole mount staining of E7.5 wildtype and *tyrn* embryos with Cleaved Caspase-3 antibodies (Red) for detection of apoptotic cells. DAPI (blue) stained nucleus of all cells. n = 3 per genotype. Scale Bar = 100 μm.

Section 2. Phenotypic analysis of *tyrn* mutants during gastrulation

2.2.1 The *tyrn* mutation does not affect anterior visceral endoderm (AVE) positioning

The mispositioned head, and the abnormal morphology of E8.5 *tyrn* mutants, indicated that the A-P axis, although established, was shifted in orientation along the proximal-distal axis. Proper formation of the A-P axis depends on the anterior migration of a

morphologically distinct population of VE cells from their position at the distal tip of the E5.5 embryo (Rivera-Perez et al., 2003); by E5.75-E6.0 this cell population will reach the anterior epiblast - extraembryonic ectoderm boundary and form the AVE (Srinivas et al., 2004). Multiple studies have shown that defects in AVE migration can lead to abnormal positioning of the A-P axis and mislocalized head phenotypes (Acampora et al., 2009; Clements et al., 2011; Kojima et al., 2014; Lu et al., 2001; Martinez-Barbera et al., 2000; Rossant and Tam, 2009b). Therefore, we asked whether the AVE resided in its normal anterior position in *tyrn* mutants at E6.5. At this stage, the *tyrn* mutants were morphologically indistinguishable from wildtype littermates. WISH showed that *tyrn* mutants expressed two archetypal AVE markers, *Dkk1* (a Wnt antagonist) and *Cerl* (a Nodal antagonist), in a pattern comparable to that of wildtype embryos (**Figure 2.11A-B**). We validated these findings by crossing in the Hhex-GFP transgene reporter to fluorescently label AVE cells in *tyrn* mutants (Rodriguez et al., 2001). Consistent with the *Dkk1* and *Cer1 in situ* hybridization results, we detected the Hhex-GFP expressing AVE cells at the anterior boundary between the embryonic and extraembryonic regions in *tyrn* embryos at E6.5 (**Figure 2.11C**). These results indicate that AVE migration and A-P axis establishment proceed normally in pre-gastrulation stage *tyrn* mutants.

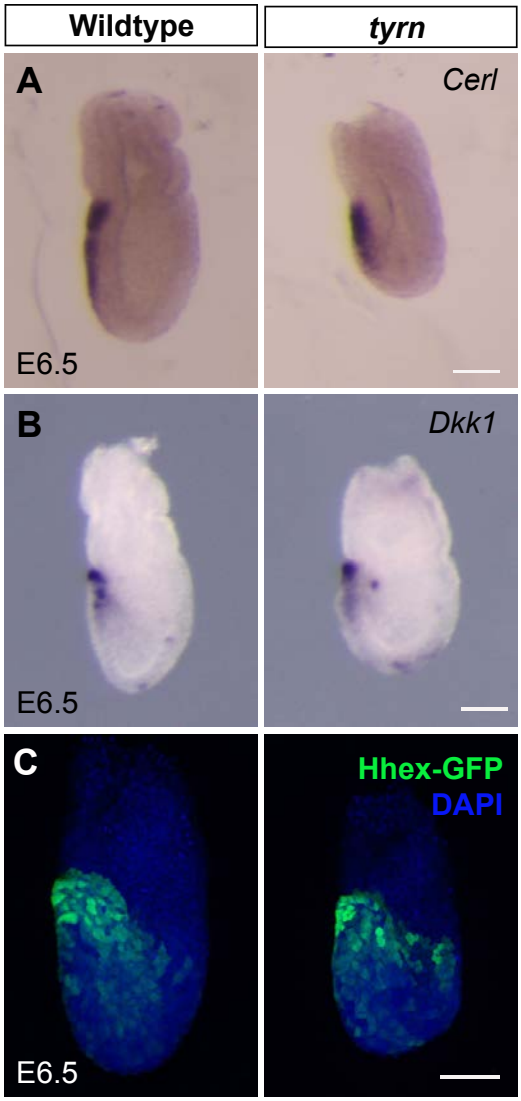

Figure 2.11 Position of Anterior Visceral Endoderm in *tyrn* mutants. *Cerl* (A) and *Dkk1* (B) were expressed in anterior visceral endoderm (AVE) in both wildtype and *tyrn* embryos at E6.5. (C) Hhex-GFP was expressed in AVE in both wildtype and *tyrn* embryos at E6.5. *n* = 3 embryos per genotype. Scale Bar = 50 μm.

2.2.2 The *tyrn* mutation affects primitive streak extension and head position at E7.5

At E6.5, the AVE resided at the expected location in *tyrn* mutants; yet the position of the *tyrn* embryo's anterior region was shifted toward the distal tip at E7.5. We examined the expression of multiple anterior-specific markers to visualize the organization of the anterior region in both wildtype and *tyrn* mutant embryos at E7.5. As depicted in **Figure 2.12A-B**, wildtype embryos expressed SOX2 uniformly throughout the anterior epiblast,

whereas the *tyrn* mutants expressed SOX2 in a discontinuous pattern, with more intense staining in the distal epiblast than in the proximal/anterior region. In the wildtype E7.5 embryo in the left panel of **Figure 2.12C-D**, the Hhex-GFP transgene labeled anterior definitive endoderm (ADE) as well as remaining AVE cells. In contrast, Hhex-GFP expression was evident predominantly in the distal region of the E7.5 *tyrn* mutant, with no obvious A-P asymmetry (**Figure 2.12C-D, right panels**). Similarly, cells expressing *Otx2*, a head organizer marker, lay distally in *tyrn* embryos compared to their anterior position in wildtype embryos (**Figure 2.12E**).

The AVE serves as a transient anterior signaling center at ~E6.5. As gastrulation progresses, AVE cells disperse into the extraembryonic/embryonic boundary and the anterior portion of the extraembryonic yolk sac (Lawson and Pedersen, 1987; Rivera-Perez et al., 2003; Shimono and Behringer, 2003; Tam et al., 2007). Meanwhile, the ADE and axial mesoderm (AME), both of which strongly express Nodal and Wnt antagonists (Arnold and Robertson, 2009), gradually migrate anteriorly and become new sources of anterior signaling. We hypothesized that the abnormal orientation of the A-P axis might reflect the distal positioning of AME and ADE. This hypothesis is consistent with the aforementioned aberrant expression pattern of Hhex-GFP, which labels both ADE and AVE cells. Furthermore, **Figure 2.12A, D, F** examined the expression of *Foxa2*, a marker of AME and ADE, in wildtype and *tyrn* embryos at E7.5. Emerging *Foxa2*-expressing ADE and AME cells reside in the distal anterior region in wildtype embryos, but these cells were observed more posteriorly in *tyrn* mutants.

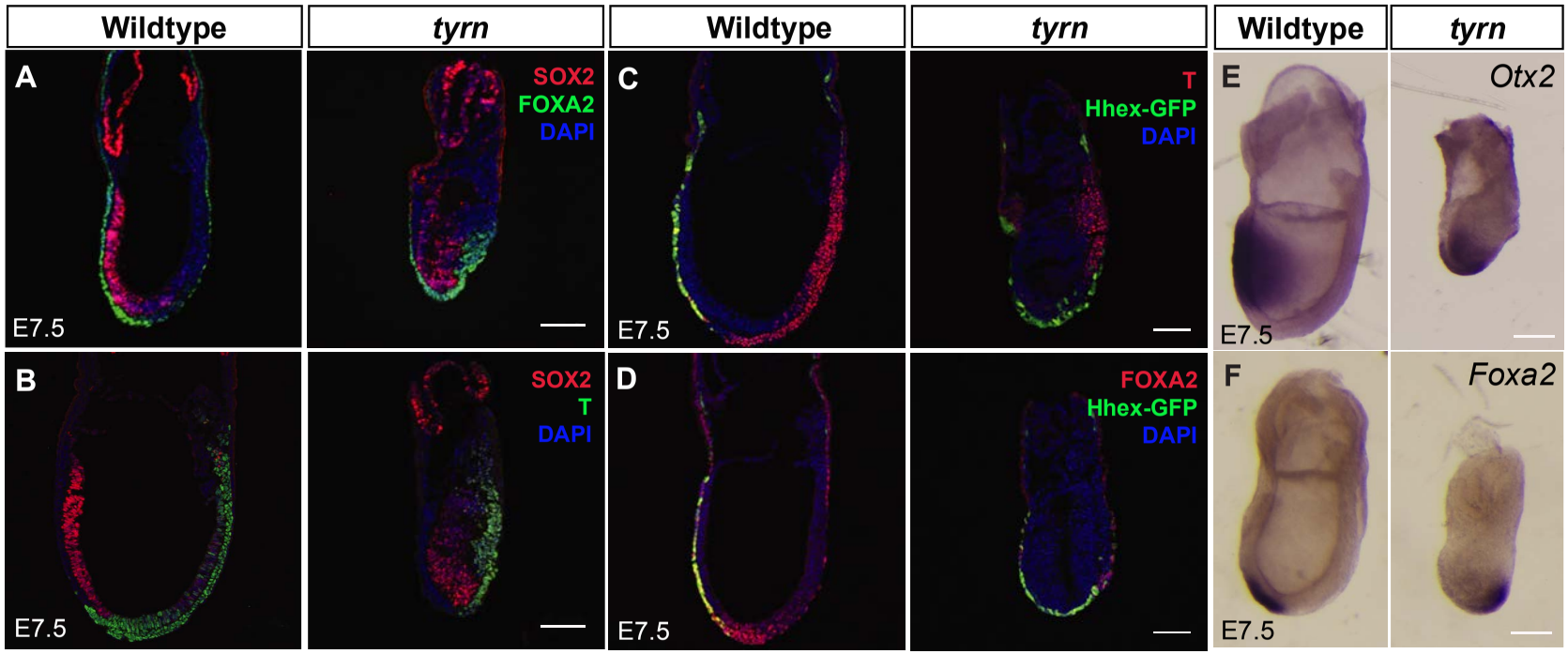
Wildtype
tyrn
Wildtype
tyrn
Wildtype
tyrn
A
SOX2
FOXA2
DAPI
E7.5
C
T
Hhex-GFP
DAPI
E7.5
E
Otx2
E7.5
B
SOX2
T
DAPI
E7.5
D
FOXA2
Hhex-GFP
DAPI
E7.5
F
Foxa2
E7.5

Figure 2.12 Characterization of anterior-posterior (A-P) patterning in *tyrn* mutants during gastrulation. Co-staining of SOX2 with FOXA2 (A) or with T (B). Co-localization of Hhex-GFP with T (C) or FOXA2 (D). The anterior marker SOX2 was strongly expressed at the distal tip in mutants. SOX2 was also expressed in chorionic ectoderm in both wildtype and *tyrn* embryos. T-staining found a shortened primitive streak in *tyrn* mutants; based on staining for Hhex-GFP and FOXA2 AME and ADE cells emerged from the midpoint of posterior side of *tyrn* mutants, in contrast to the distal/anterior region of wildtype embryos. (E) *in situ* hybridization staining of *Otx2* showed that *Otx2* expression was restricted distally in *tyrn* rather than anteriorly, as seen in wildtype embryos. (F) *Foxa2* labels axial mesoderm and definitive endoderm cells in both wildtype and *tyrn* embryos.

The aberrant posterior positioning of ADE and AME, both derivatives of the anterior primitive streak (APS) (Arnold and Robertson, 2009; Lawson, 1999; Lawson et al., 1991), suggested that primitive streak extension was defective in *tyrn* mutants. To compare the organization of the primitive between wildtype and *tyrn* embryos, we performed section immunofluorescence for T (Brachyury), a marker of nascent mesoderm emanating from the primitive streak, including AME (**Figure 2.12B-C**). In E7.5 wildtype embryos, T staining showed that the primitive streak had extended to the distal tip and generated AME derivatives of the anterior primitive streak. In contrast, T staining of E7.5 *tyrn* embryos indicated that the primitive streak had extended only to the midpoint of the posterior side (**Figure 2.12B-C**). Whole-mount embryo immunofluorescent staining showed that the defective primitive streak extension in *tyrn* embryos started to occur at E7.0 when *tyrn* mutant embryos started to show smaller size compared to wildtype embryos (**Figure 2.13A-B**). Taken together, these results suggest that the impaired extension of the primitive streak in *tyrn* embryos causes the distal positioning of the AME and ADE at E7.5. Mutant embryos underwent head morphogenesis and formed a head at the distal tip with abnormal morphology.

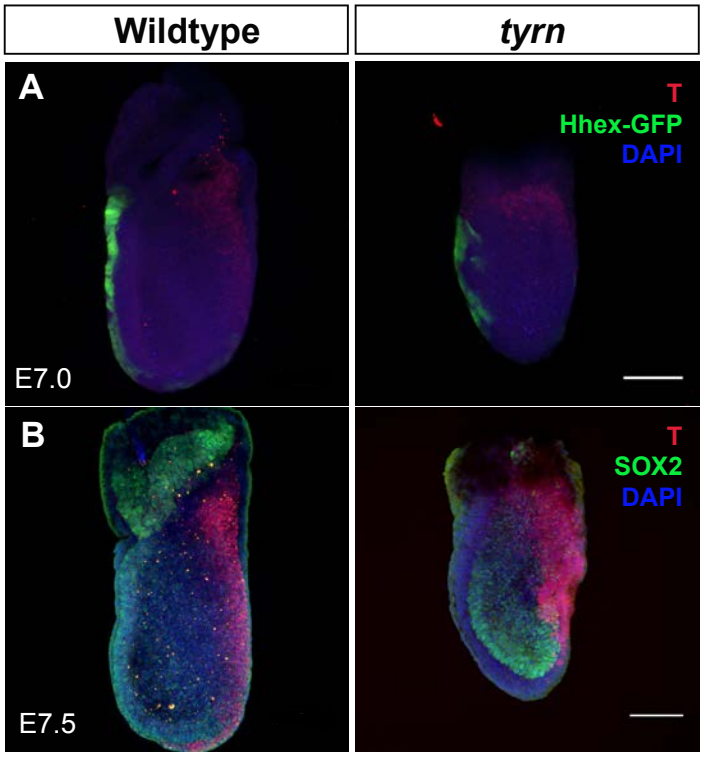

Figure 2.13 Defects in primitive streak extension in *tyrn* embryos. (A) Whole mount immunostaining of E7.0 wildtype and *tyrn* embryos. mutant embryos show reduced embryo size and the T expression area is not expanding anteriorly as long as seen in the wildtype of the same stage. Hhex-GFP labeled the AVE and emerging gut endoderm. (B) Whole mount immunostaining of E7.5 wildtype and *tyrn* embryos. T and SOX2 expression pattern were similar to the pattern in section staining (A-C). *n* = 3 embryos per genotype. Scale Bar = 100 μm.

2.2.3 The *tyrn* mutation affects mesoderm lineage allocation

The defective primitive streak elongation in *tyrn* mutants raises the question that whether the mesoderm lineage allocation is affected in *tyrn* embryos. Staining of E-Cadherin and N-cadherin at E7.5 embryos showed that the mesoderm is generated between epiblast and VE in mutant embryos, similar to the wildtype embryos (**Figure 2.14A**). Immunofluorescence staining and WISH detected irregularities in the production and positioning of paraxial and extraembryonic mesoderm. In wildtype embryos, CDX2 is expressed in ExE and the posterior side of the embryos critical for the axial elongation (Chawengsaksophak et al., 2004; van den Akker et al., 2002). However, in *tyrn* embryos,

the expression pattern of CDX2 is restricted to the posterior end (**Figure 2.14B**). Similarly, expression of *Tbx6,* a marker of paraxial mesoderm, was found along the posterior side of the wildtype embryo, down to the distal tip, it was restricted to the posterior-proximal region in *tyrn* (**Figure 2.14D**). The expression of these two markers were consistent with the short primitive streak. Expression of KDR, a marker for a subset of extraembryonic mesoderm including the blood island, amnion, and allantois (Sakurai et al., 2005), was detected in a similar place in both wildtype and *tyrn* embryos except the allantois, which is not seen in the *tyrn* embryos (**Figure 2.14C**). *Twist* expression labels two distinct mesodermal populations at E7.5; anterior mesoderm precursors to cranial mesenchyme and extraembryonic mesoderm of the allantois (Bildsoe et al., 2009). Of note, the E7.5 *tyrn* mutant generated *Twist* expressing anterior mesoderm but lacked *Twist* expressing cells of the allantois (**Figure 2.14E**). The mutant embryos also expressed greatly reduced levels of *Tbx4*, another marker of allantoic mesoderm (**Figure 2.14F**). *Mesp1* marks cardiac mesoderm at the early-streak stage and its expression is downregulated and restricted at E7.75 (Saga et al., 1999). The *Mesp1* expression in *tyrn* mutants at E7.75 resembled that seen in E7.5 wildtype embryos in published data (Saga et al., 1999), suggesting the presence of cardiac mesoderm progenitors. However, the wildtype embryos seemed to capture a transitional stage when the cardiac progenitors have migrated away and the emerging paraxial mesoderm begins expressing *Mesp1* (**Figure 2.14G**). At E8.5, *Mesp1* was expressed in posterior somites in both wildtype and mutant embryos, albeit the expression was weaker in mutants, probably due to the small somite size (**Figure 2.14H**). BMP signal gradient was observed in *tyrn* embryos. However, the signal occupied a higher proportion of embryonic area in *tyrn* mutants compared to wildtype embryos due to the smaller size, indicating a higher exposure of BMP signals along the streak (**Figure 2.15**). Taken together, these data indicate that the mesoderm lineage allocation, especially the

populations arising at the late streak stage, is perturbed by the small size, potentially through the abnormal morphogen gradient in mutant embryos.

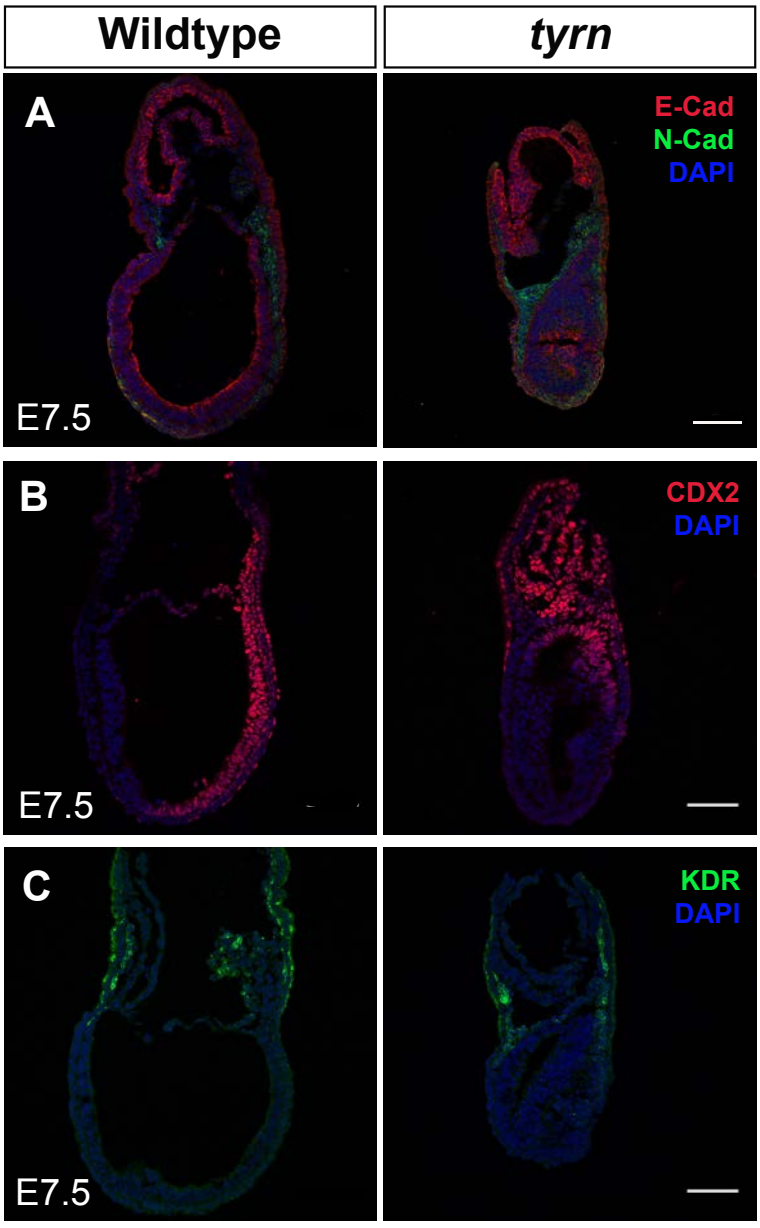

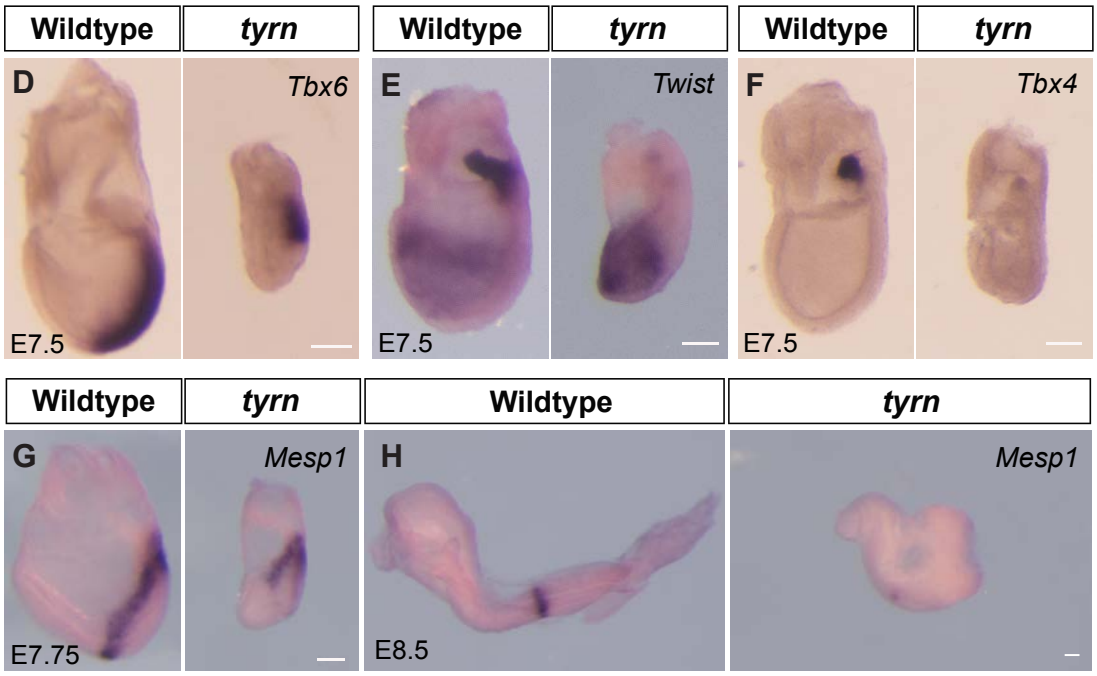

Figure 2.14 Mesoderm lineage allocation in *tyrn* mutants at late-streak stage.
(A). Costaining of N-Cadherin and E-cCdherin. N-Cadherin marked both embryonic and extraembryonic mesoderm. The mesoderm layer was formed between epiblast and VE in both wildtype and *tyrn* embryos. (B) CDX2 expression was restricted to the posterior-proximal side in *tyrn* embryos, whereas in wildtype embryos, CDX2 was expressed along the whole posterior side. (C) KDR was expressed in a subset of extraembryonic mesoderm cells located in blood island, amnion, and allantois in wildtype embryos. *tyrn* embryos showed similar expression except the allantois. (D) In wildtype embryos, the paraxial mesoderm marker *Tbx6* was expressed along the posterior side down to the distal tip. In *tyrn* mutants, *Tbx6* expression was restricted to the posterior side of the embryo. (E) In wildtype embryos, *Twist* expression labeled anterior mesodermal precursors to cranial mesenchyme and extraembryonic mesoderm of the allantois. In *tyrn* embryos, *Twist* was not expressed in allantois. (F) *Tbx4* expression in allantois was strong in wildtype embryos but not detected in mutant embryos at E7.5. (G) In wildtype embryos, *Mesp1* marked the transition stage when cardiac progenitors exited from the primitive streak while the emerging paraxial mesoderm cells started to express *Mesp1*. *Mesp1* expression was restricted to the cardiac progenitors in E7.75 mutants. (H) *Mesp1* was expressed in posterior somites in both wildtype and *tyrn* embryos at E8.5. The signal was weaker in mutant embryos. n = 3 embryos per genotype. Scale Bar=100 μm.

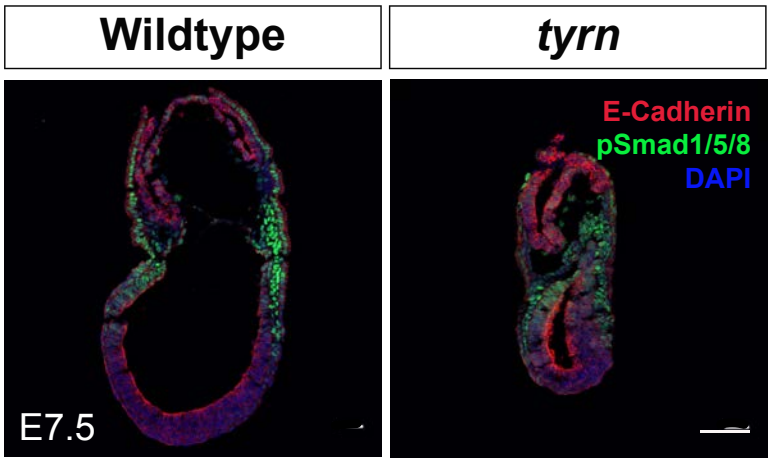

Figure 2.15 BMP signal gradient in wildtype and mutant embryos. pSmad1/5/8 reflected BMP signaling pattern. In both wildtype and *tyrn* embryos, the BMP signal was high around the boundary between the epiblast and extraembryonic tissues and became weaker to the distal. n = 3 embryos per genotype. Scale Bar=100 μm.

2.2.4 Disrupting *Pold1* in a single layer did not recapitulate phenotype in *tyrn*.

To address which germ layer mainly contributes to the phenotype observed in *tyrn* embryos, we generated homozygous *Pold1* conditional null alleles in either epiblast or VE to see which germ layer, once POLD1 is depleted, will recapitulate the *tyrn* phenotype. We took advantage of the mice harboring the *Pold1*^{tm1a} allele to generate *Pold1*$^{loxP/loxP}$ mice and crossed them with *Sox2-Cre* (Hayashi et al., 2003; Vincent and Robertson, 2003) and *Ttr-Cre* mice (Kwon and Hadjantonakis, 2009), respectively (**Figure 2.16**). No VE-specific *Pold1*-null embryos were retrieved as early as the E6.5 stage, as validated by genotyping, indicating the importance of VE formation for embryo survival at the pre-gastrulation stage. Epiblast-specific *Pold1*-null embryos were retrieved at E7.5, although a great loss of epiblast and ExE tissues were observed (**Figure 2.17A-B**). The remaining epiblast cells *Pold1*$^{+/-}$: *Sox2-Cre* embryos were still undergoing gastrulation, as shown by the sporadic T staining at the posterior side of the embryo. The VE layer was the only layer that was relatively well maintained (Fig. 2.18A).

The shrinkage of embryonic tissues was more severe in *Pold1*$^{loxP/-}$*: Sox2-Cre* embryos and did not resemble *tyrn* embryos.

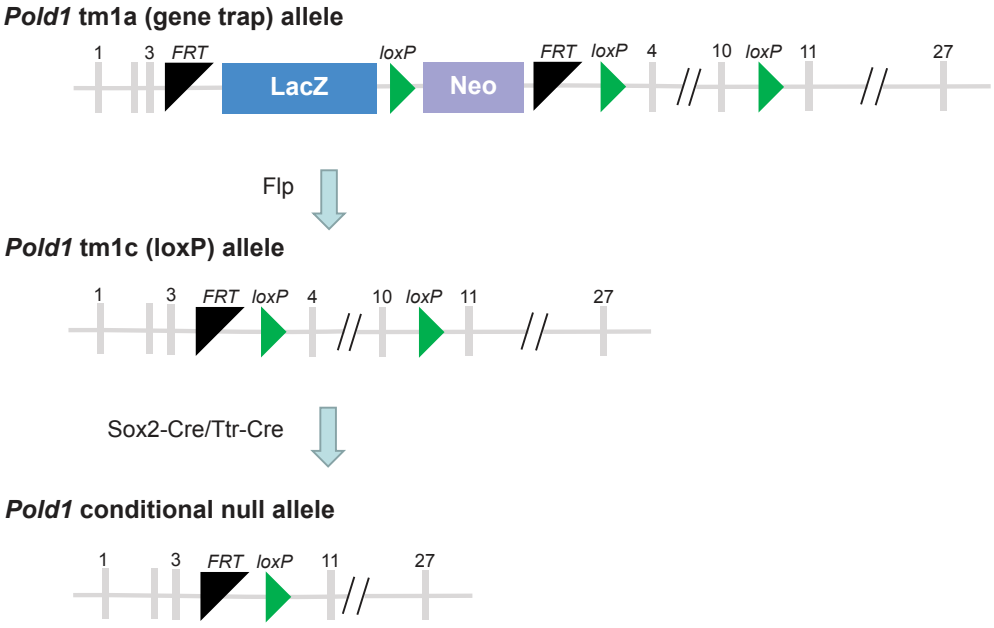

Figure 2.16 Crossing strategy of generating *Pold1* conditional null allele.
Structure of the *Pold1* tm1a (gene trap) allele and the tm1c (loxP) allele generated after Flp-mediated recombination. gene segments between loxP sites were removed after further Sox2-Cre or Ttr-Cre mediated recombination. Exons are represented in grey vertical blocks.

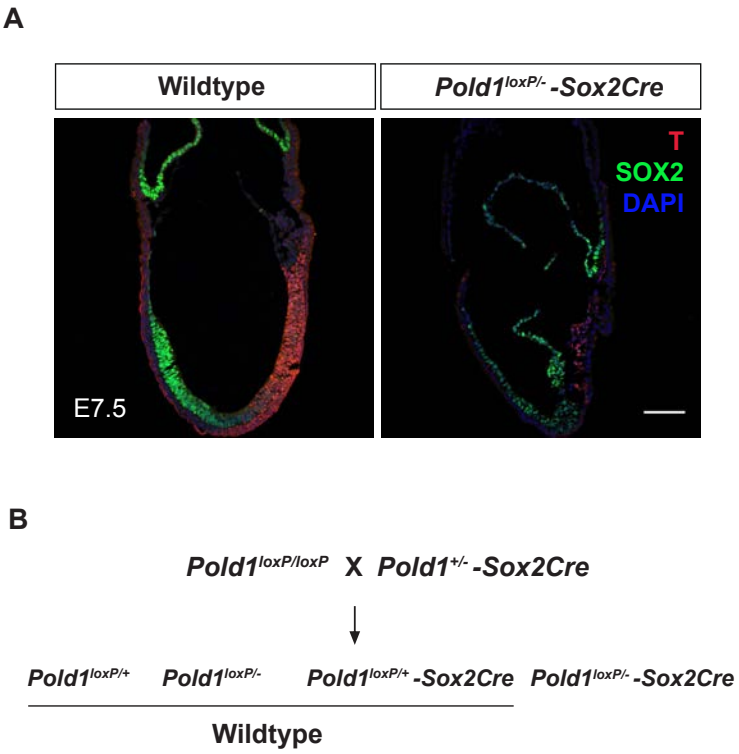

Figure 2.17 Loss of epiblast and extraembryonic ectoderm (ExE) tissues in E7.5 *Pold1* conditional null embryos. (A) Reduced epiblast and ExE tissues were observed in E7.5 *Pold1*$^{loxP/-}$*: Sox2-Cre* embryos compared to wildtype embryos by SOX2 staining. Mutant embryos underwent gastrulation as marked by T at the posterior side of the embryo. (B) Crossing strategy to generate *Pold1*$^{loxP/-}$*: Sox2-Cre* embryos. n = 3 embryos per genotype. Scale Bar=100 μm.

Given the fact that the homozygous null allele causes a more severe phenotype, we decided to combine the null allele with the *tyrn* allele in a layer-specific manner. Intriguingly, *Pold1*$^{tyrn/loxP}$*: Ttr-Cre* embryos were morphologically at the post-gastrulation stage (E10.5, the latest time point we performed the dissection), but no *Pold1*$^{tyrn/loxP}$*: Ttr-Cre* neonates were yielded. *Pold1*$^{tyrn/loxP}$*: Sox2-Cre* embryos were morphologically normal till E9.0 when *Pold1*$^{tyrn/loxP}$*-Sox2Cre* embryos did not undergo axis rotation at this stage and quickly died at E9.5 (**Figure 2.18**). These data indicate that the severity of the phenotype relies on the dosage of *Pold1* that was perturbed. The phenotypes observed in mutant embryos from different conditional allele crossing strategies also point out that the *tyrn* phenotype is caused by a global reduction of POLD1 activity.

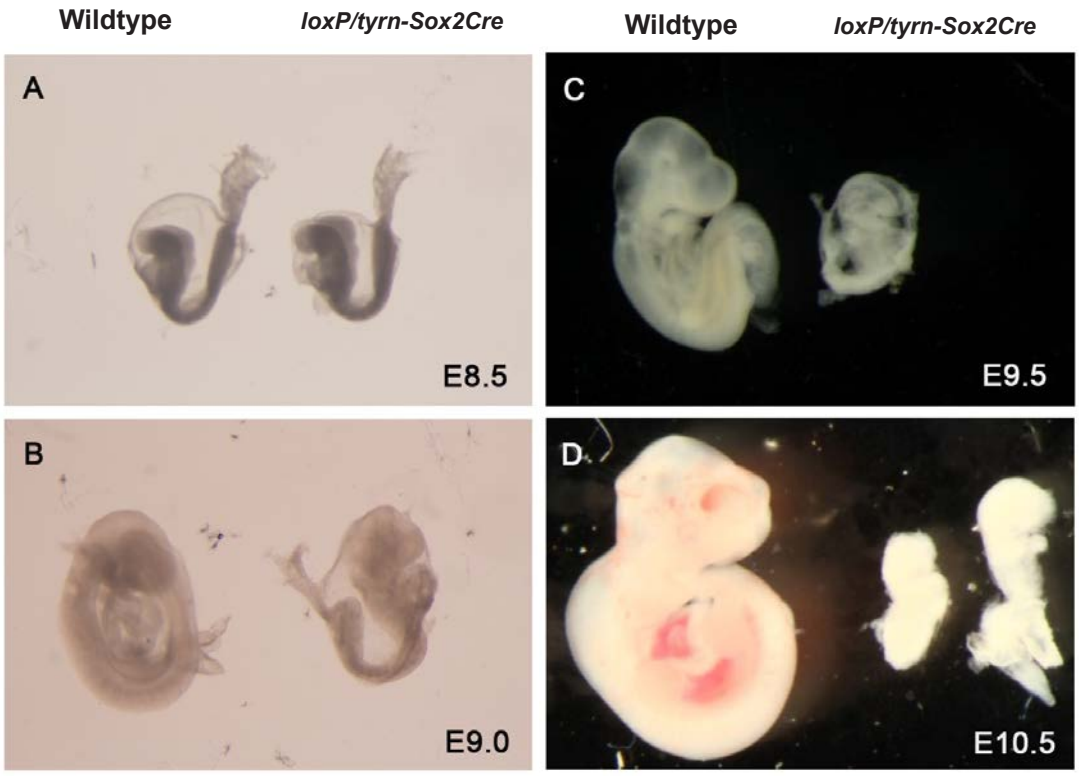

E

$$Pold1^{loxP/loxP} \times Pold1^{tyrn/+}\text{-}Sox2Cre$$

$$\downarrow$$

$$Pold1^{loxP/+} \quad Pold1^{loxP/tyrn} \quad Pold1^{loxP/+}\text{-}Sox2Cre \quad Pold1^{loxP/tyrn}\text{-}Sox2Cre$$

Wildtype

Figure 2.18 Developmental progression of *Pold1$^{loxP/tyrn}$: Sox2-Cre* embryos at post-gastrulation stage. (A) *Pold1$^{loxP/tyrn}$: Sox2-Cre* embryos were morphologically indistinguishable compared to wildtype embryos at E8.5. (B) At E9.0, mutant embryos showed reduced tissue amount and failed to undergo axis rotation along the dorsal-ventral (D-V) axis. (C) *Pold1$^{loxP/tyrn}$: Sox2-Cre* embryos embryos were smaller than wildtype embryos and started to die at E9.5 (D) E10.5, the last stage to retrieve *Pold1$^{loxP/tyrn}$: Sox2-Cre* embryos, which were already dead. (E) Crossing strategy to generate *Pold1$^{loxP/tyrn}$: Sox2-Cre* embryos. n = 3 embryos per genotype. Scale Bar=100 μm.

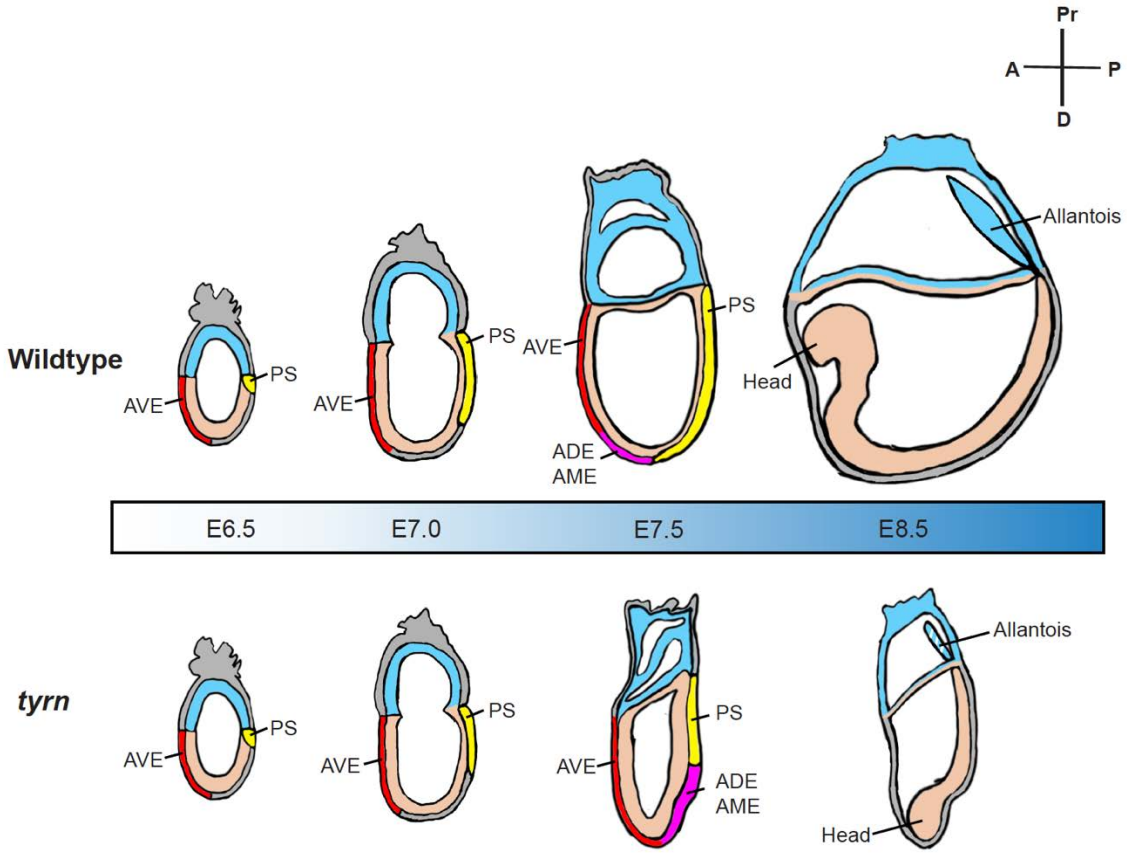

Figure 2.19 Developmental progression of wildtype and *tyrn* embryos between E6.5 and E8.5. At E6.5, wildtype and *tyrn* embryos are morphologically indistinguishable. AVE (red) is properly localized at the normal anterior region in both wildtype and mutant embryos. Gastrulation is initiated and a primitive streak (yellow) is formed. At E7.0. primitive streak elongation in *tyrn* mutants shows a slight delay compared to wildtype embryos, and there is a small though noticeable reduction in embryo size. In E7.5 wildtype embryos, the AME and ADE replace the role of AVE as the new signaling center for head formation at the anterior side of the embryo. In *tyrn* mutants, there is reduced primitive streak extension, and the AME and ADE (magenta) appear at the midpoint of the posterior side instead of migrating across the distal tip of the embryos. In addition, the head forms at the distal tip with an abnormal morphology. At E8.5, wildtype embryos show a well extended A-P axis, whereas *tyrn* mutant embryos exhibit a small, siren-like morphology with the head pointing to the distal tip of the embryo. The white stripes indicate the reduction of extraembryonic mesoderm cells in the allantois.

Chapter 3 Discussion

We assessed the impact on embryo growth and morphogenesis of a hypomorphic mutation that reduces levels of DNA proliferation at gastrulation stages. The *tyrn* mutants from our ENU mutagenesis screen provided an excellent time window for us to investigate the roles of embryo growth in gastrulation. The *tyrn* mutation disrupted the polymerase function of Pold1 and caused reduced cell proliferation *in vivo*. Mutant embryos did not merely exhibit a wildtype-like morphology with a proportionally reduced size, or a random shape with no underlying logic. Instead, it showed a siren-like morphology, with the head located closer to the distal tip rather than residing at the normal anterior region seen in the wild types. Further phenotypic analyses from E6.5-E7.5 stages revealed that the mispositioned head, as well as the general abnormal morphology seen in tyrn embryos, likely resulted from the defective primitive streak extension during gastrulation. The short primitive streak led to the distal positioning of the AME and ADE, which caused the orientation of the anterior-posterior axis to be shifted towards the distal-proximal axis (**Figure 2.19**). The *tyrn* mutants showed a remarkable impact of reduced cell proliferation during gastrulation. The impaired DNA synthesis machinery caused prolonged defects in cell proliferation, leading to a discoordination of embryo growth with lineage specification and tissue morphogenesis. Such discoordination resulted in embryos with abnormal morphology and incorrect orientation inside the decidua. These results indicate that the embryo growth needs to be highly coordinated with lineage specification and tissue morphogenesis for normal gastrulation.

The data we collected and the conclusion we have drawn so far are very superficial. The study of impacts of cell proliferation during embryo morphogenesis in the tyrn mutant raises more questions worth further investigation, some of which are not limited to the

developmental biology field. To better understand how Pold1 is involved in embryogenesis, we may need to address these questions at molecular, genomic, and cellular levels.

1. Characterizing the biochemical properties of *Pold1* D939Y

Our *in vitro* primer extension assays show reduced efficiency of DNA synthesis in mutant proteins. However, the protein we purified was the yeast orthologue of mouse POLD1 with the corresponding mutation. In the future, we can directly purify mouse POLD1^{D939Y} protein to test DNA synthesis in primer extension assay, which will be more persuasive. Based on the structure of human and yeast Pol δ, the D939Y mutation on p125 (POLD1) may potentially disrupt the structural integrity of replication complex on DNA single strands. We may also test the binding affinity of p125 with other subunits to see whether the protein-protein interaction is disrupted in POLD1^{D939Y}.

All the current biochemical data we have so far only focused on the reduced efficiency of DNA synthesis by POLD1^{D939Y}. Since *Pold1* is actively involved in DNA repair, it is possible that POLD1^{D939Y} may cause increased genome instability. Although this mutation is not localized on the exonuclease domain, it is not known whether it may have indirect effects on DNA repair. Immunofluorescence staining of cleaved caspase 3 showed increased cell apoptosis in tyrn mutants. Replication errors may occur during multiple rounds of cell proliferation. We may test the expression level of diagnostic markers for DNA damage and checkpoint response such as γ-H2AX, ATM/ATR by immunoblotting or immunofluorescence staining. Notably, some very preliminary data showed that introducing *p53* homozygous null alleles into *tyrn* mutants did not rescue

the phenotype, suggesting that the checkpoint response is not activated or the activated checkpoint response is independent of p53.

2. Investigating the behavior of *Pold1*$^{tyrn/tyrn}$ cells

The increase of cell number is significantly lower in *tyrn* mutants from E7.0. Since cell death did not become obvious until E7.5, the lower cell number growth was mainly due to defects in cell proliferation. Cell cycle controls the progression of cell proliferation and there are some important questions we may need to address: Is the cell cycle duration extended? Which phase(s) is extended during the cell cycle? Will there be more cells arrested in the G2 phase? Usually, the cell cycle analysis is performed in cultured cell lines. In our case, however, the biggest obstacle to performing cell cycle analysis is that we cannot derive stable cell lines from *tyrn* mutants. Cells cannot proliferate *in vitro* due to defective *Pold1* function, which also impedes many biochemical studies. What we can do is to pool enough embryos for analysis, which is very time-consuming and cannot address embryos until E7.5 as wildtype and *tyrn* embryos are morphologically indistinguishable before E7.5. Then we can dissociate cells directly from the embryos, though tricky, and sort these cells based on the phases where these cells are staying. Intuitively, we might see an increased ratio of cells staying in S phase due to the decreased efficiency of DNA synthesis in *Pold1*$^{tyrn/tyrn}$ cells. We might also see an increase in cells trapped in the G2 phase, if replication errors are accumulated and checkpoint responses are activated. In parallel, we can knock down *Pold1* in mouse cell lines, for example, the MEF, and perform cell cycle analysis and compare the results from cells dissociated from embryos.

The short primitive streak and generally abnormal morphology make it worthwhile to address the cell collective migration during gastrulation. Advances in embryo culture

protocols, high-resolution live imaging techniques as well as computational methods have provided strong technical support for mesoderm migration studies. By introducing mTmG into the *tyrn* background, we may visualize mesodermal cell movements via live imaging and calculate the speed and directions of individual cells. This experiment will provide visual data to reflect the whole process and understand how *tyrn* embryos adopt this morphology during these 12 hours (from E7.0 to E7.5), highlighting the importance of the coordination of cell movement and cell proliferation for tissue patterning and morphogenesis

3. Looking into the genome landscapes

The whole genome is duplicated during the S phase, which includes the synthesis of nascent DNAs and nucleosome packaging. Again, since our current study only focused on DNA synthesis. it is not known whether the epigenetic modification is affected in *Pold1*$^{tyrn/tyrn}$ cells. One study brings about the idea that Pol δ may affect histone modification in *Arabidopsis (Iglesias et al., 2015)*. We can perform ChIP-seq analysis to compare the epigenetic modifications between wildtype and *tyrn* embryos. We might observe a global change of histone modification or DNA methylation. If this is true, do the changes of epigenetic modification lead to differential gene expression in all cell types and subsequent embryo phenotypes? The global change of epigenetic modification might cause regional-specific effects in unique cell types. This might be a potential explanation for people with MDPL (mandibular hyperplasia, deafness, progeroid, and lipodystrophy) syndrome that exhibit tissue/organ-specific defects. However, questions still exist on the causative relationship between epigenetic modifications and embryo phenotypes. Another study, which is also performed in *Arabidopsis*, shows that Pol ε genetically interacts with genes involved in epigenetic

regulations (Yin et al., 2009b). We may test whether this is also true for Pol δ in mouse embryos. We may even go one step further to see whether Pol δ physically interacts with epigenetic modifiers through Co-IP.

The cell fate of mesoderm derivatives along the primitive streak is determined by differential combinations of morphogen signals these cells are exposed based on the position and timing of ingression. Our results showed that the mesoderm lineage allocation is altered in *tyrn* mutants, especially the extraembryonic mesoderm in allantois. In the meantime, we also observed an expanded BMP signal zone along the proximodistal axis in *tyrn* embryos. Based on these observations and the model of mesoderm cell lineage specification, we proposed that the establishment of morphogen gradience relies on the well-coordinated pattern signals and embryo expansion. This proposal can be further validated by looking at the transcriptional profiling of individual cells. The development of single-cell RNA seq allows us to look at the gene expression profiling at single cell level. We may depict the atlas of gene expression profiling of each cell in a high spatiotemporal resolution to get a better understanding of the cell behavior during development.

4. Beyond gastrulation, how does cell proliferation affect organogenesis?

Cell number regulation occurs throughout different stages of embryonic development. The effects of cell number perturbation on tissue/organ size and morphogenesis can vary greatly based on developmental stages and tissue/organ types. The mandibular hypoplasia, deafness, progeroid and lipodystrophy (MDPL) syndrome, a multisystem disorder, has been associated with heterozygous in-frame deletion of Ser605 that causes loss of POLD1 activity (Elouej et al., 2017; Fiorillo et al., 2018; Sasaki et al.,

2018; Weedon et al., 2013). The reported patients presented growth retardation, sensorineural deafness, loss of subcutaneous adipose tissue and insulin resistance, indicating that decreased POLD1 activity exerts organ specific effects. Other studies have also identified organ-specific responses to loss of tissue-specific progenitors. Removing the embryonic limb field in amphibians or chickens has no effect on the final limb size as the limb is capable of robust compensatory proliferation (Holder, 1981; Summerbell, 1981), and similar compensatory growth has been observed for the developing liver progenitors (Bort et al., 2006). In contrast, the final pancreas size is determined by the initial pancreatic progenitor pool and there is a lack of significant compensatory growth (Bort et al., 2006; Stanger et al., 2007). These studies demonstrate the importance of studying cell number regulation in diverse tissue and organ types at different stages of embryonic development.

Obviously, the current *tyrn* mutant is not a suitable model to address the impacts of cell proliferation in organogenesis due to the early lethality. The CRISPR/Cas9 may potentially provide a solution to address how *Pold1* could affect organ development. Theoretically, we can introduce D939Y mutation into organoids using CRISPR/Cas9 and tobserve which type(s) of organoids are sensitive to Pold1 D939Y. In the future, we may produce mice expressing tissue-specific Cas9 and gRNA targeting *Pold1* to generate D939Y mutation in an tissue-specific manner to see how POLD1 D939Y affects organ development *in vivo*. An alternative way is that we may apply reverse genetic screens to generate mice harboring mutations in *Pold1* which are milder than D393Y and show defects at later time points. This could allow us to systematically investigate the development of all types of organs when the cell proliferation is perturbed by defective *Pold1*.

5. Investigating the role of DNA polymerases in development

There are 15 DNA polymerases in mammals, with Pol δ, Pol ε and Pol α being the major polymerases required for DNA synthesis. Most of the mouse models targeting DNA polymerases are mainly applied in cancer study. The heterozygous or homozygous mutants usually develop cancer in adulthood. While it remains unclear in terms of whether and how Pol ε and Pol α contribute to embryonic development, due to lack of suitable mouse models. Homozygous deletion of Pol ε leads to embryonic lethality at E7.0, which is longer than *Pold1* knockout embryos with no detailed phenotype reported . Despite Pol δ, one mouse model targeting DNA polymerase β was created and provided some generic information in embryonic developments. DNA polymerase β is essential for base excision repair. Embryo without Pol β dies with higher mortality and increased cell apoptosis in postmitotic neurons. In conclusion, the study of DNA polymerase function in mouse development is very limited. The phenotypic analysis is also restricted to cell proliferation, DNA synthesis, cell cycle, cell death, etc. How these defects are linked to embryo development, however, has constantly been neglected and a loose conclusion is often drawn from these observations. Compared to mutations in Pol δ, these embryos have milder phenotype and are actually very useful model to study how reduced cell proliferation could affect organ development. In the future, more knock-in mouse models with various defects during embryogenesis need to be created. All the experiments we have mentioned so far can also be done in these knock-in models to explore the function of DNA polymerases in embryonic development.

In addition to mice, other model organisms also have their unique morphogenetic events and many of them become the classic models to study certain biological questions. For example, in *C.elegans*, people use the first rounds of cell division in zygotes to study the

mechanisms of asymmetrical divisions. In *Drosophila*, the ventral furrow formation and mesoderm formation are the most well-studied developmental models for topics including apical constriction, layer invagination, epithelia-mesenchymal transition. In zebrafish, epiboly is a unique morphogenetic event under constant investigation. The migratory behavior of mesendoderm cells is also a research hotspot. It will be interesting if we introduce mutations of DNA polymerases into these model organisms to see whether these typical morphogenetic events will be affected when DNA replication and cell proliferation is disrupted.

6. From model organisms to human

Studies from model organisms provide many critical insights to help us understand the developmental process in human. Although many developmental features and underlying mechanisms have been proved to be universally shared among different species, human embryonic development still has its own features which cannot be recapitulated in model organisms. Very recently, the international society of stem cell research (ISSCR) has lifted the 14-day ban on human embryo study, which allows the extended culture of human embryos. However, it is still technically challenging to culture human embryos past gastrulation. Therefore, people have been searching for alternative models to mimic the early-stage developmental progress including two-dimensional disc or organoids. The recent advances in the generation of blastoids and gastruloids from human pluripotent stem cells offers innovative opportunities to dissect the mechanisms of human embryogenesis. By combining single-cell transcriptomic analysis, we are able to continuously create new versions of these human organoids that best mimic their *in vivo* counterparts and recapitulate the dynamics of developmental events. In the future, more topics which have been deeply investigated from model organisms, especially from mouse studies, including cell proliferation in embryonic development, can be transferred

into the human *in vitro* model to get the knowledge that is, theoretically, closer to what really happens in human embryogenesis.

7. Some thoughts about this project

From my point of view, an important lesson learned from the past 7 years in the developmental biology study is “always try to think of a mutant in different ways”. For so many years, numerous transcription factors or related co-effectors, components of a certain signaling pathways, or anything that may indirectly affect the expression of the genes mentioned above, have been identified in various forward or genetic screens. These productive findings lead us to a deeper understanding of embryogenesis. However, it may also create a comfort zone that when something new or non-canonical is discovered, people eagerly try to integrate it into known signal networks. At the very beginning of this study, a lot of time has been spent on linking *Pold1* into a known signaling pathway such as Nodal, BMP, etc. For many times, I felt like going to a dead end as it is very time consuming to go through every single pathway within a limited time period. Finally, the author decided to jump out of the zone. Instead of sticking to a signaling pathway, why not going back to the gene itself and think of its basic function as a polymerase? The direct effect of defective *Pold1* function is impairs, which later affects cell cycle and cell proliferation. Everything seems normal when wildtype and mutant embryo did not show size difference. Everything becomes abnormal when embryo expansion starts to slow down. This observation finally led to a new idea that looking at embryo as a whole. The embryo is the frame for all proper signaling activities. Without normal size, the whole signaling network and cell behavior will change collectively. The embryo size has long been neglected compared to other signaling pathway specific studies. I am very glad that I find a new direction for this study and propose a model to summarize my findings. It is a great pity that I will never have the chance to share my

idea with Kathryn. The arguments between us about this mutant always brought up with new ideas and hypotheses. Without them, I would never be able to establish the current model.

Chapter 4 Materials and methods

4.1 ENU Allele Isolation and Sequencing.

The *tyrn* allele was generated by mouse ENU mutagenesis screens using C57BL/6J males and was identified based on its embryonic phenotype at E8.5, as previously described (Garcia-Garcia et al., 2005). To obtain genomic DNA, E8.5 *tyrn* mutant embryos were pooled into 3 sample groups and snap frozen on dry ice. Gentra Puregene kit (QIAGEN) was used for the genomic DNA extraction of *tyrn* mutant embryos. Whole-exome sequencing was performed at the MSKCC Integrated Genomics Operation. Exome capture was performed using the SureSelectXT kit (Agilent Technologies) and SureSelect Mouse All Exon baits (Agilent Technologies). An average of 100 million 75-bp paired reads were generated. Sequencing data analysis was performed using the methods described in (Jain et al., 2017). We examined homozygous exonic sequence variants shared among all pools of phenotypic embryos, but which were not identified in cohorts of wildtype embryo samples or separate lineages of ENU screen-derived embryos, and which were not present in a publicly available mouse genomic polymorphism database (dbSNP), 11 potential phenotype-causing lesions were found in 8 gene annotations, 6 nonsynonymous, of which *Pold1* was one: *Pold1*: NM_011131: exon23: c. G2815T: p.D939Y. After examining the known phenotypes of published alleles or functional annotations of these candidate genes, we re-examined non-exonic and heterozygous mutations and eliminated the read depth threshold to explore other possibilities. After going through the whole dataset (developed by Devanshi Jain from Scott Keeney lab) (Jain et al., 2017) containing all our exome sequencing submissions over the years to catalog universal variants we could eliminate, we confirmed that the sole candidate variant was in *Pold1.* The *tyrn* allele has a single G to T transversion in the 2815 nucleotide position of exon 23 in the *Pold1* coding sequence (G2815T), causing a nonsynonymous missense mutation in the amino

acid position 939 resulting in the substitution of aspartic acid to tyrosine, D939Y. The G2815T mutation created a RsaI restriction site used for genotyping. Embryos displaying the *tyrn* morphological defect were homozygous for the G2815T mutation.

4.2 Mouse Strains

***Pold1*$^{tm1a/+}$ mice**: The parental JM8.N4 mouse ES cell strain (strain origin: C57BL/6N, male, black coat, non-agouti, MGI ID: 4431772) (Skarnes et al., 2011) carrying one *Pold1*$^{tm1a(EUCOMM)Wtsi}$ (*Pold1*^{tm1a}) allele was imported from the European Mouse Mutant Repository (EUMMCR). The selected Pold1-G09 ES cell clone passed the karyotype analysis performed by Molecular Cytogenetics Core Facility, Memorial Sloan Kettering Cancer Center (MSKCC). The Pold1-G09 ES cell clone was injected into the female B6(Cg)-Tyr^{c-2J}/J (albino C57BL/6J, or B6-albino, non-agouti, The Jackson Laboratory) donor mice by MSKCC Mouse Genetics Core Facility. 14 out of the 19 pups alive were chimeric. Male chimeras were crossed with albino FVB/NJ (FVB, containing homozygous dominant *agouti* locus *A*/*A*) females to generate heterozygous offspring carrying the *Pold1*^{tm1a} allele. Germline transmission was determined by the presence of agouti pups and genotyping for the presence of the *LacZ* cassette present in the *tm1a* allele.

***Pold1*$^{+/tm1b}$ mice:** Mice carrying *Pold1*^{tm1b} (null) allele were generated by crossing *Pold1*$^{tm1a/+}$ mice with *CAG-Cre* transgenic mice (The Jackson Laboratory) to remove the critical exons between exon 3 to exon 10. The *lacZ* cassette remained in *Pold1*^{tm1b} allele and was used for genotyping.

***Pold1*$^{loxP/loxP}$ mice:** *Pold1*$^{+/tm1a}$ mice were crossed with mice expressing Flp recombinase to yield *Pold1*$^{+/loxP}$ offspring. The Flp recombinase removed the gene trap cassette

between exon 3 and exon 4, leaving 2 loxP sites flanking exon 4 to exon 10. Heterozygous *Pold1*$^{+/loxP}$ mice were inbred to yield homozygous *Pold1*$^{loxP/loxP}$ mice.

Other mouse strains: The Hhex-GFP strain and *Ttr-Cre* strain were gifts from Anna Katarina Hadjantonakis (Kwon and Hadjantonakis, 2009; Rodriguez et al., 2001) (MSKCC). The Flp strain (Takeuchi et al., 2002) was a gift from Alexander Joyner (MSKCC). The *Sox2-Cre* (Hayashi et al., 2003; Vincent and Robertson, 2003) strain was kindly provided by Dr. Tatiana Omelchenko. The *CAG-Cre* transgenic mice (Sakai and Miyazaki, 1997) were kindly provided by Dr. Angela Parrish.

4.3 Animal Crossing and Breeding

Mice were housed and bred under standard conditions in accordance with Institutional Animal Care and Use Committee (IACUC) guidelines. The MSKCC IACUC approved the experiments. Mice that were 8-16 weeks old were used to generate E6.5 to E8.5 embryos. For experimental crossing, 1 male and 2~3 females were set up in one cage around 5 pm in the afternoon. Plug check were done between 12pm to 4 pm starting from the next day. The plugged mice were recorded as E0.5. A second plug may occasionally occur 2-3 days after the first plug then the plugged mice were recorded as E0.5 based on the second plug time. Pregnant females were brought down to the lab and stayed for no more than 12 hours before experiments.

4.4 Embryo and mouse genotyping

Embryos and punched ear tissues from weaned young mice (~20 days after birth) were incubated in PCR buffer containing 15% Proteinase K at 55°C overnight to dissociate tissues and release DNAs. Samples were heated up at 95°C to denature Proteinase K and then diluted to 50-100 ng/μl. Sample concentration was measured by Nanodrop. For

each PCR reaction, 1 μl DNA sample was mixed in 5.118 μl PCR mastermix, 0.575 μl primer mix and 0.08 μl Platinum Taq DNA polymerase. Reaction was run on Eppendorf Thermal Cycler.

Primers for different genes and allelles were listed in the table

Programs used for PCR reactions:

Pold1 tyrn

- Step 1 94.0 °C 12 minutes
- Step 2 X 35 cycles

  94.0 °C 30 seconds

  58.0 °C 45 seconds

  72.0 °C 1 minute
- Step 3 72.0 °C 7 minutes
- Step 4 4 °C ---

Pold1 loxP/WT

- Step 1 94.0 °C 12 minutes
- Step 2 X 40 cycles

  94.0 °C 30 seconds

  62.0 °C 45 seconds

  72.0 °C 1 minute
- Step 3 72.0 °C 7 minutes
- Step 4 4 °C ---

Pold1 tm1a and tm1b

- Step 1 94.0 °C 12 minutes
- Step 2 X 35 cycles

  94.0 °C 30 seconds

  60.0 °C 30 seconds

  72.0 °C 1 minute
- Step 3 72.0 °C 7 minutes
- Step 4 4 °C ---

Hhex-GFP

- Step 1 94.0 °C 2 minutes
- Step 2 X 40 cycles

  94.0 °C 20 seconds

  55.0 °C 30 seconds

  72.0 °C 30 seconds
- Step 3 72.0 °C 10 minutes
- Step 4 4 °C ---

Cre

- Step 1 94.0 °C 2 minutes
- Step 2 X 35 cycles

  94.0 °C 30 seconds

  59.5 °C 30 seconds

  72.0 °C 1 minute
- Step 3 72.0 °C 10 minutes
- Step 4 4 °C ---

Flp-recombinase

- Step 1 94.0 °C 2 minutes
- Step 2 X 35 cycles

  94.0 °C 30 seconds

  59.5 °C 30 seconds

  72.0 °C 1 minute
- Step 3 72.0 °C 10 minutes
- Step 4 4 °C ---

For *tyrn* allele, 0.5 μl RsaI restriction enzyme, 1.5 μl enzyme buffer and 3 μl ddH_2O were added into 10 μl PCR reaction products for digestion at 37°C overnight. All PCR products were loaded onto 4% agarose-TBE gels and ran under 120 V for 40 minutes. Gels were exposed to UV to show the results using GelDoc system.

4.5 Embryo Harvesting and Dissections

Pregnant FVB female mice bearing embryos at E6.5-10.5 stages were euthanized by cervical dislocation. Uteri were harvested based on an IACUC-approved mouse protocol. Embryos were dissected from decidua inside the uterus in cold 0.4% Bovine Serum Albumin (BSA) (Sigma-Aldrich) in phosphate-buffered saline (PBS) using fine forceps and Leica dissection scope. Embryos were fixed in 4% paraformaldehyde (PFA) on ice for at least 4 hours and washed with PBS for 5 minutes X 3 times at room temperature (RT). Fixed embryos were stored in PBS at 4°C for downstream experiments.

4.6 Complementation Test

Pold1$^{tm1b/+}$ females were crossed in timed matings with *tyrn/*+ males to produce embryos. Embryos at E7.5 and E8.5 stages were harvested and grouped into wildtype and mutant cohorts based on phenotype. No *tyrn/tm1b* mutant embryos were recovered at E8.5 stage. The genotypes of E7.5 embryos corresponded with their morphological

phenotypes, verifying that a lesion in *Pold1* was the causative mutation of the *tyrn* phenotype. Embryos with abnormal morphological phenotype genotyped *Pold1*$^{tyrn/tm1b}$, whereas embryos with *Pold1*$^{+/+}$, *Pold1*$^{tyrn/+}$ *and Pold1*$^{tm1b/+}$ genotypes displayed wildtype phenotypes.

4.7 Riboprobe Preparation

Plasmids containing riboprobe sequences were linearized in the correct orientation to guarantee anti-sense probe generation. Circular plasmids were digested using desired restriction enzyme and incubated at 37°C for 2 hours. 30 μl plasmid was used in the 100 μl digestion system. Linearized plasmids were purified using the PCR purification kit (QIAGEN) to remove the restriction enzyme and diluted with depc-water to 70 μl. Combine 5ul linearized DNA, 3 μl 10X Digoxigenin NTP labeling mix, 3 μl 10X Transcription buffer, 1 μl RNase inhibitor, 2 μl T7/T3/Sp6 RNA polymerase (Sigma-Aldrich), and 16 μl deep-water to make a total of 30ul reaction sample. Samples were incubated at 37°C for 2.5~3 hours. 1 μl DNaseI (RNase-free) was added into each sample after incubation and samples were incubated at 37°C for another 30 minutes to digest plasmids. Add 70 μl depc-water to sample and spin through resin column (GE) using 100 g to remove extra DIG-NTP. Check 5 μl purified transcript on 2% agarose gel. Add 3 μl RNase inhibitor (Sigma Aldrich) into purified riboprobes and store at -20°C.

4.8 *In Situ* Hybridization

Fixed embryos were sequentially dehydrated in 25%, 50%,75% methanol in depc- PBS and 100% methanol and stored in -20°C.

Day 1: Embryos were taken out from methanol and sequentially rehydrated in 75%, 50%, 25% methanol in depc-PBS before experiments. After rehydration, embryos were placed in 12-well plated and washed in depc-PBSTween 20 for 5 minutes X 3 times.

embryos were then incubated in 1μg/mL Proteinase K-PBS solution for 3 to 7 minutes based on embryo stages, After Proteinase K treatment, embryos were washed in 2 mg/ml Glycine in depc-PBSTween 20 for 5 minutes X 2 times to stop Proteinase K reaction. Embryos were again washed in depc- PBSTween for 5 minutes X 2 times. Embryos were refixed in 4% PFA + 0.2% Glutaraldehyde for 15 minutes at room temperature and washed in depc- PBSTween 20 for 5 minutes X 3 times. Embryos were later washed in 1:1 PBSTween 20: hybridization buffer for 5 minutes at RT then 5 minutes at 70°C. After that, embryos were washed in hybridization buffer for 5 minutes at room temperature and then washed in preheated hybridization buffer for 1 hour at 70°C. Once all washes have been done embryos were incubated in hybridization solution with RNA probes at 70°C overnight.

Day 2: RNA probe solution was removed, and embryos were incubated in 800 μl warm, fresh hybridization buffer in each sample well at 70°C. 400 μl of 2X SSC buffer (pH4.5) were added into each well (without removing hybridization buffer) 3 times and embryos were washed for 5 minutes each time at 70°C. After that the buffer mix was aspirated and 2 ml 2X SSC buffer (pH7.0) + 0.15 CHAPS was added to each well to wash embryos for 30 minutes X 2 times at 70°C. After SSC wash, embryos were washed with MAB buffer for 10 minutes X 2 times at room temperature and then for 30 minutes X 2 times at 70°C. After MAB solution wash, embryos were washed in PBS for 10 minutes and then PBSTween for 5 minutes. Embryos were incubated in blocking buffer for at least 5 hours at 4°C. Embryos were incubated with anti-DIG Fab fragments (Roche, 1:10000) in blocking buffer overnight at 4°C.

Day 3: Embryos were washed in PBSTween 20 + 0.1% BSA for 45 minutes X 5 times + overnight X1 time at 4°C.

Day 4: Embryos were washed in PBSTween 20 for 30 minutes X 2 times at room temperature. Then embryos were washed in NTMT solution for 10 minutes X 2 times. Embryos were incubated in BMPurple (Roche) covered in foil until color was developed (leave at 4°C overnight or overweek if necessary). Embryos were washed in PBSTween 20 for 10 minutes X 2 times at room temperature and then re-fixed in 4% PFA for 10 minutes. Embryos were washed in PBS for 10 minutes X 3 times after fixation. Embryos were stored at 4°C before imaging.

Solution Recipe

Hybridization solution (500 ml):

- 5 g Roche Blocking Reagent
- 250 ml formamide
- 125 ml 20X SSC, pH7
- Heat to 65°C for about 1 hour to dissolve
- 59 ml ddH_2O
- 50 ml 10 mg/ml torula RNA (heat 2 minutes at 65°C to clear)
- 1 ml 50 mg/ml heparin (-80°C)
- 5 ml 10% Tween-20
- 5 ml 10% CHAPS
- 5 ml 0.5 M EDTA

store at -20°C

depc ddH_2O: 0.1% diethyl pyrocarbonate (depc) in ddH_2O, stir overnight at 37°C, autoclave 40 minutes.

depc 10X PBS: 0.5 ml depc + 500 ml 10X PBS, stir overnight, autoclave 40 minutes.

depc PBSTween 20:1X depc PBS + 0.1% Tween-20

PBSTween: 0.1% Tween 20 in 1X PBS

PBS-BSA: 0.1% BSA (powder) in 1X PBS

MAB (500 ml): 5.805 g maleic acid + 4.383 g NaCl, dissolve in ddH_2O, adjust pH to 7.5. Adjust total volume to 500 ml

20X SSC (1 L): 175.3 g NaCl + 77.4 g sodium citrate in 800ml ddH_2O, adjust pH to 7.0 with 14N HCl. Adjust total volume to 1L

2 X SSC, pH 4.5 (200 ml): 20 ml 20X SSC + 170 ml ddH_2O, adjust pH to 4.5. Adjust total volume to 200 ml.

2 X SSC, pH 7.0 (200 ml): 20 ml 20X SSC + 180 ml ddH_2O.

NTMT buffer (50 ml): 5 ml 1M Tris, pH 9.5 + 1 ml 5M NaCl + 2.5 ml 1M $MgCl_2$, add ddH_2O to 50 ml total volume.

4% PFA: 4% paraformaldehyde in PBSTween 20, lab made, stored at -80°C for long term, -20°C for short term.

4.9 EdU labeling

EdU (5-ethynyl-2'-deoxyuridine) powder (Invitrogen) was dissolved in sterile PBS into a working concentration of 2.5 mg/ml. Mice were weighed and injected with EdU solution (25 mg/kg) intraperitoneally. Embryos were harvested 2 hours after injection and fixed in 4% PFA overnight. Fixed embryos were washed with PBS+3% BSA twice and then permeabilized in PBS+0.5%Triton X-100 at RT for 20 minutes. Embryos were washed in PBS+3% BSA after permeabilization. Embryos were incubated with the reaction cocktail made from Click-iT™ EdU Cell Proliferation Kit for Imaging, Alexa Fluor 637 dye kit

(Invitrogen) at RT for 30 minutes, protected from light. The cocktail was removed after incubation and embryos were washed in PBS+3% BSA twice.

Solution Recipe

Alexa Fluor azide working solution: 70 μl DMSO + 1 vial (Alexa Fluor 647), mix well. store at -20°C for up to 1 year.

1 X Click-iT EdU reaction buffer: 4 ml 10X Click-iT EdU reaction buffer + 36 ml ddH_2O. Store buffer at 4°C for up to 6 months.

10X Click-iT EdU buffer additive: 2 ml ddH_2O + 1 vial of Click-iT EdU buffer additive powder, mix until fully dissolved. Sore at -20°C up to 1year. Discard the buffer if the color turns brown.

Click-iT reaction cocktail (1ml):

- 860 μl 1X Click-iT reaction buffer
- 40 μl $CuSO_4$
- 2.5 μl Alex Fluor azide
- 100 μl 1X reaction buffer additive

Add the above ingredients in the order and use cocktail with 15 minutes of preparation.

4.10 Immunofluorescence and Confocal Microscopy

Fixed embryos were store in PBS at 4°C before use. Embryos for cryosection were dehydrated in 30% Sucrose-PBS at 4°C overnight. Embryos were embedded in Tissue-Tek® O.C.T Compound (Sakura Finetek) and frozen on smashed dry ice immediately after embedding. Embedded embryos were stored in -80°C before use.

Day 1: Embryos were sectioned in 10 mm using Leica CM1520 Cryostat. Section slides were stored in -80°C before use. For whole-mount staining embryos, embryos were permeabilized with PBS+0.5%Triton X-100 for 1 hour at RT. For section staining, slides

were dried for 30 minutes and incubated in blocking buffer (0.1% TritonX-100, 1% heat-inactivated donkey serum [Gemini: Bio-produces] in PBS) for 1 hour at RT. Primary antibodies were diluted with the optimized diluting ratio in blocking buffer: Embryos and slides were incubated with primary antibodies at 4°C overnight on rotator.

The dilution ratio of primary antibodies used in this study were listed below:
FOXA2 (Abcam,1:300), T (Cell Signaling Technology,1:400), Cleaved Caspase-3 (Cell Signaling Technology,1:300), SOX2 (R and D Systems 1:300), N-cadherin (Cell Signaling Technology, 1:300), E-Cadherin (Sigma Aldrich, 1:300), pSmad1/5/9 (Cell Signaling Technology, 1:200), KDR (BD Pharmingen, 1:100), CDX2 (Abcam, 1:200).

Day 2: Embryos and slides were washed with PBS for 10 minutes X 3 times the next day. Section slides or embryos were incubated in blocking buffer containing specific secondary antibodies (Invitrogen,1:500) and DAPI (1:1000) for 2 hours at RT. For whole mount staining embryos, embryos were washed in PBS for 5 minutes X 3 times and incubated in FocusClear (CelExplorer.Co) for 20 minutes at RT, protected from light. Embryos were mounted with MountClear (CelExplorer.Co) and stored at 4°C. For cryosection staining, slides were washed in PBS for 5 minutes X 3 times and mounted with ProLong Gold Antifade Mountant (Thermo Fisher Scientific) and stored at 4°C. Both embryos and sections were imaged using Leica SP8 inverted laser scanning confocal microscope. Confocal images were reconstructed using Fiji (ImageJ) open-source image processing software.

4.11 Immunoblotting
E8.5 wildtype and mutant embryos were harvested and pooled separately and stored in -80°C before experiments.

Day 1: Tissues were homogenized in cold lysis buffer on ice. Lysate was left on shaker at 4°C for another 30 minutes. Lysate was centrifuged at maximum speed (12000 rpm) to collect supernatant. Protein concentration was determined through BSA-based protein assay using Quick Start Bradford 1X Dye Reagent (BIORAD) and adjusted to 2 μg/μl. Samples were mixed 1:1 with 2X SDS loading buffer and denatured at 95°C for 5 minutes. Samples were loaded in equal amounts onto 8% SDS-PAGE gels and ran for 2 hours under 150V in 1X SDS at RT. Proteins were transferred to PVDF membranes under 15V overnight at 4°C. Membranes were incubated in blocking buffer containing (TBST+5% BSA) for 1hour at RT and incubated with primary antibody in blocking buffer at 4°C overnight: POLD1 (Abcam Cat# ab168827,1:500); GAPDH (Santa Cruz Biotechnology Cat# sc-32233, RRID:AB_627679, 1:1000).

Day 2: Membranes were incubated in blocking buffer containing (TBST+5% BSA) for 1hour at RT and incubated with primary antibody in blocking buffer at 4°C overnight: POLD1 (Abcam Cat# ab168827,1:500); GAPDH (Santa Cruz Biotechnology Cat# sc-32233, RRID: AB_627679, 1:1000). Membranes were washed with 1X TBSTween and incubated with specific secondary antibodies (1: 5000~10000) for 1 hour at room temperature. Membranes were washed with 1X TBSTween and incubated with Pierce™ ECL Western Blotting Substrate (Thermo Fisher Scientific) for 5 minutes before film exposure.

Solution Recipe:

lysis buffer (10 ml)

- 500 μl 1 M Tris-HCl, pH 7.2
- 500 μl 5 M NaCl

- 200 μl 200 mM EDTA
- phosphatase inhibitor mixture I and II (Calbiochem)
- one tablet of Minicomplete (Roche)
- 8.8 ml ddH_2O

2 X SDS sample loading buffer: 4% SDS, 100 mM Tris-HCl pH 6.8, 0.2% bromophenol blue, 20% glycerol, 200 mM β-mercaptoethanol (add before use)

10 X SDS running buffer (1 L): dissolve 30.2 g Tris-base, 144 g glycine, 10g SDS in 900 ml ddH_2O, adjust total volume to 1L.

1 X SDS running buffer (1 L): 100 ml 10 X SDS running buffer + 900 ml ddH_2O

10 X transfer buffer (1 L, no methanol): dissolve 30.2 g Tris-base, 144 g glycine in 900 ml ddH_2O, and adjust the total volume to 1 L.

1X transfer buffer (1 L): 100 ml 10X transfer buffer + 200 ml methanol + 700 ml ddH_2O.

10X TBS buffer (1 L): dissolve 24 g Tris-base, 88 g NaCl in 900 ml ddH_2O, adjust pH to 7.6 with 12 N HCl. Adjust total volume to 1 L

1X TBSTween buffer (1 L) 0.1% Tween 20 in 100 ml 10X TBS + 900 ml ddH_2O

separation gel (8%)

- 4.7 ml ddH_2O.
- 2.7 ml 30% Acrylamide/bis
- 2.5 ml 1.5 M Tris-HCl, pH 8.8
- 100 μl 10% SDS
- 10 μl TEMED
- 32 μl 10% Ammonium persulfate (APS)

stacking gel (4%)

- 6.1 ml ddH_2O
- 1.3 ml 30% Acrylamide/bis

- 2.5 ml 0.5 M Tris-HCl, pH6.8
- 100 μl 10% SDS
- 10 μl TEMED
- 100 μl 10% Ammonium persulfate (APS)

4.12 Primer Extension Assay

Primer extension reactions were performed at 30°C in polymerization buffer (25 mM Tris-HCl pH 7.5, 8 mM Magnesium Acetate, 5 mM Potassium Glutamate, 5% Glycerol). Purified proteins used in the primer extension assays were purified as previously described (Devbhandari and Remus, 2020). DNA template for the assay was generated by annealing a primer (5′-CCCAGTCACGACGTTGTAAAACG-3′) to M13mp18 single-stranded DNA (New England Biolabs, N4040S). The assay was initiated by incubation of 1nM of DNA template with 1 mM ATP, 1 mM DTT, 80 μM dATP, 80 μM dGTP, 80 μM dCTP and 400 nM of RPA for 5 minutes. PCNA and RFC were then added to 70 nM and 4 nM, respectively, and incubation was continued for 5 minutes. Then, 33 nM of a-^{32}P-dATP (3,000 Ci per mmol) and 4 nM of either Pol δ^{WT} or Pol δ^{D941Y} was added to the reaction resulting in a primer extension by 9 base pairs (due to lack of dTTP). After 5 min, 80 μM dTTP were added to the mix for synchronous primer extension. Equal volume aliquots of this reaction (18 μl) were removed from the master reaction (100 μl) at indicated times and stopped by adding EDTA and SDS to final concentrations of 40 mM and 0.25%, respectively. Products were fractionated on a 0.8% alkaline agarose gel (30 mM NaOH and 2 mM EDTA), dried and imaged using Typhoon FLA 7000. Quantification of the gel images was performed using the ImageJ.

4.13 Quantitation of Total Cells, EdU Signal Intensity, EdU-Positive Cells

E6.0, E6.5, and E7.0 whole mount EdU-labeled embryos were imaged using Leica SP8 inverted laser scanning confocal microscope and confocal z stacks of embryos were generated. *tyrn* mutant and wildtype embryos of the same stage were imaged under the same conditions. For each stage, 3 embryos per genotype were imaged for quantification. Optical sections of each embryo were imported into Imaris (version 9.5, Oxford Instruments), and 3D-reconstitution along Z-axis was performed for data analysis. We used spots function in Imaris to automatically segment all DAPI-positive cells (in both embryonic and extraembryonic tissues) to obtain a total cell count for each embryo. EdU signal intensity of each segmented cell was automatically measured, and the background signal was subtracted. Cells with EdU signal above 10 arbitrary units were considered EdU positive and counted as EdU positive cells by the software. We used Prism 9 (GraphPad) to perform normalization of EdU signal intensity. At each stage, the EdU signal of each EdU positive cell was normalized to the maximum EdU signal intensity. Data points were presented as box plots to show the distribution of EdU signal intensity among EdU positive cell population. Within the box plot, the median is represented by the horizontal dividing line and the top and bottom of the box represent the seventy-fifth and twenty-fifth percentile, with the whiskers indicating the maximum and minimum points. Two-tailed Student's *t*-test was performed to evaluate the significance of all measurements.

4.14 Statistics and Graphs

Embryo images n = 3 for all the experiments. For primer extension assay, 3 biological replicates were performed. We used Prism 9 to perform a 2-tailed Student's *t-test* to evaluate the significance of all measurements and generated box plots and non-linear fitted curves. For the structure of human DNA polymerase δ, the original structure was

imported and processed in PyMOL (The PyMOL Molecular Graphics System, Version 1.2r3pre. Schrödinger, LLC)

4.15 Data availability

The structure of the human DNA polymerase delta holoenzyme was pulled from the protein data bank (PDB). PDB DOI: 10.2210/pdb6TNY/pdb. EM Map EMD-10539: EMDB EMDataResource.

Appendix

List of solutions and stocks

Name	Ingredient Concentration
4% PFA solution	4% PFA (v/v), 0.1% Tween 20 (v/v), 137 mM NaCl, 2.7 mM KCl, 10 mM Na_2HPO_4, 1.8 mM KH_2PO_4
APS stock solution	10% $(NH_4)_2S_2O_8$ (ammonium persulfate) (w/v)
Blocking buffer (immunostaining)	1% heat-inactivated donkey serum (v/v), 0.1% Triton X-100 (v/v), 137 mM NaCl, 2.7 mM KCl, 10 mM Na_2HPO_4, 1.8 mM KH_2PO_4
Blocking buffer (in situ hybridization)	1% heat-inactivated goat serum(v/v), 0.1% Triton X-100 (v/v), 137 mM NaCl, 2.7 mM KCl, 10 mM Na_2HPO_4, 1.8 mM KH_2PO_4
Blocking buffer (western blot)	5% milk (w/v), 150 mM NaCl, 50 mM Tris-HCl, pH 7.6
EDTA stock solution	200 mM EDTA
MAB buffer	100 mM Maleic acid, 150 mM NaCl, pH 7.5
MgCl2 stock solution	1 M
NaCl stock solution	5 M
NTMT buffer	0.1 Tween 20 (v/v), 100 mM Tris HCl, 50mM $MgCl_2$, 100mM NaCl,
PBS 1 X	137 mM NaCl, 2.7 mM KCl, 10 mM Na_2HPO_4, 1.8 mM KH_2PO_4

PBS 10 X	1.3 M NaCl, 27 mM KCl, 100 mM Na_2HPO_4, 18 mM KH_2PO_4
PBS-BSA (EdU staining)	3% BSA (w/v), 137 mM NaCl, 2.7 mM KCl, 10 mM Na_2HPO_4, 1.8 mM KH_2PO_4
PBS-BSA (embryo dissection)	0.4% BSA (w/v), 137 mM NaCl, 2.7 mM KCl, 10 mM Na_2HPO_4, 1.8 mM KH_2PO_4
PBS-BSA (in situ hybridization)	0.1% BSA (w/v), 137 mM NaCl, 2.7 mM KCl, 10 mM Na_2HPO_4, 1.8 mM KH_2PO_4
PBS-Triton X (section slides immunofluorescence)	0.1% Triton X-100 (v/v), 137 mM NaCl, 2.7 mM KCl, 10 mM Na_2HPO_4, 1.8 mM KH_2PO_4
PBS-Triton X (whole-mount immunofluorescence)	0.3% Triton X-100 (v/v), 137 mM NaCl, 2.7 mM KCl, 10 mM Na_2HPO_4, 1.8 mM KH_2PO_4
PBS-Tween 20	0.1% Tween 20 (v/v), 137 mM NaCl, 2.7 mM KCl, 10 mM Na_2HPO_4, 1.8 mM KH_2PO_4
PCR buffer 10 X	200 mM Tris-HCl, 500 mM KCl, pH 8.4
Proteinase K solution (genotyping)	15% Proteinase K (v/v), 20 mM Tris-HCl, 50 mM KCl, pH 8.4
Proteinase K solution (in situ hybridization)	0.1% Proteinase K (v/v), 20 mM Tris-HCl, 50 mM KCl, pH 8.4
SDS stock solution 100X	10% SDS (w/v)
SSC 20 X	3 M NaCl, 0.3 M $Na_3C_6H_5O_7$ (Sodium Citrate), pH 7.0

SSC, pH 4.5 2 X	0.3 M NaCl, 30 mM $Na_3C_6H_5O_7$, pH 4.5
SSC, pH 7.0 2 X	0.3 M NaCl, 30 mM $Na_3C_6H_5O_7$, pH 7.0
TBE buffer 1 X	100 mM Tris-base, 90 mM Boric acid, 1 mM EDTA
TBE buffer 10 X	1 M Tris-base, 0.9 M Boric acid, 10 mM EDTA
TBS 10 X	1.5 M NaCl, 500 mM Tris-HCl, pH 7.6
TBS-Tween 20 1 X	150 mM NaCl, 50 mM Tris-HCl, pH 7.6
Tris HCl stock solution pH 7.2	1 M Tris-HCl, pH 7.2
Tris HCl stock solution pH 9.5	1 M Tris-base, pH 9.5

List of reagents and antibodies

Name	Catalog Number	Brand
Human/Mouse/Rat SOX2 Antibody, Polyclonal Goat IgG	AF 2018	R & D SYSTEMS
T (Brachyury) Rabbit mAb	816945	Cell Signaling
Recombinant Anti-FOXA2 antibody [EPR4466]	ab108422	Abcam
N-Cadherin (D4R1H) XP Rabbit mAb	13116T	Cell Signaling
Monoclonal Anti-Uvomorulin/E-Cadherin antibody	U3254	Sigma-Aldrich
Phospho-Smad1/5/9 Rabbit mAb	13820	Cell Signaling
Purified Rat Anti-Mouse Flk-1	555307	BD Pharmingen
CDX2 (D11D10) Rabbit mAb	12306S	Cell Signaling
Anti-POLD1 antibody	ab168827	Abcam
Donkey anti-Rat IgG(H+L) Highly Cross-Absorbed Secondary Antibody, Alexa Fluor plus 594	A-211209	Invitrogen
Donkey anti-Rabbit IgG(H+L) Cross-Absorbed Secondary Antibody, Alexa Fluor 594	A-21207	Invitrogen
Donkey anti-Rabbit IgG(H+L) Cross-Absorbed Secondary Antibody, Alexa Fluor 568	A-10042	Invitrogen

Donkey anti-Goat IgG (H+L) Cross-Absorbed Secondary Antibody, Alexa Fluor 488	A-11055	Invitrogen
Donkey anti-Goat IgG (H+L) Cross-Absorbed Secondary Antibody, Alexa Fluor 488	A-32790	Invitrogen
Donkey anti-Goat IgG (H+L) Cross-Absorbed Secondary Antibody, Alexa Fluor Plus 647	A32849	Invitrogen
Amersham ECL Rabbit IgG, HRP-linked whole Ab (from donkey)	NA934	Cytiva Life Sciences
4,6-diamidino-2-phenylindole dihydrochloride (DAPI)	D9542	Sigma-Aldrich
RsaI	R0167L	New England Biolabs
HindIII	R0104S	New England Biolabs
BamHI	R0136S	New England Biolabs
XbaI	R0145S	New England Biolabs
rCutsmart Buffer	B6004S	New England Biolabs
NEBuffer 2	B7003S	New England Biolabs
NEBuffer 3.1	B7002S	New England Biolabs
Platinum Taq DNA Polymerase	10966026	Invitrogen
Deoxynucleoside Triphosphate Set, PCR Grade, sodium salt	11969064001	Roche
Proteinase K, recombinant, PCR Grade	3115828001	Roche

Phusion High-Fidelity DNA Polymerase	M0530S	New England Biolabs
Donor Donkey Serum	101-151	GeminiBio
Donor Goat serum	100-109	GeminiBio
Bovine Serum Albumin	A7906	Sigma-Aldrich
QIAquick PCR Purification Kit	28106	QIAGEN
QIAquick Gel Extraction Kit	28706	QIAGEN
QIAquick Spin Miniprep Kit	27106	QIAGEN
Gentra Puregene Kit	158667	QIAGEN
One Shot TOP10 Chemically Competent *E.Coli*	C404010	Invitrogen
DIG RNA Labeling Mix	11277073910	Roche
Anti-Digoxigenin-AP, Fab fragments	11093274910	Roche
Click-iT EdU Cell Proliferation Kit for Imaging, Alexa Fluor 647 dye	C10340	Invitrogen
TEMED	1610800	Bio-Rad Laboratories
30% Acrylamide/Bis Solution	1610158	Bio-Rad Laboratories
Quick Start Bradford 1X Dye Reagent	5000205	Bio-Rad Laboratories
Gibson Assembly Master Mix	E2611S	New England Biolabs
Gel Loading Dye, Purple (6X)	B7024S	New England Biolabs
RNase*Zap* RNase Decontamination Solution	AM9780	Invitrogen
Blocking Reagent	11096176001	Roche
BM-Purple	11442074001	Roche

List of primers

Target gene (allele)	Forward 5'-3'	Reverse 5'-3'
Pold1 (*tyrn*)	atgcttctgacccctgcacc	gagtgtcgatgggcaggctg
Pold1 (wildtype)	ggagttgctcctgtggaagacc	aggaatgaggtgaaccacatcccg
Pold1 (tm1a or *tm1b, LacZ* reporter)	atcctctgcatggtcaggtc	cgtggcctgattcattcc
Cre	attgctgtcacttggtcgtggc	ggaaaatgcttctgtccgtttgc
Hhex-GFP	aagttcatctgcaccaccg	tccttgaagaagatggtgcg
Pol3 Gibson Assembly Insertion Piece 1	ggcgaagaattgttaattaag agctcttaccacttagac	agttgtacaacagagctgaatac ccattgttcgttttggaaaac
Pol3 Gibson Assembly Insertion Piece 2	ttcagctctgttgtacaacttatcg	cgaattcaaccctcactaaaggg cggccgcaatgtctccaattttggg
Flp (*flippase*)	gtggatcgatcctacccttgcg	ggtccaactgcagcccaagcttcc
Pold1 (*loxP*)	acgaagttatggtctgagctcgcc	ggcagattcccctctgtgca

List of chemicals

Name	Catalog Number	Brand
Glycine, 2kg	1610724	Bio-Rad Laboratories
SDS (Sodium Dodecyl Sulfate)	1610302	Bio-Rad Laboratories
Agarose	BP 160-500	Fisher Bioreagents
Boric Acid	A73-1	Fisher Bioreagents
D-Sucrose	BP220-212	Fisher Bioreagents
Ethylenediaminetetraacetic Acid, Disodium Salt Dihydrate	S311-100	Fisher Bioreagents
Magnesium Chloride Hexahydrate	M33-500	Fisher Bioreagents
Potassium Chloride	P217-500	Fisher Bioreagents
Potassium Phosphate Monobasic	BP362-500	Fisher Bioreagents
Sodium Chloride	BP358-10	Fisher Bioreagents
Sodium Citrate Dihydrate	S279-3	Fisher Bioreagents
Sodium Phosphate Dibasic Heptahydrate	BP331-500	Fisher Bioreagents
Sodium Phosphate Monobasic Monohydrate	BP330-500	Fisher Bioreagents

Tris Base	BP152-25	Fisher Bioreagents
Tris Hydrochloride	BP153-500	Fisher Bioreagents
Triton X- 100	AAA160460F	Fisher Bioreagents
Tween 20	BP337-100	Fisher Bioreagents
Ammonium Persulfate	A3678	Sigma Aldrich
CHAPS Hydrate	C3023	Sigma Aldrich
Diethyl pyrocarbonate	D5758	Sigma Aldrich
Formamide	221198	Sigma Aldrich
Heparin sodium salt from porcine intestinal mucosa	H3393	Sigma Aldrich
Maleic acid	MX0100	Sigma Aldrich
Ribonucleic acid from torula yeast	R6625-25G	Sigma Aldrich

Bibliography

Acampora, D., Di Giovannantonio, L. G., Di Salvio, M., Mancuso, P. and Simeone, A. (2009). Selective inactivation of Otx2 mRNA isoforms reveals isoform-specific requirement for visceral endoderm anteriorization and head morphogenesis and highlights cell diversity in the visceral endoderm. *Mech Dev* **126**, 882-897.

Ahsan, K., Singh, N., Rocha, M., Huang, C. and Prince, V. E. (2019). Prickle1 is required for EMT and migration of zebrafish cranial neural crest. *Dev Biol* **448**, 16-35.

Alarcon, V. B. (2010). Cell polarity regulator PARD6B is essential for trophectoderm formation in the preimplantation mouse embryo. *Biol Reprod* **83**, 347-358.

Alexandre, H. (1979). The utilization of an inhibitor of spermidine and spermine synthesis as a tool for the study of the determination of cavitation in the preimplantation mouse embryo. *J Embryol Exp Morphol* **53**, 145-162.

Amack, J. D. (2021). Cellular dynamics of EMT: lessons from live in vivo imaging of embryonic development. *Cell Commun Signal* **19**, 79.

Anderson, K. V., Jurgens, G. and Nusslein-Volhard, C. (1985). Establishment of dorsal-ventral polarity in the Drosophila embryo: genetic studies on the role of the Toll gene product. *Cell* **42**, 779-789.

Andreazzoli, M., Gestri, G., Cremisi, F., Casarosa, S., Dawid, I. B. and Barsacchi, G. (2003). Xrx1 controls proliferation and neurogenesis in Xenopus anterior neural plate. *Development* **130**, 5143-5154.

Ang, S. L., Jin, O., Rhinn, M., Daigle, N., Stevenson, L. and Rossant, J. (1996). A targeted mouse Otx2 mutation leads to severe defects in gastrulation and formation of axial mesoderm and to deletion of rostral brain. *Development* **122**, 243-252.

Ang, S. L. and Rossant, J. (1994). HNF-3 beta is essential for node and notochord formation in mouse development. *Cell* **78**, 561-574.

Aoki, T. O., David, N. B., Minchiotti, G., Saint-Etienne, L., Dickmeis, T., Persico, G. M., Strahle, U., Mourrain, P. and Rosa, F. M. (2002). Molecular integration of casanova in the Nodal signalling pathway controlling endoderm formation. *Development* **129**, 275-286.

Aria, V. and Yeeles, J. T. (2019). Mechanism of bidirectional leading-strand synthesis establishment at eukaryotic DNA replication origins. *Molecular cell* **73**, 199-211. e110.

Arkell, R. M. and Tam, P. P. (2012). Initiating head development in mouse embryos: integrating signalling and transcriptional activity. *Open Biol* **2**, 120030.

Arnold, S. J., Hofmann, U. K., Bikoff, E. K. and Robertson, E. J. (2008). Pivotal roles for eomesodermin during axis formation, epithelium-to-mesenchyme transition and endoderm specification in the mouse. *Development* **135**, 501-511.

Arnold, S. J. and Robertson, E. J. (2009). Making a commitment: cell lineage allocation and axis patterning in the early mouse embryo. *Nat Rev Mol Cell Biol* **10**, 91-103.

Arroyo, M. and Raychaudhuri, P. (1992). Retinoblastoma-repression of E2F-dependent transcription depends on the ability of the retinoblastoma protein to interact with E2F and is abrogated by the adenovirus E1A oncoprotein. *Nucleic Acids Res* **20**, 5947-5954.

Artavanis-Tsakonas, S., Matsuno, K. and Fortini, M. E. (1995). Notch signaling. *Science* **268**, 225-232.

Artus, J. and Chazaud, C. (2014). A close look at the mammalian blastocyst: epiblast and primitive endoderm formation. *Cellular and molecular life sciences* **71**, 3327-3338.

Artus, J., Piliszek, A. and Hadjantonakis, A. K. (2011). The primitive endoderm lineage of the mouse blastocyst: sequential transcription factor activation and regulation of differentiation by Sox17. *Dev Biol* **350**, 393-404.

Axelrod, J. D., Miller, J. R., Shulman, J. M., Moon, R. T. and Perrimon, N. (1998). Differential recruitment of Dishevelled provides signaling specificity in the planar cell polarity and Wingless signaling pathways. *Genes Dev* **12**, 2610-2622.

Azar, Y. and Eyal-Giladi, H. (1979). Marginal zone cells--the primitive streak-inducing component of the primary hypoblast in the chick. *J Embryol Exp Morphol* **52**, 79-88.
---- (1981). Interaction of epiblast and hypoblast in the formation of the primitive streak and the embryonic axis in chick, as revealed by hypoblast-rotation experiments. *J Embryol Exp Morphol* **61**, 133-144.
Azpiazu, N. and Frasch, M. (1993). tinman and bagpipe: two homeo box genes that determine cell fates in the dorsal mesoderm of Drosophila. *Genes Dev* **7**, 1325-1340.
Bachiller, D., Klingensmith, J., Kemp, C., Belo, J. A., Anderson, R. M., May, S. R., McMahon, J. A., McMahon, A. P., Harland, R. M., Rossant, J., et al. (2000). The organizer factors Chordin and Noggin are required for mouse forebrain development. *Nature* **403**, 658-661.
Bachvarova, R. F., Skromne, I. and Stern, C. D. (1998). Induction of primitive streak and Hensen's node by the posterior marginal zone in the early chick embryo. *Development* **125**, 3521-3534.
Bailles, A., Collinet, C., Philippe, J. M., Lenne, P. F., Munro, E. and Lecuit, T. (2019). Genetic induction and mechanochemical propagation of a morphogenetic wave. *Nature* **572**, 467-473.
Baker, R. and Schubiger, G. (1995). Ectoderm induces muscle-specific gene expression in Drosophila embryos. *Development* **121**, 1387-1398.
Balakrishnan, L. and Bambara, R. A. (2013). Flap endonuclease 1. *Annu Rev Biochem* **82**, 119-138.
Bandara, L. R. and La Thangue, N. B. (1991). Adenovirus E1a prevents the retinoblastoma gene product from complexing with a cellular transcription factor. *Nature* **351**, 494-497.
Banerjee, S., Gordon, L., Donn, T. M., Berti, C., Moens, C. B., Burden, S. J. and Granato, M. (2011). A novel role for MuSK and non-canonical Wnt signaling during segmental neural crest cell migration. *Development* **138**, 3287-3296.
Bardot, E., Calderon, D., Santoriello, F., Han, S., Cheung, K., Jadhav, B., Burtscher, I., Artap, S., Jain, R., Epstein, J., et al. (2017). Foxa2 identifies a cardiac progenitor population with ventricular differentiation potential. *Nat Commun* **8**, 14428.
Bardot, E. S. and Hadjantonakis, A.-K. (2020). Mouse gastrulation: coordination of tissue patterning, specification and diversification of cell fate. *Mechanisms of development* **163**, 103617.
Barrett, K., Leptin, M. and Settleman, J. (1997). The Rho GTPase and a putative RhoGEF mediate a signaling pathway for the cell shape changes in Drosophila gastrulation. *Cell* **91**, 905-915.
Barriga, E. H., Franze, K., Charras, G. and Mayor, R. (2018). Tissue stiffening coordinates morphogenesis by triggering collective cell migration in vivo. *Nature* **554**, 523-527.
Bazzi, H., Soroka, E., Alcorn, H. L. and Anderson, K. V. (2017). STRIP1, a core component of STRIPAK complexes, is essential for normal mesoderm migration in the mouse embryo. *Proc Natl Acad Sci U S A* **114**, E10928-E10936.
Beck, F., Erler, T., Russell, A. and James, R. (1995). Expression of Cdx-2 in the mouse embryo and placenta: possible role in patterning of the extra-embryonic membranes. *Dev Dyn* **204**, 219-227.
Beese, L. S. and Steitz, T. A. (1991). Structural basis for the 3'-5' exonuclease activity of Escherichia coli DNA polymerase I: a two metal ion mechanism. *EMBO J* **10**, 25-33.
Belo, J. A., Bouwmeester, T., Leyns, L., Kertesz, N., Gallo, M., Follettie, M. and De Robertis, E. M. (1997). Cerberus-like is a secreted factor with neutralizing activity expressed in the anterior primitive endoderm of the mouse gastrula. *Mech Dev* **68**, 45-57.
Ben-Haim, N., Lu, C., Guzman-Ayala, M., Pescatore, L., Mesnard, D., Bischofberger, M., Naef, F., Robertson, E. J. and Constam, D. B. (2006). The nodal precursor acting

via activin receptors induces mesoderm by maintaining a source of its convertases and BMP4. *Dev Cell* **11**, 313-323.
Bene, F. D., Tessmar-Raible, K. and Wittbrodt, J. (2004). Direct interaction of geminin and Six3 in eye development. *Nature* **427**, 745-749.
Bennett, J. T., Joubin, K., Cheng, S., Aanstad, P., Herwig, R., Clark, M., Lehrach, H. and Schier, A. F. (2007). Nodal signaling activates differentiation genes during zebrafish gastrulation. *Dev Biol* **304**, 525-540.
Berndt, J. D., Clay, M. R., Langenberg, T. and Halloran, M. C. (2008). Rho-kinase and myosin II affect dynamic neural crest cell behaviors during epithelial to mesenchymal transition in vivo. *Dev Biol* **324**, 236-244.
Berthet, C., Aleem, E., Coppola, V., Tessarollo, L. and Kaldis, P. (2003). Cdk2 knockout mice are viable. *Curr Biol* **13**, 1775-1785.
Bertocchini, F. and Stern, C. D. (2002). The hypoblast of the chick embryo positions the primitive streak by antagonizing nodal signaling. *Dev Cell* **3**, 735-744.
Bessonnard, S., De Mot, L., Gonze, D., Barriol, M., Dennis, C., Goldbeter, A., Dupont, G. and Chazaud, C. (2014). Gata6, Nanog and Erk signaling control cell fate in the inner cell mass through a tristable regulatory network. *Development* **141**, 3637-3648.
Bildsoe, H., Loebel, D. A., Jones, V. J., Chen, Y. T., Behringer, R. R. and Tam, P. P. (2009). Requirement for Twist1 in frontonasal and skull vault development in the mouse embryo. *Dev Biol* **331**, 176-188.
Bilinski, S. M. (1998). Ovaries, oogenesis and insect phylogeny. Introductory remarks. *Folia Histochem Cytobiol* **36**, 143-145.
Bisgrove, B. W., Essner, J. J. and Yost, H. J. (1999). Regulation of midline development by antagonism of lefty and nodal signaling. *Development* **126**, 3253-3262.
Bisgrove, B. W., Su, Y. C. and Yost, H. J. (2017). Maternal Gdf3 is an obligatory cofactor in Nodal signaling for embryonic axis formation in zebrafish. *Elife* **6**.
Blakeley, P., Fogarty, N. M., Del Valle, I., Wamaitha, S. E., Hu, T. X., Elder, K., Snell, P., Christie, L., Robson, P. and Niakan, K. K. (2015). Defining the three cell lineages of the human blastocyst by single-cell RNA-seq. *Development* **142**, 3613.
Blow, J. J. and Laskey, R. A. (1988). A role for the nuclear envelope in controlling DNA replication within the cell cycle. *Nature* **332**, 546-548.
Bollum, F. and Potter, V. R. (1957). Thymidine incorporation into deoxyribonucleic acid of rat liver homogenates. *Journal of the American Chemical Society* **79**, 3603-3604.
Boroviak, T., Loos, R., Lombard, P., Okahara, J., Behr, R., Sasaki, E., Nichols, J., Smith, A. and Bertone, P. (2015). Lineage-Specific Profiling Delineates the Emergence and Progression of Naive Pluripotency in Mammalian Embryogenesis. *Dev Cell* **35**, 366-382.
Bort, R., Signore, M., Tremblay, K., Martinez Barbera, J. P. and Zaret, K. S. (2006). Hex homeobox gene controls the transition of the endoderm to a pseudostratified, cell emergent epithelium for liver bud development. *Dev Biol* **290**, 44-56.
Boulet, A., Simon, M., Faye, G., Bauer, G. A. and Burgers, P. M. (1989). Structure and function of the Saccharomyces cerevisiae CDC2 gene encoding the large subunit of DNA polymerase III. *EMBO J* **8**, 1849-1854.
Bourdais, R., Rousseau, B., Pujals, A., Boussion, H., Joly, C., Guillemin, A., Baumgaertner, I., Neuzillet, C. and Tournigand, C. (2017). Polymerase proofreading domain mutations: New opportunities for immunotherapy in hypermutated colorectal cancer beyond MMR deficiency. *Crit Rev Oncol Hematol* **113**, 242-248.
Bousquet, E., Calvayrac, O., Mazieres, J., Lajoie-Mazenc, I., Boubekeur, N., Favre, G. and Pradines, A. (2016). RhoB loss induces Rac1-dependent mesenchymal cell invasion in lung cells through PP2A inhibition. *Oncogene* **35**, 1760-1769.

Bovolenta, P., Mallamaci, A., Puelles, L. and Boncinelli, E. (1998). Expression pattern of cSix3, a member of the Six/sine oculis family of transcription factors. *Mech Dev* **70**, 201-203.
Boward, B., Wu, T. and Dalton, S. (2016). Concise Review: Control of Cell Fate Through Cell Cycle and Pluripotency Networks. *Stem Cells* **34**, 1427-1436.
Brand, M. and Campos-Ortega, J. A. (1988). Two groups of interrelated genes regulate early neurogenesis in Drosophila melanogaster. *Rouxs Arch Dev Biol* **197**, 457-470.
Brandeis, M., Rosewell, I., Carrington, M., Crompton, T., Jacobs, M. A., Kirk, J., Gannon, J. and Hunt, T. (1998). Cyclin B2-null mice develop normally and are fertile whereas cyclin B1-null mice die in utero. *Proc Natl Acad Sci U S A* **95**, 4344-4349.
Bravo, R., Frank, R., Blundell, P. A. and Macdonald-Bravo, H. (1987). Cyclin/PCNA is the auxiliary protein of DNA polymerase-delta. *Nature* **326**, 515-517.
Brennan, J., Lu, C. C., Norris, D. P., Rodriguez, T. A., Beddington, R. S. and Robertson, E. J. (2001). Nodal signalling in the epiblast patterns the early mouse embryo. *Nature* **411**, 965-969.
Briggs, S. and Tomlinson, I. (2013). Germline and somatic polymerase epsilon and delta mutations define a new class of hypermutated colorectal and endometrial cancers. *J Pathol* **230**, 148-153.
Brocas, C., Charbonnier, J. B., Dherin, C., Gangloff, S. and Maloisel, L. (2010). Stable interactions between DNA polymerase delta catalytic and structural subunits are essential for efficient DNA repair. *DNA Repair (Amst)* **9**, 1098-1111.
Buehr, M. and McLaren, A. (1974). Size regulation in chimaeric mouse embryos. *J Embryol Exp Morphol* **31**, 229-234.
Buning, J. (1993). Germ cell cluster formation in insect ovaries. *International Journal of Insect Morphology and Embryology* **22**, 237-253.
Büning, J. (1994). *The insect ovary: ultrastructure, previtellogenic growth and evolution*: Springer Science & Business Media.
Burgers, P. M. (1991). Saccharomyces cerevisiae replication factor C. II. Formation and activity of complexes with the proliferating cell nuclear antigen and with DNA polymerases delta and epsilon. *J Biol Chem* **266**, 22698-22706.
Burmeister, M., Novak, J., Liang, M. Y., Basu, S., Ploder, L., Hawes, N. L., Vidgen, D., Hoover, F., Goldman, D., Kalnins, V. I., et al. (1996). Ocular retardation mouse caused by Chx10 homeobox null allele: impaired retinal progenitor proliferation and bipolar cell differentiation. *Nat Genet* **12**, 376-384.
Burtscher, I. and Lickert, H. (2009). Foxa2 regulates polarity and epithelialization in the endoderm germ layer of the mouse embryo. *Development* **136**, 1029-1038.
Bury, M., Le Calvé, B., Ferbeyre, G., Blank, V. and Lessard, F. (2021). New insights into CDK regulators: novel opportunities for cancer therapy. *Trends in Cell Biology* **31**, 331-344.
Busanello, A., Battistelli, C., Carbone, M., Mostocotto, C. and Maione, R. (2012). MyoD regulates p57kip2 expression by interacting with a distant cis-element and modifying a higher order chromatin structure. *Nucleic Acids Res* **40**, 8266-8275.
Butler, M. T. and Wallingford, J. B. (2017). Planar cell polarity in development and disease. *Nat Rev Mol Cell Biol* **18**, 375-388.
Byrnes, J. J., Downey, K. M., Black, V. L. and So, A. G. (1976). A new mammalian DNA polymerase with 3' to 5' exonuclease activity: DNA polymerase delta. *Biochemistry* **15**, 2817-2823.
Callebaut, M. and Van Nueten, E. (1994). Rauber's (Koller's) sickle: the early gastrulation organizer of the avian blastoderm. *Eur J Morphol* **32**, 35-48.
Campbell, K. H., Loi, P., Otaegui, P. J. and Wilmut, I. (1996). Cell cycle co-ordination in embryo cloning by nuclear transfer. *Rev Reprod* **1**, 40-46.
Campbell, K. H., Ritchie, W. A. and Wilmut, I. (1993). Nuclear-cytoplasmic interactions during the first cell cycle of nuclear transfer reconstructed bovine embryos:

implications for deoxyribonucleic acid replication and development. *Biol Reprod* **49**, 933-942.

Camus, A., Davidson, B. P., Billiards, S., Khoo, P., Rivera-Perez, J. A., Wakamiya, M., Behringer, R. R. and Tam, P. P. (2000). The morphogenetic role of midline mesendoderm and ectoderm in the development of the forebrain and the midbrain of the mouse embryo. *Development* **127**, 1799-1813.

Camus, A., Perea-Gomez, A., Moreau, A. and Collignon, J. (2006). Absence of Nodal signaling promotes precocious neural differentiation in the mouse embryo. *Dev Biol* **295**, 743-755.

Canizo, J. R., Ynsaurralde Rivolta, A. E., Vazquez Echegaray, C., Suva, M., Alberio, V., Aller, J. F., Guberman, A. S., Salamone, D. F., Alberio, R. H. and Alberio, R. (2019). A dose-dependent response to MEK inhibition determines hypoblast fate in bovine embryos. *BMC Dev Biol* **19**, 13.

Canning, D. R. and Stern, C. D. (1988). Changes in the expression of the carbohydrate epitope HNK-1 associated with mesoderm induction in the chick embryo. *Development* **104**, 643-655.

Cano, A., Perez-Moreno, M. A., Rodrigo, I., Locascio, A., Blanco, M. J., del Barrio, M. G., Portillo, F. and Nieto, M. A. (2000). The transcription factor snail controls epithelial-mesenchymal transitions by repressing E-cadherin expression. *Nat Cell Biol* **2**, 76-83.

Cao, Z., Carey, T. S., Ganguly, A., Wilson, C. A., Paul, S. and Knott, J. G. (2015). Transcription factor AP-2gamma induces early Cdx2 expression and represses HIPPO signaling to specify the trophectoderm lineage. *Development* **142**, 1606-1615.

Capek, D., Smutny, M., Tichy, A. M., Morri, M., Janovjak, H. and Heisenberg, C. P. (2019). Light-activated Frizzled7 reveals a permissive role of non-canonical wnt signaling in mesendoderm cell migration. *Elife* **8**.

Carmany-Rampey, A. and Schier, A. F. (2001). Single-cell internalization during zebrafish gastrulation. *Curr Biol* **11**, 1261-1265.

Carney, T. J., Dutton, K. A., Greenhill, E., Delfino-Machin, M., Dufourcq, P., Blader, P. and Kelsh, R. N. (2006). A direct role for Sox10 in specification of neural crest-derived sensory neurons. *Development* **133**, 4619-4630.

Carver, E. A., Jiang, R., Lan, Y., Oram, K. F. and Gridley, T. (2001). The mouse snail gene encodes a key regulator of the epithelial-mesenchymal transition. *Mol Cell Biol* **21**, 8184-8188.

Casanova, J. (1990). Pattern formation under the control of the terminal system in the Drosophila embryo. *Development* **110**, 621-628.

Casarosa, S., Amato, M. A., Andreazzoli, M., Gestri, G., Barsacchi, G. and Cremisi, F. (2003). Xrx1 controls proliferation and multipotency of retinal progenitors. *Mol Cell Neurosci* **22**, 25-36.

Casarosa, S., Andreazzoli, M., Simeone, A. and Barsacchi, G. (1997). Xrx1, a novel Xenopus homeobox gene expressed during eye and pineal gland development. *Mech Dev* **61**, 187-198.

Chambers, I., Colby, D., Robertson, M., Nichols, J., Lee, S., Tweedie, S. and Smith, A. (2003). Functional expression cloning of Nanog, a pluripotency sustaining factor in embryonic stem cells. *Cell* **113**, 643-655.

Chan, S. W., Lim, C. J., Guo, F., Tan, I., Leung, T. and Hong, W. (2013). Actin-binding and cell proliferation activities of angiomotin family members are regulated by Hippo pathway-mediated phosphorylation. *J Biol Chem* **288**, 37296-37307.

Chang, L. M. (1977). DNA polymerases from bakers' yeast. *J Biol Chem* **252**, 1873-1880.

Chapman, D. L., Agulnik, I., Hancock, S., Silver, L. M. and Papaioannou, V. E. (1996). Tbx6, a mouse T-Box gene implicated in paraxial mesoderm formation at gastrulation. *Dev Biol* **180**, 534-542.

Chawengsaksophak, K., de Graaff, W., Rossant, J., Deschamps, J. and Beck, F. (2004). Cdx2 is essential for axial elongation in mouse development. *Proc Natl Acad Sci U S A* **101**, 7641-7645.
Chazaud, C. and Rossant, J. (2006). Disruption of early proximodistal patterning and AVE formation in Apc mutants. *Development* **133**, 3379-3387.
Chazaud, C. and Yamanaka, Y. (2016). Lineage specification in the mouse preimplantation embryo. *Development* **143**, 1063-1074.
Chazaud, C., Yamanaka, Y., Pawson, T. and Rossant, J. (2006). Early lineage segregation between epiblast and primitive endoderm in mouse blastocysts through the Grb2-MAPK pathway. *Dev Cell* **10**, 615-624.
Chellappan, S. P., Hiebert, S., Mudryj, M., Horowitz, J. M. and Nevins, J. R. (1991). The E2F transcription factor is a cellular target for the RB protein. *Cell* **65**, 1053-1061.
Chen, C. M. and Cepko, C. L. (2000). Expression of Chx10 and Chx10-1 in the developing chicken retina. *Mech Dev* **90**, 293-297.
Chen, H. and Sukumar, S. (2003). Role of homeobox genes in normal mammary gland development and breast tumorigenesis. *J Mammary Gland Biol Neoplasia* **8**, 159-175.
Chen, X., Ji, Z., Webber, A. and Sharrocks, A. D. (2016). Genome-wide binding studies reveal DNA binding specificity mechanisms and functional interplay amongst Forkhead transcription factors. *Nucleic Acids Res* **44**, 1566-1578.
Chen, Y. and Schier, A. F. (2001). The zebrafish Nodal signal Squint functions as a morphogen. *Nature* **411**, 607-610.
Chilkova, O., Stenlund, P., Isoz, I., Stith, C. M., Grabowski, P., Lundstrom, E. B., Burgers, P. M. and Johansson, E. (2007). The eukaryotic leading and lagging strand DNA polymerases are loaded onto primer-ends via separate mechanisms but have comparable processivity in the presence of PCNA. *Nucleic Acids Res* **35**, 6588-6597.
Chittenden, T., Livingston, D. M. and Kaelin Jr, W. G. (1991). The T/E1A-binding domain of the retinoblastoma product can interact selectively with a sequence-specific DNA-binding protein. *Cell* **65**, 1073-1082.
Chng, S. C., Ho, L., Tian, J. and Reversade, B. (2013). ELABELA: a hormone essential for heart development signals via the apelin receptor. *Dev Cell* **27**, 672-680.
Choksi, S. P., Southall, T. D., Bossing, T., Edoff, K., de Wit, E., Fischer, B. E., van Steensel, B., Micklem, G. and Brand, A. H. (2006). Prospero acts as a binary switch between self-renewal and differentiation in Drosophila neural stem cells. *Dev Cell* **11**, 775-789.
Chu-LaGraff, Q. and Doe, C. Q. (1993). Neuroblast specification and formation regulated by wingless in the Drosophila CNS. *Science* **261**, 1594-1597.
Chung, D. W., Zhang, J. A., Tan, C. K., Davie, E. W., So, A. G. and Downey, K. M. (1991). Primary structure of the catalytic subunit of human DNA polymerase delta and chromosomal location of the gene. *Proc Natl Acad Sci U S A* **88**, 11197-11201.
Ciruna, B. and Rossant, J. (2001). FGF signaling regulates mesoderm cell fate specification and morphogenetic movement at the primitive streak. *Dev Cell* **1**, 37-49.
Ciruna, B. G., Schwartz, L., Harpal, K., Yamaguchi, T. P. and Rossant, J. (1997). Chimeric analysis of fibroblast growth factor receptor-1 (Fgfr1) function: a role for FGFR1 in morphogenetic movement through the primitive streak. *Development* **124**, 2829-2841.
Clark, I. B., Muha, V., Klingseisen, A., Leptin, M. and Müller, H.-A. J. (2011). Fibroblast growth factor signalling controls successive cell behaviours during mesoderm layer formation in Drosophila. *Development* **138**, 2705-2715.
Clausen, A. R., Lujan, S. A., Burkholder, A. B., Orebaugh, C. D., Williams, J. S., Clausen, M. F., Malc, E. P., Mieczkowski, P. A., Fargo, D. C., Smith, D. J., et al.

(2015). Tracking replication enzymology in vivo by genome-wide mapping of ribonucleotide incorporation. *Nat Struct Mol Biol* **22**, 185-191.
Clements, M., Pernaute, B., Vella, F. and Rodriguez, T. A. (2011). Crosstalk between Nodal/activin and MAPK p38 signaling is essential for anterior-posterior axis specification. *Curr Biol* **21**, 1289-1295.
Conlon, F. L., Lyons, K. M., Takaesu, N., Barth, K. S., Kispert, A., Herrmann, B. and Robertson, E. J. (1994). A primary requirement for nodal in the formation and maintenance of the primitive streak in the mouse. *Development* **120**, 1919-1928.
Connell-Crowley, L., Harper, J. W. and Goodrich, D. W. (1997). Cyclin D1/Cdk4 regulates retinoblastoma protein-mediated cell cycle arrest by site-specific phosphorylation. *Molecular biology of the cell* **8**, 287-301.
Coopman, P. and Djiane, A. (2016). Adherens Junction and E-Cadherin complex regulation by epithelial polarity. *Cell Mol Life Sci* **73**, 3535-3553.
Copp, A. (1979). Interaction between inner cell mass and trophectoderm of the mouse blastocyst: II. The fate of the polar trophectoderm.
Corson, L. B., Yamanaka, Y., Lai, K.-M. V. and Rossant, J. (2003). Spatial and temporal patterns of ERK signaling during mouse embryogenesis.
COSTA, M. (1993). Gastrulation in Drosophila: cellular mechanisms of morphogenetic movements. *The development of Drosophila melanogaster* **1**, 425-465.
Costa, M., Wilson, E. T. and Wieschaus, E. (1994). A putative cell signal encoded by the folded gastrulation gene coordinates cell shape changes during Drosophila gastrulation. *Cell* **76**, 1075-1089.
Costello, I., Pimeisl, I. M., Drager, S., Bikoff, E. K., Robertson, E. J. and Arnold, S. J. (2011). The T-box transcription factor Eomesodermin acts upstream of Mesp1 to specify cardiac mesoderm during mouse gastrulation. *Nat Cell Biol* **13**, 1084-1091.
Cox, D. N., Lu, B., Sun, T. Q., Williams, L. T. and Jan, Y. N. (2001). Drosophila par-1 is required for oocyte differentiation and microtubule organization. *Curr Biol* **11**, 75-87.
Cox, R. T. and Spradling, A. C. (2003). A Balbiani body and the fusome mediate mitochondrial inheritance during Drosophila oogenesis. *Development* **130**, 1579-1590.
Crompton, L. A., Du Roure, C. and Rodriguez, T. A. (2007). Early embryonic expression patterns of the mouse Flamingo and Prickle orthologues. *Dev Dyn* **236**, 3137-3143.
Cuevas, D. J., Kawakami, E. and Patricio, F. R. (1997). [Evaluation of small intestine mucosal biopsies obtained simultaneously by suction capsule and endoscopic forceps in children with suspected enteropathy]. *Arq Gastroenterol* **34**, 248-253.
Cullmann, G., Hindges, R., Berchtold, M. W. and Hubscher, U. (1993). Cloning of a mouse cDNA encoding DNA polymerase delta: refinement of the homology boxes. *Gene* **134**, 191-200.
Cvekl, A. and Duncan, M. K. (2007). Genetic and epigenetic mechanisms of gene regulation during lens development. *Prog Retin Eye Res* **26**, 555-597.
Czochor, J. R., Sulkowski, P. and Glazer, P. M. (2016). miR-155 Overexpression Promotes Genomic Instability by Reducing High-fidelity Polymerase Delta Expression and Activating Error-Prone DSB Repair. *Mol Cancer Res* **14**, 363-373.
Daigaku, Y., Keszthelyi, A., Muller, C. A., Miyabe, I., Brooks, T., Retkute, R., Hubank, M., Nieduszynski, C. A. and Carr, A. M. (2015). A global profile of replicative polymerase usage. *Nat Struct Mol Biol* **22**, 192-198.
Daigneault, B. W., Vilarino, M., Rajput, S. K., Frum, T., Smith, G. W. and Ross, P. J. (2018). CRISPR editing validation, immunostaining and DNA sequencing of individual fixed bovine embryos. *Biotechniques* **65**, 281-283.
Darzynkiewicz, Z., Gong, J., Juan, G., Ardelt, B. and Traganos, F. (1996). Cytometry of cyclin proteins. *Cytometry* **25**, 1-13.
David, N. B. and Rosa, F. M. (2001). Cell autonomous commitment to an endodermal fate and behaviour by activation of Nodal signalling. *Development* **128**, 3937-3947.

Dawes-Hoang, R. E., Parmar, K. M., Christiansen, A. E., Phelps, C. B., Brand, A. H. and Wieschaus, E. F. (2005). folded gastrulation, cell shape change and the control of myosin localization. *Development* **132**, 4165-4178.
De Cuevas, M. and Spradling, A. C. (1998). Morphogenesis of the Drosophila fusome and its implications for oocyte specification. *Development* **125**, 2781-2789.
De Paepe, C., Cauffman, G., Verloes, A., Sterckx, J., Devroey, P., Tournaye, H., Liebaers, I. and Van de Velde, H. (2013). Human trophectoderm cells are not yet committed. *Hum Reprod* **28**, 740-749.
Dean, W. L. and Rossant, J. (1984). Effect of delaying DNA replication on blastocyst formation in the mouse. *Differentiation* **26**, 134-137.
Degelmann, A., Hardy, P. A., Perrimon, N. and Mahowald, A. P. (1986). Developmental analysis of the torso-like phenotype in Drosophila produced by a maternal-effect locus. *Dev Biol* **115**, 479-489.
Deglincerti, A., Croft, G. F., Pietila, L. N., Zernicka-Goetz, M., Siggia, E. D. and Brivanlou, A. H. (2016). Self-organization of the in vitro attached human embryo. *Nature* **533**, 251-254.
Del Bene, F. and Wittbrodt, J. (2005). Cell cycle control by homeobox genes in development and disease. *Semin Cell Dev Biol* **16**, 449-460.
Deng, W. and Lin, H. (1997). Spectrosomes and Fusomes Anchor Mitotic Spindles during Asymmetric Germ Cell Divisions and Facilitate the Formation of a Polarized Microtubule Array for Oocyte Specification inDrosophila. *Developmental biology* **189**, 79-94.
Devbhandari, S., Jiang, J., Kumar, C., Whitehouse, I. and Remus, D. (2017). Chromatin Constrains the Initiation and Elongation of DNA Replication. *Mol Cell* **65**, 131-141.
Devbhandari, S. and Remus, D. (2020). Rad53 limits CMG helicase uncoupling from DNA synthesis at replication forks. *Nat Struct Mol Biol* **27**, 461-471.
Devenport, D. (2016). Tissue morphodynamics: Translating planar polarity cues into polarized cell behaviors. *Semin Cell Dev Biol* **55**, 99-110.
Di-Gregorio, A., Sancho, M., Stuckey, D. W., Crompton, L. A., Godwin, J., Mishina, Y. and Rodriguez, T. A. (2007). BMP signalling inhibits premature neural differentiation in the mouse embryo. *Development* **134**, 3359-3369.
Di Tullio, A. and Graf, T. (2012). C/EBP α bypasses cell cycle-dependency during immune cell transdifferentiation. *Cell Cycle* **11**, 2739-2746.
Dickmeis, T., Aanstad, P., Clark, M., Fischer, N., Herwig, R., Mourrain, P., Blader, P., Rosa, F., Lehrach, H. and Strahle, U. (2001). Identification of nodal signaling targets by array analysis of induced complex probes. *Dev Dyn* **222**, 571-580.
Dietrich, J. E. and Hiiragi, T. (2007). Stochastic patterning in the mouse pre-implantation embryo. *Development* **134**, 4219-4231.
Ding, J., Yang, L., Yan, Y. T., Chen, A., Desai, N., Wynshaw-Boris, A. and Shen, M. M. (1998). Cripto is required for correct orientation of the anterior-posterior axis in the mouse embryo. *Nature* **395**, 702-707.
Dougan, S. T., Warga, R. M., Kane, D. A., Schier, A. F. and Talbot, W. S. (2003). The role of the zebrafish nodal-related genes squint and cyclops in patterning of mesendoderm. *Development* **130**, 1837-1851.
Dubrulle, J., Jordan, B. M., Akhmetova, L., Farrell, J. A., Kim, S. H., Solnica-Krezel, L. and Schier, A. F. (2015). Response to Nodal morphogen gradient is determined by the kinetics of target gene induction. *Elife* **4**.
Dumortier, J. G. and David, N. B. (2015). The TORC2 component, Sin1, controls migration of anterior mesendoderm during zebrafish gastrulation. *PLoS One* **10**, e0118474.
Dumortier, J. G., Martin, S., Meyer, D., Rosa, F. M. and David, N. B. (2012). Collective mesendoderm migration relies on an intrinsic directionality signal transmitted through cell contacts. *Proc Natl Acad Sci U S A* **109**, 16945-16950.

Dunn, N. R., Vincent, S. D., Oxburgh, L., Robertson, E. J. and Bikoff, E. K. (2004). Combinatorial activities of Smad2 and Smad3 regulate mesoderm formation and patterning in the mouse embryo. *Development* **131**, 1717-1728.
Dyer, M. A., Livesey, F. J., Cepko, C. L. and Oliver, G. (2003). Prox1 function controls progenitor cell proliferation and horizontal cell genesis in the mammalian retina. *Nat Genet* **34**, 53-58.
Dynlacht, B. D., Flores, O., Lees, J. A. and Harlow, E. (1994). Differential regulation of E2F transactivation by cyclin/cdk2 complexes. *Genes Dev* **8**, 1772-1786.
Egli, D., Birkhoff, G. and Eggan, K. (2008). Mediators of reprogramming: transcription factors and transitions through mitosis. *Nat Rev Mol Cell Biol* **9**, 505-516.
Elouej, S., Beleza-Meireles, A., Caswell, R., Colclough, K., Ellard, S., Desvignes, J. P., Beroud, C., Levy, N., Mohammed, S. and De Sandre-Giovannoli, A. (2017). Exome sequencing reveals a de novo POLD1 mutation causing phenotypic variability in mandibular hypoplasia, deafness, progeroid features, and lipodystrophy syndrome (MDPL). *Metabolism* **71**, 213-225.
Enders, A. C. and King, B. F. (1988). Formation and differentiation of extraembryonic mesoderm in the rhesus monkey. *American journal of anatomy* **181**, 327-340.
Eyal-Giladi, H. and Khaner, O. (1989). The chick's marginal zone and primitive streak formation: II. Quantification of the marginal zone's potencies—Temporal and spatial aspects. *Developmental biology* **134**, 215-221.
Eyal-Giladi, H. and Kochav, S. (1976). From cleavage to primitive streak formation: a complementary normal table and a new look at the first stages of the development of the chick: I. General morphology. *Developmental biology* **49**, 321-337.
Faast, R., White, J., Cartwright, P., Crocker, L., Sarcevic, B. and Dalton, S. (2004). Cdk6-cyclin D3 activity in murine ES cells is resistant to inhibition by p16(INK4a). *Oncogene* **23**, 491-502.
Fan, Y., Min, Z., Alsolami, S., Ma, Z., Zhang, E., Chen, W., Zhong, K., Pei, W., Kang, X., Zhang, P., et al. (2021). Generation of human blastocyst-like structures from pluripotent stem cells. *Cell Discov* **7**, 81.
Feldman, B., Concha, M. L., Saude, L., Parsons, M. J., Adams, R. J., Wilson, S. W. and Stemple, D. L. (2002). Lefty antagonism of Squint is essential for normal gastrulation. *Curr Biol* **12**, 2129-2135.
Feldman, B., Dougan, S. T., Schier, A. F. and Talbot, W. S. (2000). Nodal-related signals establish mesendodermal fate and trunk neural identity in zebrafish. *Curr Biol* **10**, 531-534.
Feldman, B., Gates, M. A., Egan, E. S., Dougan, S. T., Rennebeck, G., Sirotkin, H. I., Schier, A. F. and Talbot, W. S. (1998). Zebrafish organizer development and germ-layer formation require nodal-related signals. *Nature* **395**, 181-185.
Ferretti, E. and Hadjantonakis, A. K. (2019). Mesoderm specification and diversification: from single cells to emergent tissues. *Curr Opin Cell Biol* **61**, 110-116.
Fiorillo, C., D'Apice, M. R., Trucco, F., Murdocca, M., Spitalieri, P., Assereto, S., Baratto, S., Morcaldi, G., Minetti, C., Sangiuolo, F., et al. (2018). Characterization of MDPL Fibroblasts Carrying the Recurrent p.Ser605del Mutation in POLD1 Gene. *DNA Cell Biol*.
FOE, V. E. (1993). Mitosis and morphogenesis in the Drosophila embryo: point and counterpoint. *The development of Drosophila melanogaster*, 149-300.
Foe, V. E. and Alberts, B. M. (1983). Studies of nuclear and cytoplasmic behaviour during the five mitotic cycles that precede gastrulation in Drosophila embryogenesis. *Journal of cell science* **61**, 31-70.
Fogarty, N. M. E., McCarthy, A., Snijders, K. E., Powell, B. E., Kubikova, N., Blakeley, P., Lea, R., Elder, K., Wamaitha, S. E., Kim, D., et al. (2017). Genome editing reveals a role for OCT4 in human embryogenesis. *Nature* **550**, 67-73.

Fohn, L. E. and Behringer, R. R. (2001). ESX1L, a novel X chromosome-linked human homeobox gene expressed in the placenta and testis. *Genomics* **74**, 105-108.
Foley, A. C., Skromne, I. and Stern, C. D. (2000). Reconciling different models of forebrain induction and patterning: a dual role for the hypoblast. *Development* **127**, 3839-3854.
Fortune, J. M., Pavlov, Y. I., Welch, C. M., Johansson, E., Burgers, P. M. and Kunkel, T. A. (2005). Saccharomyces cerevisiae DNA polymerase delta: high fidelity for base substitutions but lower fidelity for single- and multi-base deletions. *J Biol Chem* **280**, 29980-29987.
Francesconi, S., Park, H. and Wang, T. S. (1993). Fission yeast with DNA polymerase delta temperature-sensitive alleles exhibits cell division cycle phenotype. *Nucleic Acids Res* **21**, 3821-3828.
Frankenberg, S., Gerbe, F., Bessonnard, S., Belville, C., Pouchin, P., Bardot, O. and Chazaud, C. (2011). Primitive endoderm differentiates via a three-step mechanism involving Nanog and RTK signaling. *Dev Cell* **21**, 1005-1013.
Franklin, M. C., Wang, J. and Steitz, T. A. (2001). Structure of the replicating complex of a pol alpha family DNA polymerase. *Cell* **105**, 657-667.
Frohnhofer, H. G., Lehmann, R. and Nusslein-Volhard, C. (1986). Manipulating the anteroposterior pattern of the Drosophila embryo. *J Embryol Exp Morphol* **97 Suppl**, 169-179.
Fu, Y. V., Yardimci, H., Long, D. T., Ho, T. V., Guainazzi, A., Bermudez, V. P., Hurwitz, J., van Oijen, A., Scharer, O. D. and Walter, J. C. (2011). Selective bypass of a lagging strand roadblock by the eukaryotic replicative DNA helicase. *Cell* **146**, 931-941.
Fujikura, J., Yamato, E., Yonemura, S., Hosoda, K., Masui, S., Nakao, K., Miyazaki Ji, J. and Niwa, H. (2002). Differentiation of embryonic stem cells is induced by GATA factors. *Genes Dev* **16**, 784-789.
Furukawa, T., Kozak, C. A. and Cepko, C. L. (1997). rax, a novel paired-type homeobox gene, shows expression in the anterior neural fold and developing retina. *Proc Natl Acad Sci U S A* **94**, 3088-3093.
Furuno, N., den Elzen, N. and Pines, J. (1999). Human cyclin A is required for mitosis until mid prophase. *J Cell Biol* **147**, 295-306.
Ganier, O., Bocquet, S., Peiffer, I., Brochard, V., Arnaud, P., Puy, A., Jouneau, A., Feil, R., Renard, J. P. and Mechali, M. (2011). Synergic reprogramming of mammalian cells by combined exposure to mitotic Xenopus egg extracts and transcription factors. *Proc Natl Acad Sci U S A* **108**, 17331-17336.
Garbacz, M. A., Lujan, S. A., Burkholder, A. B., Cox, P. B., Wu, Q., Zhou, Z. X., Haber, J. E. and Kunkel, T. A. (2018). Evidence that DNA polymerase delta contributes to initiating leading strand DNA replication in Saccharomyces cerevisiae. *Nat Commun* **9**, 858.
Garcia-Garcia, M. J., Eggenschwiler, J. T., Caspary, T., Alcorn, H. L., Wyler, M. R., Huangfu, D., Rakeman, A. S., Lee, J. D., Feinberg, E. H., Timmer, J. R., et al. (2005). Analysis of mouse embryonic patterning and morphogenesis by forward genetics. *Proc Natl Acad Sci U S A* **102**, 5913-5919.
Gardner, R., Papaioannou, V. and Barton, S. (1973). Origin of the ectoplacental cone and secondary giant cells in mouse blastocysts reconstituted from isolated trophoblast and inner cell mass. *Development* **30**, 561-572.
Garg, P., Stith, C. M., Sabouri, N., Johansson, E. and Burgers, P. M. (2004). Idling by DNA polymerase delta maintains a ligatable nick during lagging-strand DNA replication. *Genes Dev* **18**, 2764-2773.
Gehring, W. J., Qian, Y. Q., Billeter, M., Furukubo-Tokunaga, K., Schier, A. F., Resendez-Perez, D., Affolter, M., Otting, G. and Wuthrich, K. (1994). Homeodomain-DNA recognition. *Cell* **78**, 211-223.

Geng, Y., Yu, Q., Sicinska, E., Das, M., Schneider, J. E., Bhattacharya, S., Rideout, W. M., Bronson, R. T., Gardner, H. and Sicinski, P. (2003). Cyclin E ablation in the mouse. *Cell* **114**, 431-443.

Georgescu, R., Yuan, Z., Bai, L., de Luna Almeida Santos, R., Sun, J., Zhang, D., Yurieva, O., Li, H. and O'Donnell, M. E. (2017). Structure of eukaryotic CMG helicase at a replication fork and implications to replisome architecture and origin initiation. *Proc Natl Acad Sci U S A* **114**, E697-E706.

Georgescu, R. E., Langston, L., Yao, N. Y., Yurieva, O., Zhang, D., Finkelstein, J., Agarwal, T. and O'Donnell, M. E. (2014). Mechanism of asymmetric polymerase assembly at the eukaryotic replication fork. *Nat Struct Mol Biol* **21**, 664-670.

Gerbe, F., Cox, B., Rossant, J. and Chazaud, C. (2008). Dynamic expression of Lrp2 pathway members reveals progressive epithelial differentiation of primitive endoderm in mouse blastocyst. *Dev Biol* **313**, 594-602.

Gerik, K. J., Li, X., Pautz, A. and Burgers, P. M. (1998). Characterization of the two small subunits of Saccharomyces cerevisiae DNA polymerase delta. *J Biol Chem* **273**, 19747-19755.

Gerri, C., McCarthy, A., Alanis-Lobato, G., Demtschenko, A., Bruneau, A., Loubersac, S., Fogarty, N. M. E., Hampshire, D., Elder, K., Snell, P., et al. (2020). Initiation of a conserved trophectoderm program in human, cow and mouse embryos. *Nature* **587**, 443-447.

Gheisari, E., Aakhte, M. and Muller, H. J. (2020). Gastrulation in Drosophila melanogaster: Genetic control, cellular basis and biomechanics. *Mech Dev* **163**, 103629.

Ghysen, A., Dambly-Chaudiere, C., Jan, L. Y. and Jan, Y. N. (1993). Cell interactions and gene interactions in peripheral neurogenesis. *Genes Dev* **7**, 723-733.

Girard, F., Strausfeld, U., Fernandez, A. and Lamb, N. J. (1991). Cyclin A is required for the onset of DNA replication in mammalian fibroblasts. *Cell* **67**, 1169-1179.

Goissis, M. D. and Cibelli, J. B. (2014). Functional characterization of CDX2 during bovine preimplantation development in vitro. *Mol Reprod Dev* **81**, 962-970.

Gomer, R. H. and Firtel, R. A. (1987). Cell-autonomous determination of cell-type choice in Dictyostelium development by cell-cycle phase. *Science* **237**, 758-762.

Gore, A. V., Maegawa, S., Cheong, A., Gilligan, P. C., Weinberg, E. S. and Sampath, K. (2005). The zebrafish dorsal axis is apparent at the four-cell stage. *Nature* **438**, 1030-1035.

Gorski, D. H. and Leal, A. J. (2003). Inhibition of endothelial cell activation by the homeobox gene Gax. *J Surg Res* **111**, 91-99.

Gorski, D. H., LePage, D. F., Patel, C. V., Copeland, N. G., Jenkins, N. A. and Walsh, K. (1993). Molecular cloning of a diverged homeobox gene that is rapidly down-regulated during the G0/G1 transition in vascular smooth muscle cells. *Mol Cell Biol* **13**, 3722-3733.

Goswami, P., Abid Ali, F., Douglas, M. E., Locke, J., Purkiss, A., Janska, A., Eickhoff, P., Early, A., Nans, A., Cheung, A. M. C., et al. (2018). Structure of DNA-CMG-Pol epsilon elucidates the roles of the non-catalytic polymerase modules in the eukaryotic replisome. *Nat Commun* **9**, 5061.

Gottesfeld, J. M. and Forbes, D. J. (1997). Mitotic repression of the transcriptional machinery. *Trends Biochem Sci* **22**, 197-202.

Gottesfeld, J. M., Wolf, V. J., Dang, T., Forbes, D. J. and Hartl, P. (1994). Mitotic repression of RNA polymerase III transcription in vitro mediated by phosphorylation of a TFIIIB component. *Science* **263**, 81-84.

Grabarek, J. B. and Plusa, B. (2012). Live imaging of primitive endoderm precursors in the mouse blastocyst. *Methods Mol Biol* **916**, 275-285.

Grapin-Botton, A. and Constam, D. (2007). Evolution of the mechanisms and molecular control of endoderm formation. *Mech Dev* **124**, 253-278.

Grau, Y., Carteret, C. and Simpson, P. (1984). Mutations and Chromosomal Rearrangements Affecting the Expression of Snail, a Gene Involved in Embryonic Patterning in DROSOPHILA MELANOGASTER. *Genetics* **108**, 347-360.
Gray, R. S., Roszko, I. and Solnica-Krezel, L. (2011). Planar cell polarity: coordinating morphogenetic cell behaviors with embryonic polarity. *Dev Cell* **21**, 120-133.
Green, E. S., Stubbs, J. L. and Levine, E. M. (2003). Genetic rescue of cell number in a mouse model of microphthalmia: interactions between Chx10 and G1-phase cell cycle regulators. *Development* **130**, 539-552.
Gritsman, K., Talbot, W. S. and Schier, A. F. (2000). Nodal signaling patterns the organizer. *Development* **127**, 921-932.
Gritsman, K., Zhang, J., Cheng, S., Heckscher, E., Talbot, W. S. and Schier, A. F. (1999). The EGF-CFC protein one-eyed pinhead is essential for nodal signaling. *Cell* **97**, 121-132.
Gu, Z., Nomura, M., Simpson, B. B., Lei, H., Feijen, A., van den Eijnden-van Raaij, J., Donahoe, P. K. and Li, E. (1998). The type I activin receptor ActRIB is required for egg cylinder organization and gastrulation in the mouse. *Genes Dev* **12**, 844-857.
Guan, K. L., Jenkins, C. W., Li, Y., Nichols, M. A., Wu, X., O'Keefe, C. L., Matera, A. G. and Xiong, Y. (1994). Growth suppression by p18, a p16INK4/MTS1- and p14INK4B/MTS2-related CDK6 inhibitor, correlates with wild-type pRb function. *Genes Dev* **8**, 2939-2952.
Guilliam, T. A. and Yeeles, J. T. (2020a). An updated perspective on the polymerase division of labor during eukaryotic DNA replication. *Critical reviews in biochemistry and molecular biology* **55**, 469-481.
Guilliam, T. A. and Yeeles, J. T. P. (2020b). Reconstitution of translesion synthesis reveals a mechanism of eukaryotic DNA replication restart. *Nat Struct Mol Biol* **27**, 450-460.
Guo, G., Huss, M., Tong, G. Q., Wang, C., Li Sun, L., Clarke, N. D. and Robson, P. (2010). Resolution of cell fate decisions revealed by single-cell gene expression analysis from zygote to blastocyst. *Dev Cell* **18**, 675-685.
Guo, G., Stirparo, G. G., Strawbridge, S. E., Spindlow, D., Yang, J., Clarke, J., Dattani, A., Yanagida, A., Li, M. A., Myers, S., et al. (2021). Human naive epiblast cells possess unrestricted lineage potential. *Cell Stem Cell* **28**, 1040-1056 e1046.
Guo, K. and Walsh, K. (1997). Inhibition of myogenesis by multiple cyclin-Cdk complexes. Coordinate regulation of myogenesis and cell cycle activity at the level of E2F. *J Biol Chem* **272**, 791-797.
Hacker, U. and Perrimon, N. (1998). DRhoGEF2 encodes a member of the Dbl family of oncogenes and controls cell shape changes during gastrulation in Drosophila. *Genes Dev* **12**, 274-284.
Hagos, E. G. and Dougan, S. T. (2007). Time-dependent patterning of the mesoderm and endoderm by Nodal signals in zebrafish. *BMC Dev Biol* **7**, 22.
Halevy, O., Novitch, B. G., Spicer, D. B., Skapek, S. X., Rhee, J., Hannon, G. J., Beach, D. and Lassar, A. B. (1995). Correlation of terminal cell cycle arrest of skeletal muscle with induction of p21 by MyoD. *Science* **267**, 1018-1021.
Halley-Stott, R. P., Jullien, J., Pasque, V. and Gurdon, J. (2014). Mitosis gives a brief window of opportunity for a change in gene transcription. *PLoS Biol* **12**, e1001914.
Hallonet, M., Kaestner, K. H., Martin-Parras, L., Sasaki, H., Betz, U. A. and Ang, S. L. (2002). Maintenance of the specification of the anterior definitive endoderm and forebrain depends on the axial mesendoderm: a study using HNF3beta/Foxa2 conditional mutants. *Dev Biol* **243**, 20-33.
Hamburger, V. and Hamilton, H. L. (1951). A series of normal stages in the development of the chick embryo. *J Morphol* **88**, 49-92.
Handyside, A. H. and Hunter, S. (1986). Cell division and death in the mouse blastocyst before implantation. *Rouxs Arch Dev Biol* **195**, 519-526.

Harborth, J., Elbashir, S. M., Bechert, K., Tuschl, T. and Weber, K. (2001). Identification of essential genes in cultured mammalian cells using small interfering RNAs. *J Cell Sci* **114**, 4557-4565.
Hardwick, L. J. and Philpott, A. (2014). Nervous decision-making: to divide or differentiate. *Trends Genet* **30**, 254-261.
Hart, A. H., Hartley, L., Sourris, K., Stadler, E. S., Li, R., Stanley, E. G., Tam, P. P., Elefanty, A. G. and Robb, L. (2002). Mixl1 is required for axial mesendoderm morphogenesis and patterning in the murine embryo. *Development* **129**, 3597-3608.
Hartenstein, V. (1993). Early pattern of neuronal differentiation in the Xenopus embryonic brainstem and spinal cord. *J Comp Neurol* **328**, 213-231.
Hartenstein, V. and Campos-Ortega, J. A. (1985). Fate-mapping in wild-typeDrosophila melanogaster. *Wilhelm Roux's archives of developmental biology* **194**, 181-195.
Hartenstein, V. and Posakony, J. W. (1990). Sensillum development in the absence of cell division: the sensillum phenotype of the Drosophila mutant string. *Dev Biol* **138**, 147-158.
Hartenstein, V., Younossi-Hartenstein, A. and Lekven, A. (1994). Delamination and division in the Drosophila neurectoderm: spatiotemporal pattern, cytoskeletal dynamics, and common control by neurogenic and segment polarity genes. *Dev Biol* **165**, 480-499.
Harvey, S. A. and Smith, J. C. (2009). Visualisation and quantification of morphogen gradient formation in the zebrafish. *PLoS biology* **7**, e1000101.
Hayashi, S., Tenzen, T. and McMahon, A. P. (2003). Maternal inheritance of Cre activity in a Sox2Cre deleter strain. *Genesis* **37**, 51-53.
Heallen, T., Zhang, M., Wang, J., Bonilla-Claudio, M., Klysik, E., Johnson, R. L. and Martin, J. F. (2011). Hippo pathway inhibits Wnt signaling to restrain cardiomyocyte proliferation and heart size. *Science* **332**, 458-461.
Heisenberg, C. P., Tada, M., Rauch, G. J., Saude, L., Concha, M. L., Geisler, R., Stemple, D. L., Smith, J. C. and Wilson, S. W. (2000). Silberblick/Wnt11 mediates convergent extension movements during zebrafish gastrulation. *Nature* **405**, 76-81.
Heix, J., Vente, A., Voit, R., Budde, A., Michaelidis, T. M. and Grummt, I. (1998). Mitotic silencing of human rRNA synthesis: inactivation of the promoter selectivity factor SL1 by cdc2/cyclin B-mediated phosphorylation. *EMBO J* **17**, 7373-7381.
Hemavathy, K., Meng, X. and Ip, Y. T. (1997). Differential regulation of gastrulation and neuroectodermal gene expression by Snail in the Drosophila embryo. *Development* **124**, 3683-3691.
Hernandez-Martinez, R., Ramkumar, N. and Anderson, K. V. (2019). p120-catenin regulates WNT signaling and EMT in the mouse embryo. *Proc Natl Acad Sci U S A* **116**, 16872-16881.
Hirai, H., Roussel, M. F., Kato, J. Y., Ashmun, R. A. and Sherr, C. J. (1995). Novel INK4 proteins, p19 and p18, are specific inhibitors of the cyclin D-dependent kinases CDK4 and CDK6. *Mol Cell Biol* **15**, 2672-2681.
Hirano, T., Kobayashi, R. and Hirano, M. (1997). Condensins, chromosome condensation protein complexes containing XCAP-C, XCAP-E and a Xenopus homolog of the Drosophila Barren protein. *Cell* **89**, 511-521.
Hirano, T. and Mitchison, T. J. (1994). A heterodimeric coiled-coil protein required for mitotic chromosome condensation in vitro. *Cell* **79**, 449-458.
Hirate, Y., Hirahara, S., Inoue, K., Kiyonari, H., Niwa, H. and Sasaki, H. (2015). Par-aPKC-dependent and -independent mechanisms cooperatively control cell polarity, Hippo signaling, and cell positioning in 16-cell stage mouse embryos. *Dev Growth Differ* **57**, 544-556.
Hirate, Y., Hirahara, S., Inoue, K., Suzuki, A., Alarcon, V. B., Akimoto, K., Hirai, T., Hara, T., Adachi, M., Chida, K., et al. (2013). Polarity-dependent distribution of angiomotin localizes Hippo signaling in preimplantation embryos. *Curr Biol* **23**, 1181-1194.

Ho, R. K. and Kimmel, C. B. (1993). Commitment of cell fate in the early zebrafish embryo. *Science* **261**, 109-111.
Hocke, S., Guo, Y., Job, A., Orth, M., Ziesch, A., Lauber, K., De Toni, E. N., Gress, T. M., Herbst, A., Goke, B., et al. (2016). A synthetic lethal screen identifies ATR-inhibition as a novel therapeutic approach for POLD1-deficient cancers. *Oncotarget* **7**, 7080-7095.
Holder, N. (1981). Regeneration and compensatory growth. *Br Med Bull* **37**, 227-232.
Hong, H., Takahashi, K., Ichisaka, T., Aoi, T., Kanagawa, O., Nakagawa, M., Okita, K. and Yamanaka, S. (2009). Suppression of induced pluripotent stem cell generation by the p53-p21 pathway. *Nature* **460**, 1132-1135.
Hoshino, H., Shioi, G. and Aizawa, S. (2015). AVE protein expression and visceral endoderm cell behavior during anterior-posterior axis formation in mouse embryos: Asymmetry in OTX2 and DKK1 expression. *Dev Biol* **402**, 175-191.
Howe, J. A., Howell, M., Hunt, T. and Newport, J. W. (1995). Identification of a developmental timer regulating the stability of embryonic cyclin A and a new somatic A-type cyclin at gastrulation. *Genes Dev* **9**, 1164-1176.
Howell, M., Mohun, T. J. and Hill, C. S. (2001). Xenopus Smad3 is specifically expressed in the chordoneural hinge, notochord and in the endocardium of the developing heart. *Mech Dev* **104**, 147-150.
Hu, G., Lee, H., Price, S. M., Shen, M. M. and Abate-Shen, C. (2001). Msx homeobox genes inhibit differentiation through upregulation of cyclin D1. *Development* **128**, 2373-2384.
Huangfu, D., Liu, A., Rakeman, A. S., Murcia, N. S., Niswander, L. and Anderson, K. V. (2003). Hedgehog signalling in the mouse requires intraflagellar transport proteins. *Nature* **426**, 83-87.
Huelsken, J., Vogel, R., Brinkmann, V., Erdmann, B., Birchmeier, C. and Birchmeier, W. (2000). Requirement for beta-catenin in anterior-posterior axis formation in mice. *J Cell Biol* **148**, 567-578.
Hughes, P., Tratner, I., Ducoux, M., Piard, K. and Baldacci, G. (1999). Isolation and identification of the third subunit of mammalian DNA polymerase delta by PCNA-affinity chromatography of mouse FM3A cell extracts. *Nucleic Acids Res* **27**, 2108-2114.
Hume, C. R. and Dodd, J. (1993). Cwnt-8C: a novel Wnt gene with a potential role in primitive streak formation and hindbrain organization. *Development* **119**, 1147-1160.
Huynh, J. R., Shulman, J. M., Benton, R. and St Johnston, D. (2001). PAR-1 is required for the maintenance of oocyte fate in Drosophila. *Development* **128**, 1201-1209.
Iams, K., Larson, E. D. and Drummond, J. T. (2002). DNA template requirements for human mismatch repair in vitro. *J Biol Chem* **277**, 30805-30814.
Iglesias, F. M., Bruera, N. A., Dergan-Dylon, S., Marino-Buslje, C., Lorenzi, H., Mateos, J. L., Turck, F., Coupland, G. and Cerdan, P. D. (2015). The arabidopsis DNA polymerase delta has a role in the deposition of transcriptionally active epigenetic marks, development and flowering. *PLoS Genet* **11**, e1004975.
Ip, C. K., Fossat, N., Jones, V., Lamonerie, T. and Tam, P. P. (2014). Head formation: OTX2 regulates Dkk1 and Lhx1 activity in the anterior mesendoderm. *Development* **141**, 3859-3867.
Ip, Y. T., Levine, M. and Bier, E. (1994). Neurogenic expression of snail is controlled by separable CNS and PNS promoter elements. *Development* **120**, 199-207.
Izpisua-Belmonte, J. C., De Robertis, E. M., Storey, K. G. and Stern, C. D. (1993). The homeobox gene goosecoid and the origin of organizer cells in the early chick blastoderm. *Cell* **74**, 645-659.
Jaglarz, M. K. (1998). The number that counts. Phylogenetic implications of the number of nurse cells in ovarian follicles of Coleoptera-Adephaga. *Folia Histochem Cytobiol* **36**, 167-178.

Jain, D., Meydan, C., Lange, J., Claeys Bouuaert, C., Lailler, N., Mason, C. E., Anderson, K. V. and Keeney, S. (2017). rahu is a mutant allele of Dnmt3c, encoding a DNA methyltransferase homolog required for meiosis and transposon repression in the mouse male germline. *PLoS Genet* **13**, e1006964.

Jain, R., Aggarwal, A. K. and Rechkoblit, O. (2018). Eukaryotic DNA polymerases. *Curr Opin Struct Biol* **53**, 77-87.

Jain, R., Hammel, M., Johnson, R. E., Prakash, L., Prakash, S. and Aggarwal, A. K. (2009). Structural insights into yeast DNA polymerase delta by small angle X-ray scattering. *J Mol Biol* **394**, 377-382.

Jan, Y. N. and Jan, L. Y. (2001). Asymmetric cell division in the Drosophila nervous system. *Nat Rev Neurosci* **2**, 772-779.

Jean, D., Bernier, G. and Gruss, P. (1999). Six6 (Optx2) is a novel murine Six3-related homeobox gene that demarcates the presumptive pituitary/hypothalamic axis and the ventral optic stalk. *Mech Dev* **84**, 31-40.

Jiang, Q., Liu, D., Gong, Y., Wang, Y., Sun, S., Gui, Y. and Song, H. (2009). Yap is required for the development of brain, eyes, and neural crest in zebrafish. *Biochemical and biophysical research communications* **384**, 114-119.

Jin, Y. H., Obert, R., Burgers, P. M., Kunkel, T. A., Resnick, M. A. and Gordenin, D. A. (2001). The 3'-->5' exonuclease of DNA polymerase delta can substitute for the 5' flap endonuclease Rad27/Fen1 in processing Okazaki fragments and preventing genome instability. *Proc Natl Acad Sci U S A* **98**, 5122-5127.

Job, A., Tatura, M., Schafer, C., Lutz, V., Schneider, H., Lankat-Buttgereit, B., Zielinski, A., Borgmann, K., Bauer, C., Gress, T. M., et al. (2020). The POLD1(R689W) variant increases the sensitivity of colorectal cancer cells to ATR and CHK1 inhibitors. *Sci Rep* **10**, 18924.

Johansson, E., Garg, P. and Burgers, P. M. (2004). The Pol32 subunit of DNA polymerase delta contains separable domains for processive replication and proliferating cell nuclear antigen (PCNA) binding. *J Biol Chem* **279**, 1907-1915.

Joo, H. Y., Zhai, L., Yang, C., Nie, S., Erdjument-Bromage, H., Tempst, P., Chang, C. and Wang, H. (2007). Regulation of cell cycle progression and gene expression by H2A deubiquitination. *Nature* **449**, 1068-1072.

Jopling, C., Sleep, E., Raya, M., Marti, M., Raya, A. and Izpisua Belmonte, J. C. (2010). Zebrafish heart regeneration occurs by cardiomyocyte dedifferentiation and proliferation. *Nature* **464**, 606-609.

Jurgens, G. and Weigel, D. (1988). Terminal versus segmental development in the Drosophila embryo: the role of the homeotic gene fork head. *Rouxs Arch Dev Biol* **197**, 345-354.

Kadyrov, F. A., Genschel, J., Fang, Y., Penland, E., Edelmann, W. and Modrich, P. (2009). A possible mechanism for exonuclease 1-independent eukaryotic mismatch repair. *Proc Natl Acad Sci U S A* **106**, 8495-8500.

Kagawa, H., Javali, A., Khoei, H. H., Sommer, T. M., Sestini, G., Novatchkova, M., Scholte Op Reimer, Y., Castel, G., Bruneau, A., Maenhoudt, N., et al. (2022). Human blastoids model blastocyst development and implantation. *Nature* **601**, 600-605.

Kam, Z., Minden, J. S., Agard, D. A., Sedat, J. W. and Leptin, M. (1991). Drosophila gastrulation: analysis of cell shape changes in living embryos by three-dimensional fluorescence microscopy. *Development* **112**, 365-370.

Kamb, A., Gruis, N. A., Weaver-Feldhaus, J., Liu, Q., Harshman, K., Tavtigian, S. V., Stockert, E., Day, R. S., 3rd, Johnson, B. E. and Skolnick, M. H. (1994). A cell cycle regulator potentially involved in genesis of many tumor types. *Science* **264**, 436-440.

Kanai-Azuma, M., Kanai, Y., Gad, J. M., Tajima, Y., Taya, C., Kurohmaru, M., Sanai, Y., Yonekawa, H., Yazaki, K., Tam, P. P., et al. (2002). Depletion of definitive gut endoderm in Sox17-null mutant mice. *Development* **129**, 2367-2379.
Kaneko, K. J. and DePamphilis, M. L. (2013). TEAD4 establishes the energy homeostasis essential for blastocoel formation. *Development* **140**, 3680-3690.
Kang, E., Wu, G., Ma, H., Li, Y., Tippner-Hedges, R., Tachibana, M., Sparman, M., Wolf, D. P., Scholer, H. R. and Mitalipov, S. (2014). Nuclear reprogramming by interphase cytoplasm of two-cell mouse embryos. *Nature* **509**, 101-104.
Kang, M., Piliszek, A., Artus, J. and Hadjantonakis, A. K. (2013). FGF4 is required for lineage restriction and salt-and-pepper distribution of primitive endoderm factors but not their initial expression in the mouse. *Development* **140**, 267-279.
Karkhanis, V., Wang, L., Tae, S., Hu, Y. J., Imbalzano, A. N. and Sif, S. (2012). Protein arginine methyltransferase 7 regulates cellular response to DNA damage by methylating promoter histones H2A and H4 of the polymerase delta catalytic subunit gene, POLD1. *J Biol Chem* **287**, 29801-29814.
Kawabe, T., Muslin, A. J. and Korsmeyer, S. J. (1997). HOX11 interacts with protein phosphatases PP2A and PP1 and disrupts a G2/M cell-cycle checkpoint. *Nature* **385**, 454-458.
Kawakami, K., Sato, S., Ozaki, H. and Ikeda, K. (2000). Six family genes--structure and function as transcription factors and their roles in development. *Bioessays* **22**, 616-626.
Kawamura, T., Suzuki, J., Wang, Y. V., Menendez, S., Morera, L. B., Raya, A., Wahl, G. M. and Izpisua Belmonte, J. C. (2009). Linking the p53 tumour suppressor pathway to somatic cell reprogramming. *Nature* **460**, 1140-1144.
Keller, P. J., Schmidt, A. D., Wittbrodt, J. and Stelzer, E. H. (2008). Reconstruction of zebrafish early embryonic development by scanned light sheet microscopy. *Science* **322**, 1065-1069.
Kemp, C., Willems, E., Abdo, S., Lambiv, L. and Leyns, L. (2005). Expression of all Wnt genes and their secreted antagonists during mouse blastocyst and postimplantation development. *Dev Dyn* **233**, 1064-1075.
Kemper, R. R., Ahn, E. R., Zhang, P., Lee, M. Y. and Rabin, M. (1992). Human DNA polymerase delta gene maps to region 19q13.3-q13.4 by in situ hybridization. *Genomics* **14**, 205-206.
Kerridge, S., Munjal, A., Philippe, J. M., Jha, A., de las Bayonas, A. G., Saurin, A. J. and Lecuit, T. (2016). Modular activation of Rho1 by GPCR signalling imparts polarized myosin II activation during morphogenesis. *Nat Cell Biol* **18**, 261-270.
Khaner, O. and Eyal-Giladi, H. (1986). The embryo-forming potency of the posterior marginal zone in stages X through XII of the chick. *Developmental biology* **115**, 275-281.
---- (1989). The chick's marginal zone and primitive streak formation: I. Coordinative effect of induction and inhibition. *Developmental biology* **134**, 206-214.
Khaner, O., Mitrani, E. and Eyal-Giladi, H. (1985). Developmental potencies of area opaca and marginal zone areas of early chick blastoderms.
Kiecker, C., Bates, T. and Bell, E. (2016). Molecular specification of germ layers in vertebrate embryos. *Cell Mol Life Sci* **73**, 923-947.
Kimura-Yoshida, C., Nakano, H., Okamura, D., Nakao, K., Yonemura, S., Belo, J. A., Aizawa, S., Matsui, Y. and Matsuo, I. (2005). Canonical Wnt signaling and its antagonist regulate anterior-posterior axis polarization by guiding cell migration in mouse visceral endoderm. *Dev Cell* **9**, 639-650.
Kimura, K., Cuvier, O. and Hirano, T. (2001). Chromosome condensation by a human condensin complex in Xenopus egg extracts. *J Biol Chem* **276**, 5417-5420.
Kimura, K., Hirano, M., Kobayashi, R. and Hirano, T. (1998). Phosphorylation and activation of 13S condensin by Cdc2 in vitro. *Science* **282**, 487-490.

Kinder, S. J., Tsang, T. E., Quinlan, G. A., Hadjantonakis, A. K., Nagy, A. and Tam, P. P. (1999). The orderly allocation of mesodermal cells to the extraembryonic structures and the anteroposterior axis during gastrulation of the mouse embryo. *Development* **126**, 4691-4701.

King, R. C. (1970). Ovarian development in Drosophila melanogaster.

King, R. W., Jackson, P. K. and Kirschner, M. W. (1994). Mitosis in transition. *Cell* **79**, 563-571.

Kirchhof, N., Carnwath, J. W., Lemme, E., Anastassiadis, K., Scholer, H. and Niemann, H. (2000). Expression pattern of Oct-4 in preimplantation embryos of different species. *Biol Reprod* **63**, 1698-1705.

Kitajima, S., Takagi, A., Inoue, T. and Saga, Y. (2000). MesP1 and MesP2 are essential for the development of cardiac mesoderm. *Development* **127**, 3215-3226.

Klaus, A., Saga, Y., Taketo, M. M., Tzahor, E. and Birchmeier, W. (2007). Distinct roles of Wnt/beta-catenin and Bmp signaling during early cardiogenesis. *Proc Natl Acad Sci U S A* **104**, 18531-18536.

Kloc, M., Bilinski, S., Dougherty, M. T., Brey, E. M. and Etkin, L. D. (2004). Formation, architecture and polarity of female germline cyst in Xenopus. *Dev Biol* **266**, 43-61.

Knoblich, J. A. and Lehner, C. F. (1993). Synergistic action of Drosophila cyclins A and B during the G2-M transition. *The EMBO journal* **12**, 65-74.

Kobayashi, M., Nishikawa, K., Suzuki, T. and Yamamoto, M. (2001). The homeobox protein Six3 interacts with the Groucho corepressor and acts as a transcriptional repressor in eye and forebrain formation. *Dev Biol* **232**, 315-326.

Kobayashi, M., Toyama, R., Takeda, H., Dawid, I. B. and Kawakami, K. (1998). Overexpression of the forebrain-specific homeobox gene six3 induces rostral forebrain enlargement in zebrafish. *Development* **125**, 2973-2982.

Kochav, S., Ginsburg, M. and Eyal-Giladi, H. (1980). From cleavage to primitive streak formation: a complementary normal table and a new look at the first stages of the development of the chick. II. Microscopic anatomy and cell population dynamics. *Dev Biol* **79**, 296-308.

Koh, K. D., Balachander, S., Hesselberth, J. R. and Storici, F. (2015). Ribose-seq: global mapping of ribonucleotides embedded in genomic DNA. *Nat Methods* **12**, 251-257, 253 p following 257.

Kojima, Y., Tam, O. H. and Tam, P. P. (2014). Timing of developmental events in the early mouse embryo. *Semin Cell Dev Biol* **34**, 65-75.

Kolsch, V., Seher, T., Fernandez-Ballester, G. J., Serrano, L. and Leptin, M. (2007). Control of Drosophila gastrulation by apical localization of adherens junctions and RhoGEF2. *Science* **315**, 384-386.

Korotkevich, E., Niwayama, R., Courtois, A., Friese, S., Berger, N., Buchholz, F. and Hiiragi, T. (2017). The Apical Domain Is Required and Sufficient for the First Lineage Segregation in the Mouse Embryo. *Dev Cell* **40**, 235-247 e237.

Korzh, V., Edlund, T. and Thor, S. (1993). Zebrafish primary neurons initiate expression of the LIM homeodomain protein Isl-1 at the end of gastrulation. *Development* **118**, 417-425.

Kozar, K., Ciemerych, M. A., Rebel, V. I., Shigematsu, H., Zagozdzon, A., Sicinska, E., Geng, Y., Yu, Q., Bhattacharya, S., Bronson, R. T., et al. (2004). Mouse development and cell proliferation in the absence of D-cyclins. *Cell* **118**, 477-491.

Krawchuk, D., Honma-Yamanaka, N., Anani, S. and Yamanaka, Y. (2013). FGF4 is a limiting factor controlling the proportions of primitive endoderm and epiblast in the ICM of the mouse blastocyst. *Dev Biol* **384**, 65-71.

Krek, W., Ewen, M. E., Shirodkar, S., Arany, Z., Kaelin, W. G., Jr. and Livingston, D. M. (1994). Negative regulation of the growth-promoting transcription factor E2F-1 by a stably bound cyclin A-dependent protein kinase. *Cell* **78**, 161-172.

Krek, W., Xu, G. and Livingston, D. M. (1995). Cyclin A-kinase regulation of E2F-1 DNA binding function underlies suppression of an S phase checkpoint. *Cell* **83**, 1149-1158.

Krieg, M., Arboleda-Estudillo, Y., Puech, P. H., Kafer, J., Graner, F., Muller, D. J. and Heisenberg, C. P. (2008). Tensile forces govern germ-layer organization in zebrafish. *Nat Cell Biol* **10**, 429-436.

Kroll, K. L., Salic, A. N., Evans, L. M. and Kirschner, M. W. (1998). Geminin, a neuralizing molecule that demarcates the future neural plate at the onset of gastrulation. *Development* **125**, 3247-3258.

Kruhlak, M. J., Hendzel, M. J., Fischle, W., Bertos, N. R., Hameed, S., Yang, X. J., Verdin, E. and Bazett-Jones, D. P. (2001). Regulation of global acetylation in mitosis through loss of histone acetyltransferases and deacetylases from chromatin. *J Biol Chem* **276**, 38307-38319.

Krupinski, P., Chickarmane, V. and Peterson, C. (2011). Simulating the mammalian blastocyst--molecular and mechanical interactions pattern the embryo. *PLoS Comput Biol* **7**, e1001128.

Kubrakiewicz, J. (1997). Germ cells cluster organization in polytrophic ovaries of neuroptera. *Tissue Cell* **29**, 221-228.

Kuijk, E. W., Du Puy, L., Van Tol, H. T., Oei, C. H., Haagsman, H. P., Colenbrander, B. and Roelen, B. A. (2008). Differences in early lineage segregation between mammals. *Dev Dyn* **237**, 918-927.

Kuijk, E. W., van Tol, L. T., Van de Velde, H., Wubbolts, R., Welling, M., Geijsen, N. and Roelen, B. A. (2012). The roles of FGF and MAP kinase signaling in the segregation of the epiblast and hypoblast cell lineages in bovine and human embryos. *Development* **139**, 871-882.

Kumar, A., Lualdi, M., Lyozin, G. T., Sharma, P., Loncarek, J., Fu, X. Y. and Kuehn, M. R. (2015). Nodal signaling from the visceral endoderm is required to maintain Nodal gene expression in the epiblast and drive DVE/AVE migration. *Dev Biol* **400**, 1-9.

Kunath, T., Yamanaka, Y., Detmar, J., MacPhee, D., Caniggia, I., Rossant, J. and Jurisicova, A. (2014). Developmental differences in the expression of FGF receptors between human and mouse embryos. *Placenta* **35**, 1079-1088.

Kunkel, T. A. and Erie, D. A. (2005). DNA mismatch repair. *Annu Rev Biochem* **74**, 681-710.

Kuo, J. C., Han, X., Hsiao, C. T., Yates, J. R., 3rd and Waterman, C. M. (2011). Analysis of the myosin-II-responsive focal adhesion proteome reveals a role for beta-Pix in negative regulation of focal adhesion maturation. *Nat Cell Biol* **13**, 383-393.

Kurimoto, K., Yabuta, Y., Ohinata, Y., Ono, Y., Uno, K. D., Yamada, R. G., Ueda, H. R. and Saitou, M. (2006). An improved single-cell cDNA amplification method for efficient high-density oligonucleotide microarray analysis. *Nucleic Acids Res* **34**, e42.

Kwan, J., Sczaniecka, A., Heidary Arash, E., Nguyen, L., Chen, C. C., Ratkovic, S., Klezovitch, O., Attisano, L., McNeill, H., Emili, A., et al. (2016). DLG5 connects cell polarity and Hippo signaling protein networks by linking PAR-1 with MST1/2. *Genes Dev* **30**, 2696-2709.

Kwon, D. H., Kapadia, S. R., Tuzcu, E. M., Halley, C. M., Gorodeski, E. Z., Curtin, R. J., Thamilarasan, M., Smedira, N. G., Lytle, B. W., Lever, H. M., et al. (2008a). Long-term outcomes in high-risk symptomatic patients with hypertrophic cardiomyopathy undergoing alcohol septal ablation. *JACC Cardiovasc Interv* **1**, 432-438.

Kwon, G. S. and Hadjantonakis, A. K. (2009). Transthyretin mouse transgenes direct RFP expression or Cre-mediated recombination throughout the visceral endoderm. *Genesis* **47**, 447-455.

Kwon, G. S., Viotti, M. and Hadjantonakis, A. K. (2008b). The endoderm of the mouse embryo arises by dynamic widespread intercalation of embryonic and extraembryonic lineages. *Dev Cell* **15**, 509-520.

Lakso, M., Pichel, J. G., Gorman, J. R., Sauer, B., Okamoto, Y., Lee, E., Alt, F. W. and Westphal, H. (1996). Efficient in vivo manipulation of mouse genomic sequences at the zygote stage. *Proc Natl Acad Sci U S A* **93**, 5860-5865.

Lancey, C., Tehseen, M., Raducanu, V. S., Rashid, F., Merino, N., Ragan, T. J., Savva, C. G., Zaher, M. S., Shirbini, A., Blanco, F. J., et al. (2020). Structure of the processive human Pol delta holoenzyme. *Nat Commun* **11**, 1109.

Lange, L., Marks, M., Liu, J., Wittler, L., Bauer, H., Piehl, S., Blass, G., Timmermann, B. and Herrmann, B. G. (2017). Patterning and gastrulation defects caused by the t(w18) lethal are due to loss of Ppp2r1a. *Biol Open* **6**, 752-764.

Langston, L. D., Zhang, D., Yurieva, O., Georgescu, R. E., Finkelstein, J., Yao, N. Y., Indiani, C. and O'Donnell, M. E. (2014). CMG helicase and DNA polymerase epsilon form a functional 15-subunit holoenzyme for eukaryotic leading-strand DNA replication. *Proc Natl Acad Sci U S A* **111**, 15390-15395.

Latimer, A. and Jessen, J. R. (2010). Extracellular matrix assembly and organization during zebrafish gastrulation. *Matrix Biol* **29**, 89-96.

Lawson, K. A. (1999). Fate mapping the mouse embryo. *Int J Dev Biol* **43**, 773-775.

Lawson, K. A., Dunn, N. R., Roelen, B. A., Zeinstra, L. M., Davis, A. M., Wright, C. V., Korving, J. P. and Hogan, B. L. (1999). Bmp4 is required for the generation of primordial germ cells in the mouse embryo. *Genes Dev* **13**, 424-436.

Lawson, K. A., Meneses, J. J. and Pedersen, R. A. (1986). Cell fate and cell lineage in the endoderm of the presomite mouse embryo, studied with an intracellular tracer. *Dev Biol* **115**, 325-339.

---- (1991). Clonal analysis of epiblast fate during germ layer formation in the mouse embryo. *Development* **113**, 891-911.

Lawson, K. A. and Pedersen, R. A. (1987). Cell fate, morphogenetic movement and population kinetics of embryonic endoderm at the time of germ layer formation in the mouse. *Development* **101**, 627-652.

---- (1992). Clonal analysis of cell fate during gastrulation and early neurulation in the mouse. *Ciba Found Symp* **165**, 3-21; discussion 21-26.

Lee, M. Y., Tan, C. K., Downey, K. M. and So, A. G. (1984). Further studies on calf thymus DNA polymerase. delta. purified to homogeneity by a new procedure. *Biochemistry* **23**, 1906-1913.

Lee, M. Y., Zhang, S., Lin, S. H., Wang, X., Darzynkiewicz, Z., Zhang, Z. and Lee, E. Y. (2014). The tail that wags the dog: p12, the smallest subunit of DNA polymerase delta, is degraded by ubiquitin ligases in response to DNA damage and during cell cycle progression. *Cell Cycle* **13**, 23-31.

Lee, S. H., Eki, T. and Hurwitz, J. (1989). Synthesis of DNA containing the simian virus 40 origin of replication by the combined action of DNA polymerases alpha and delta. *Proc Natl Acad Sci U S A* **86**, 7361-7365.

Lees, J., Buchkovich, K., Marshak, D., Anderson, C. and Harlow, E. (1991). The retinoblastoma protein is phosphorylated on multiple sites by human cdc2. *The EMBO journal* **10**, 4279-4290.

Lemaitre, J. M., Danis, E., Pasero, P., Vassetzky, Y. and Mechali, M. (2005). Mitotic remodeling of the replicon and chromosome structure. *Cell* **123**, 787-801.

Leptin, M. and Grunewald, B. (1990). Cell shape changes during gastrulation in Drosophila. *Development* **110**, 73-84.

Leung, C. Y. and Zernicka-Goetz, M. (2013). Angiomotin prevents pluripotent lineage differentiation in mouse embryos via Hippo pathway-dependent and -independent mechanisms. *Nat Commun* **4**, 2251.

Leung, T., Bischof, J., Soll, I., Niessing, D., Zhang, D., Ma, J., Jackle, H. and Driever, W. (2003). bozozok directly represses bmp2b transcription and mediates the earliest dorsoventral asymmetry of bmp2b expression in zebrafish. *Development* **130**, 3639-3649.

Levine, E. M., Passini, M., Hitchcock, P. F., Glasgow, E. and Schechter, N. (1997). Vsx-1 and Vsx-2: two Chx10-like homeobox genes expressed in overlapping domains in the adult goldfish retina. *J Comp Neurol* **387**, 439-448.
Lewis, N. E. and Rossant, J. (1982). Mechanism of size regulation in mouse embryo aggregates. *J Embryol Exp Morphol* **72**, 169-181.
Lewis, S. L., Khoo, P. L., De Young, R. A., Steiner, K., Wilcock, C., Mukhopadhyay, M., Westphal, H., Jamieson, R. V., Robb, L. and Tam, P. P. (2008). Dkk1 and Wnt3 interact to control head morphogenesis in the mouse. *Development* **135**, 1791-1801.
Li, B. and Lee, M. Y. (2001). Transcriptional regulation of the human DNA polymerase delta catalytic subunit gene POLD1 by p53 tumor suppressor and Sp1. *J Biol Chem* **276**, 29729-29739.
Li, L. and Vaessin, H. (2000). Pan-neural Prospero terminates cell proliferation during Drosophila neurogenesis. *Genes Dev* **14**, 147-151.
Li, R., Zhong, C., Yu, Y., Liu, H., Sakurai, M., Yu, L., Min, Z., Shi, L., Wei, Y., Takahashi, Y., et al. (2019). Generation of Blastocyst-like Structures from Mouse Embryonic and Adult Cell Cultures. *Cell* **179**, 687-702 e618.
Li, V. C., Ballabeni, A. and Kirschner, M. W. (2012). Gap 1 phase length and mouse embryonic stem cell self-renewal. *Proc Natl Acad Sci U S A* **109**, 12550-12555.
Li, X., Perissi, V., Liu, F., Rose, D. W. and Rosenfeld, M. G. (2002). Tissue-specific regulation of retinal and pituitary precursor cell proliferation. *Science* **297**, 1180-1183.
Lin, H. and Spradling, A. C. (1995). Fusome asymmetry and oocyte determination in Drosophila. *Dev Genet* **16**, 6-12.
Lister, R., Pelizzola, M., Dowen, R. H., Hawkins, R. D., Hon, G., Tonti-Filippini, J., Nery, J. R., Lee, L., Ye, Z., Ngo, Q. M., et al. (2009). Human DNA methylomes at base resolution show widespread epigenomic differences. *Nature* **462**, 315-322.
Lister, R., Pelizzola, M., Kida, Y. S., Hawkins, R. D., Nery, J. R., Hon, G., Antosiewicz-Bourget, J., O'Malley, R., Castanon, R., Klugman, S., et al. (2011). Hotspots of aberrant epigenomic reprogramming in human induced pluripotent stem cells. *Nature* **471**, 68-73.
Liu, D., Matzuk, M. M., Sung, W. K., Guo, Q., Wang, P. and Wolgemuth, D. J. (1998). Cyclin A1 is required for meiosis in the male mouse. *Nat Genet* **20**, 377-380.
Liu, I. S., Chen, J. D., Ploder, L., Vidgen, D., van der Kooy, D., Kalnins, V. I. and McInnes, R. R. (1994). Developmental expression of a novel murine homeobox gene (Chx10): evidence for roles in determination of the neuroretina and inner nuclear layer. *Neuron* **13**, 377-393.
Liu, J., He, X., Corbett, S. A., Lowry, S. F., Graham, A. M., Fassler, R. and Li, S. (2009). Integrins are required for the differentiation of visceral endoderm. *J Cell Sci* **122**, 233-242.
Liu, L., Mo, J., Rodriguez-Belmonte, E. M. and Lee, M. Y. (2000). Identification of a fourth subunit of mammalian DNA polymerase delta. *J Biol Chem* **275**, 18739-18744.
Liu, P., Wakamiya, M., Shea, M. J., Albrecht, U., Behringer, R. R. and Bradley, A. (1999). Requirement for Wnt3 in vertebrate axis formation. *Nat Genet* **22**, 361-365.
Liu, X., Tan, J. P., Schroder, J., Aberkane, A., Ouyang, J. F., Mohenska, M., Lim, S. M., Sun, Y. B. Y., Chen, J., Sun, G., et al. (2021). Modelling human blastocysts by reprogramming fibroblasts into iBlastoids. *Nature* **591**, 627-632.
Liu, Z., Woo, S. and Weiner, O. D. (2018). Nodal signaling has dual roles in fate specification and directed migration during germ layer segregation in zebrafish. *Development* **145**.
Londin, E. R., Mentzer, L. and Sirotkin, H. I. (2007). Churchill regulates cell movement and mesoderm specification by repressing Nodal signaling. *BMC Dev Biol* **7**, 120.
Long, S., Ahmad, N. and Rebagliati, M. (2003). The zebrafish nodal-related gene southpaw is required for visceral and diencephalic left-right asymmetry. *Development* **130**, 2303-2316.

Longley, M. J., Pierce, A. J. and Modrich, P. (1997). DNA polymerase delta is required for human mismatch repair in vitro. *J Biol Chem* **272**, 10917-10921.

Loosli, F., Koster, R. W., Carl, M., Krone, A. and Wittbrodt, J. (1998). Six3, a medaka homologue of the Drosophila homeobox gene sine oculis is expressed in the anterior embryonic shield and the developing eye. *Mech Dev* **74**, 159-164.

Loosli, F., Staub, W., Finger-Baier, K. C., Ober, E. A., Verkade, H., Wittbrodt, J. and Baier, H. (2003). Loss of eyes in zebrafish caused by mutation of chokh/rx3. *EMBO Rep* **4**, 894-899.

Loosli, F., Winkler, S., Burgtorf, C., Wurmbach, E., Ansorge, W., Henrich, T., Grabher, C., Arendt, D., Carl, M., Krone, A., et al. (2001). Medaka eyeless is the key factor linking retinal determination and eye growth. *Development* **128**, 4035-4044.

Loosli, F., Winkler, S. and Wittbrodt, J. (1999). Six3 overexpression initiates the formation of ectopic retina. *Genes & development* **13**, 649-654.

Lopez-Rios, J., Gallardo, M. E., Rodriguez de Cordoba, S. and Bovolenta, P. (1999). Six9 (Optx2), a new member of the six gene family of transcription factors, is expressed at early stages of vertebrate ocular and pituitary development. *Mech Dev* **83**, 155-159.

Lopez-Rios, J., Tessmar, K., Loosli, F., Wittbrodt, J. and Bovolenta, P. (2003). Six3 and Six6 activity is modulated by members of the groucho family. *Development* **130**, 185-195.

Lorthongpanich, C., Messerschmidt, D. M., Chan, S. W., Hong, W., Knowles, B. B. and Solter, D. (2013). Temporal reduction of LATS kinases in the early preimplantation embryo prevents ICM lineage differentiation. *Genes Dev* **27**, 1441-1446.

Lu, C. C., Brennan, J. and Robertson, E. J. (2001). From fertilization to gastrulation: axis formation in the mouse embryo. *Curr Opin Genet Dev* **11**, 384-392.

Lu, C. C. and Robertson, E. J. (2004). Multiple roles for Nodal in the epiblast of the mouse embryo in the establishment of anterior-posterior patterning. *Dev Biol* **273**, 149-159.

Lu, F. I., Thisse, C. and Thisse, B. (2011). Identification and mechanism of regulation of the zebrafish dorsal determinant. *Proc Natl Acad Sci U S A* **108**, 15876-15880.

Lujan, S. A., Clausen, A. R., Clark, A. B., MacAlpine, H. K., MacAlpine, D. M., Malc, E. P., Mieczkowski, P. A., Burkholder, A. B., Fargo, D. C., Gordenin, D. A., et al. (2014). Heterogeneous polymerase fidelity and mismatch repair bias genome variation and composition. *Genome Res* **24**, 1751-1764.

Lujan, S. A., Williams, J. S. and Kunkel, T. A. (2016). Eukaryotic genome instability in light of asymmetric DNA replication. *Crit Rev Biochem Mol Biol* **51**, 43-52.

Lujan, S. A., Williams, J. S., Pursell, Z. F., Abdulovic-Cui, A. A., Clark, A. B., Nick McElhinny, S. A. and Kunkel, T. A. (2012). Mismatch repair balances leading and lagging strand DNA replication fidelity. *PLoS Genet* **8**, e1003016.

Luo, L., Yang, X., Takihara, Y., Knoetgen, H. and Kessel, M. (2004). The cell-cycle regulator geminin inhibits Hox function through direct and polycomb-mediated interactions. *Nature* **427**, 749-753.

Lv, X. B., Liu, C. Y., Wang, Z., Sun, Y. P., Xiong, Y., Lei, Q. Y. and Guan, K. L. (2015). PARD3 induces TAZ activation and cell growth by promoting LATS1 and PP1 interaction. *EMBO Rep* **16**, 975-985.

Mac Auley, A., Werb, Z. and Mirkes, P. E. (1993). Characterization of the unusually rapid cell cycles during rat gastrulation. *Development* **117**, 873-883.

Machacek, M., Hodgson, L., Welch, C., Elliott, H., Pertz, O., Nalbant, P., Abell, A., Johnson, G. L., Hahn, K. M. and Danuser, G. (2009). Coordination of Rho GTPase activities during cell protrusion. *Nature* **461**, 99-103.

Madeja, Z. E., Sosnowski, J., Hryniewicz, K., Warzych, E., Pawlak, P., Rozwadowska, N., Plusa, B. and Lechniak, D. (2013). Changes in sub-cellular localisation of trophoblast and inner cell mass specific transcription factors during bovine preimplantation development. *BMC Dev Biol* **13**, 32.

Madsen, C. D., Hooper, S., Tozluoglu, M., Bruckbauer, A., Fletcher, G., Erler, J. T., Bates, P. A., Thompson, B. and Sahai, E. (2015). STRIPAK components determine mode of cancer cell migration and metastasis. *Nat Cell Biol* **17**, 68-80.

Malumbres, M., Sotillo, R., Santamaria, D., Galan, J., Cerezo, A., Ortega, S., Dubus, P. and Barbacid, M. (2004). Mammalian cells cycle without the D-type cyclin-dependent kinases Cdk4 and Cdk6. *Cell* **118**, 493-504.

Mana-Capelli, S., Paramasivam, M., Dutta, S. and McCollum, D. (2014). Angiomotins link F-actin architecture to Hippo pathway signaling. *Mol Biol Cell* **25**, 1676-1685.

Manning, A. J., Peters, K. A., Peifer, M. and Rogers, S. L. (2013). Regulation of epithelial morphogenesis by the G protein-coupled receptor mist and its ligand fog. *Sci Signal* **6**, ra98.

Manser, E., Loo, T. H., Koh, C. G., Zhao, Z. S., Chen, X. Q., Tan, L., Tan, I., Leung, T. and Lim, L. (1998). PAK kinases are directly coupled to the PIX family of nucleotide exchange factors. *Mol Cell* **1**, 183-192.

Margottin-Goguet, F., Hsu, J. Y., Loktev, A., Hsieh, H. M., Reimann, J. D. and Jackson, P. K. (2003). Prophase destruction of Emi1 by the SCF(betaTrCP/Slimb) ubiquitin ligase activates the anaphase promoting complex to allow progression beyond prometaphase. *Dev Cell* **4**, 813-826.

Martin, A. C., Gelbart, M., Fernandez-Gonzalez, R., Kaschube, M. and Wieschaus, E. F. (2010). Integration of contractile forces during tissue invagination. *J Cell Biol* **188**, 735-749.

Martinez-Barbera, J. P., Rodriguez, T. A. and Beddington, R. S. (2000). The homeobox gene Hesx1 is required in the anterior neural ectoderm for normal forebrain formation. *Dev Biol* **223**, 422-430.

Masserdotti, G., Gascon, S. and Gotz, M. (2016). Direct neuronal reprogramming: learning from and for development. *Development* **143**, 2494-2510.

Mathers, P. H., Grinberg, A., Mahon, K. A. and Jamrich, M. (1997). The Rx homeobox gene is essential for vertebrate eye development. *Nature* **387**, 603-607.

Matsuo, K., Shimada, M., Yokota, H., Satoh, T., Katabuchi, H., Kodama, S., Sasaki, H., Matsumura, N., Mikami, M. and Sugiyama, T. (2017). Effectiveness of adjuvant systemic chemotherapy for intermediate-risk stage IB cervical cancer. *Oncotarget* **8**, 106866-106875.

McDole, K., Guignard, L., Amat, F., Berger, A., Malandain, G., Royer, L. A., Turaga, S. C., Branson, K. and Keller, P. J. (2018). In Toto Imaging and Reconstruction of Post-Implantation Mouse Development at the Single-Cell Level. *Cell* **175**, 859-876 e833.

McElhinny, S. A. N., Gordenin, D. A., Stith, C. M., Burgers, P. M. and Kunkel, T. A. (2008). Division of labor at the eukaryotic replication fork. *Molecular cell* **30**, 137-144.

McElhinny, S. A. N., Kumar, D., Clark, A. B., Watt, D. L., Watts, B. E., Lundström, E.-B., Johansson, E., Chabes, A. and Kunkel, T. A. (2010). Genome instability due to ribonucleotide incorporation into DNA. *Nature chemical biology* **6**, 774-781.

McGarry, T. J. and Kirschner, M. W. (1998). Geminin, an inhibitor of DNA replication, is degraded during mitosis. *Cell* **93**, 1043-1053.

McManus, K. J. and Hendzel, M. J. (2006). The relationship between histone H3 phosphorylation and acetylation throughout the mammalian cell cycle. *Biochem Cell Biol* **84**, 640-657.

Meilhac, S. M., Adams, R. J., Morris, S. A., Danckaert, A., Le Garrec, J. F. and Zernicka-Goetz, M. (2009). Active cell movements coupled to positional induction are involved in lineage segregation in the mouse blastocyst. *Dev Biol* **331**, 210-221.

Meistermann, D., Bruneau, A., Loubersac, S., Reignier, A., Firmin, J., Francois-Campion, V., Kilens, S., Lelievre, Y., Lammers, J., Feyeux, M., et al. (2021). Integrated pseudotime analysis of human pre-implantation embryo single-cell

transcriptomes reveals the dynamics of lineage specification. *Cell Stem Cell* **28**, 1625-1640 e1626.
Melby, A. E., Beach, C., Mullins, M. and Kimelman, D. (2000). Patterning the early zebrafish by the opposing actions of bozozok and vox/vent. *Dev Biol* **224**, 275-285.
Meng, X., Zhou, Y., Lee, E. Y., Lee, M. Y. and Frick, D. N. (2010). The p12 subunit of human polymerase delta modulates the rate and fidelity of DNA synthesis. *Biochemistry* **49**, 3545-3554.
Meng, X., Zhou, Y., Zhang, S., Lee, E. Y., Frick, D. N. and Lee, M. Y. (2009). DNA damage alters DNA polymerase delta to a form that exhibits increased discrimination against modified template bases and mismatched primers. *Nucleic Acids Res* **37**, 647-657.
Menko, A. S. (2002). Lens epithelial cell differentiation. *Experimental eye research* **75**, 485-490.
Meno, C., Gritsman, K., Ohishi, S., Ohfuji, Y., Heckscher, E., Mochida, K., Shimono, A., Kondoh, H., Talbot, W. S., Robertson, E. J., et al. (1999). Mouse Lefty2 and zebrafish antivin are feedback inhibitors of nodal signaling during vertebrate gastrulation. *Mol Cell* **4**, 287-298.
Miao, H., Vanderleest, T. E., Jewett, C. E., Loerke, D. and Blankenship, J. T. (2019). Cell ratcheting through the Sbf RabGEF directs force balancing and stepped apical constriction. *J Cell Biol* **218**, 3845-3860.
Migeotte, I., Grego-Bessa, J. and Anderson, K. V. (2011). Rac1 mediates morphogenetic responses to intercellular signals in the gastrulating mouse embryo. *Development* **138**, 3011-3020.
Migeotte, I., Omelchenko, T., Hall, A. and Anderson, K. V. (2010). Rac1-dependent collective cell migration is required for specification of the anterior-posterior body axis of the mouse. *PLoS Biol* **8**, e1000442.
Mihajlovic, A. I., Thamodaran, V. and Bruce, A. W. (2015). The first two cell-fate decisions of preimplantation mouse embryo development are not functionally independent. *Sci Rep* **5**, 15034.
Mishina, Y., Crombie, R., Bradley, A. and Behringer, R. R. (1999). Multiple roles for activin-like kinase-2 signaling during mouse embryogenesis. *Dev Biol* **213**, 314-326.
Mishina, Y., Suzuki, A., Ueno, N. and Behringer, R. R. (1995). Bmpr encodes a type I bone morphogenetic protein receptor that is essential for gastrulation during mouse embryogenesis. *Genes Dev* **9**, 3027-3037.
Mitrani, E., Shimoni, Y. and Eyal-Giladi, H. (1983). Nature of the hypoblastic influence on the chick embryo epiblast. *J Embryol Exp Morphol* **75**, 21-30.
Mitsui, K., Tokuzawa, Y., Itoh, H., Segawa, K., Murakami, M., Takahashi, K., Maruyama, M., Maeda, M. and Yamanaka, S. (2003). The homeoprotein Nanog is required for maintenance of pluripotency in mouse epiblast and ES cells. *Cell* **113**, 631-642.
Miyabe, I., Kunkel, T. A. and Carr, A. M. (2011). The major roles of DNA polymerases epsilon and delta at the eukaryotic replication fork are evolutionarily conserved. *PLoS Genet* **7**, e1002407.
Miyagi, C., Yamashita, S., Ohba, Y., Yoshizaki, H., Matsuda, M. and Hirano, T. (2004). STAT3 noncell-autonomously controls planar cell polarity during zebrafish convergence and extension. *The Journal of cell biology* **166**, 975-981.
Mizoguchi, T., Verkade, H., Heath, J. K., Kuroiwa, A. and Kikuchi, Y. (2008). Sdf1/Cxcr4 signaling controls the dorsal migration of endodermal cells during zebrafish gastrulation. *Development* **135**, 2521-2529.
Mlodzik, M., Fjose, A. and Gehring, W. J. (1985). Isolation of caudal, a Drosophila homeo box-containing gene with maternal expression, whose transcripts form a concentration gradient at the pre-blastoderm stage. *EMBO J* **4**, 2961-2969.
Mlodzik, M. and Gehring, W. J. (1987). Expression of the caudal gene in the germ line of Drosophila: formation of an RNA and protein gradient during early embryogenesis. *Cell* **48**, 465-478.

Modrich, P. (1997). Strand-specific mismatch repair in mammalian cells. *J Biol Chem* **272**, 24727-24730.
---- (2006). Mechanisms in eukaryotic mismatch repair. *J Biol Chem* **281**, 30305-30309.
Mohamed, O. A., Clarke, H. J. and Dufort, D. (2004). Beta-catenin signaling marks the prospective site of primitive streak formation in the mouse embryo. *Dev Dyn* **231**, 416-424.
Montague, T. G. and Schier, A. F. (2017). Vg1-Nodal heterodimers are the endogenous inducers of mesendoderm. *Elife* **6**.
Montero, J. A., Carvalho, L., Wilsch-Brauninger, M., Kilian, B., Mustafa, C. and Heisenberg, C. P. (2005). Shield formation at the onset of zebrafish gastrulation. *Development* **132**, 1187-1198.
Montero, J. A., Kilian, B., Chan, J., Bayliss, P. E. and Heisenberg, C. P. (2003). Phosphoinositide 3-kinase is required for process outgrowth and cell polarization of gastrulating mesendodermal cells. *Curr Biol* **13**, 1279-1289.
Moody, S. A. and Kline, M. J. (1990). Segregation of fate during cleavage of frog (Xenopus laevis) blastomeres. *Anat Embryol (Berl)* **182**, 347-362.
Moore, J. D., Kirk, J. A. and Hunt, T. (2003). Unmasking the S-phase-promoting potential of cyclin B1. *Science* **300**, 987-990.
Moore, R., Cai, K. Q., Escudero, D. O. and Xu, X. X. (2009). Cell adhesive affinity does not dictate primitive endoderm segregation and positioning during murine embryoid body formation. *Genesis* **47**, 579-589.
Morgan, D. O. (1997). Cyclin-dependent kinases: engines, clocks, and microprocessors. *Annu Rev Cell Dev Biol* **13**, 261-291.
Morize, P., Christiansen, A. E., Costa, M., Parks, S. and Wieschaus, E. (1998). Hyperactivation of the folded gastrulation pathway induces specific cell shape changes. *Development* **125**, 589-597.
Morris, S. A., Graham, S. J., Jedrusik, A. and Zernicka-Goetz, M. (2013). The differential response to Fgf signalling in cells internalized at different times influences lineage segregation in preimplantation mouse embryos. *Open Biol* **3**, 130104.
Morris, S. A., Teo, R. T., Li, H., Robson, P., Glover, D. M. and Zernicka-Goetz, M. (2010). Origin and formation of the first two distinct cell types of the inner cell mass in the mouse embryo. *Proc Natl Acad Sci U S A* **107**, 6364-6369.
Morrison, A., Araki, H., Clark, A. B., Hamatake, R. K. and Sugino, A. (1990). A third essential DNA polymerase in S. cerevisiae. *Cell* **62**, 1143-1151.
Morrison, A., Bell, J. B., Kunkel, T. A. and Sugino, A. (1991). Eukaryotic DNA polymerase amino acid sequence required for 3'----5' exonuclease activity. *Proc Natl Acad Sci U S A* **88**, 9473-9477.
Morrison, A., Johnson, A. L., Johnston, L. H. and Sugino, A. (1993). Pathway correcting DNA replication errors in Saccharomyces cerevisiae. *EMBO J* **12**, 1467-1473.
Mudrak, I., Ogris, E., Rotheneder, H. and Wintersberger, E. (1994). Coordinated trans activation of DNA synthesis- and precursor-producing enzymes by polyomavirus large T antigen through interaction with the retinoblastoma protein. *Mol Cell Biol* **14**, 1886-1892.
Mukhopadhyay, M., Shtrom, S., Rodriguez-Esteban, C., Chen, L., Tsukui, T., Gomer, L., Dorward, D. W., Glinka, A., Grinberg, A., Huang, S. P., et al. (2001). Dickkopf1 is required for embryonic head induction and limb morphogenesis in the mouse. *Dev Cell* **1**, 423-434.
Mukhopadhyay, M., Teufel, A., Yamashita, T., Agulnick, A. D., Chen, L., Downs, K. M., Schindler, A., Grinberg, A., Huang, S. P., Dorward, D., et al. (2003). Functional ablation of the mouse Ldb1 gene results in severe patterning defects during gastrulation. *Development* **130**, 495-505.

Mummery, C. L., van Rooijen, M. A., van den Brink, S. E. and de Laat, S. W. (1987). Cell cycle analysis during retinoic acid induced differentiation of a human embryonal carcinoma-derived cell line. *Cell Differ* **20**, 153-160.
Mur, P., Garcia-Mulero, S., Del Valle, J., Magraner-Pardo, L., Vidal, A., Pineda, M., Cinnirella, G., Martin-Ramos, E., Pons, T., Lopez-Doriga, A., et al. (2020). Role of POLE and POLD1 in familial cancer. *Genet Med* **22**, 2089-2100.
Murphy, M., Stinnakre, M. G., Senamaud-Beaufort, C., Winston, N. J., Sweeney, C., Kubelka, M., Carrington, M., Brechot, C. and Sobczak-Thepot, J. (1997). Delayed early embryonic lethality following disruption of the murine cyclin A2 gene. *Nat Genet* **15**, 83-86.
Muzumdar, M. D., Tasic, B., Miyamichi, K., Li, L. and Luo, L. (2007). A global double-fluorescent Cre reporter mouse. *Genesis* **45**, 593-605.
Myers, D. C., Sepich, D. S. and Solnica-Krezel, L. (2002). Bmp activity gradient regulates convergent extension during zebrafish gastrulation. *Dev Biol* **243**, 81-98.
Nair, S. and Schilling, T. F. (2008). Chemokine signaling controls endodermal migration during zebrafish gastrulation. *Science* **322**, 89-92.
Nakamura, M., Matsumoto, K., Iwamoto, Y., Muguruma, T., Nakazawa, N., Hatori, R., Taniguchi, K., Maeda, R. and Matsuno, K. (2013). Reduced cell number in the hindgut epithelium disrupts hindgut left-right asymmetry in a mutant of pebble, encoding a RhoGEF, in Drosophila embryos. *Mech Dev* **130**, 169-180.
Nakaya, Y., Sukowati, E. W., Wu, Y. and Sheng, G. (2008). RhoA and microtubule dynamics control cell-basement membrane interaction in EMT during gastrulation. *Nat Cell Biol* **10**, 765-775.
Neganova, I., Zhang, X., Atkinson, S. and Lako, M. (2009). Expression and functional analysis of G1 to S regulatory components reveals an important role for CDK2 in cell cycle regulation in human embryonic stem cells. *Oncogene* **28**, 20-30.
Niakan, K. K. and Eggan, K. (2013). Analysis of human embryos from zygote to blastocyst reveals distinct gene expression patterns relative to the mouse. *Dev Biol* **375**, 54-64.
Niakan, K. K., Ji, H., Maehr, R., Vokes, S. A., Rodolfa, K. T., Sherwood, R. I., Yamaki, M., Dimos, J. T., Chen, A. E., Melton, D. A., et al. (2010). Sox17 promotes differentiation in mouse embryonic stem cells by directly regulating extraembryonic gene expression and indirectly antagonizing self-renewal. *Genes Dev* **24**, 312-326.
Nichols, J., Silva, J., Roode, M. and Smith, A. (2009). Suppression of Erk signalling promotes ground state pluripotency in the mouse embryo. *Development* **136**, 3215-3222.
Nichols, J., Zevnik, B., Anastassiadis, K., Niwa, H., Klewe-Nebenius, D., Chambers, I., Scholer, H. and Smith, A. (1998). Formation of pluripotent stem cells in the mammalian embryo depends on the POU transcription factor Oct4. *Cell* **95**, 379-391.
Nicolas, E., Golemis, E. A. and Arora, S. (2016). POLD1: Central mediator of DNA replication and repair, and implication in cancer and other pathologies. *Gene* **590**, 128-141.
Nieuwkoop, P. D. (1967). The "organization centre". 3. Segregation and pattern formation in morphogenetic fields. *Acta Biotheor* **17**, 178-194.
Nishioka, N., Inoue, K., Adachi, K., Kiyonari, H., Ota, M., Ralston, A., Yabuta, N., Hirahara, S., Stephenson, R. O., Ogonuki, N., et al. (2009). The Hippo signaling pathway components Lats and Yap pattern Tead4 activity to distinguish mouse trophectoderm from inner cell mass. *Dev Cell* **16**, 398-410.
Nishioka, N., Nagano, S., Nakayama, R., Kiyonari, H., Ijiri, T., Taniguchi, K., Shawlot, W., Hayashizaki, Y., Westphal, H., Behringer, R. R., et al. (2005). Ssdp1 regulates head morphogenesis of mouse embryos by activating the Lim1-Ldb1 complex. *Development* **132**, 2535-2546.

Nishioka, N., Yamamoto, S., Kiyonari, H., Sato, H., Sawada, A., Ota, M., Nakao, K. and Sasaki, H. (2008). Tead4 is required for specification of trophectoderm in pre-implantation mouse embryos. *Mech Dev* **125**, 270-283.

Niwa, H., Miyazaki, J. and Smith, A. G. (2000). Quantitative expression of Oct-3/4 defines differentiation, dedifferentiation or self-renewal of ES cells. *Nat Genet* **24**, 372-376.

Niwa, H., Toyooka, Y., Shimosato, D., Strumpf, D., Takahashi, K., Yagi, R. and Rossant, J. (2005). Interaction between Oct3/4 and Cdx2 determines trophectoderm differentiation. *Cell* **123**, 917-929.

Norris, D. P. and Robertson, E. J. (1999). Asymmetric and node-specific nodal expression patterns are controlled by two distinct cis-acting regulatory elements. *Genes Dev* **13**, 1575-1588.

Norris, M. L., Pauli, A., Gagnon, J. A., Lord, N. D., Rogers, K. W., Mosimann, C., Zon, L. I. and Schier, A. F. (2017). Toddler signaling regulates mesodermal cell migration downstream of Nodal signaling. *Elife* **6**.

Nowotschin, S., Costello, I., Piliszek, A., Kwon, G. S., Mao, C. A., Klein, W. H., Robertson, E. J. and Hadjantonakis, A. K. (2013). The T-box transcription factor Eomesodermin is essential for AVE induction in the mouse embryo. *Genes Dev* **27**, 997-1002.

Nowotschin, S., Setty, M., Kuo, Y. Y., Liu, V., Garg, V., Sharma, R., Simon, C. S., Saiz, N., Gardner, R., Boutet, S. C., et al. (2019). The emergent landscape of the mouse gut endoderm at single-cell resolution. *Nature* **569**, 361-367.

Nüsslein-Volhard, C. (1979). Maternal effect mutations that alter the spatial coordinates of the embryo of Drosophila melanogaster. *Determinants of spatial organization* **28**.

Nusslein-Volhard, C., Frohnhofer, H. G. and Lehmann, R. (1987). Determination of anteroposterior polarity in Drosophila. *Science* **238**, 1675-1681.

Oda, H., Tsukita, S. and Takeichi, M. (1998). Dynamic behavior of the cadherin-based cell-cell adhesion system during Drosophila gastrulation. *Dev Biol* **203**, 435-450.

Ohnishi, Y., Huber, W., Tsumura, A., Kang, M., Xenopoulos, P., Kurimoto, K., Oles, A. K., Arauzo-Bravo, M. J., Saitou, M., Hadjantonakis, A. K., et al. (2014). Cell-to-cell expression variability followed by signal reinforcement progressively segregates early mouse lineages. *Nat Cell Biol* **16**, 27-37.

Ohtoshi, A., Maeda, T., Higashi, H., Ashizawa, S. and Hatakeyama, M. (2000). Human p55(CDC)/Cdc20 associates with cyclin A and is phosphorylated by the cyclin A-Cdk2 complex. *Biochem Biophys Res Commun* **268**, 530-534.

Ohtsubo, M., Theodoras, A. M., Schumacher, J., Roberts, J. M. and Pagano, M. (1995). Human cyclin E, a nuclear protein essential for the G1-to-S phase transition. *Mol Cell Biol* **15**, 2612-2624.

Ohuchi, H., Tomonari, S., Itoh, H., Mikawa, T. and Noji, S. (1999). Identification of chick rax/rx genes with overlapping patterns of expression during early eye and brain development. *Mech Dev* **85**, 193-195.

Okumura-Nakanishi, S., Saito, M., Niwa, H. and Ishikawa, F. (2005). Oct-3/4 and Sox2 regulate Oct-3/4 gene in embryonic stem cells. *J Biol Chem* **280**, 5307-5317.

Olguin, H. C. and Olwin, B. B. (2004). Pax-7 up-regulation inhibits myogenesis and cell cycle progression in satellite cells: a potential mechanism for self-renewal. *Dev Biol* **275**, 375-388.

Oliver, G., Mailhos, A., Wehr, R., Copeland, N. G., Jenkins, N. A. and Gruss, P. (1995). Six3, a murine homologue of the sine oculis gene, demarcates the most anterior border of the developing neural plate and is expressed during eye development. *Development* **121**, 4045-4055.

Omelchenko, T., Hall, A. and Anderson, K. V. (2020). beta-Pix-dependent cellular protrusions propel collective mesoderm migration in the mouse embryo. *Nat Commun* **11**, 6066.

Omelchenko, T., Rabadan, M. A., Hernandez-Martinez, R., Grego-Bessa, J., Anderson, K. V. and Hall, A. (2014). beta-Pix directs collective migration of anterior visceral endoderm cells in the early mouse embryo. *Genes Dev* **28**, 2764-2777.

Ong, S. and Tan, C. (2010). Germline cyst formation and incomplete cytokinesis during Drosophila melanogaster oogenesis. *Dev Biol* **337**, 84-98.

Ortega, S., Prieto, I., Odajima, J., Martin, A., Dubus, P., Sotillo, R., Barbero, J. L., Malumbres, M. and Barbacid, M. (2003). Cyclin-dependent kinase 2 is essential for meiosis but not for mitotic cell division in mice. *Nat Genet* **35**, 25-31.

Oustanina, S., Hause, G. and Braun, T. (2004). Pax7 directs postnatal renewal and propagation of myogenic satellite cells but not their specification. *EMBO J* **23**, 3430-3439.

Ozawa, H., Ashizawa, S., Naito, M., Yanagihara, M., Ohnishi, N., Maeda, T., Matsuda, Y., Jo, Y., Higashi, H., Kakita, A., et al. (2004). Paired-like homeodomain protein ESXR1 possesses a cleavable C-terminal region that inhibits cyclin degradation. *Oncogene* **23**, 6590-6602.

Pagano, M., Pepperkok, R., Lukas, J., Baldin, V., Ansorge, W., Bartek, J. and Draetta, G. (1993). Regulation of the cell cycle by the cdk2 protein kinase in cultured human fibroblasts. *J Cell Biol* **121**, 101-111.

Pagano, M., Pepperkok, R., Verde, F., Ansorge, W. and Draetta, G. (1992). Cyclin A is required at two points in the human cell cycle. *EMBO J* **11**, 961-971.

Palles, C., Cazier, J. B., Howarth, K. M., Domingo, E., Jones, A. M., Broderick, P., Kemp, Z., Spain, S. L., Guarino, E., Salguero, I., et al. (2013). Germline mutations affecting the proofreading domains of POLE and POLD1 predispose to colorectal adenomas and carcinomas. *Nat Genet* **45**, 136-144.

Pan, D. (2010). The hippo signaling pathway in development and cancer. *Dev Cell* **19**, 491-505.

Parker, S. B., Eichele, G., Zhang, P., Rawls, A., Sands, A. T., Bradley, A., Olson, E. N., Harper, J. W. and Elledge, S. J. (1995). p53-independent expression of p21Cip1 in muscle and other terminally differentiating cells. *Science* **267**, 1024-1027.

Parsons, J. L., Preston, B. D., O'Connor, T. R. and Dianov, G. L. (2007). DNA polymerase delta-dependent repair of DNA single strand breaks containing 3'-end proximal lesions. *Nucleic Acids Res* **35**, 1054-1063.

Pasteels, J. (1940). Un apercu comparatif de la gastrulation chez les chordes. *Biological Reviews* **15**, 59-106.

Pauklin, S., Madrigal, P., Bertero, A. and Vallier, L. (2016). Initiation of stem cell differentiation involves cell cycle-dependent regulation of developmental genes by Cyclin D. *Genes Dev* **30**, 421-433.

Pauklin, S. and Vallier, L. (2013). The cell-cycle state of stem cells determines cell fate propensity. *Cell* **155**, 135-147.

Pauli, A., Norris, M. L., Valen, E., Chew, G. L., Gagnon, J. A., Zimmerman, S., Mitchell, A., Ma, J., Dubrulle, J., Reyon, D., et al. (2014). Toddler: an embryonic signal that promotes cell movement via Apelin receptors. *Science* **343**, 1248636.

Pavlov, Y. I., Mian, I. M. and Kunkel, T. A. (2003). Evidence for preferential mismatch repair of lagging strand DNA replication errors in yeast. *Curr Biol* **13**, 744-748.

Pelliccia, J. L., Jindal, G. A. and Burdine, R. D. (2017). Gdf3 is required for robust Nodal signaling during germ layer formation and left-right patterning. *Elife* **6**, e28635.

Pepling, M. E., de Cuevas, M. and Spradling, A. C. (1999). Germline cysts: a conserved phase of germ cell development? *Trends Cell Biol* **9**, 257-262.

Perdiguero, E. and Nebreda, A. R. (2004). Regulation of Cdc25C activity during the meiotic G2/M transition. *Cell Cycle* **3**, 733-737.

Perea-Gomez, A., Vella, F. D., Shawlot, W., Oulad-Abdelghani, M., Chazaud, C., Meno, C., Pfister, V., Chen, L., Robertson, E., Hamada, H., et al. (2002). Nodal

antagonists in the anterior visceral endoderm prevent the formation of multiple primitive streaks. *Dev Cell* **3**, 745-756.

Peters, K. A. and Rogers, S. L. (2013). Drosophila Ric-8 interacts with the Galpha12/13 subunit, Concertina, during activation of the Folded gastrulation pathway. *Mol Biol Cell* **24**, 3460-3471.

Petropoulos, S., Edsgard, D., Reinius, B., Deng, Q., Panula, S. P., Codeluppi, S., Reyes, A. P., Linnarsson, S., Sandberg, R. and Lanner, F. (2016). Single-Cell RNA-Seq Reveals Lineage and X Chromosome Dynamics in Human Preimplantation Embryos. *Cell* **167**, 285.

Pezeron, G., Mourrain, P., Courty, S., Ghislain, J., Becker, T. S., Rosa, F. M. and David, N. B. (2008). Live analysis of endodermal layer formation identifies random walk as a novel gastrulation movement. *Curr Biol* **18**, 276-281.

Phippard, D. J., Weber-Hall, S. J., Sharpe, P. T., Naylor, M. S., Jayatalake, H., Maas, R., Woo, I., Roberts-Clark, D., Francis-West, P. H., Liu, Y. H., et al. (1996). Regulation of Msx-1, Msx-2, Bmp-2 and Bmp-4 during foetal and postnatal mammary gland development. *Development* **122**, 2729-2737.

Piacentino, M. L., Li, Y. and Bronner, M. E. (2020). Epithelial-to-mesenchymal transition and different migration strategies as viewed from the neural crest. *Curr Opin Cell Biol* **66**, 43-50.

Pierce, G. B., Aguilar, D., Hood, G. and Wells, R. S. (1984). Trophectoderm in control of murine embryonal carcinoma. *Cancer Res* **44**, 3987-3996.

Pijuan-Sala, B., Griffiths, J. A., Guibentif, C., Hiscock, T. W., Jawaid, W., Calero-Nieto, F. J., Mulas, C., Ibarra-Soria, X., Tyser, R. C. V., Ho, D. L. L., et al. (2019). A single-cell molecular map of mouse gastrulation and early organogenesis. *Nature* **566**, 490-495.

Pines, J. (1991). Cyclins: wheels within wheels. *Cell Growth Differ* **2**, 305-310.

---- (1995). Cyclins and cyclin-dependent kinases: a biochemical view. *Biochem J* **308 (Pt 3)**, 697-711.

Pinheiro, D. and Heisenberg, C. P. (2020). Zebrafish gastrulation: Putting fate in motion. *Curr Top Dev Biol* **136**, 343-375.

Plaster, N., Sonntag, C., Busse, C. E. and Hammerschmidt, M. (2006). p53 deficiency rescues apoptosis and differentiation of multiple cell types in zebrafish flathead mutants deficient for zygotic DNA polymerase delta1. *Cell Death Differ* **13**, 223-235.

Plusa, B., Piliszek, A., Frankenberg, S., Artus, J. and Hadjantonakis, A. K. (2008). Distinct sequential cell behaviours direct primitive endoderm formation in the mouse blastocyst. *Development* **135**, 3081-3091.

Podust, V. N., Chang, L. S., Ott, R., Dianov, G. L. and Fanning, E. (2002). Reconstitution of human DNA polymerase delta using recombinant baculoviruses: the p12 subunit potentiates DNA polymerizing activity of the four-subunit enzyme. *J Biol Chem* **277**, 3894-3901.

Pogoda, H. M., Solnica-Krezel, L., Driever, W. and Meyer, D. (2000). The zebrafish forkhead transcription factor FoxH1/Fast1 is a modulator of nodal signaling required for organizer formation. *Curr Biol* **10**, 1041-1049.

Polyak, K., Kato, J. Y., Solomon, M. J., Sherr, C. J., Massague, J., Roberts, J. M. and Koff, A. (1994a). p27Kip1, a cyclin-Cdk inhibitor, links transforming growth factor-beta and contact inhibition to cell cycle arrest. *Genes Dev* **8**, 9-22.

Polyak, K., Lee, M. H., Erdjument-Bromage, H., Koff, A., Roberts, J. M., Tempst, P. and Massague, J. (1994b). Cloning of p27Kip1, a cyclin-dependent kinase inhibitor and a potential mediator of extracellular antimitogenic signals. *Cell* **78**, 59-66.

Posfai, E., Petropoulos, S., de Barros, F. R. O., Schell, J. P., Jurisica, I., Sandberg, R., Lanner, F. and Rossant, J. (2017). Position- and Hippo signaling-dependent plasticity during lineage segregation in the early mouse embryo. *Elife* **6**.

Posfai, E., Schell, J. P., Janiszewski, A., Rovic, I., Murray, A., Bradshaw, B., Yamakawa, T., Pardon, T., El Bakkali, M., Talon, I., et al. (2021). Evaluating totipotency using criteria of increasing stringency. *Nat Cell Biol* **23**, 49-60.
Poss, K. D., Wilson, L. G. and Keating, M. T. (2002). Heart regeneration in zebrafish. *Science* **298**, 2188-2190.
Poulson, D. (1950). Histogenesis, organogenesis, and differentiation in the embryo of Drosophila melanogaster Meigen. *Biology of Drosophila*, 168-274.
Power, M. A. and Tam, P. P. (1993). Onset of gastrulation, morphogenesis and somitogenesis in mouse embryos displaying compensatory growth. *Anat Embryol (Berl)* **187**, 493-504.
Prelich, G. and Stillman, B. (1988). Coordinated leading and lagging strand synthesis during SV40 DNA replication in vitro requires PCNA. *Cell* **53**, 117-126.
Pursell, Z. F., Isoz, I., Lundstrom, E. B., Johansson, E. and Kunkel, T. A. (2007). Regulation of B family DNA polymerase fidelity by a conserved active site residue: characterization of M644W, M644L and M644F mutants of yeast DNA polymerase epsilon. *Nucleic Acids Res* **35**, 3076-3086.
Raffaelli, A. and Stern, C. D. (2020). Signaling events regulating embryonic polarity and formation of the primitive streak in the chick embryo. *Curr Top Dev Biol* **136**, 85-111.
Rakeman, A. S. and Anderson, K. V. (2006). Axis specification and morphogenesis in the mouse embryo require Nap1, a regulator of WAVE-mediated actin branching. *Development* **133**, 3075-3083.
Ralston, A., Cox, B. J., Nishioka, N., Sasaki, H., Chea, E., Rugg-Gunn, P., Guo, G., Robson, P., Draper, J. S. and Rossant, J. (2010). Gata3 regulates trophoblast development downstream of Tead4 and in parallel to Cdx2. *Development* **137**, 395-403.
Ralston, A. and Rossant, J. (2005). Genetic regulation of stem cell origins in the mouse embryo. *Clin Genet* **68**, 106-112.
---- (2008). Cdx2 acts downstream of cell polarization to cell-autonomously promote trophectoderm fate in the early mouse embryo. *Dev Biol* **313**, 614-629.
Ramkumar, N., Omelchenko, T., Silva-Gagliardi, N. F., McGlade, C. J., Wijnholds, J. and Anderson, K. V. (2016). Crumbs2 promotes cell ingression during the epithelial-to-mesenchymal transition at gastrulation. *Nat Cell Biol* **18**, 1281-1291.
Rane, S. G., Dubus, P., Mettus, R. V., Galbreath, E. J., Boden, G., Reddy, E. P. and Barbacid, M. (1999). Loss of Cdk4 expression causes insulin-deficient diabetes and Cdk4 activation results in beta-islet cell hyperplasia. *Nat Genet* **22**, 44-52.
Rao, S. S., Chu, C. and Kohtz, D. S. (1994). Ectopic expression of cyclin D1 prevents activation of gene transcription by myogenic basic helix-loop-helix regulators. *Mol Cell Biol* **14**, 5259-5267.
Rashbass, P., Cooke, L. A., Herrmann, B. G. and Beddington, R. S. (1991). A cell autonomous function of Brachyury in T/T embryonic stem cell chimaeras. *Nature* **353**, 348-351.
Rashbass, P., Wilson, V., Rosen, B. and Beddington, R. S. (1994). Alterations in gene expression during mesoderm formation and axial patterning in Brachyury (T) embryos. *Int J Dev Biol* **38**, 35-44.
Rayner, E., van Gool, I. C., Palles, C., Kearsey, S. E., Bosse, T., Tomlinson, I. and Church, D. N. (2016). A panoply of errors: polymerase proofreading domain mutations in cancer. *Nat Rev Cancer* **16**, 71-81.
Rayon, T., Menchero, S., Nieto, A., Xenopoulos, P., Crespo, M., Cockburn, K., Canon, S., Sasaki, H., Hadjantonakis, A. K., de la Pompa, J. L., et al. (2014). Notch and hippo converge on Cdx2 to specify the trophectoderm lineage in the mouse blastocyst. *Dev Cell* **30**, 410-422.
Reginensi, A., Scott, R. P., Gregorieff, A., Bagherie-Lachidan, M., Chung, C., Lim, D. S., Pawson, T., Wrana, J. and McNeill, H. (2013). Yap- and Cdc42-dependent

nephrogenesis and morphogenesis during mouse kidney development. *PLoS Genet* **9**, e1003380.
Reha-Krantz, L. J. (2010). DNA polymerase proofreading: Multiple roles maintain genome stability. *Biochim Biophys Acta* **1804**, 1049-1063.
Reijns, M. A. M., Kemp, H., Ding, J., de Proce, S. M., Jackson, A. P. and Taylor, M. S. (2015). Lagging-strand replication shapes the mutational landscape of the genome. *Nature* **518**, 502-506.
Reimann, J. D., Freed, E., Hsu, J. Y., Kramer, E. R., Peters, J.-M. and Jackson, P. K. (2001). Emi1 is a mitotic regulator that interacts with Cdc20 and inhibits the anaphase promoting complex. *Cell* **105**, 645-655.
Rembold, M., Ciglar, L., Yanez-Cuna, J. O., Zinzen, R. P., Girardot, C., Jain, A., Welte, M. A., Stark, A., Leptin, M. and Furlong, E. E. (2014). A conserved role for Snail as a potentiator of active transcription. *Genes Dev* **28**, 167-181.
Rivera-Perez, J. A. and Hadjantonakis, A. K. (2014). The Dynamics of Morphogenesis in the Early Mouse Embryo. *Cold Spring Harb Perspect Biol* **7**.
Rivera-Perez, J. A., Mager, J. and Magnuson, T. (2003). Dynamic morphogenetic events characterize the mouse visceral endoderm. *Dev Biol* **261**, 470-487.
Rivron, N. C., Frias-Aldeguer, J., Vrij, E. J., Boisset, J. C., Korving, J., Vivie, J., Truckenmuller, R. K., van Oudenaarden, A., van Blitterswijk, C. A. and Geijsen, N. (2018). Blastocyst-like structures generated solely from stem cells. *Nature* **557**, 106-111.
Robertson, E. J. (2014). Dose-dependent Nodal/Smad signals pattern the early mouse embryo. *Semin Cell Dev Biol* **32**, 73-79.
Rodaway, A., Takeda, H., Koshida, S., Broadbent, J., Price, B., Smith, J. C., Patient, R. and Holder, N. (1999). Induction of the mesendoderm in the zebrafish germ ring by yolk cell-derived TGF-beta family signals and discrimination of mesoderm and endoderm by FGF. *Development* **126**, 3067-3078.
Rodes, B., Garcia, F., Gutierrez, C., Martinez-Picado, J., Aguilera, A., Saumoy, M., Vallejo, A., Domingo, P., Dalmau, D., Ribas, M. A., et al. (2005). Impact of drug resistance genotypes on CD4+ counts and plasma viremia in heavily antiretroviral-experienced HIV-infected patients. *J Med Virol* **77**, 23-28.
Rodgers, H. M., Huffman, V. J., Voronina, V. A., Lewandoski, M. and Mathers, P. H. (2018). The role of the Rx homeobox gene in retinal progenitor proliferation and cell fate specification. *Mech Dev* **151**, 18-29.
Rodriguez, T. A., Casey, E. S., Harland, R. M., Smith, J. C. and Beddington, R. S. (2001). Distinct enhancer elements control Hex expression during gastrulation and early organogenesis. *Dev Biol* **234**, 304-316.
Rogulja, D. and Irvine, K. D. (2005). Regulation of cell proliferation by a morphogen gradient. *Cell* **123**, 449-461.
Roode, M., Blair, K., Snell, P., Elder, K., Marchant, S., Smith, A. and Nichols, J. (2012). Human hypoblast formation is not dependent on FGF signalling. *Dev Biol* **361**, 358-363.
Rossant, J. and Tam, P. P. (2009a). Blastocyst lineage formation, early embryonic asymmetries and axis patterning in the mouse.
Rossant, J. and Tam, P. P. (2009b). Blastocyst lineage formation, early embryonic asymmetries and axis patterning in the mouse. *Development* **136**, 701-713.
Rossant, J. and Tam, P. P. L. (2017). New Insights into Early Human Development: Lessons for Stem Cell Derivation and Differentiation. *Cell Stem Cell* **20**, 18-28.
Roszko, I., Sawada, A. and Solnica-Krezel, L. (2009). Regulation of convergence and extension movements during vertebrate gastrulation by the Wnt/PCP pathway. *Semin Cell Dev Biol* **20**, 986-997.

Roth, S., Hiromi, Y., Godt, D. and Nusslein-Volhard, C. (1991). cactus, a maternal gene required for proper formation of the dorsoventral morphogen gradient in Drosophila embryos. *Development* **112**, 371-388.

Rozbicki, E., Chuai, M., Karjalainen, A. I., Song, F., Sang, H. M., Martin, R., Knolker, H. J., MacDonald, M. P. and Weijer, C. J. (2015). Myosin-II-mediated cell shape changes and cell intercalation contribute to primitive streak formation. *Nat Cell Biol* **17**, 397-408.

Rudkin, G. T. (1972). Replication in polytene chromosomes. *Developmental studies on giant chromosomes*, 59-85.

Ruiz, S., Panopoulos, A. D., Herrerias, A., Bissig, K. D., Lutz, M., Berggren, W. T., Verma, I. M. and Izpisua Belmonte, J. C. (2011). A high proliferation rate is required for cell reprogramming and maintenance of human embryonic stem cell identity. *Curr Biol* **21**, 45-52.

Ryu, S. L., Fujii, R., Yamanaka, Y., Shimizu, T., Yabe, T., Hirata, T., Hibi, M. and Hirano, T. (2001). Regulation of dharma/bozozok by the Wnt pathway. *Dev Biol* **231**, 397-409.

Saga, Y., Miyagawa-Tomita, S., Takagi, A., Kitajima, S., Miyazaki, J. and Inoue, T. (1999). MesP1 is expressed in the heart precursor cells and required for the formation of a single heart tube. *Development* **126**, 3437-3447.

Saiz, N., Grabarek, J. B., Sabherwal, N., Papalopulu, N. and Plusa, B. (2013). Atypical protein kinase C couples cell sorting with primitive endoderm maturation in the mouse blastocyst. *Development* **140**, 4311-4322.

Saiz, N., Williams, K. M., Seshan, V. E. and Hadjantonakis, A. K. (2016). Asynchronous fate decisions by single cells collectively ensure consistent lineage composition in the mouse blastocyst. *Nat Commun* **7**, 13463.

Sakai, K. and Miyazaki, J. (1997). A transgenic mouse line that retains Cre recombinase activity in mature oocytes irrespective of the cre transgene transmission. *Biochem Biophys Res Commun* **237**, 318-324.

Sakaue-Sawano, A., Kurokawa, H., Morimura, T., Hanyu, A., Hama, H., Osawa, H., Kashiwagi, S., Fukami, K., Miyata, T., Miyoshi, H., et al. (2008). Visualizing spatiotemporal dynamics of multicellular cell-cycle progression. *Cell* **132**, 487-498.

Sako, K., Pradhan, S. J., Barone, V., Ingles-Prieto, A., Muller, P., Ruprecht, V., Capek, D., Galande, S., Janovjak, H. and Heisenberg, C. P. (2016). Optogenetic Control of Nodal Signaling Reveals a Temporal Pattern of Nodal Signaling Regulating Cell Fate Specification during Gastrulation. *Cell Rep* **16**, 866-877.

Sakurai, Y., Ohgimoto, K., Kataoka, Y., Yoshida, N. and Shibuya, M. (2005). Essential role of Flk-1 (VEGF receptor 2) tyrosine residue 1173 in vasculogenesis in mice. *Proc Natl Acad Sci U S A* **102**, 1076-1081.

Sandmann, T., Girardot, C., Brehme, M., Tongprasit, W., Stolc, V. and Furlong, E. E. (2007). A core transcriptional network for early mesoderm development in Drosophila melanogaster. *Genes Dev* **21**, 436-449.

Sasaki, H., Yanagi, K., Ugi, S., Kobayashi, K., Ohkubo, K., Tajiri, Y., Maegawa, H., Kashiwagi, A. and Kaname, T. (2018). Definitive diagnosis of mandibular hypoplasia, deafness, progeroid features and lipodystrophy (MDPL) syndrome caused by a recurrent de novo mutation in the POLD1 gene. *Endocr J* **65**, 227-238.

Satokata, I., Ma, L., Ohshima, H., Bei, M., Woo, I., Nishizawa, K., Maeda, T., Takano, Y., Uchiyama, M., Heaney, S., et al. (2000). Msx2 deficiency in mice causes pleiotropic defects in bone growth and ectodermal organ formation. *Nat Genet* **24**, 391-395.

Saykali, B., Mathiah, N., Nahaboo, W., Racu, M. L., Hammou, L., Defrance, M. and Migeotte, I. (2019). Distinct mesoderm migration phenotypes in extra-embryonic and embryonic regions of the early mouse embryo. *Elife* **8**.

Schafer, G., Narasimha, M., Vogelsang, E. and Leptin, M. (2014). Cadherin switching during the formation and differentiation of the Drosophila mesoderm - implications for epithelial-to-mesenchymal transitions. *J Cell Sci* **127**, 1511-1522.
Schier, A. F. and Talbot, W. S. (2005). Molecular genetics of axis formation in zebrafish. *Annu Rev Genet* **39**, 561-613.
Schmitt, M. W., Matsumoto, Y. and Loeb, L. A. (2009). High fidelity and lesion bypass capability of human DNA polymerase delta. *Biochimie* **91**, 1163-1172.
Schneider, S., Steinbeisser, H., Warga, R. M. and Hausen, P. (1996). Beta-catenin translocation into nuclei demarcates the dorsalizing centers in frog and fish embryos. *Mech Dev* **57**, 191-198.
Schrode, N., Saiz, N., Di Talia, S. and Hadjantonakis, A. K. (2014). GATA6 levels modulate primitive endoderm cell fate choice and timing in the mouse blastocyst. *Dev Cell* **29**, 454-467.
Schroter, C., Rue, P., Mackenzie, J. P. and Martinez Arias, A. (2015). FGF/MAPK signaling sets the switching threshold of a bistable circuit controlling cell fate decisions in embryonic stem cells. *Development* **142**, 4205-4216.
Schulte-Merker, S., Lee, K. J., McMahon, A. P. and Hammerschmidt, M. (1997). The zebrafish organizer requires chordino. *Nature* **387**, 862-863.
Schupbach, T. and Wieschaus, E. (1986). Maternal-effect mutations altering the anterior-posterior pattern of the Drosophila embryo. *Rouxs Arch Dev Biol* **195**, 302-317.
Schweisguth, F. (2015). Asymmetric cell division in the Drosophila bristle lineage: from the polarization of sensory organ precursor cells to Notch-mediated binary fate decision. *Wiley Interdiscip Rev Dev Biol* **4**, 299-309.
Scott, M. P., Tamkun, J. W. and Hartzell, G. W., 3rd (1989). The structure and function of the homeodomain. *Biochim Biophys Acta* **989**, 25-48.
Seale, P., Asakura, A. and Rudnicki, M. A. (2001). The potential of muscle stem cells. *Dev Cell* **1**, 333-342.
Seale, P., Sabourin, L. A., Girgis-Gabardo, A., Mansouri, A., Gruss, P. and Rudnicki, M. A. (2000). Pax7 is required for the specification of myogenic satellite cells. *Cell* **102**, 777-786.
Seimiya, M. and Gehring, W. J. (2000). The Drosophila homeobox gene optix is capable of inducing ectopic eyes by an eyeless-independent mechanism. *Development* **127**, 1879-1886.
Seleiro, E. A., Connolly, D. J. and Cooke, J. (1996). Early developmental expression and experimental axis determination by the chicken Vg1 gene. *Curr Biol* **6**, 1476-1486.
Seo, H. C., Drivenes, Ellingsen, S. and Fjose, A. (1998). Expression of two zebrafish homologues of the murine Six3 gene demarcates the initial eye primordia. *Mech Dev* **73**, 45-57.
Sepich, D. S., Calmelet, C., Kiskowski, M. and Solnica-Krezel, L. (2005). Initiation of convergence and extension movements of lateral mesoderm during zebrafish gastrulation. *Dev Dyn* **234**, 279-292.
Serrano, M., Hannon, G. J. and Beach, D. (1993). A new regulatory motif in cell-cycle control causing specific inhibition of cyclin D/CDK4. *Nature* **366**, 704-707.
Shah, S. B., Skromne, I., Hume, C. R., Kessler, D. S., Lee, K. J., Stern, C. D. and Dodd, J. (1997). Misexpression of chick Vg1 in the marginal zone induces primitive streak formation. *Development* **124**, 5127-5138.
Shawlot, W. and Behringer, R. R. (1995). Requirement for Lim1 in head-organizer function. *Nature* **374**, 425-430.
Shimizu, T., Yamanaka, Y., Nojima, H., Yabe, T., Hibi, M. and Hirano, T. (2002). A novel repressor-type homeobox gene, ved, is involved in dharma/bozozok-mediated dorsal organizer formation in zebrafish. *Mech Dev* **118**, 125-138.
Shimizu, T., Yamanaka, Y., Ryu, S. L., Hashimoto, H., Yabe, T., Hirata, T., Bae, Y. K., Hibi, M. and Hirano, T. (2000). Cooperative roles of Bozozok/Dharma and Nodal-

related proteins in the formation of the dorsal organizer in zebrafish. *Mech Dev* **91**, 293-303.

Shimono, A. and Behringer, R. R. (2003). Angiomotin regulates visceral endoderm movements during mouse embryogenesis. *Curr Biol* **13**, 613-617.

Sicinski, P., Donaher, J. L., Geng, Y., Parker, S. B., Gardner, H., Park, M. Y., Robker, R. L., Richards, J. S., McGinnis, L. K., Biggers, J. D., et al. (1996). Cyclin D2 is an FSH-responsive gene involved in gonadal cell proliferation and oncogenesis. *Nature* **384**, 470-474.

Sicinski, P., Donaher, J. L., Parker, S. B., Li, T., Fazeli, A., Gardner, H., Haslam, S. Z., Bronson, R. T., Elledge, S. J. and Weinberg, R. A. (1995). Cyclin D1 provides a link between development and oncogenesis in the retina and breast. *Cell* **82**, 621-630.

Simon, C. S., Downes, D. J., Gosden, M. E., Telenius, J., Higgs, D. R., Hughes, J. R., Costello, I., Bikoff, E. K. and Robertson, E. J. (2017). Functional characterisation of cis-regulatory elements governing dynamic Eomes expression in the early mouse embryo. *Development* **144**, 1249-1260.

Simon, M., Giot, L. and Faye, G. (1991). The 3' to 5' exonuclease activity located in the DNA polymerase delta subunit of Saccharomyces cerevisiae is required for accurate replication. *EMBO J* **10**, 2165-2170.

Simpson, P. (1983). Maternal-Zygotic Gene Interactions during Formation of the Dorsoventral Pattern in Drosophila Embryos. *Genetics* **105**, 615-632.

Singh, A. M., Chappell, J., Trost, R., Lin, L., Wang, T., Tang, J., Matlock, B. K., Weller, K. P., Wu, H., Zhao, S., et al. (2013). Cell-cycle control of developmentally regulated transcription factors accounts for heterogeneity in human pluripotent cells. *Stem Cell Reports* **1**, 532-544.

Singh, A. M., Hamazaki, T., Hankowski, K. E. and Terada, N. (2007). A heterogeneous expression pattern for Nanog in embryonic stem cells. *Stem Cells* **25**, 2534-2542.

Singh, A. M., Sun, Y., Li, L., Zhang, W., Wu, T., Zhao, S., Qin, Z. and Dalton, S. (2015). Cell-Cycle Control of Bivalent Epigenetic Domains Regulates the Exit from Pluripotency. *Stem Cell Reports* **5**, 323-336.

Sitney, K. C., Budd, M. E. and Campbell, J. L. (1989). DNA polymerase III, a second essential DNA polymerase, is encoded by the S. cerevisiae CDC2 gene. *Cell* **56**, 599-605.

Skapek, S. X., Rhee, J., Spicer, D. B. and Lassar, A. B. (1995). Inhibition of myogenic differentiation in proliferating myoblasts by cyclin D1-dependent kinase. *Science* **267**, 1022-1024.

Skarnes, W. C., Rosen, B., West, A. P., Koutsourakis, M., Bushell, W., Iyer, V., Mujica, A. O., Thomas, M., Harrow, J., Cox, T., et al. (2011). A conditional knockout resource for the genome-wide study of mouse gene function. *Nature* **474**, 337-342.

Skeath, J. B. and Carroll, S. B. (1992). Regulation of proneural gene expression and cell fate during neuroblast segregation in the Drosophila embryo. *Development* **114**, 939-946.

Skopicki, H. A., Lyons, G. E., Schatteman, G., Smith, R. C., Andres, V., Schirm, S., Isner, J. and Walsh, K. (1997). Embryonic expression of the Gax homeodomain protein in cardiac, smooth, and skeletal muscle. *Circ Res* **80**, 452-462.

Skromne, I. and Stern, C. D. (2001). Interactions between Wnt and Vg1 signalling pathways initiate primitive streak formation in the chick embryo. *Development* **128**, 2915-2927.

Smith, A. V. and Orr-Weaver, T. L. (1991). The regulation of the cell cycle during Drosophila embryogenesis: the transition to polyteny. *Development* **112**, 997-1008.

Smith, R. C., Branellec, D., Gorski, D. H., Guo, K., Perlman, H., Dedieu, J.-F., Pastore, C., Mahfoudi, A., Denèfle, P. and Isner, J. M. (1997). p21CIP1-mediated inhibition of cell proliferation by overexpression of the gax homeodomain gene. *Genes & Development* **11**, 1674-1689.

Smutny, M., Akos, Z., Grigolon, S., Shamipour, S., Ruprecht, V., Capek, D., Behrndt, M., Papusheva, E., Tada, M., Hof, B., et al. (2017). Friction forces position the neural anlage. *Nat Cell Biol* **19**, 306-317.

Snell, G. and Stevens, L. (1966). Early embryology. In "Biology of the Laboratory Mouse"(EL Green, ed.). McGraw-Hill, New York.

Snow, M. (1977). Gastrulation in the mouse: growth and regionalization of the epiblast.

Snow, M. H. and Bennett, D. (1978). Gastrulation in the mouse: assessment of cell populations in the epiblast of tw18/tw18 embryos. *J Embryol Exp Morphol* **47**, 39-52.

Snow, M. H. and Tam, P. P. (1979). Is compensatory growth a complicating factor in mouse teratology? *Nature* **279**, 555-557.

Solnica-Krezel, L. and Sepich, D. S. (2012). Gastrulation: making and shaping germ layers. *Annu Rev Cell Dev Biol* **28**, 687-717.

Solnica-Krezel, L., Stemple, D. L., Mountcastle-Shah, E., Rangini, Z., Neuhauss, S. C., Malicki, J., Schier, A. F., Stainier, D. Y., Zwartkruis, F., Abdelilah, S., et al. (1996). Mutations affecting cell fates and cellular rearrangements during gastrulation in zebrafish. *Development* **123**, 67-80.

Song, J., Hong, P., Liu, C., Zhang, Y., Wang, J. and Wang, P. (2015). Human POLD1 modulates cell cycle progression and DNA damage repair. *BMC Biochem* **16**, 14.

Song, J. Y., Park, R., Kim, J. Y., Hughes, L., Lu, L., Kim, S., Johnson, R. L. and Cho, S. H. (2014). Dual function of Yap in the regulation of lens progenitor cells and cellular polarity. *Dev Biol* **386**, 281-290.

Song, N., Zhu, X., Shi, L., An, J., Wu, Y. and Sang, J. (2009). Identification and functional analysis of a CDE/CHR element in the POLD1 promoter. *Sci China C Life Sci* **52**, 551-559.

Soufi, A., Donahue, G. and Zaret, K. S. (2012). Facilitators and impediments of the pluripotency reprogramming factors' initial engagement with the genome. *Cell* **151**, 994-1004.

Soufi, A., Garcia, M. F., Jaroszewicz, A., Osman, N., Pellegrini, M. and Zaret, K. S. (2015). Pioneer transcription factors target partial DNA motifs on nucleosomes to initiate reprogramming. *Cell* **161**, 555-568.

Sozen, B., Cox, A. L., De Jonghe, J., Bao, M., Hollfelder, F., Glover, D. M. and Zernicka-Goetz, M. (2019). Self-Organization of Mouse Stem Cells into an Extended Potential Blastoid. *Dev Cell* **51**, 698-712 e698.

Sozen, B., Jorgensen, V., Weatherbee, B. A. T., Chen, S., Zhu, M. and Zernicka-Goetz, M. (2021). Reconstructing aspects of human embryogenesis with pluripotent stem cells. *Nat Commun* **12**, 5550.

Spencer, C. A., Kruhlak, M. J., Jenkins, H. L., Sun, X. and Bazett-Jones, D. P. (2000). Mitotic transcription repression in vivo in the absence of nucleosomal chromatin condensation. *J Cell Biol* **150**, 13-26.

Spiegelman, M. and Bennett, D. (1974). Fine structural study of cell migration in the early mesoderm of normal and mutant mouse embryos (T-locus: t-9/t-9). *J Embryol Exp Morphol* **32**, 723-728.

Spratt Jr, N. T. (1942). Location of organ-specific regions and their relationship to the development of the primitive streak in the early chick blastoderm. *Journal of Experimental Zoology* **89**, 69-101.

Srinivas, S., Rodriguez, T., Clements, M., Smith, J. C. and Beddington, R. S. (2004). Active cell migration drives the unilateral movements of the anterior visceral endoderm. *Development* **131**, 1157-1164.

Stachel, S. E., Grunwald, D. J. and Myers, P. Z. (1993). Lithium perturbation and goosecoid expression identify a dorsal specification pathway in the pregastrula zebrafish. *Development* **117**, 1261-1274.

Stanger, B. Z., Tanaka, A. J. and Melton, D. A. (2007). Organ size is limited by the number of embryonic progenitor cells in the pancreas but not the liver. *Nature* **445**, 886-891.

Stead, E., White, J., Faast, R., Conn, S., Goldstone, S., Rathjen, J., Dhingra, U., Rathjen, P., Walker, D. and Dalton, S. (2002). Pluripotent cell division cycles are driven by ectopic Cdk2, cyclin A/E and E2F activities. *Oncogene* **21**, 8320-8333.
Stern, C. D. (1990). The marginal zone and its contribution to the hypoblast and primitive streak of the chick embryo. *Development* **109**, 667-682.
Stern, C. D. and Canning, D. R. (1990). Origin of cells giving rise to mesoderm and endoderm in chick embryo. *Nature* **343**, 273-275.
Stirparo, G. G., Boroviak, T., Guo, G., Nichols, J., Smith, A. and Bertone, P. (2018). Integrated analysis of single-cell embryo data yields a unified transcriptome signature for the human pre-implantation epiblast. *Development* **145**.
Streit, A., Berliner, A. J., Papanayotou, C., Sirulnik, A. and Stern, C. D. (2000). Initiation of neural induction by FGF signalling before gastrulation. *Nature* **406**, 74-78.
Strumpf, D., Mao, C. A., Yamanaka, Y., Ralston, A., Chawengsaksophak, K., Beck, F. and Rossant, J. (2005). Cdx2 is required for correct cell fate specification and differentiation of trophectoderm in the mouse blastocyst. *Development* **132**, 2093-2102.
Stuckey, D. W., Clements, M., Di-Gregorio, A., Senner, C. E., Le Tissier, P., Srinivas, S. and Rodriguez, T. A. (2011). Coordination of cell proliferation and anterior-posterior axis establishment in the mouse embryo. *Development* **138**, 1521-1530.
Su, T. T. and O'Farrell, P. H. (1997). Chromosome association of minichromosome maintenance proteins in Drosophila mitotic cycles. *The Journal of cell biology* **139**, 13-21.
Su, T. T. and O'Farrell, P. H. (1998). Chromosome association of minichromosome maintenance proteins in Drosophila endoreplication cycles. *J Cell Biol* **140**, 451-460.
Sugino, A. (1995). Yeast DNA polymerases and their role at the replication fork. *Trends Biochem Sci* **20**, 319-323.
Sulston, J. E., Schierenberg, E., White, J. G. and Thomson, J. N. (1983). The embryonic cell lineage of the nematode Caenorhabditis elegans. *Dev Biol* **100**, 64-119.
Summerbell, D. (1981). Evidence for regulation of growth, size and pattern in the developing chick limb bud. *J Embryol Exp Morphol* **65 Suppl**, 129-150.
Sun, J., Shi, Y., Georgescu, R. E., Yuan, Z., Chait, B. T., Li, H. and O'Donnell, M. E. (2015). The architecture of a eukaryotic replisome. *Nat Struct Mol Biol* **22**, 976-982.
Sun, X., Meyers, E. N., Lewandoski, M. and Martin, G. R. (1999). Targeted disruption of Fgf8 causes failure of cell migration in the gastrulating mouse embryo. *Genes Dev* **13**, 1834-1846.
Sutherland, A. E., Speed, T. P. and Calarco, P. G. (1990). Inner cell allocation in the mouse morula: the role of oriented division during fourth cleavage. *Dev Biol* **137**, 13-25.
Swan, M. K., Johnson, R. E., Prakash, L., Prakash, S. and Aggarwal, A. K. (2009). Structural basis of high-fidelity DNA synthesis by yeast DNA polymerase delta. *Nat Struct Mol Biol* **16**, 979-986.
Sweeney, C., Murphy, M., Kubelka, M., Ravnik, S. E., Hawkins, C. F., Wolgemuth, D. J. and Carrington, M. (1996). A distinct cyclin A is expressed in germ cells in the mouse. *Development* **122**, 53-64.
Sweeton, D., Parks, S., Costa, M. and Wieschaus, E. (1991). Gastrulation in Drosophila: the formation of the ventral furrow and posterior midgut invaginations. *Development* **112**, 775-789.
Syvaoja, J., Suomensaari, S., Nishida, C., Goldsmith, J. S., Chui, G. S., Jain, S. and Linn, S. (1990). DNA polymerases alpha, delta, and epsilon: three distinct enzymes from HeLa cells. *Proc Natl Acad Sci U S A* **87**, 6664-6668.
Tabrizian, K., Shahraki, J., Bazzi, M., Rezaee, R., Jahantigh, H. and Hashemzaei, M. (2017). Neuro-Protective Effects of Resveratrol on Carbon Monoxide-Induced Toxicity in Male Rats. *Phytother Res* **31**, 1310-1315.

Tada, M. and Heisenberg, C. P. (2012). Convergent extension: using collective cell migration and cell intercalation to shape embryos. *Development* **139**, 3897-3904.
Tada, S., Li, A., Maiorano, D., Mechali, M. and Blow, J. J. (2001). Repression of origin assembly in metaphase depends on inhibition of RLF-B/Cdt1 by geminin. *Nat Cell Biol* **3**, 107-113.
Takaoka, K., Nishimura, H. and Hamada, H. (2017). Both Nodal signalling and stochasticity select for prospective distal visceral endoderm in mouse embryos. *Nature Communications* **8**, 1492.
Takaoka, K., Yamamoto, M. and Hamada, H. (2011). Origin and role of distal visceral endoderm, a group of cells that determines anterior-posterior polarity of the mouse embryo. *Nat Cell Biol* **13**, 743-752.
Takaoka, K., Yamamoto, M., Shiratori, H., Meno, C., Rossant, J., Saijoh, Y. and Hamada, H. (2006). The mouse embryo autonomously acquires anterior-posterior polarity at implantation. *Dev Cell* **10**, 451-459.
Takashima, S. and Murakami, R. (2001). Regulation of pattern formation in the Drosophila hindgut by wg, hh, dpp, and en. *Mech Dev* **101**, 79-90.
Takeuchi, T., Nomura, T., Tsujita, M., Suzuki, M., Fuse, T., Mori, H. and Mishina, M. (2002). Flp recombinase transgenic mice of C57BL/6 strain for conditional gene targeting. *Biochem Biophys Res Commun* **293**, 953-957.
Tam, P. P. and Beddington, R. S. (1987). The formation of mesodermal tissues in the mouse embryo during gastrulation and early organogenesis. *Development* **99**, 109-126.
Tam, P. P., Khoo, P. L., Lewis, S. L., Bildsoe, H., Wong, N., Tsang, T. E., Gad, J. M. and Robb, L. (2007). Sequential allocation and global pattern of movement of the definitive endoderm in the mouse embryo during gastrulation. *Development* **134**, 251-260.
Tam, P. P., Williams, E. A. and Chan, W. Y. (1993). Gastrulation in the mouse embryo: ultrastructural and molecular aspects of germ layer morphogenesis. *Microsc Res Tech* **26**, 301-328.
ten Klooster, J. P., Jaffer, Z. M., Chernoff, J. and Hordijk, P. L. (2006). Targeting and activation of Rac1 are mediated by the exchange factor β-Pix. *The Journal of cell biology* **172**, 759-769.
Tepass, U. and Hartenstein, V. (1994). The development of cellular junctions in the Drosophila embryo. *Dev Biol* **161**, 563-596.
Tepass, U., Theres, C. and Knust, E. (1990). crumbs encodes an EGF-like protein expressed on apical membranes of Drosophila epithelial cells and required for organization of epithelia. *Cell* **61**, 787-799.
Tessmar, K., Loosli, F. and Wittbrodt, J. (2002). A screen for co-factors of Six3. *Mech Dev* **117**, 103-113.
Tetsu, O. and McCormick, F. (2003). Proliferation of cancer cells despite CDK2 inhibition. *Cancer Cell* **3**, 233-245.
Thisse, B., Stoetzel, C., Gorostiza-Thisse, C. and Perrin-Schmitt, F. (1988). Sequence of the twist gene and nuclear localization of its protein in endomesodermal cells of early Drosophila embryos. *EMBO J* **7**, 2175-2183.
Thisse, B. and Thisse, C. (2005). Functions and regulations of fibroblast growth factor signaling during embryonic development. *Dev Biol* **287**, 390-402.
Thisse, B., Wright, C. V. and Thisse, C. (2000). Activin- and Nodal-related factors control antero-posterior patterning of the zebrafish embryo. *Nature* **403**, 425-428.
Thomas, P. Q., Brown, A. and Beddington, R. S. (1998). Hex: a homeobox gene revealing peri-implantation asymmetry in the mouse embryo and an early transient marker of endothelial cell precursors. *Development* **125**, 85-94.
Thomsen, G. H. and Melton, D. A. (1993). Processed Vg1 protein is an axial mesoderm inducer in Xenopus. *Cell* **74**, 433-441.

Torres-Padilla, M. E., Richardson, L., Kolasinska, P., Meilhac, S. M., Luetke-Eversloh, M. V. and Zernicka-Goetz, M. (2007). The anterior visceral endoderm of the mouse embryo is established from both preimplantation precursor cells and by de novo gene expression after implantation. *Dev Biol* **309**, 97-112.

Toy, J., Yang, J. M., Leppert, G. S. and Sundin, O. H. (1998). The optx2 homeobox gene is expressed in early precursors of the eye and activates retina-specific genes. *Proc Natl Acad Sci U S A* **95**, 10643-10648.

Toyoshima, H. and Hunter, T. (1994). p27, a novel inhibitor of G1 cyclin-Cdk protein kinase activity, is related to p21. *Cell* **78**, 67-74.

Tran, L. D., Hino, H., Quach, H., Lim, S., Shindo, A., Mimori-Kiyosue, Y., Mione, M., Ueno, N., Winkler, C., Hibi, M., et al. (2012). Dynamic microtubules at the vegetal cortex predict the embryonic axis in zebrafish. *Development* **139**, 3644-3652.

Treutlein, B., Lee, Q. Y., Camp, J. G., Mall, M., Koh, W., Shariati, S. A., Sim, S., Neff, N. F., Skotheim, J. M., Wernig, M., et al. (2016). Dissecting direct reprogramming from fibroblast to neuron using single-cell RNA-seq. *Nature* **534**, 391-395.

Tsurimoto, T., Melendy, T. and Stillman, B. (1990). Sequential initiation of lagging and leading strand synthesis by two different polymerase complexes at the SV40 DNA replication origin. *Nature* **346**, 534-539.

Tsurimoto, T. and Stillman, B. (1991). Replication factors required for SV40 DNA replication in vitro. II. Switching of DNA polymerase alpha and delta during initiation of leading and lagging strand synthesis. *J Biol Chem* **266**, 1961-1968.

Tsutsui, T., Hesabi, B., Moons, D. S., Pandolfi, P. P., Hansel, K. S., Koff, A. and Kiyokawa, H. (1999). Targeted disruption of CDK4 delays cell cycle entry with enhanced p27(Kip1) activity. *Mol Cell Biol* **19**, 7011-7019.

Tupler, R., Perini, G. and Green, M. R. (2001). Expressing the human genome. *Nature* **409**, 832-833.

Turner, F. R. and Mahowald, A. P. (1977). Scanning electron microscopy of Drosophila melanogaster embryogenesis. II. Gastrulation and segmentation. *Dev Biol* **57**, 403-416.

Ubersax, J. A., Woodbury, E. L., Quang, P. N., Paraz, M., Blethrow, J. D., Shah, K., Shokat, K. M. and Morgan, D. O. (2003). Targets of the cyclin-dependent kinase Cdk1. *Nature* **425**, 859-864.

Uchimura, A., Hidaka, Y., Hirabayashi, T., Hirabayashi, M. and Yagi, T. (2009). DNA polymerase delta is required for early mammalian embryogenesis. *PLoS One* **4**, e4184.

Ulrich, F., Concha, M. L., Heid, P. J., Voss, E., Witzel, S., Roehl, H., Tada, M., Wilson, S. W., Adams, R. J., Soll, D. R., et al. (2003). Slb/Wnt11 controls hypoblast cell migration and morphogenesis at the onset of zebrafish gastrulation. *Development* **130**, 5375-5384.

Umar, A., Buermeyer, A. B., Simon, J. A., Thomas, D. C., Clark, A. B., Liskay, R. M. and Kunkel, T. A. (1996). Requirement for PCNA in DNA mismatch repair at a step preceding DNA resynthesis. *Cell* **87**, 65-73.

Urban, N., van den Berg, D. L., Forget, A., Andersen, J., Demmers, J. A., Hunt, C., Ayrault, O. and Guillemot, F. (2016). Return to quiescence of mouse neural stem cells by degradation of a proactivation protein. *Science* **353**, 292-295.

Utikal, J., Polo, J. M., Stadtfeld, M., Maherali, N., Kulalert, W., Walsh, R. M., Khalil, A., Rheinwald, J. G. and Hochedlinger, K. (2009). Immortalization eliminates a roadblock during cellular reprogramming into iPS cells. *Nature* **460**, 1145-1148.

Vakaet, L. (1967). Contribution a l'etude de la pregastrulation et de la gastrulation de l'embryon de poulet en culture'in vitro'. *Mem. Acad. Roy. Med. Belg*, 235-257.

Vakaet, L. (1970). Cinephotomicrographic investigations of gastrulation in the chick blastoderm. *Arch Biol (Liege)* **81**, 387-426.

Valle, L., Hernandez-Illan, E., Bellido, F., Aiza, G., Castillejo, A., Castillejo, M. I., Navarro, M., Segui, N., Vargas, G., Guarinos, C., et al. (2014). New insights into POLE and POLD1 germline mutations in familial colorectal cancer and polyposis. *Hum Mol Genet* **23**, 3506-3512.

van Boxtel, A. L., Chesebro, J. E., Heliot, C., Ramel, M.-C., Stone, R. K. and Hill, C. S. (2015). A temporal window for signal activation dictates the dimensions of a nodal signaling domain. *Developmental cell* **35**, 175-185.

Van Boxtel, A. L., Economou, A. D., Heliot, C. and Hill, C. S. (2018). Long-range signaling activation and local inhibition separate the mesoderm and endoderm lineages. *Developmental cell* **44**, 179-191. e175.

van den Akker, E., Forlani, S., Chawengsaksophak, K., de Graaff, W., Beck, F., Meyer, B. I. and Deschamps, J. (2002). Cdx1 and Cdx2 have overlapping functions in anteroposterior patterning and posterior axis elongation. *Development* **129**, 2181-2193.

van den Heuvel, S. and Harlow, E. (1993). Distinct roles for cyclin-dependent kinases in cell cycle control. *Science* **262**, 2050-2054.

Venkatesan, R. N., Hsu, J. J., Lawrence, N. A., Preston, B. D. and Loeb, L. A. (2006). Mutator phenotypes caused by substitution at a conserved motif A residue in eukaryotic DNA polymerase delta. *J Biol Chem* **281**, 4486-4494.

Venkatesan, R. N., Treuting, P. M., Fuller, E. D., Goldsby, R. E., Norwood, T. H., Gooley, T. A., Ladiges, W. C., Preston, B. D. and Loeb, L. A. (2007). Mutation at the polymerase active site of mouse DNA polymerase delta increases genomic instability and accelerates tumorigenesis. *Mol Cell Biol* **27**, 7669-7682.

Vierbuchen, T., Ostermeier, A., Pang, Z. P., Kokubu, Y., Sudhof, T. C. and Wernig, M. (2010). Direct conversion of fibroblasts to functional neurons by defined factors. *Nature* **463**, 1035-1041.

Vincent, S. D., Dunn, N. R., Hayashi, S., Norris, D. P. and Robertson, E. J. (2003). Cell fate decisions within the mouse organizer are governed by graded Nodal signals. *Genes Dev* **17**, 1646-1662.

Vincent, S. D. and Robertson, E. J. (2003). Highly efficient transgene-independent recombination directed by a maternally derived SOX2CRE transgene. *Genesis* **37**, 54-56.

Viotti, M., Niu, L., Shi, S. H. and Hadjantonakis, A. K. (2012). Role of the gut endoderm in relaying left-right patterning in mice. *PLoS Biol* **10**, e1001276.

Viotti, M., Nowotschin, S. and Hadjantonakis, A. K. (2014). SOX17 links gut endoderm morphogenesis and germ layer segregation. *Nat Cell Biol* **16**, 1146-1156.

Visvader, J. E. and Lindeman, G. J. (2003). Transcriptional regulators in mammary gland development and cancer. *Int J Biochem Cell Biol* **35**, 1034-1051.

Voiculescu, O., Bertocchini, F., Wolpert, L., Keller, R. E. and Stern, C. D. (2007). The amniote primitive streak is defined by epithelial cell intercalation before gastrulation. *Nature* **449**, 1049-1052.

Voiculescu, O., Bodenstein, L., Lau, I. J. and Stern, C. D. (2014). Local cell interactions and self-amplifying individual cell ingression drive amniote gastrulation. *Elife* **3**, e01817.

von Gise, A., Lin, Z., Schlegelmilch, K., Honor, L. B., Pan, G. M., Buck, J. N., Ma, Q., Ishiwata, T., Zhou, B. and Camargo, F. D. (2012). YAP1, the nuclear target of Hippo signaling, stimulates heart growth through cardiomyocyte proliferation but not hypertrophy. *Proceedings of the National Academy of Sciences* **109**, 2394-2399.

Waddington, C. (1933). Induction by the endoderm in birds. *Wilhelm Roux'Archiv für Entwicklungsmechanik der Organismen* **128**, 502-521.

Waddington, C. H. (1932). III. Experiments on the development of chick and duck embryos, cultivated in vitro. *Philosophical Transactions of the Royal Society of London. Series B, Containing Papers of a Biological Character* **221**, 179-230.

Waldrip, W. R., Bikoff, E. K., Hoodless, P. A., Wrana, J. L. and Robertson, E. J. (1998). Smad2 signaling in extraembryonic tissues determines anterior-posterior polarity of the early mouse embryo. *Cell* **92**, 797-808.

Wamaitha, S. E., del Valle, I., Cho, L. T., Wei, Y., Fogarty, N. M., Blakeley, P., Sherwood, R. I., Ji, H. and Niakan, K. K. (2015). Gata6 potently initiates reprograming of pluripotent and differentiated cells to extraembryonic endoderm stem cells. *Genes Dev* **29**, 1239-1255.

Wang, Y., Zhang, Q., Chen, H., Li, X., Mai, W., Chen, K., Zhang, S., Lee, E. Y., Lee, M. Y. and Zhou, Y. (2011). P50, the small subunit of DNA polymerase delta, is required for mediation of the interaction of polymerase delta subassemblies with PCNA. *PLoS One* **6**, e27092.

Warga, R. M. and Kimmel, C. B. (1990). Cell movements during epiboly and gastrulation in zebrafish. *Development* **108**, 569-580.

Warga, R. M. and Nusslein-Volhard, C. (1999). Origin and development of the zebrafish endoderm. *Development* **126**, 827-838.

Warr, N., Powles-Glover, N., Chappell, A., Robson, J., Norris, D. and Arkell, R. M. (2008). Zic2-associated holoprosencephaly is caused by a transient defect in the organizer region during gastrulation. *Hum Mol Genet* **17**, 2986-2996.

Washimi, O., Nagatake, M., Osada, H., Ueda, R., Koshikawa, T., Seki, T., Takahashi, T. and Takahashi, T. (1995). In vivo occurrence of p16 (MTS1) and p15 (MTS2) alterations preferentially in non-small cell lung cancers. *Cancer Res* **55**, 514-517.

Weedon, M. N., Ellard, S., Prindle, M. J., Caswell, R., Lango Allen, H., Oram, R., Godbole, K., Yajnik, C. S., Sbraccia, P., Novelli, G., et al. (2013). An in-frame deletion at the polymerase active site of POLD1 causes a multisystem disorder with lipodystrophy. *Nat Genet* **45**, 947-950.

Weigel, D., Jurgens, G., Klingler, M. and Jackle, H. (1990). Two gap genes mediate maternal terminal pattern information in Drosophila. *Science* **248**, 495-498.

Weinberg, D. H. and Kelly, T. J. (1989). Requirement for two DNA polymerases in the replication of simian virus 40 DNA in vitro. *Proc Natl Acad Sci U S A* **86**, 9742-9746.

Weinberg, R. A. (1995). The retinoblastoma protein and cell cycle control. *Cell* **81**, 323-330.

Wells, R. S. (1982). An in vitro assay for growth regulation of embryonal carcinoma by the blastocyst. *Cancer Res* **42**, 2736-2741.

Weng, M. and Wieschaus, E. (2017). Polarity protein Par3/Bazooka follows myosin-dependent junction repositioning. *Dev Biol* **422**, 125-134.

Wheeler, S. R., Carrico, M. L., Wilson, B. A. and Skeath, J. B. (2005). The Tribolium columnar genes reveal conservation and plasticity in neural precursor patterning along the embryonic dorsal-ventral axis. *Dev Biol* **279**, 491-500.

White, J., Stead, E., Faast, R., Conn, S., Cartwright, P. and Dalton, S. (2005). Developmental activation of the Rb-E2F pathway and establishment of cell cycle-regulated cyclin-dependent kinase activity during embryonic stem cell differentiation. *Mol Biol Cell* **16**, 2018-2027.

Williams, M., Burdsal, C., Periasamy, A., Lewandoski, M. and Sutherland, A. (2012). Mouse primitive streak forms in situ by initiation of epithelial to mesenchymal transition without migration of a cell population. *Dev Dyn* **241**, 270-283.

Williams, M. L. and Solnica-Krezel, L. (2017). Regulation of gastrulation movements by emergent cell and tissue interactions. *Curr Opin Cell Biol* **48**, 33-39.

Wilson, S. W. and Houart, C. (2004). Early steps in the development of the forebrain. *Dev Cell* **6**, 167-181.

Wilson, V. and Beddington, R. S. (1996). Cell fate and morphogenetic movement in the late mouse primitive streak. *Mech Dev* **55**, 79-89.

Wilson, V., Manson, L., Skarnes, W. C. and Beddington, R. (1995). The T gene is necessary for normal mesodermal morphogenetic cell movements during gastrulation. *Development* **121**, 877-886.

Winklbauer, R. and Muller, H. A. (2011). Mesoderm layer formation in Xenopus and Drosophila gastrulation. *Phys Biol* **8**, 045001.

Winnier, G., Blessing, M., Labosky, P. A. and Hogan, B. L. (1995). Bone morphogenetic protein-4 is required for mesoderm formation and patterning in the mouse. *Genes Dev* **9**, 2105-2116.

Winston, N., Bourgain-Guglielmetti, F., Ciemerych, M. A., Kubiak, J. Z., Senamaud-Beaufort, C., Carrington, M., Brechot, C. and Sobczak-Thepot, J. (2000). Early development of mouse embryos null mutant for the cyclin A2 gene occurs in the absence of maternally derived cyclin A2 gene products. *Dev Biol* **223**, 139-153.

Wintersberger, U. and Wintersberger, E. (1970). Studies on deoxyribonucleic acid polymerases from yeast. 2. Partial purification and characterization of mitochondrial DNA polymerase from wild type and respiration-deficient yeast cells. *Eur J Biochem* **13**, 20-27.

Wohlschlegel, J. A., Dwyer, B. T., Dhar, S. K., Cvetic, C., Walter, J. C. and Dutta, A. (2000). Inhibition of eukaryotic DNA replication by geminin binding to Cdt1. *Science* **290**, 2309-2312.

Woo, S., Housley, M. P., Weiner, O. D. and Stainier, D. Y. (2012). Nodal signaling regulates endodermal cell motility and actin dynamics via Rac1 and Prex1. *J Cell Biol* **198**, 941-952.

Xenopoulos, P., Kang, M., Puliafito, A., Di Talia, S. and Hadjantonakis, A. K. (2015). Heterogeneities in Nanog Expression Drive Stable Commitment to Pluripotency in the Mouse Blastocyst. *Cell Rep* **10**, 1508-1520.

Xiao, Z., Patrakka, J., Nukui, M., Chi, L., Niu, D., Betsholtz, C., Pikkarainen, T., Vainio, S. and Tryggvason, K. (2011). Deficiency in Crumbs homolog 2 (Crb2) affects gastrulation and results in embryonic lethality in mice. *Dev Dyn* **240**, 2646-2656.

Xin, M., Kim, Y., Sutherland, L. B., Qi, X., McAnally, J., Schwartz, R. J., Richardson, J. A., Bassel-Duby, R. and Olson, E. N. (2011). Regulation of insulin-like growth factor signaling by Yap governs cardiomyocyte proliferation and embryonic heart size. *Sci Signal* **4**, ra70.

Yagi, R., Kohn, M. J., Karavanova, I., Kaneko, K. J., Vullhorst, D., DePamphilis, M. L. and Buonanno, A. (2007). Transcription factor TEAD4 specifies the trophectoderm lineage at the beginning of mammalian development. *Development* **134**, 3827-3836.

Yamaguchi, T. P., Harpal, K., Henkemeyer, M. and Rossant, J. (1994). fgfr-1 is required for embryonic growth and mesodermal patterning during mouse gastrulation. *Genes Dev* **8**, 3032-3044.

Yamamoto, M., Beppu, H., Takaoka, K., Meno, C., Li, E., Miyazono, K. and Hamada, H. (2009). Antagonism between Smad1 and Smad2 signaling determines the site of distal visceral endoderm formation in the mouse embryo. *J Cell Biol* **184**, 323-334.

Yamamoto, M., Saijoh, Y., Perea-Gomez, A., Shawlot, W., Behringer, R. R., Ang, S. L., Hamada, H. and Meno, C. (2004). Nodal antagonists regulate formation of the anteroposterior axis of the mouse embryo. *Nature* **428**, 387-392.

Yamanaka, Y., Lanner, F. and Rossant, J. (2010). FGF signal-dependent segregation of primitive endoderm and epiblast in the mouse blastocyst. *Development* **137**, 715-724.

Yamanaka, Y., Mizuno, T., Sasai, Y., Kishi, M., Takeda, H., Kim, C. H., Hibi, M. and Hirano, T. (1998). A novel homeobox gene, dharma, can induce the organizer in a non-cell-autonomous manner. *Genes Dev* **12**, 2345-2353.

Yamashita, S., Miyagi, C., Carmany-Rampey, A., Shimizu, T., Fujii, R., Schier, A. F. and Hirano, T. (2002). Stat3 Controls Cell Movements during Zebrafish Gastrulation. *Dev Cell* **2**, 363-375.

Yamashita, S., Miyagi, C., Fukada, T., Kagara, N., Che, Y. S. and Hirano, T. (2004). Zinc transporter LIVI controls epithelial-mesenchymal transition in zebrafish gastrula organizer. *Nature* **429**, 298-302.

Yan, L., Chen, J., Zhu, X., Sun, J., Wu, X., Shen, W., Zhang, W., Tao, Q. and Meng, A. (2018). Maternal Huluwa dictates the embryonic body axis through beta-catenin in vertebrates. *Science* **362**.

Yan, L., Yang, M., Guo, H., Yang, L., Wu, J., Li, R., Liu, P., Lian, Y., Zheng, X., Yan, J., et al. (2013). Single-cell RNA-Seq profiling of human preimplantation embryos and embryonic stem cells. *Nat Struct Mol Biol* **20**, 1131-1139.

Yanagida, A., Corujo-Simon, E., Revell, C. K., Sahu, P., Stirparo, G. G., Aspalter, I. M., Winkel, A. K., Peters, R., De Belly, H., Cassani, D. A. D., et al. (2022). Cell surface fluctuations regulate early embryonic lineage sorting. *Cell* **185**, 1258.

Yang, D. H., Smith, E. R., Roland, I. H., Sheng, Z., He, J., Martin, W. D., Hamilton, T. C., Lambeth, J. D. and Xu, X. X. (2002). Disabled-2 is essential for endodermal cell positioning and structure formation during mouse embryogenesis. *Dev Biol* **251**, 27-44.

Yang, J., Ryan, D. J., Wang, W., Tsang, J. C., Lan, G., Masaki, H., Gao, X., Antunes, L., Yu, Y., Zhu, Z., et al. (2017a). Establishment of mouse expanded potential stem cells. *Nature* **550**, 393-397.

Yang, Q. E., Fields, S. D., Zhang, K., Ozawa, M., Johnson, S. E. and Ealy, A. D. (2011). Fibroblast growth factor 2 promotes primitive endoderm development in bovine blastocyst outgrowths. *Biol Reprod* **85**, 946-953.

Yang, Y., Liu, B., Xu, J., Wang, J., Wu, J., Shi, C., Xu, Y., Dong, J., Wang, C., Lai, W., et al. (2017b). Derivation of Pluripotent Stem Cells with In Vivo Embryonic and Extraembryonic Potency. *Cell* **169**, 243-257 e225.

Yang, Y. and Mlodzik, M. (2015). Wnt-Frizzled/planar cell polarity signaling: cellular orientation by facing the wind (Wnt). *Annu Rev Cell Dev Biol* **31**, 623-646.

Ye, X. and Weinberg, R. A. (2015). Epithelial-Mesenchymal Plasticity: A Central Regulator of Cancer Progression. *Trends Cell Biol* **25**, 675-686.

Yeeles, J. T., Deegan, T. D., Janska, A., Early, A. and Diffley, J. F. (2015). Regulated eukaryotic DNA replication origin firing with purified proteins. *Nature* **519**, 431-435.

Yeeles, J. T., Janska, A., Early, A. and Diffley, J. F. (2017). How the eukaryotic replisome achieves rapid and efficient DNA replication. *Molecular cell* **65**, 105-116.

Yin, C., Ciruna, B. and Solnica-Krezel, L. (2009a). Convergence and extension movements during vertebrate gastrulation. *Curr Top Dev Biol* **89**, 163-192.

Yin, H., Zhang, X., Liu, J., Wang, Y., He, J., Yang, T., Hong, X., Yang, Q. and Gong, Z. (2009b). Epigenetic regulation, somatic homologous recombination, and abscisic acid signaling are influenced by DNA polymerase ϵ mutation in Arabidopsis. *The Plant Cell* **21**, 386-402.

Yu, F. X., Zhao, B. and Guan, K. L. (2015). Hippo Pathway in Organ Size Control, Tissue Homeostasis, and Cancer. *Cell* **163**, 811-828.

Yu, L., Wei, Y., Duan, J., Schmitz, D. A., Sakurai, M., Wang, L., Wang, K., Zhao, S., Hon, G. C. and Wu, J. (2021). Blastocyst-like structures generated from human pluripotent stem cells. *Nature* **591**, 620-626.

Zalokar, M. (1976). Division and migration of nuclei during early embryogenesis of Drosophila melanogaster. *J. Microsc. Biol. Cell.* **25**, 97-106.

Zarkowska, T. and Mittnacht, S. (1997). Differential phosphorylation of the retinoblastoma protein by G1/S cyclin-dependent kinases. *Journal of Biological Chemistry* **272**, 12738-12746.

Zecca, M., Basler, K. and Struhl, G. (1995). Sequential organizing activities of engrailed, hedgehog and decapentaplegic in the Drosophila wing. *Development* **121**, 2265-2278.

Zeng, L., Fagotto, F., Zhang, T., Hsu, W., Vasicek, T. J., Perry, W. L., 3rd, Lee, J. J., Tilghman, S. M., Gumbiner, B. M. and Costantini, F. (1997). The mouse Fused locus encodes Axin, an inhibitor of the Wnt signaling pathway that regulates embryonic axis formation. *Cell* **90**, 181-192.

Zhao, L. and Chang, L. S. (1997). The human POLD1 gene. Identification of an upstream activator sequence, activation by Sp1 and Sp3, and cell cycle regulation. *J Biol Chem* **272**, 4869-4882.
Zhou, Q., Brown, J., Kanarek, A., Rajagopal, J. and Melton, D. A. (2008). In vivo reprogramming of adult pancreatic exocrine cells to beta-cells. *Nature* **455**, 627-632.
Zhou, X. and Anderson, K. V. (2010). Development of head organizer of the mouse embryo depends on a high level of mitochondrial metabolism. *Dev Biol* **344**, 185-195.
Zhou, X., Hollemann, T., Pieler, T. and Gruss, P. (2000). Cloning and expression of xSix3, the Xenopus homologue of murine Six3. *Mech Dev* **91**, 327-330.
Zhou, Y., Chen, H., Li, X., Wang, Y., Chen, K., Zhang, S., Meng, X., Lee, E. Y. and Lee, M. Y. (2011). Production of recombinant human DNA polymerase delta in a Bombyx mori bioreactor. *PloS one* **6**, e22224.
Zhou, Y., Meng, X., Zhang, S., Lee, E. Y. and Lee, M. Y. (2012). Characterization of human DNA polymerase delta and its subassemblies reconstituted by expression in the MultiBac system. *PLoS One* **7**, e39156.
Zhou, Z. X., Lujan, S. A., Burkholder, A. B., Garbacz, M. A. and Kunkel, T. A. (2019). Roles for DNA polymerase delta in initiating and terminating leading strand DNA replication. *Nat Commun* **10**, 3992.
Zhu, C. C., Dyer, M. A., Uchikawa, M., Kondoh, H., Lagutin, O. V. and Oliver, G. (2002). Six3-mediated auto repression and eye development requires its interaction with members of the Groucho-related family of co-repressors. *Development* **129**, 2835-2849.
Zhu, M., Shahbazi, M., Martin, A., Zhang, C., Sozen, B., Borsos, M., Mandelbaum, R. S., Paulson, R. J., Mole, M. A., Esbert, M., et al. (2021). Human embryo polarization requires PLC signaling to mediate trophectoderm specification. *Elife* **10**.
Zou, H., McGarry, T. J., Bernal, T. and Kirschner, M. W. (1999). Identification of a vertebrate sister-chromatid separation inhibitor involved in transformation and tumorigenesis. *Science* **285**, 418-422.
Zuber, M. E., Perron, M., Philpott, A., Bang, A. and Harris, W. A. (1999). Giant eyes in Xenopus laevis by overexpression of XOptx2. *Cell* **98**, 341-352.
Zusman, S. B. and Wieschaus, E. F. (1985). Requirements for zygotic gene activity during gastrulation in Drosophila melanogaster. *Dev Biol* **111**, 359-371.